NATIONAL TECHNICAL UNIVERSITY OF ATHENS
School of Mechanical Engineering

INTERDISCIPLINARY POSTGRADUATE SPECILIAZATION
PROGRAMME «AUTOMATION SYSTEMS»

THESIS

«DAMAGE TOLERANCE IN DESIGN OF AIRCRAFT STRUCTURES»

ZOI PAPPA

Approved by:

Professor: D. Manolakos, School of Mechanical Engineering

ATHENS, OCTOBER 2018

Abstract

Damage tolerance design is becoming a mandatory part of the design of modern aircrafts, related to the any structure's ability of sustaining the defects in an acceptable fail-safely level. A whole damage tolerance methodology has been developed during the last decades, specifically in aerospace engineering field, where the approach of designing is based both on the flaws existence and monitoring the extension of cracks. Principles of fracture mechanics are used recently in predicting residual strength and crack growth. Most commonly, the structure considered to be damage tolerant if a maintenance program has been implemented that will result in the detection and repair of accidental damage, corrosion and fatigue cracking before such damage reduces the residual strength of structure below the acceptable limit.

The thesis consists of four main sections: The first section reviews the damage tolerant methodology, which based on crack propagation laws (including linear and non-linear ranges and spectrum loading effects) in fracture mechanics field, the residual strength principles and the life prediction methodology. The second part presents the damage characterization in accordance with several non-destructive methods and the analysis of cracking behavior under spectrum loading conditions and environmental conditions. The comparison of the test results and analysis verification tests provide data that define the accuracy of the damage tolerance analysis for predicting the crack growth behavior of the structure and control damage under operational conditions. This damage tolerance testing methodology and evaluation of material/quality/analysis and structural hardware tests data are represented in the third part of this paper. In latter part of this thesis, the structural elements of an aircraft are divided into two main categories as primary structural or secondary structure elements carrying flight/ground/pressurization loads or only air /inertial loads accordingly. Some examples of corrosion, cracks and damage growth incidents are also shown. Additionally, the experimental tests for the development of reinforced panels for the reduction of fatigue crack growth and the increase of residual strength of the aircraft skin as an attempt to improve their application to aircraft structures.

This thesis is a general approach to critically review some damage tolerance design approaches and adopt the knowledge of stress concentration and crack propagation damage in aerostructures. Damage fail-safe control as a strong suggestion for the manufacturers of transport aircrafts to retain the large damage-tolerance capability designed into the first wide-bodied aircraft and to modify their methodology to establish inspection thresholds for those structures incapable of sustaining large obviously detectable damage

Table of Content

List of Figures

SECTION 1: ABSTRACT

Damage tolerance design is becoming a mandatory part of the design of modern aircrafts, related to the any structure's ability of sustaining the defects in an acceptable fail-safely level. A whole damage tolerance methodology has been developed during the last decades, specifically in aerospace engineering field, where the approach of designing is based both on the flaws existence and monitoring the extension of cracks. Principles of fracture mechanics are used recently in predicting residual strength and crack growth. Most commonly, the structure considered to be damage tolerant if a maintenance program has been implemented that will result in the detection and repair of accidental damage, corrosion and fatigue cracking before such damage reduces the residual strength of structure below the acceptable limit.

The thesis consists of four main sections: The first section reviews the damage tolerant methodology, which based on crack propagation laws (including linear and non-linear ranges and spectrum loading effects) in fracture mechanics field, the residual strength principles and the life prediction methodology. The second part presents the damage characterization in accordance with several non-destructive methods and the analysis of cracking behavior under spectrum loading conditions and environmental conditions. The comparison of the test results and analysis verification tests provide data that define the accuracy of the damage tolerance analysis for predicting the crack growth behavior of the structure and control damage under operational conditions. This damage tolerance testing methodology and evaluation of material/quality/analysis and structural hardware tests data are represented in the third part of this paper. In latter part of this thesis, the structural elements of an aircraft are divided into two main categories as primary structural or secondary structure elements carrying flight/ground/pressurization loads or only air /inertial loads accordingly. Some examples of corrosion, cracks and damage growth incidents are also shown. Additionally, the experimental tests for the development of reinforced panels for the reduction of fatigue crack growth and the increase of residual strength of the aircraft skin as an attempt to improve their application to aircraft structures.

This thesis is a general approach to critically review some damage tolerance design approaches and adopt the knowledge of stress concentration and crack propagation damage in aerostructures. Damage fail-safe control as a strong suggestion for the manufacturers of transport aircrafts to retain the large damage-tolerance capability designed into the first wide-bodied aircraft and to modify their methodology to establish inspection thresholds for those structures incapable of sustaining large obviously detectable damage.

This paper is also dedicated to my friends and colleagues, Mr. Jason Aivaliotis for giving me inspiration and motivation to choose a "safe life" criterion in aviation, Ms. Lydia Katsimiga for her passion on each assigned academic project through her outstanding performance into continuous research and Mr. Georgios Davanos for his constant persistence on completing successfully all primary goals set on time.

Special regards to Professor Dimitrios Manolakos for his guidance through this project, his discrete acceptance and flexibility to issues for the implementation of this thesis.

SECTION 2: DAMAGE TOLERANT METHODOLOGY

In this section, the fundamentals of the damage tolerant methodology are presented. The crack growth behavior is analyzed from the initial flaw to the failure of the structure by taking into account the factors affecting the rate growth.

The Damage Tolerant Methodology is based on fracture mechanics, residual strength principles and life prediction methodology and the detailed presentation of them follows in the subsections below.

SECTION 2.1: INTRODUCTION IN DAMAGE TOLERANT METHODOLOGY

For ensuring the structural safety, the consideration of initial damage in the form of cracks or equivalent damage is necessary. This common practice where the damage accumulation process as entirely crack growth with zero time to initiate the crack is a result of information derived from tests of structures under simulated flight loading and analyses of in-service fractures, cracking instances etc… These sources indicated that the time of the crack initiation from most structural details (sharp corners or holes) is short and the majority of the life is spent growing the resultant cracks to failure. Another conclusion is that the major source of cracks occurred by initial manufacturing defects such as sharp corners tool marks and the like. So, the life prediction is based on the crack growth where the crack length is the measure of the damage and the crack growth rate define the rate of damage accumulation.

Firstly, the typical crack growth behavior being observed in a structural element is presented on the schematic below Figure 2.1.

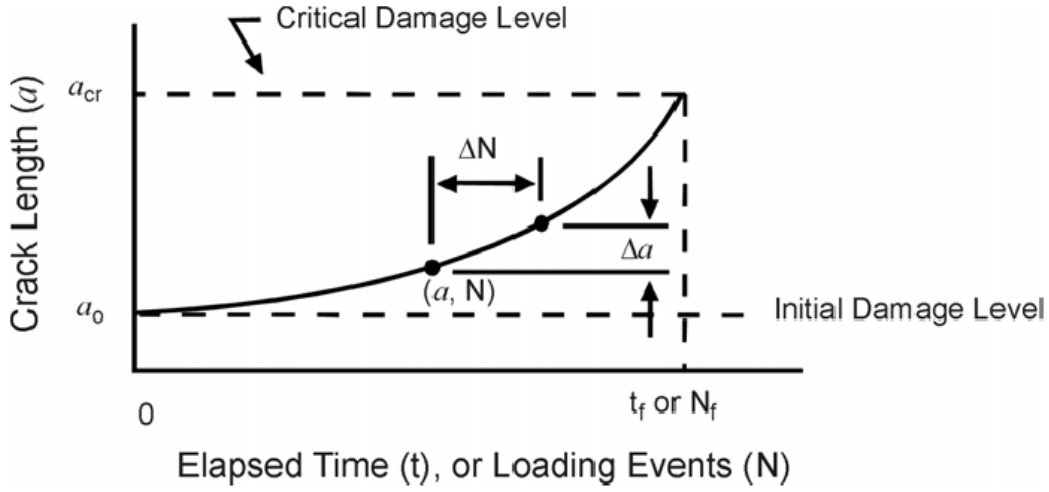

Figure 2.1. Schematic of Observed Crack Growth Behavior for a Typical Structural Cracking Problem

The crack growth evolves from the initial damage size (initial crack length α_o) to a damage size causing structural failure (critical crack length α_{cr}). The x-axis represents the elapsed time t of loading application (operational flight hours) or the number of applied loading events N (number of aircraft's flights). The y-axis represents the length of the crack observed in the structure α. For the definition of the function, the increment of a crack Δα resulting from a ΔN number of loading events gives the curve of the crack growth. When the crack length reaches the critical damage level, the growth is unstable and thus the failure is reached. So, the structural life limit t_f or N_f is expressed as the maximum allowable service time or number of accumulated service events. The objective of the Damage Tolerant Requirements is the definition of the expected lifetime t_s or N_s as safe levels that could not impair the safety of the aircraft (t_f or N_f must be greater than t_s or N_s).

Another important observation is the close relationship between the length of the crack at failure and the load or stress. As observed in Figure 2.1, the smaller the crack length is, the slower growth rate exhibits. So, a smaller length of a crack could have a greater residual strength. This leads to a function between crack length and residual strength.

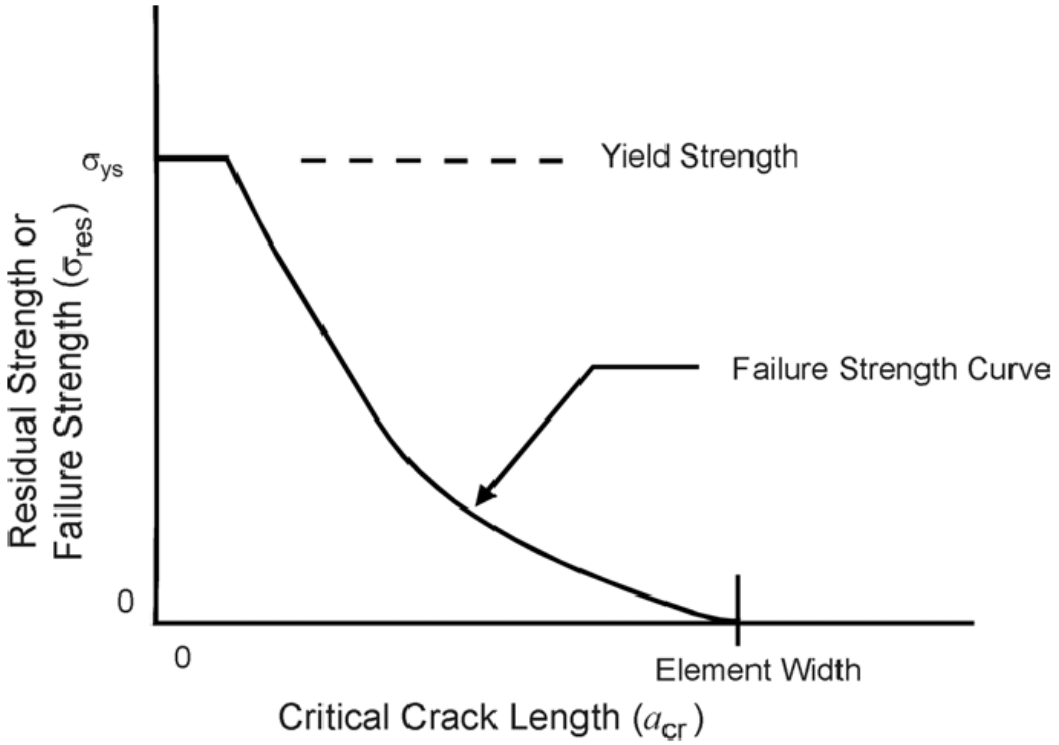

Figure 2.2: Schematic of Relationship between Failure Strength and Crack Length for a Typical Single Element Type Structure

By combining Figure 2.1 and Figure 2.2, a direct relationship between residual strength and elapsed time t or number of loading events N is excluded.

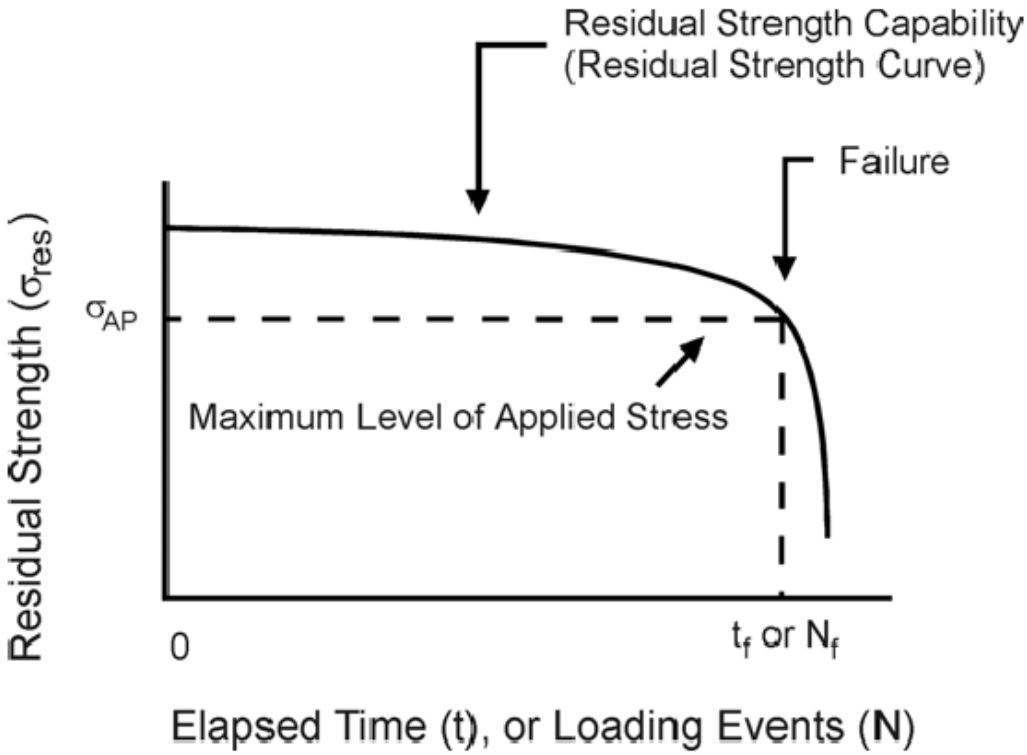

Figure 2.3: Residual Strength Diagram Relationship between Residual Strength Capacity and Elapsed Time

The residual strength diagram shows that while the structure is young ($t << t_f$) the residual strength capacity is basically unimpaired because the crack is both small and doesn't grow much with time. As the structure starts to age, the residual strength capacity is shown to decrease and just prior to failure, the rate of decrease in residual strength capacity is accelerating because now the crack is rapidly becoming very large. When the residual strength capacity equals the level of the maximum stress in the operational history, failure occurs. When the loads in the operational history change, the subcritical crack growth process changes its pattern of growth and this in turn affects the residual strength diagram and the allowable structural life.

There are four major parameters that affect the crack growth life and residual strength capacity of structures. These parameters are in the realm of quality (initial crack size), usage (loading history), material (material properties), and geometry (structural properties). Their schematic representation in function of the structure's lifetime is presented in Figure 2.4.

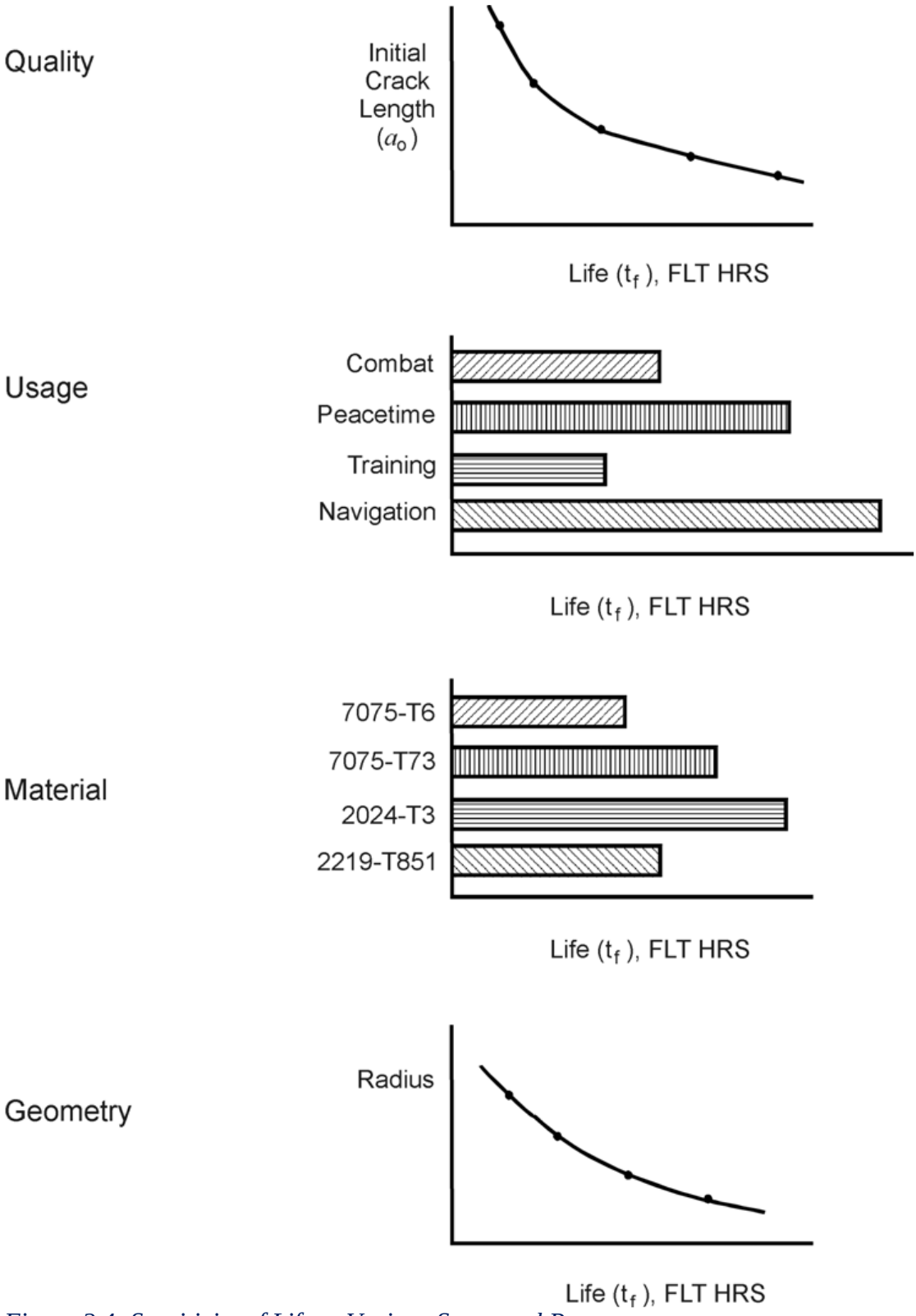

Figure 2.4: Sensitivity of Life to Various Structural Parameters

SECTION 2.2: FRACTURE MECHANICS

The realization that component fractures that result from the extension of small crack-like defects are failures that depend on localized phenomena leads to the modeling of cracking phenomena with the technology of Fracture Mechanics. Since the material tolerance to flaws resides in a material's ability to deform locally, this modeling focuses on the crack tip region where the material must resist crack extension. A mechanical model characterizing a crack movement in structural components fabricated from materials having low tolerance to flaws is used.

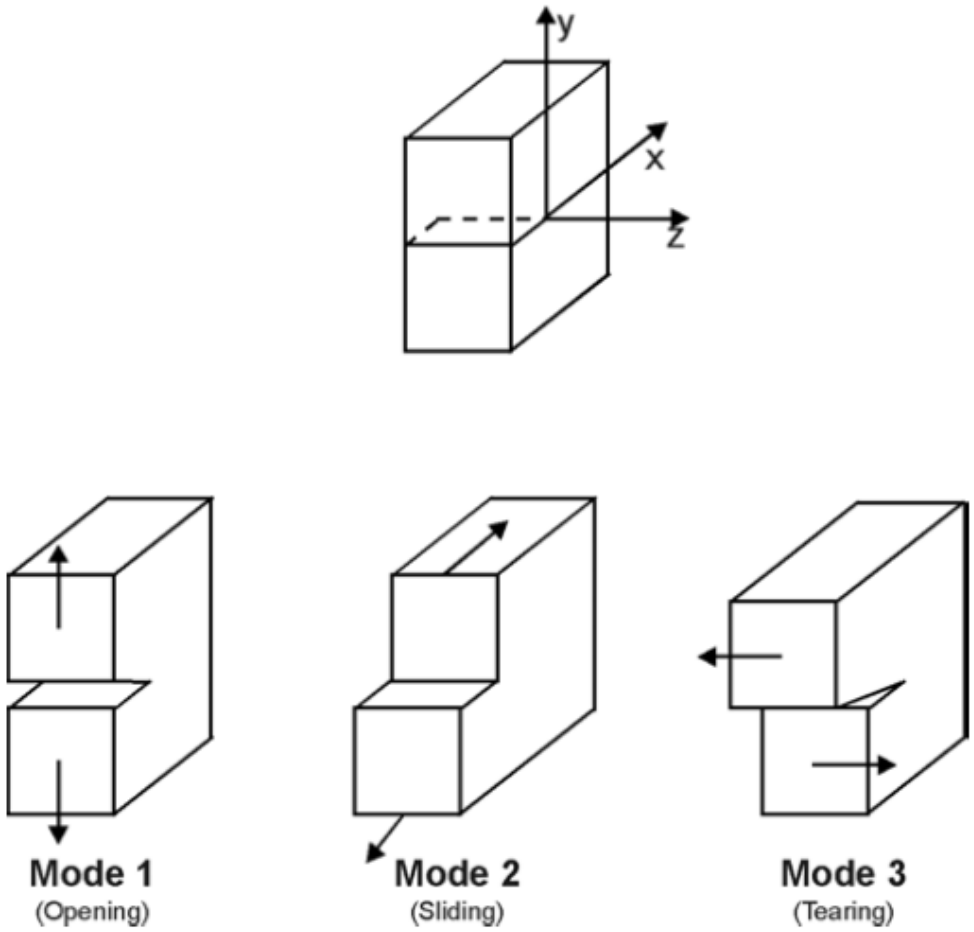

Figure 2.5: The Three Modes of Crack Extension

It is essential that the three modes of crack extension be introduced. Since improvement of a material's tensile opening (Mode 1) fracture resistance will also improve the resistance to the combined mode action and shear stresses fractures are rather infrequent, this section will emphasize on Mode 1 crack extension behavior.

A linear elastic analysis of a cracked body provides a good first approximation to the localized stress state in materials that fracture at gross section stresses below the yield strength. No additional refinements in the analysis are necessary if the gross section stresses at failure are below $0.7\sigma_{ys}$. The elastic analysis when modified to account for restricted amounts of stress relaxation due to crack tip plastic deformation provides an adequate description of fracture that occurs above $0.7\sigma_{ys}$.

The linear elastic fracture mechanics model is a method for determining the resistance of a material to below-yield strength fractures based on the assumption that at the initiation of fracture any localized plastic deformation is small and considered within the surrounding elastic stress field. For the calculation of the crack tip stress field, an infinite plate with a flaw that extends through thickness is used.

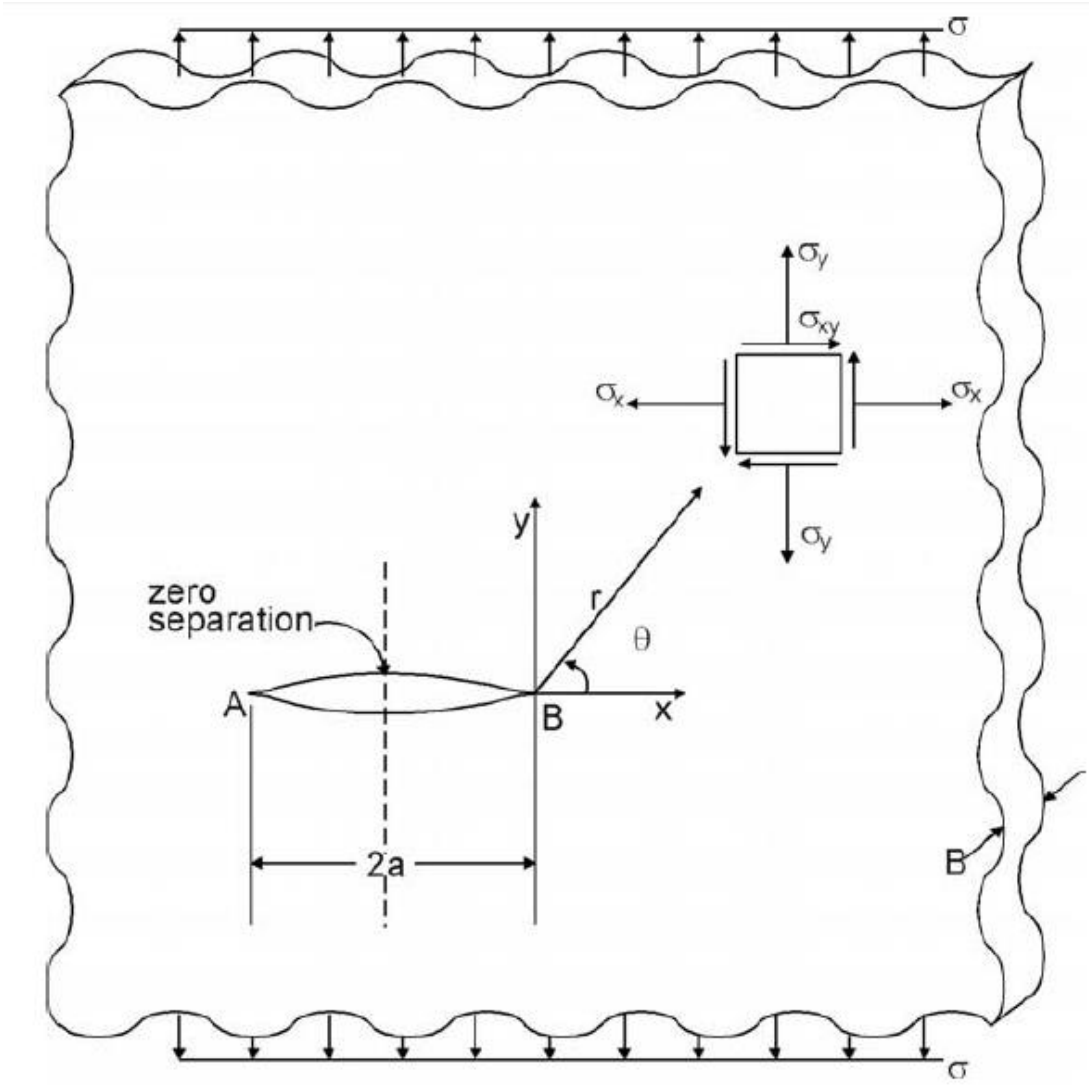

Figure 2.6: Infinite Plate with a Flaw that Extends Through Thickness

The local stress field (within r < a/10) is given by [Irwin, 1957; Williams, 1957; Sneddon & Lowengrub, 1969; Rice, 1968a]:

$$\sigma_x = \frac{K}{\sqrt{2\pi r}} cos\frac{\theta}{2}\left[1 - sin\frac{\theta}{2} sin\frac{3\theta}{2}\right]$$

$$\sigma_y = \frac{K}{\sqrt{2\pi r}} cos\frac{\theta}{2}\left[1 + sin\frac{\theta}{2} sin\frac{3\theta}{2}\right]$$

$$\sigma_{xy} = \frac{K}{\sqrt{2\pi r}} sin\frac{\theta}{2}\left[cos\frac{\theta}{2} cos\frac{3\theta}{2}\right]$$

These equations represent the crack tip stress field for the Mode 1 crack extension. The stress in the third direction are given by $\sigma_z = \sigma_{xz} = \sigma_{yz} = 0$ for the plane stress problem, and when the third directional strains are zero (plane strain problem), the out of plane stresses become $\sigma_{xz} = \sigma_{yz} = 0$ and $\sigma_z = \nu (\sigma_x + \sigma_y)$. While the geometry and loading of a component may change, as long as the crack opens in a direction normal to the crack path, the crack tip stresses are found to be as given by the equations above.

Three variables appear in the stress field equation: the crack tip polar coordinates r and θ and the parameter K. The functions of the coordinates determine how the stresses vary with distance from the right hand crack tip (point B) and with angular displacement from the x-axis. As the stress element is moved closer to the crack tip, the stresses are seen to become infinite and this is a general feature of most cracking solutions as most cracks have the same geometrical shape at their tip. The parameter K is the stress intensity factor because its magnitude determines the intensity or magnitude of the stresses in the crack tip region. It is a single parameter characterization of the crack tip stress field and can be calculated as:

$$K = \sigma\beta\sqrt{\pi a}$$

where the factor β is used to relate gross geometrical features to the stress intensity factors. A structural analyst should be able to determine analytically, numerically, or experimentally the stress-intensity factor relationship for almost any conceivable cracked body geometry and loading.

If the level of crack tip stress intensity factor exceeds a critical value, unstable fracture will occur [Irwin, 1957; Irwin & Kies, 1954; Irwin, et al., 1958]. Mathematically, this is expressed as: if $K = K_c$ where K_c is called fracture toughness, then catastrophic crack extension (fracture) occurs.

For the validation that the fracture toughness concept can be used to adequately describe fractures that initiate at gross sectional stress below 70% of the yield strength, the results of a wide plate fracture study are used [Boeing, 1962].

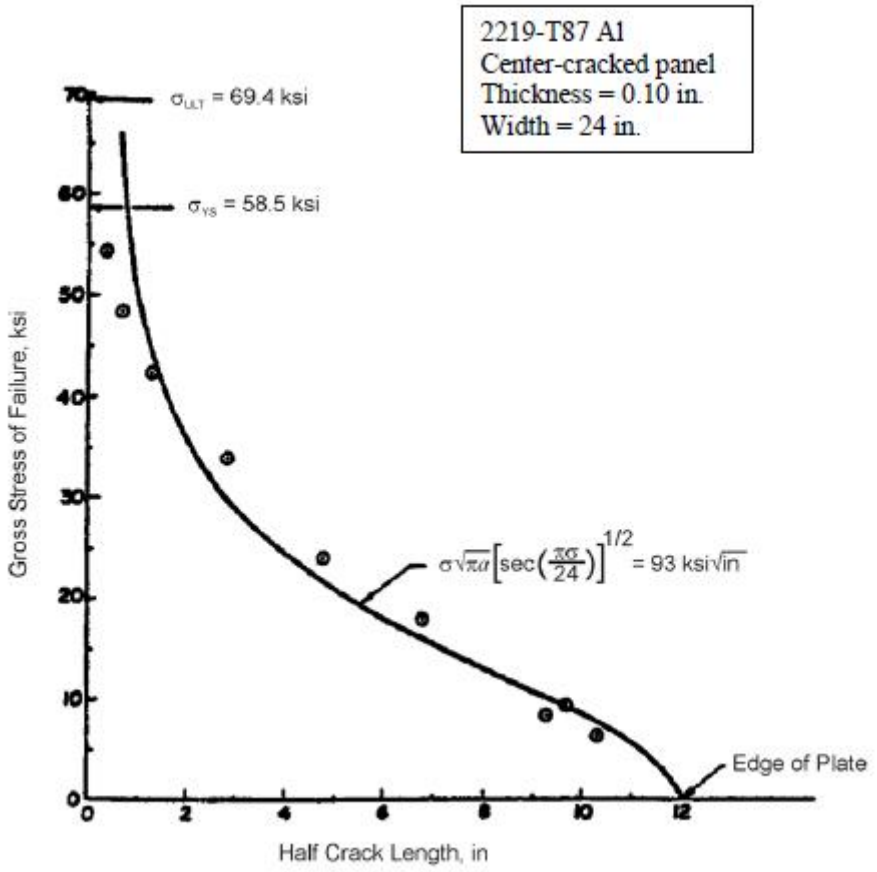

Figure 2.7: Results of a Wide Plate Fracture Study Compared with a Fracture Toughness Curve Calculated Using the Finite Width Plate Stress Intensity Factor Equation

The stress-intensity factor for the uniformly-loaded center-cracked finite-width panel is given by:

$$K = \sigma\left[\pi a \sec\frac{\pi a}{W}\right]^{1/2}$$

where W is the panel width.

Since plastic deformation is assumed negligible in the linear elastic analysis, the equation does not describe the crack growth behavior for small cracks in plastic stress fields.

Fracture toughness (K_c) is a mechanical property that measures a material's resistance to fracture and is strongly dependent on the amount of crack tip constraint due to component thickness because of its influence on the pattern of crack tip plastic deformation. For "thin" plane stress type components, a 45 degree through the thickness yielding pattern develops; in "thicker" plane strain components of the same material, the hinge-type plastic deformation pattern predominates [Hahn, & Rosenfield, 1965].

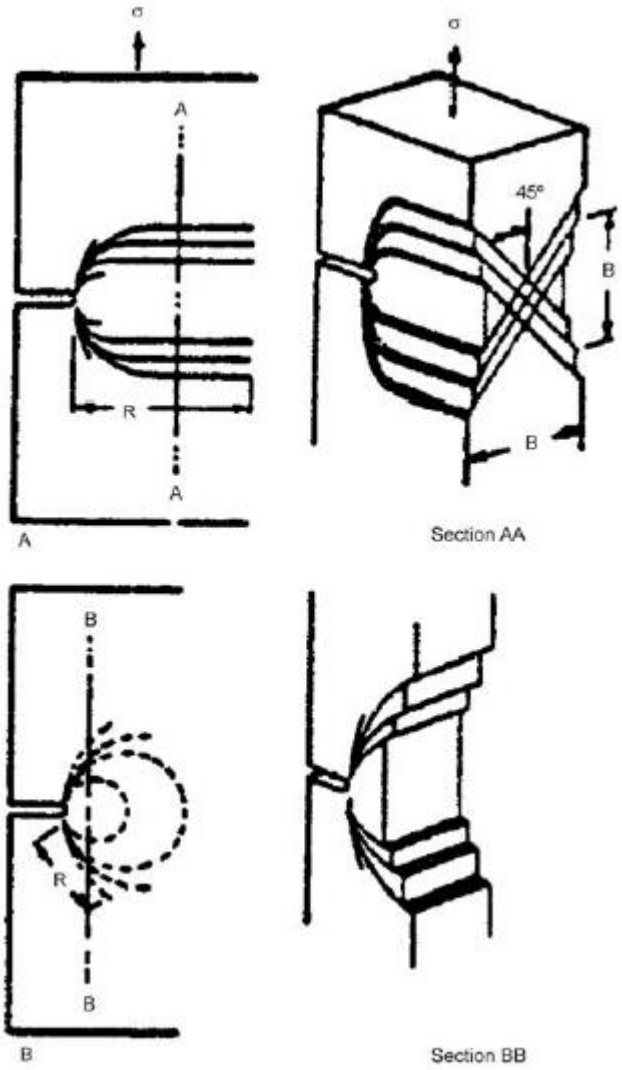

Figure 2.8: Yield Zone Observed on the Surface and Cross Section of a Cracked Sheet Under Uni-axial Tensile Loading in: A-Plane Stress, 45 degree Shear Type; B-Plane Strain, Hinge Type

The linear elastic fracture mechanics approach can only be expected to characterize fracture when the region in which plastic deformation occurs is contained within the elastic crack tip stress field. When the crack tip plastic deformation is unrestricted by elastic material around the crack, the engineer must resort to using elasto-plastic techniques to predict the critical crack size at fracture.

As plastic deformation will occur at the crack tip as a result of the high stresses that are generated by the sharp stress concentration and in order to estimate the extent of this plastic deformation, Irwin equated the yield strength to the y-direction stress along the x-axis and solved for the radius.

$$r_y = \frac{1}{2\pi}\left(\frac{K}{\sigma_{ys}}\right)^2$$

Subsequent investigations have shown that the stresses within the crack tip region are lower than the elastic stresses and that the size of the plastic deformation zone in advance of the crack is between r_y and $2r_y$. Models of an elastic, perfectly plastic material have shown that the material outside the plastic zone is stressed as if the crack were centered in

the plastic zone. If the extent of the plastic zone is small with respect to features of the structural geometry and to the physical length of the crack, linear elastic fracture mechanics analyses apply. As this concept of contained yielding is referred to as small scale yielding, most structural problems of interest to the aerospace community can be characterized by linear elastic fracture mechanics parameters because the extent of yielding is contained within a small region around the crack tip.

As cracks impair the load-carrying characteristics of a structure, the only quantifiable measure of sub-critical damage is a crack. By taking into account the stress intensity factor, a crack mechanics approach to solve sub-critical crack growth problems was developed [Paris, et al., 1961; Donaldson & Anderson, 1961; Paris, 1964]. If the crack tip stress state and its waveform are the same in a given time period for two separate geometry and loading conditions, then the crack growth rate behavior observed by the two cracks should be the same for that time period and the equation representing the sub-critical crack growth hypothesis is:

$$\frac{\Delta a}{\Delta t} = f(K(t))$$

or

$$\frac{\Delta a}{\Delta N} = f(K(t))$$

where it is stated that a material's rate of crack growth is a function of the stress intensity factor and the stress intensity factor shown to explicitly depend on time in order to indicate the influence of its waveform on the crack growth rate. For the verification of this hypothesis, fatigue crack growth data were generated under constant amplitude type repeated loading.

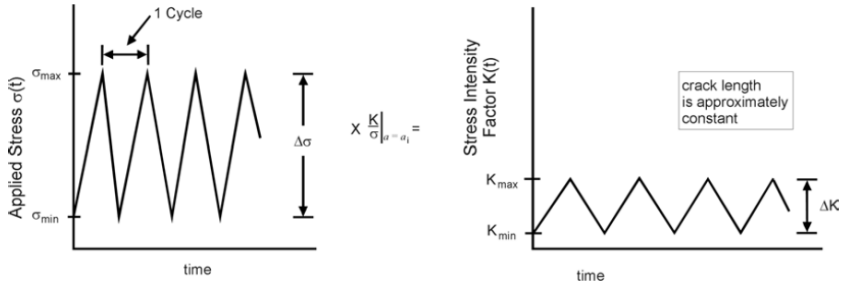

Figure 2.9: Parameters that Define Constant Amplitude Load Histories for Fatigue Crack Growth. The Figure also Illustrates the Transformation between Stress History Loading and Stress-Intensity-Factor Loading at One Crack Length Position

On the left diagram of the Figure 2.9, a repeating constant amplitude cycle with a maximum stress of σ_{max}, a minimum stress of σ_{min}, and a stress range of $\Delta\sigma$ is described. The stress ratio (R) is given by the ratio of the minimum stress to the maximum stress. In describing constant amplitude stress histories, it is only necessary to define two of the above four parameters; typically $\Delta\sigma$ and R or σ_{max} and R. A stress history is converted into a stress-intensity factor history by multiplying the stresses by the stress-intensity-factor coefficient (K/σ). As can be noted from the figure, the coefficient is evaluated at the current crack length a_i and the stress-intensity-factor history is shown to be a repeating cyclic history in the diagram on the right. The terms K_{max}, K_{min} and ΔK define the

maximum, the minimum and range of stress-intensity factor, respectively. Strictly speaking, the stress-intensity factor history should not be shown constant but reflective of the changes in the stress-intensity-factor coefficient as the crack grows. For small changes in crack length, however, the stress-intensity factor coefficient does not change much, so it is reasonably accurate for the number of cycles shown.

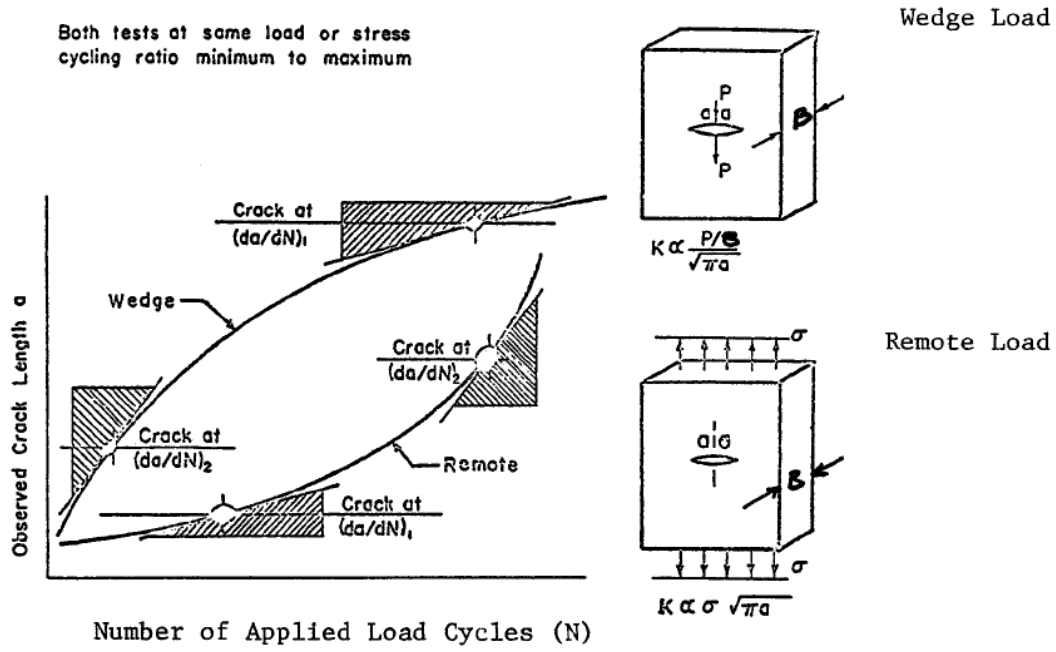

Figure 2.10: Description of Crack Growth Behavior Observed for Two Very Different Structural Geometries

The fatigue crack growth rate behaviors exhibited by a plate structure subjected to two extreme loading conditions (but at the same nominal stress level) are compared in Figure 2.10[Donaldson & Anderson, 1961; Anderson & James, 1970]. These loading conditions are referred to as wedge loading and remote loading. In the remote loaded structure, the rate of crack length change accelerates as the crack grows. An opposite growth rate behavior is exhibited by the wedge loaded structure. These two extreme loading conditions provide a good test for the application of the fracture mechanics approach to the study of fatigue crack growth rates. If the approach can be used to describe these opposite growth rate behaviors, then it should be generally applicable to any other type of structure or loading.

The appropriate stress intensity parameter for fatigue crack propagation should be the difference between the maximum and minimum stress-intensity factors in a cycle of fatigue loading. This difference in the stress-intensity factors is the stress intensity range (ΔK) and it measures the alternating intensity of the crack tip stress field responsible for inducing reversed plastic deformation. The stress-intensity range as a function of crack length is obtained from the static stress-intensity-factor formulas where the range in stress (load) replaces the static stress (load). Drawing tangents to the cyclic crack length curves provides estimates of the cyclic (fatigue) crack growth rates at various crack lengths. Calculation of corresponding stress-intensity ranges for these same crack lengths provides the data plotted below[Donaldson & Anderson, 1961; Anderson & James, 1970] where the same stress-intensity range (ΔK), the same crack growth rate (da/dN) is observed, even though both the form of the stress-intensity equations and the cycle-crack length curves are very different.

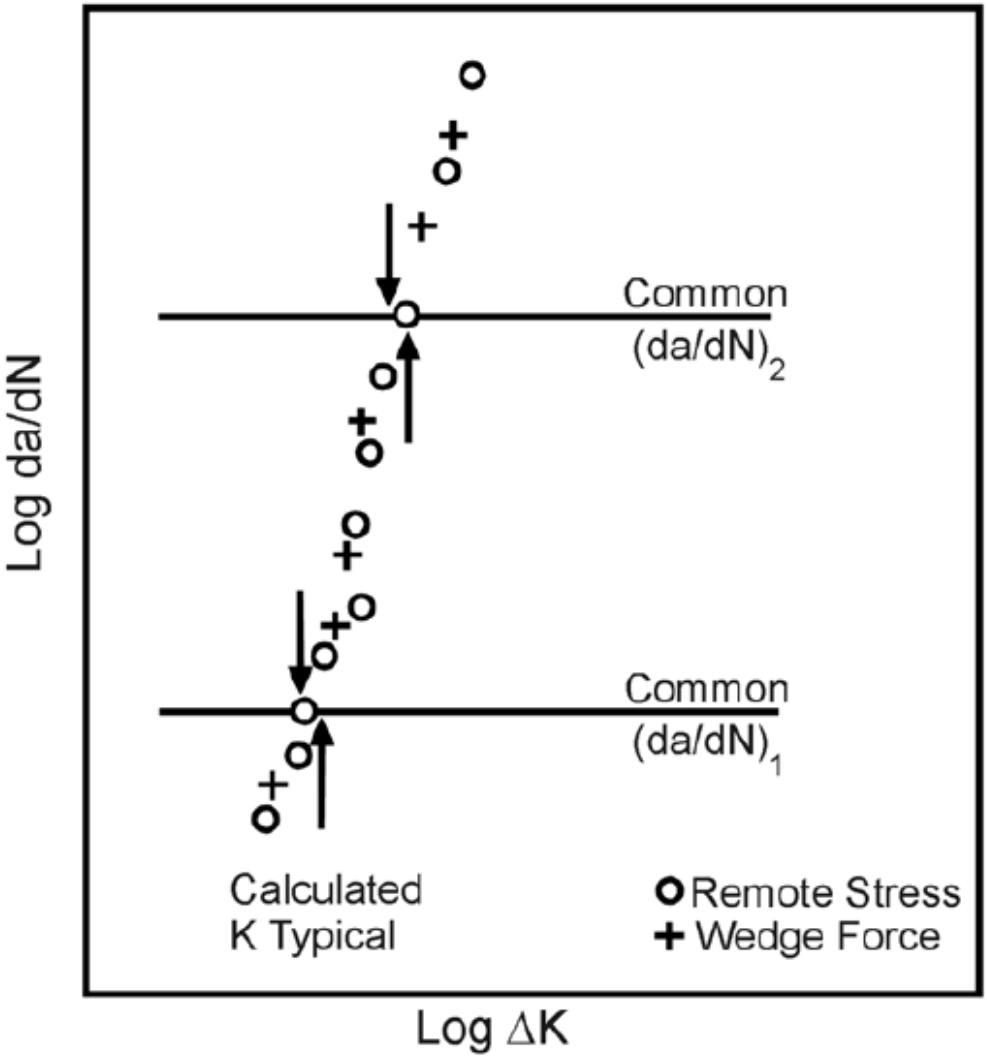

Figure 2.11: Comparison of Crack Growth Rate Results for the Two Structural Geometries.

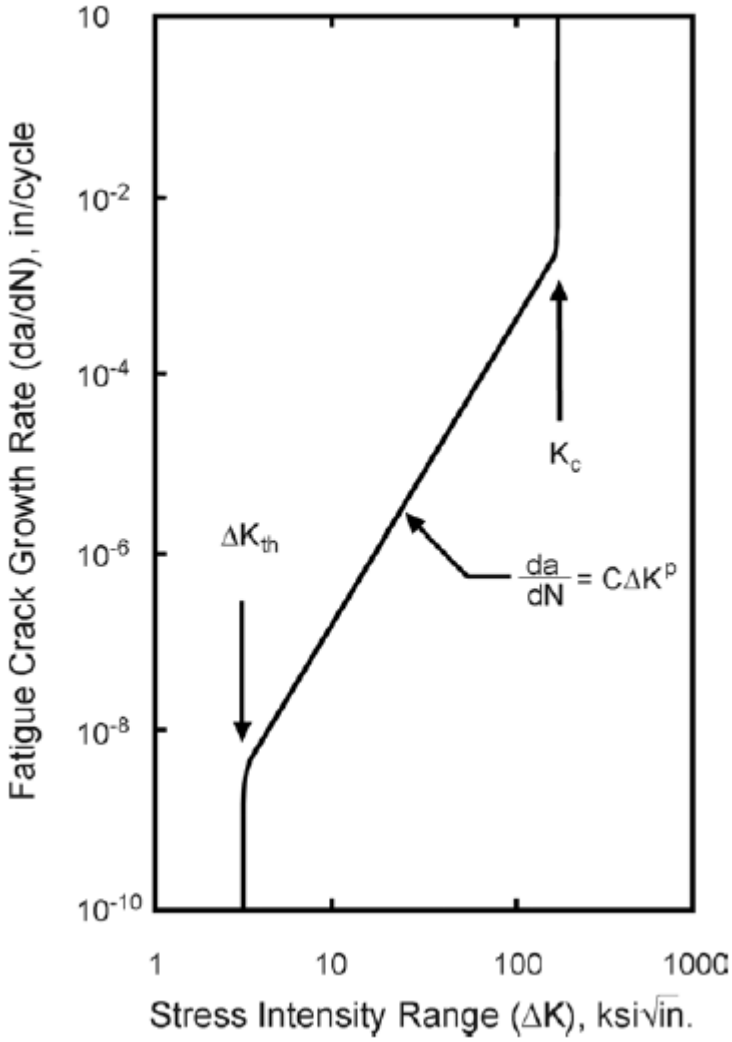

Figure 2.12: Schematic Illustration of the Fatigue Crack Growth Rate as a Function of Stress Intensity Range

The general fatigue cracking behavior pattern exhibited by most structural materials is shown in Figure 2.12, where the shape of the curve is sigmoidal with no crack growth being observed below a given threshold level of stress-intensity range and rapid crack propagation occurring when the maximum stress-intensity-factor in the fatigue cycle approaches the fracture toughness of the material. In the sub-critical growth region, numerous investigators have indicated that the rate of cyclic growth (da/dN) can be described using a power law relation

$$\frac{da}{dN} = C(\Delta K)^p$$

where C and p are experimentally developed constants.

Given crack growth rate data, the designer integrates the crack growth rate as a function of the stress-intensity factor for the structure through the crack growth interval of interest. Other investigations have demonstrated that sub-critical crack growth processes that result from variable amplitude loading, stress corrosion cracking, hydrogen embrittlement and liquid metal embrittlement can in general be described using

$$\frac{\Delta a}{\Delta t} = f(K(t))$$

or

$$\frac{\Delta a}{\Delta N} = f(K(t))$$

.

The sub-critical cracking of structural materials has been successfully modeled with fracture mechanics tools primarily because the plastic deformation processes accompanying cracks are localized and thereby controlled by the surrounding stress field. As suspected, the magnitude in the elastic crack tip stress field is found to correlate well with the rate of sub-critical crack advance.

SECTION 2.3: RESIDUAL STRENGTH

The presence of a crack significantly lowers the strength of a structure. The load carrying capacity of a cracked structure is the residual strength of that structure. It is a function of material toughness, crack size, crack geometry and structural configuration and its evaluation throughout the expected service life may prevent a catastrophic failure.

The basic concept of the damage tolerance design is to maintain a minimum required residual strength so that catastrophic failure of the structure is prevented. The major sequence of events that ultimately define the residual strength requirements starts with the identification of a safety-of-flight-critical element and either its structural configuration or its degree of inspectability will establish the allowable structural design concept and the inspection level categories. Every safety-of-flight-critical element must be qualified in at least one design concept category and in one inspection category. Each allowable combination of design concept and inspection category is coupled in JSSG-2006 to a residual strength requirement, a service life requirement, and a requirement to assume a level of initial damage.

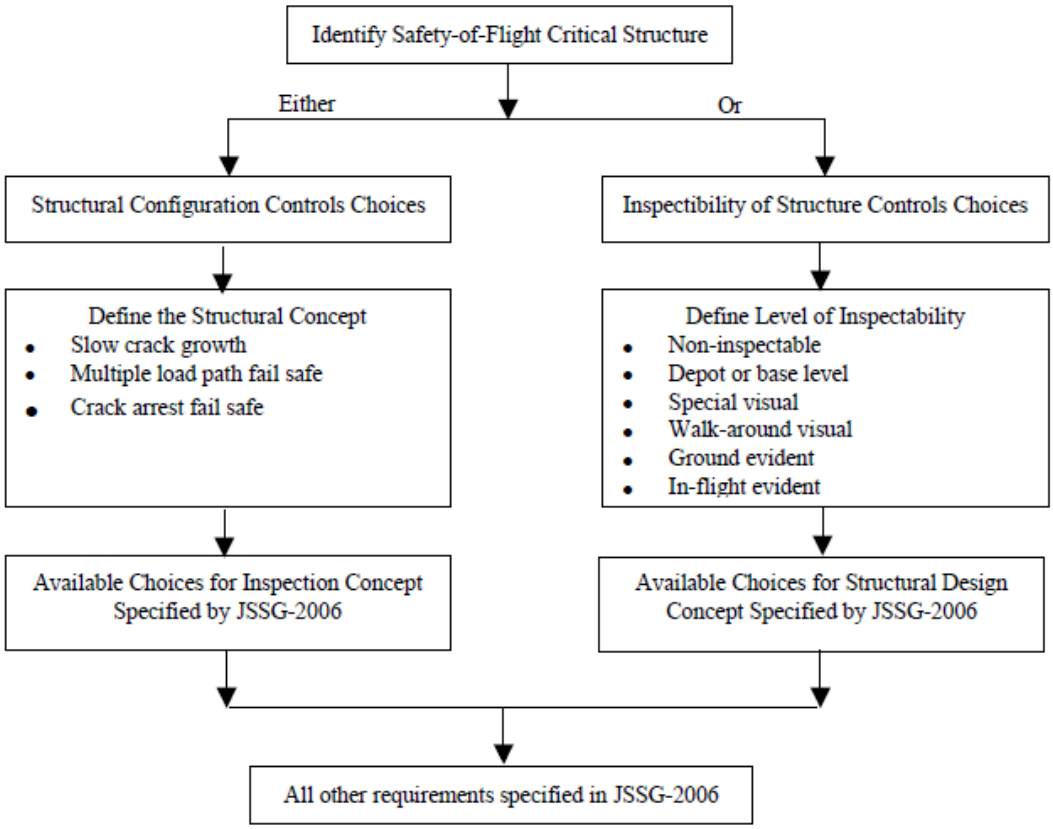

Figure 2.13: The Structural Configuration or Degree of Inspectability Controls the Subsequent Choices of Design Concept and Inspection Level

With the use of the residual strength capability curve, the level of load that the structure can withstand without failing in the presence of a growing crack may be defined.

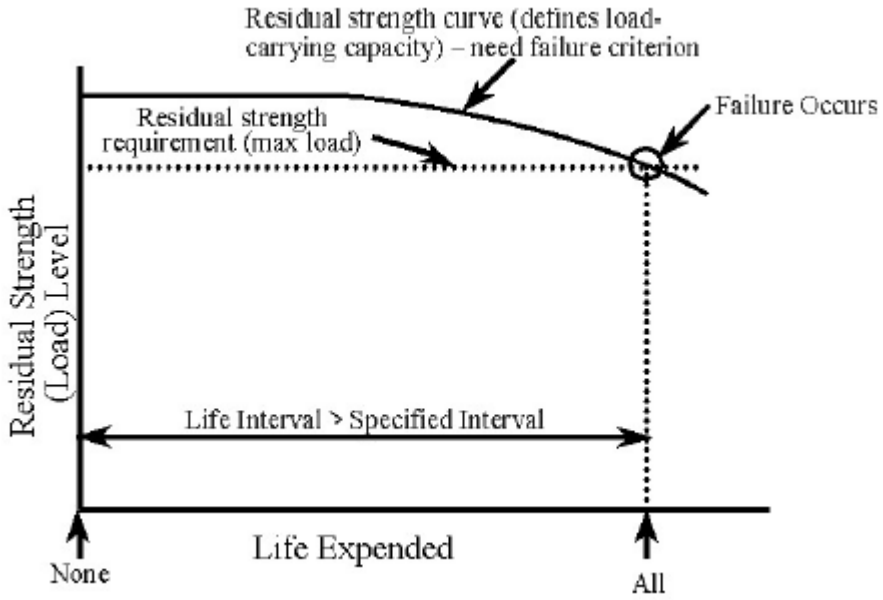

Figure 2.14: Relationship Between the Life Expended and Residual Strength Capability Showing a Monotonic Decrease in Load Carrying Capacity Due to Damage

The crack-growth-life curve and its various properties is necessary for determining the crack size as a function of time as the change in residual strength capacity is a function of time.

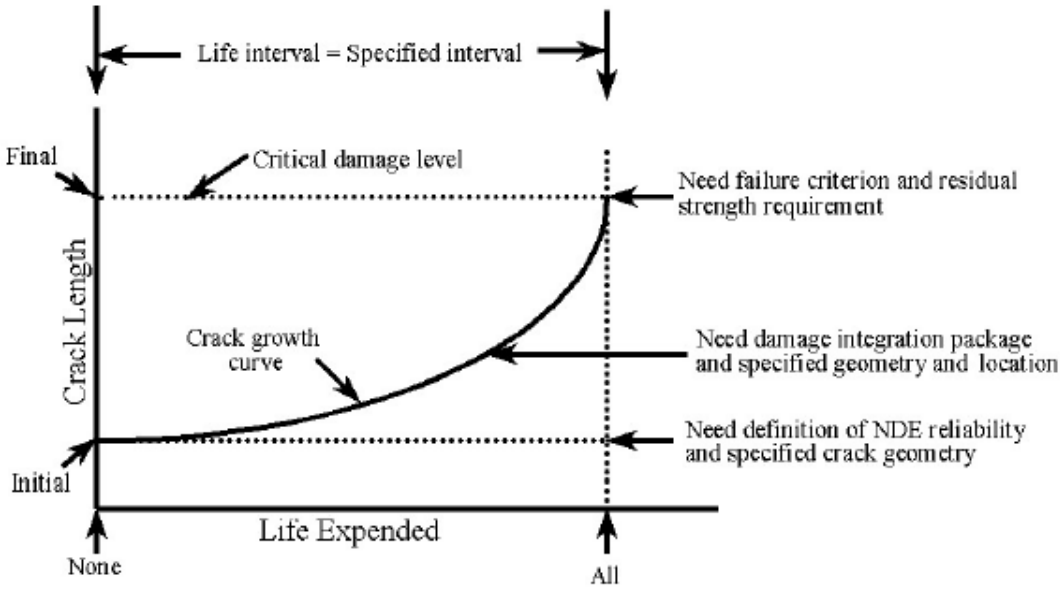

Figure 2.15: Relationship Between Crack Length and Life Expended Showing a Monotonic Increase in Crack Length Up Until Failure

In Figure 2.15, the various technology and specification requirements needed to define the crack growth curve which, in turn, establishes the life limit are also shown.

When the residual strength of the structure falls below the maximum stress in the service load history, failure can be expected. To avoid such a failure, a thorough understanding of the problem is essential. Significant advances have been made in recent years in procedures for analyzing damaged structures. Assessments now consider residual strength, damage growth, interactive multiple damage sites and quantitative structural maintenance and in-service evaluations.

The application of existing fracture mechanics solution techniques has yielded effective methods for analyzing the residual strength of the cracked structure.

The most important factor to consider in residual strength prediction of a cracked built-up structure is to decide whether the structure is skin or stiffener critical. Normally, a short crack length is likely to be a skin critical case and a long crack length a stiffener critical case. However, there is no clear cut demarcation between the two cases. Factors such as percentage stiffening, spacing of stringers, lands in the structure, and other structural details will influence the type of failure. Hence, a good technique is to determine the residual strength of a given structure based on both skin critical and stiffener critical cases. The minimum fracture stress of the two will then represent the residual strength of the structure and should be considered to be the governing case.

In a slow crack growth structure, the damage tolerance must be assured by the maintenance of a slow rate of crack growth, a residual strength capacity, and the assurance that subcritical damage will either be detected at the depot or will not reach unstable dimensions within the design lifetime of the structure.

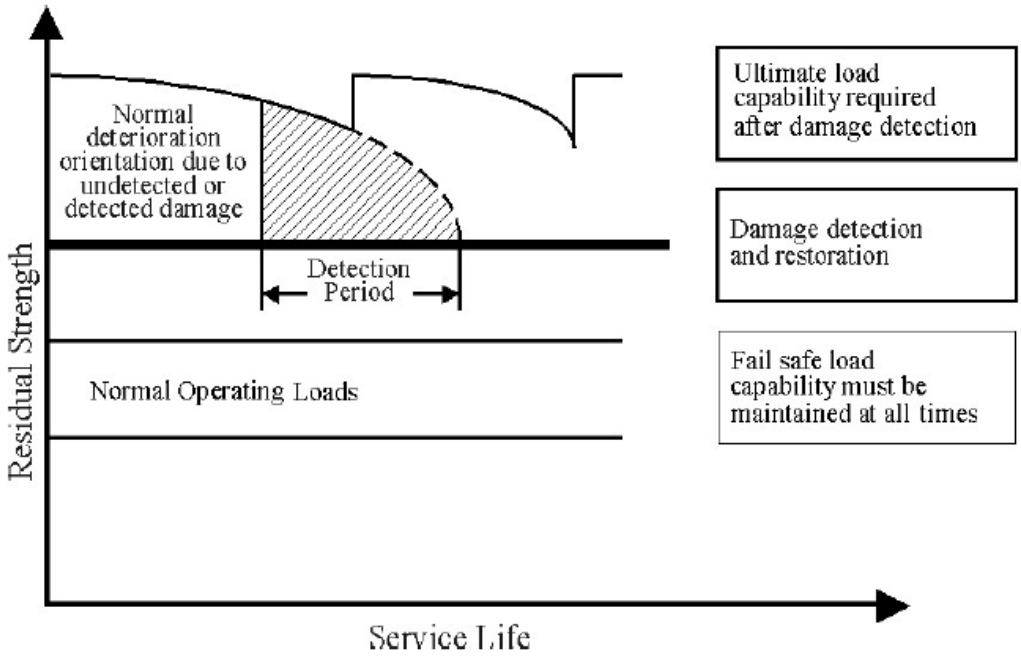

Figure 2.16: Strength Criteria for Periodically Inspected Damage Tolerant Structure

As a result of the inspections, the initially assumed cracks do not grow to a critical size and the structure is restored to its original load carrying capability when an inspection capability equal to that of the manufacturer's is employed.

Single-load-path "monolithic" structure must be qualified in this category; the residual strength estimation procedure for this type of structure is fairly straightforward. Built-up (multiple-load-path) structure can be qualified either in this category or in the fail-safe category.

The residual strength requirement of a fail-safe structure is to assure damage tolerance following a partial failure of the structure. Damage tolerance is maintained through detection of this failure prior to total loss of the structure and sufficient residual strength capability for operating safely within the partial failure prior to inspection. The fail-safe structure is typically a built-up structure with multiple load paths or crack arrest features in its design. In the event of failure of a structural member, its load must be transferred to and withstood by the remainder of the structure, which also contains crack damage, without causing the loss of whole structure. The residual strength of the built-up structure must be determined under such critical circumstances so that the fail-safe design requirements are met.

The analysis of residual strength capability for built-up structure requires the estimation of the critical stress level at which the partial failure occurs, as well as an understanding of the capability of the total structure to withstand this partial failure at and subsequent to the time of failure. The required load associated with the time subsequent to failure is based on the inspection category and, the partially-failed structure must be able to maintain this load until the time of inspection.

The determination of residual strength for uncracked structures is straightforward because the ultimate strength of the material is the residual strength. A crack in a structure causes a high stress concentration resulting in a reduced residual strength. When the load on the structure exceeds a certain limit, the crack will extend. The crack extension may become immediately unstable and the crack may propagate in a fast uncontrollable manner causing complete fracture of the component.

The simplest failure criterion assumes that failure occurs at the ultimate (or yield) strength of the material.

$$\sigma_f = F_{tu}$$

where σ_f is the fracture stress and F_{tu} is the ultimate strength.

In past analyses of failure of built-up structure, the residual strength of stiffeners was based upon this criterion. When the main panel between the stiffeners fails due to catastrophic crack growth, the panel loads are transferred to the stringers (or stiffeners). The transferred loads may increase the stress level in the stringer so it is high enough to reach the value of σ_f, causing stiffener failure.

In a cracked structure, the stress intensity factor (K) interrelates the local stresses in the region of the crack tip with crack geometry, structural geometry, and the level of load on the structure. When the applied load level increases, the K value also increases and reaches a critical value at which time the crack growth becomes unstable.

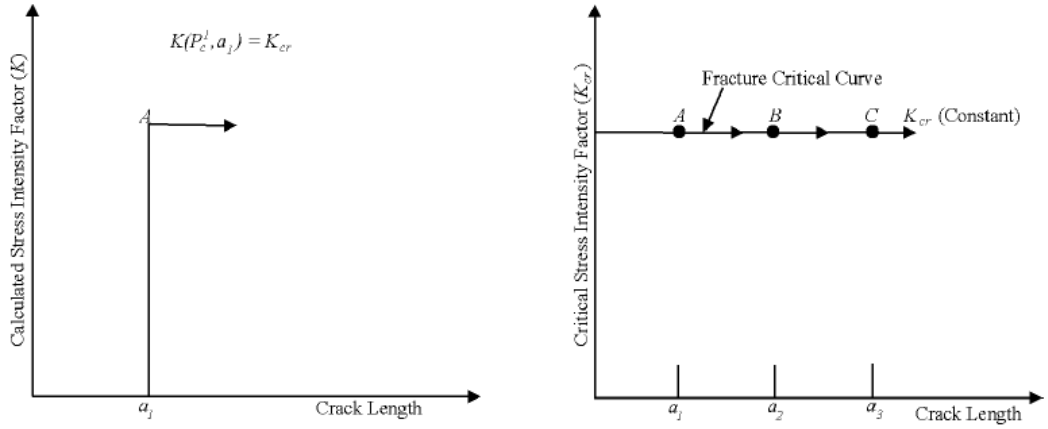

(a) Stress Intesity Factor Calculated as a Function of Load and Crack Length

(b) Critical Stress Intesity Factor Levels Described as a Function of Crack Length

Figure 2.17: The Fracture Mechanics Basis for Establishing Residual Strength

This critical level of K, which is independent of the crack length, is a material property called fracture toughness. The fracture toughness is a measure of the material's resistance to unstable cracking. Several test procedures are available to evaluate the fracture toughness. Also, various theoretical and numerical solution techniques are available, as already discussed, which can be used to estimate the (applied) stress intensity factor, K, for a given structure.

The failure criterion (Irwin's Criterion) states that abrupt fracture occurs when the crack-tip stress-intensity factor reaches or exceeds the fracture toughness of the material. The corresponding applied stress at failure is called the fracture strength. The failure criterion becomes simple

$$K \geq K_{cr}$$

where K_{cr} is the material's fracture toughness.

The critical K_{cr} for abrupt fracture mode is denoted as K_{Ic} for plane strain conditions and K_c for plane stress conditions; the conditions for plane stress or plane strain are determined by experiment.

In general, a material's toughness depends on thickness. When the thickness is such that the crack tip plastic zone size is on the order of the plate thickness, the toughness reaches a maximum value, $K_{c(max)}$. With increasing thickness of the plate, the plastic zone size reduces and thus the toughness gradually decreases, from $K_{c(max)}$ to K_{Ic}. When the thickness is large enough that the crack tip deformation is not affected by the thickness,

plane strain conditions prevail at the crack tip. The toughness in the plane strain regime is virtually independent of thickness. For increasing thickness, the toughness asymptotically approaches the plane strain fracture toughness, K_{Ic}.

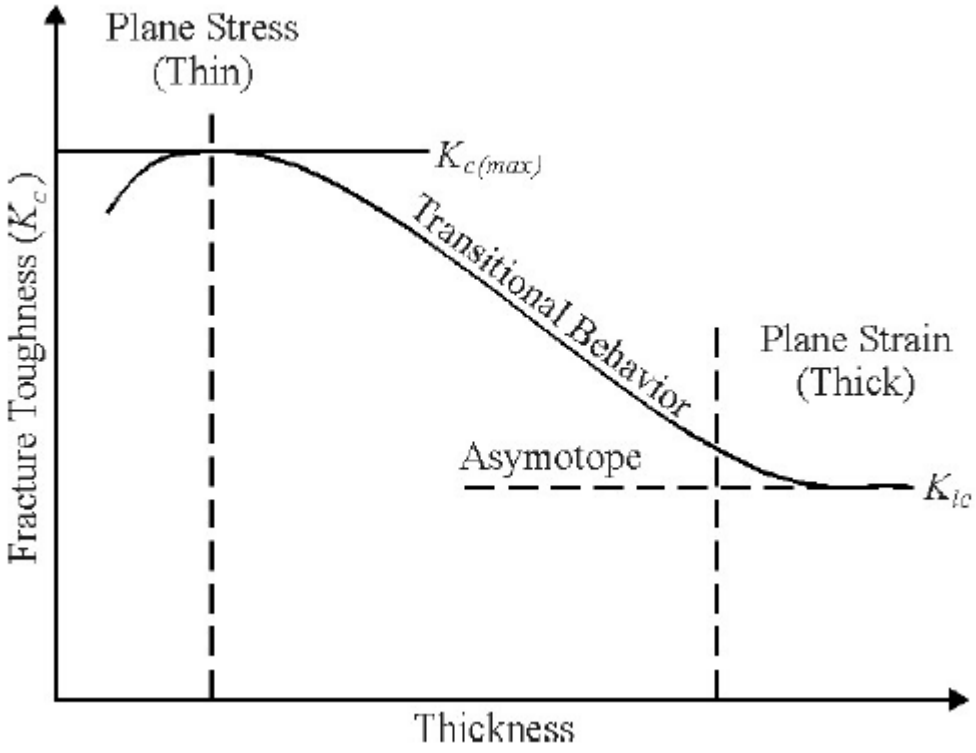

Figure 2.18: Fracture Toughness as a Function of Thickness

When the crack extends by a tearing mode of fracture, which typically occurs in thin metal sheets or in tough materials, the crack extension is essentially slow and stable. The failure condition for tearing fractures depends on the crack growth resistance (K_R) behavior of the material and the applied stress-intensity factor K, which in turn depends on the crack and structural configurations.

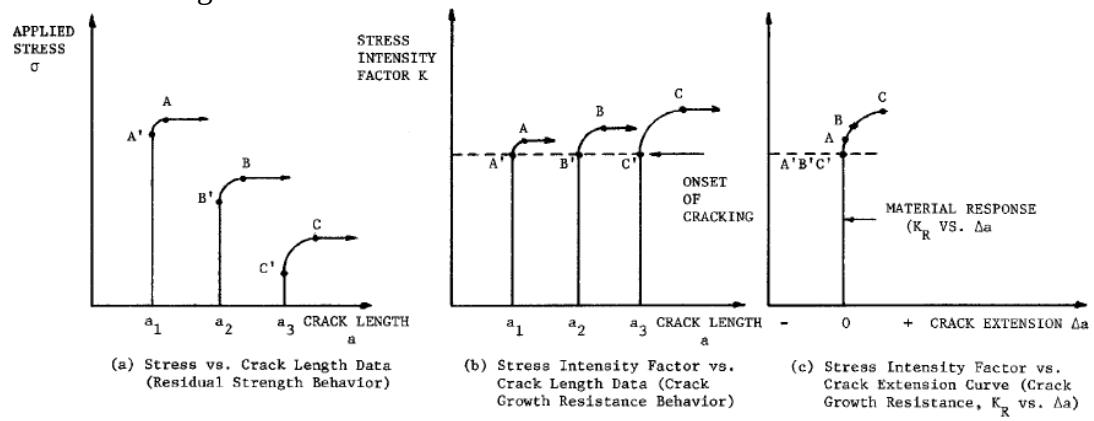

Figure 2.19: Schematic Illustration of Tearing Fracture Behavior and the Development of a Crack Growth Resistance Curve (R-Curve)

While the shape of the resistance curve is basically independent of crack length or other geometrical effects, the fracture level is a function of crack length.

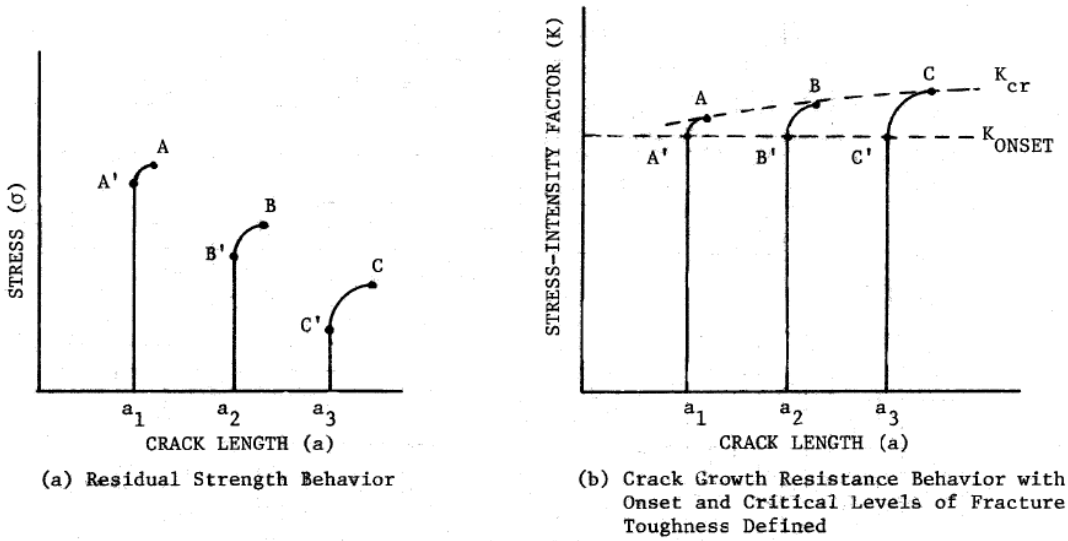

Figure 2.20: Schematic Illustration of Tearing Fracture Behavior Which Further Defines the Change in Critical Level of Fracture Toughness as a Function of Crack Length

Due to the complexity of the two parameter fracture criteria for tearing fracture behavior, engineers sometimes obtain preliminary estimates for the residual strength using a single parameter fracture toughness criterion. The stress-crack length levels are associated with the onset of cracking ($K = K_{ONSET}$) and fast fracture ($K = K_{cr}$) conditions for a tearing material. Intermediate between the two curves established from material observations is a third curve referred to as the apparent fracture curve. The apparent fracture toughness (K_{APP}) is established from the same data employed to derive K_{ONSET} and K_{cr}. The calculation procedure uses the onset (or initial) crack length (a_i) and the final recorded stress level (σ_{cr}) for the tests conducted. Thus, K_{APP} represents a fracture toughness level bounded by the onset and fast fracture levels.

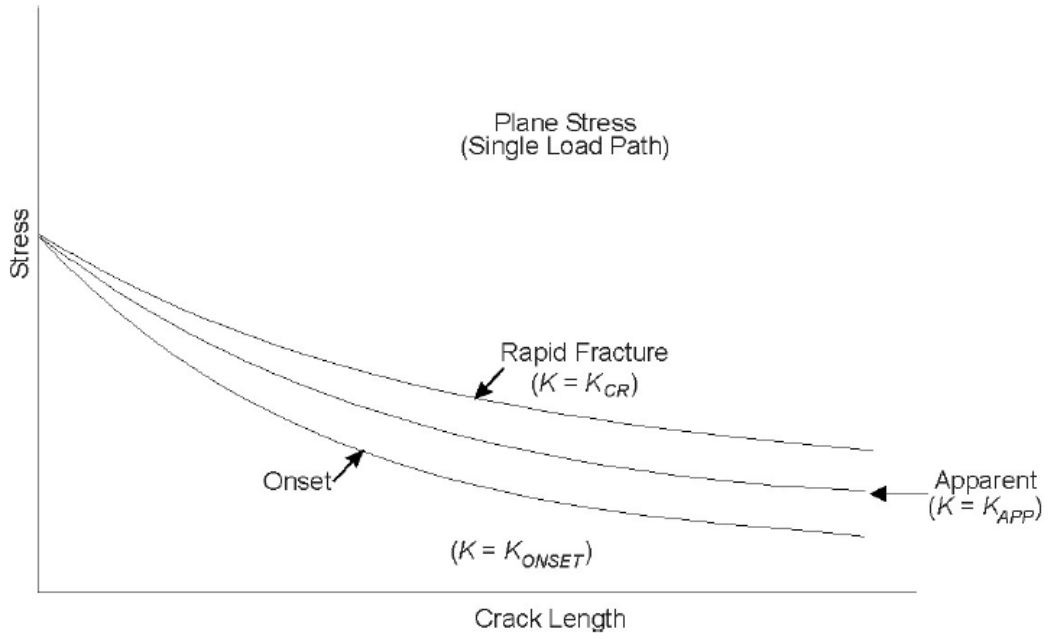

Figure 2.21: Description of the Three Fracture Toughness Criteria that are Utilized to Estimate Residual Strength Under Tearing Fracture Conditions

As an abrupt failure criterion for a tearing fracture, for lower bound estimates of the residual strength for fast fracture of a tearing material, one could equate the level of

applied stress-intensity factor (K) to the apparent fracture toughness (K_{APP}) in order to determine the critical level of stress.

If the crack tip plastic zone size is estimated to be on the order of the structural thickness but substantially smaller than other geometrical variables (crack length, ligament size, height, etc.), a linear elastic fracture mechanics analysis can still be sensibly used to predict the catastrophic cracking event. The failure criterion for tearing type fractures under these conditions states that fracture will occur when the stress-intensity factor K reaches or exceeds the material's fracture resistance K_R and the rate of change of K (with respect to crack length) reaches or exceeds the rate of change of K_R (with respect to crack length). Physically, the criterion means that at failure, the energy available to extend the crack equals or exceeds the material resistance to crack growth.

The corresponding applied stress, σ_f, at this point is defined as the fracture stress that determines the residual strength of the cracked structure. This two-parameters criterion can be mathematically expressed:

$$K \geq K_R; \quad \frac{\partial K}{\partial a} \geq \frac{\partial K_R}{\partial a}$$

To interpret the meaning of this criterion, first consider the structural parameters that are a function of the geometry and stress, i.e. K and $\partial K/\partial a$.

Since this R-curve is assumed to be independent of the initial crack length, it can be superimposed on the plot of K versus a. The tangency point between the applied stress intensity factor curve (K vs. a) and the R-curve (K_R vs. Δa) determines the commencement of unstable crack propagation. In general, the accurate method of determining the tangency point involves the numerical solution based on the experimentally obtained R-curve. Using a least squares determined polynomial expression for R-curve and knowing an expression for K in terms of crack length, the common tangent point can be obtained by equating the functional values ($K = K_R$) and also the first derivatives with respect to the crack length of these two expressions.

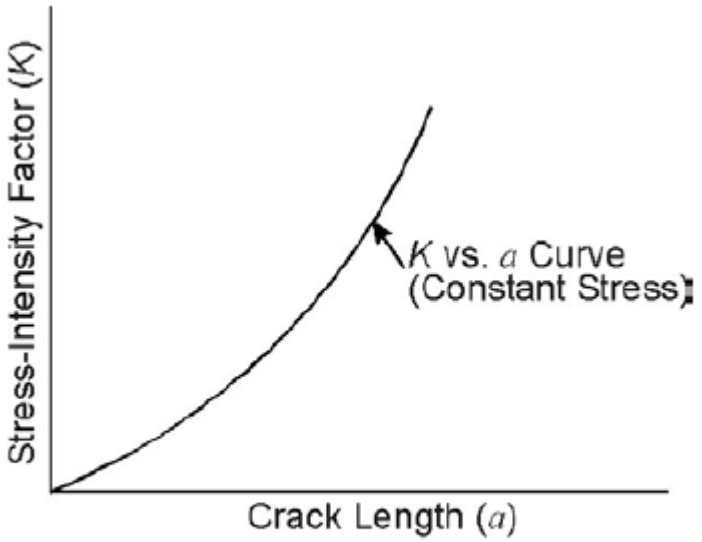

(a) Driving Force

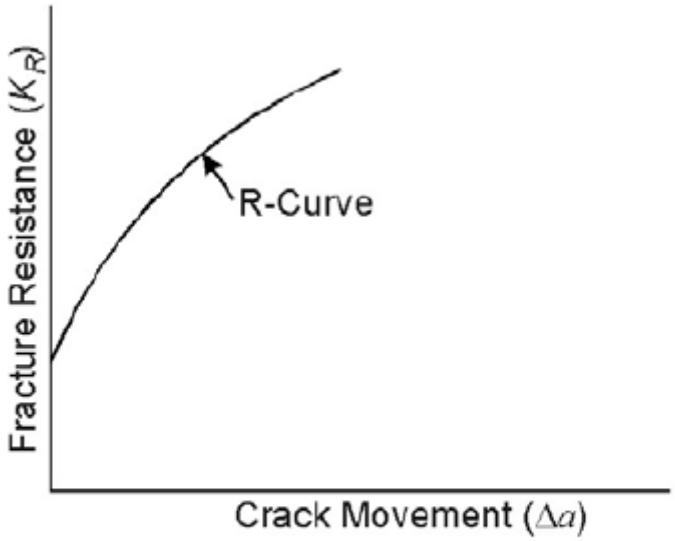

(b) Resistance to Crack Growth

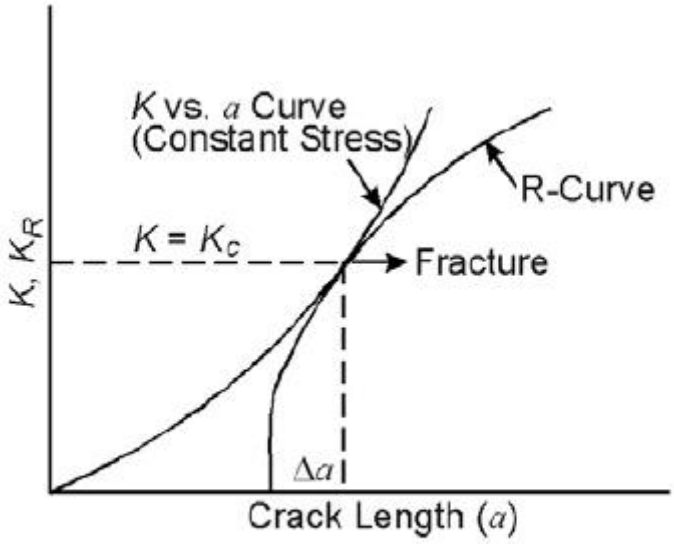

(c) Establishment of Critical Conditions

Figure 2.22: Schematic Illustration of the Individual and Collective Parts of a K_R Fracture Analysis

The crack growth resistance curve (K_R) has shown good promise for materials where limited (small-scale) yielding occurs in front of the crack tip. Difficulties in estimating crack tip plasticity under large-scale yielding conditions, led to an alternate failure criterion based on the J-integral [Rice, 1968]. J-integral criterion is similar to the K_R -curve criterion; it states that failure will occur when the following conditions are met:

$$\sqrt{J} \geq \sqrt{J_R}; \frac{d\sqrt{J}}{da} \geq \frac{\partial\sqrt{J_R}}{\partial a}$$

where J is the value of the applied J-integral and J_R is the value of the J-integral representing the material resistance to fracture. The applied stress (σ_f) is defined as the fracture stress. Since the effect of large-scale yielding can be appropriately incorporated through a suitable elastic-plastic model in the estimation of J-integral, it becomes an effective parameter for predicting failure under plane stress conditions where the plastic zone size is significantly large.

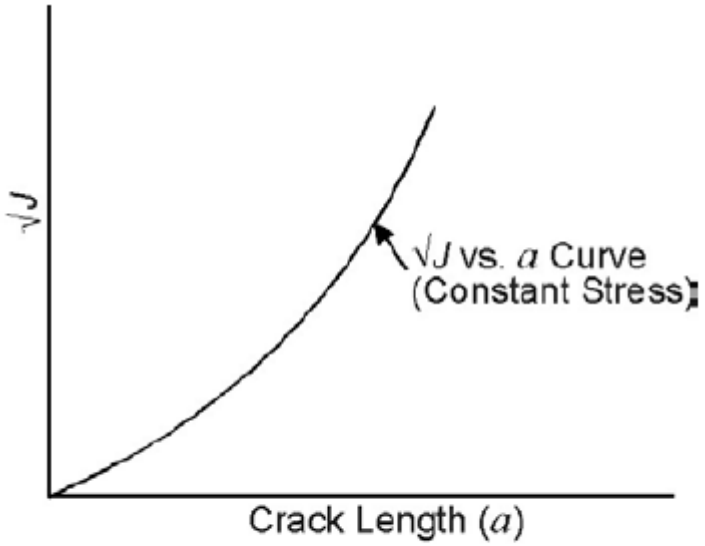

(a) Driving Force

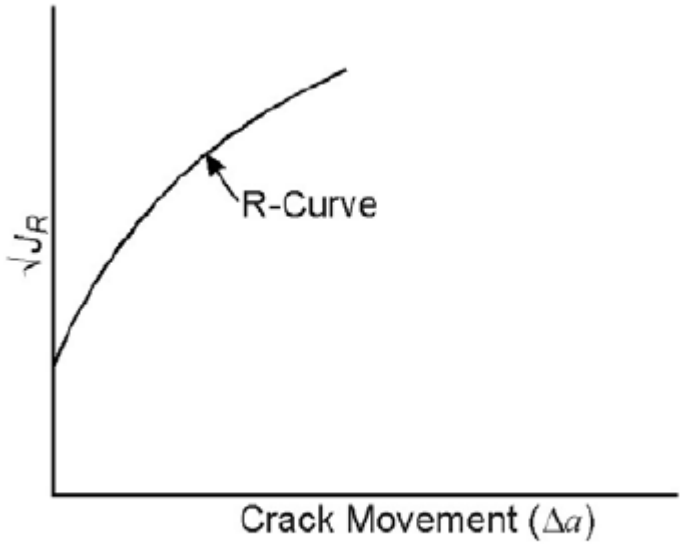

(b) Resistance to Crack Growth

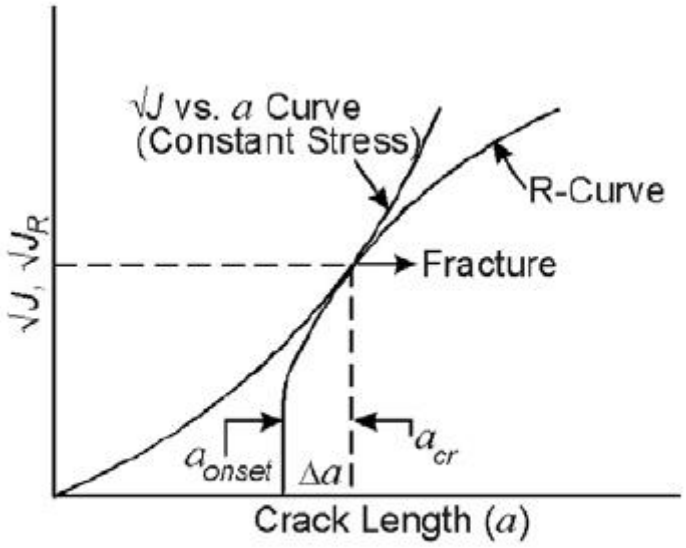

(c) Establishment of Critical Conditions

Figure 2.23: Schematic Illustration of the Individual and Collective Parts of a J_R Fracture Analysis

To establish the residual strength capability of a given structure under certain loading conditions, prediction techniques must be developed with a thorough understanding of the complexities involved in evaluating the residual strength. For monolithic or single load path structures which must be classified as slow crack growth structures, the estimation of residual strength capability is straightforward. In multiple load path, built-up structures, whether classified as slow crack growth or fail-safe structures, the strength analysis can become complicated due to the complex geometric construction of the built-up components. In general, the prediction techniques are based on the critical value of the stress-intensity factor for a given geometry and loading. Using fracture toughness failure criteria as explained earlier, the decay in critical stress can be obtained in terms of crack size.

For a single load path structure, such as an unstiffened panel, the residual strength diagram under plane strain conditions, consists of a single curve. The procedure for developing the residual strength diagram involves the calculation of the critical stress σ_f, for the critical crack length a_c, using the relationship:

$$K_{cr} = \sigma_f \beta \sqrt{\pi a_c}$$

where K_{cr} is the known value of fracture toughness of the material.

The plot of σ_f vs. a_c then provides the necessary residual strength diagram required in design analysis for the simple configuration.

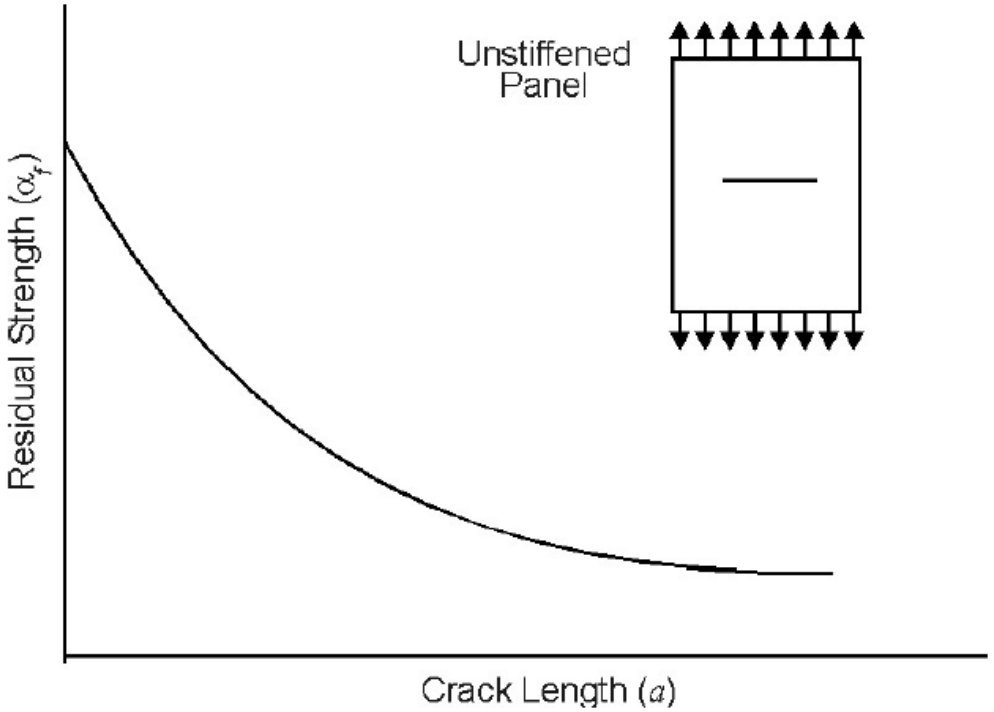

Figure 2.24: Residual Strength Diagram for Abrupt Failure of a Single Load Path Structure

Depending on the complexity of the structure, K can be calculated either numerically or through closed form solutions. These techniques, in conjunction with an appropriate failure criterion, can then be used to determine the residual strength capabilities of a given structure.

In general, the construction of a residual strength diagram involves three steps:

(a) The development of the relationship between the applied stress σ, the crack length parameter a, and the applied stress-intensity factor K for the given structural configuration.

(b) The selection of an appropriate failure criterion based for the expected material behavior at the crack tip.

(c) The fracture strength (σ_f) values for critical crack sizes (a_c) are obtained utilizing the results of the first two steps and residual strength diagram (σ_f vs. a_c) for the given structural configuration is plotted.

In single load path structures, the residual strength analysis involved only one failure criterion for a given structural geometry. In built-up structures, due to the complex geometrical configuration, one or more failure criterion may have to be considered in the determination of residual strength for the whole structure. Safety can be achieved by designing aircraft structure either as slow crack growth or as fail-safe. Fail-safe case can further be classified into two cases: Multiple Load Path and Crack Arrest. Typically, both Multiple Load Path and Crack Arrest structures are built-up structures. The structure shown in Figure 2.25 is analyzed to further explain the features inherent in multiple load path, built-up structure.

As long as the central member is not failed, all three elements carry a share of the total load P. In the event of failure of the center member, the total load P (actually 1.15P) must be transmitted by the other two members at the instant of failure, if the structure is to stay intact.

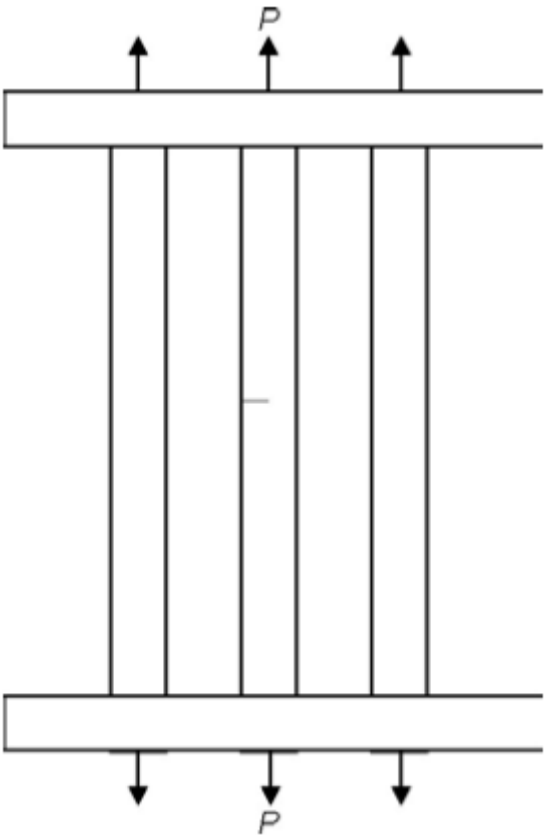

Figure 2.25: Multiple Load Path (Built-up) Structure with a Crack in the Central Member

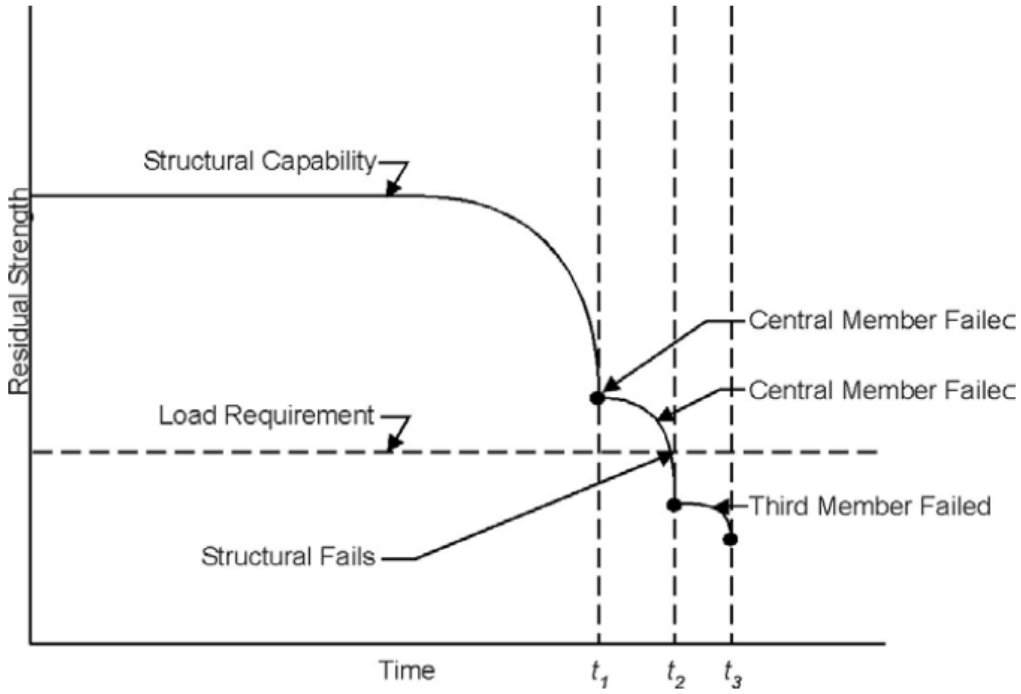

Figure 2.26: Reduction of Residual Strength During Successive Failure of Members in the Structure

When one element fails, the remaining parallel members are able to carry the required load without failure. The residual capability is shown to degrade as the crack in the central

member extends and as the cracks in the remaining elements fail. Is is also shown that the discontinuous change in the strength capability is a result of element failures. Since the load levels in other members dramatically increase, if the load P must be maintained, the remaining members will have short lives. Thus, the second member may fail after the time (t_2). The residual strength capability is shown to drop below the safe level somewhere in time between t_1 and t_2. The duration of the time interval between the failure of the first element and the failure of the structure may be short or long depending on the "type of failure" of the first member and the load requirements subsequent to this failure. This time interval is available for the detection of the failure of the first member and the repair of the structure.

The failure stress or the critical flaw size level of the central member (any one of the parallel members) can be estimated by treating the problem in a manner similar to the single load path structure. Using a fatigue crack growth analysis, the crack propagation curve is obtained from the minimum detectable crack size to the critical crack length.

In multiple load path structure, partial failure of the structure can occur during its operating period. But this failure must be detected at an inspection before catastrophic failure of the entire structure occurs. A suitable inspection schedule must include analysis of structural characteristics along with the operational requirements for the intervals between inspections.

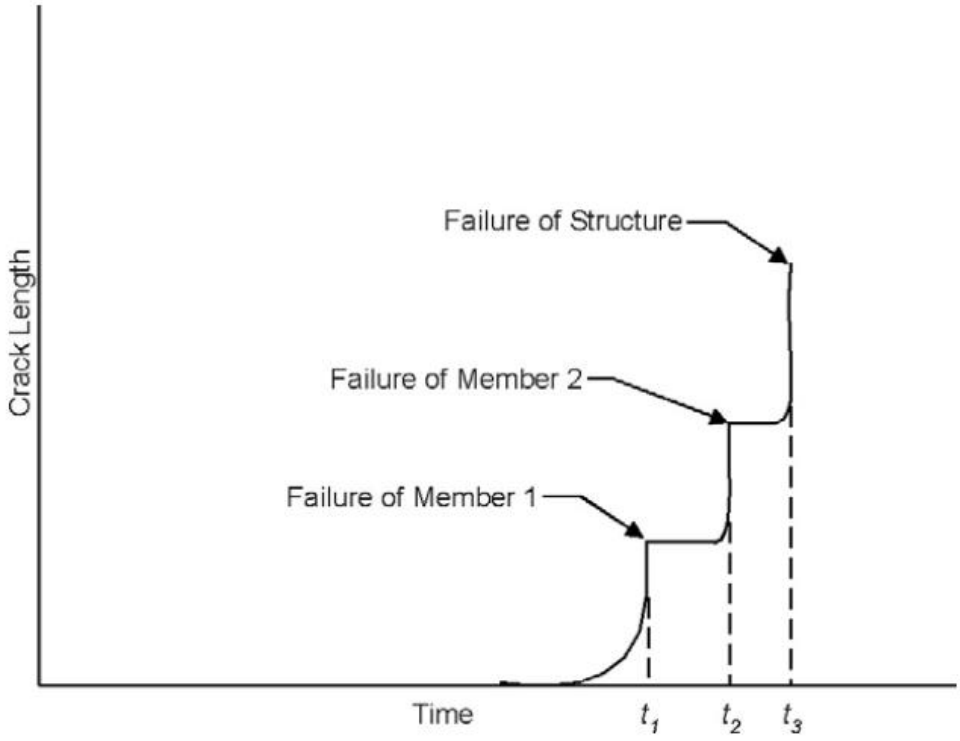

Figure 2.27: Crack Growth for Multiple Load Path Structure

To illustrate the analysis involved in the estimation of residual strength of complex structures, consider an axially loaded skin-stringer combination with longitudinal stiffening.

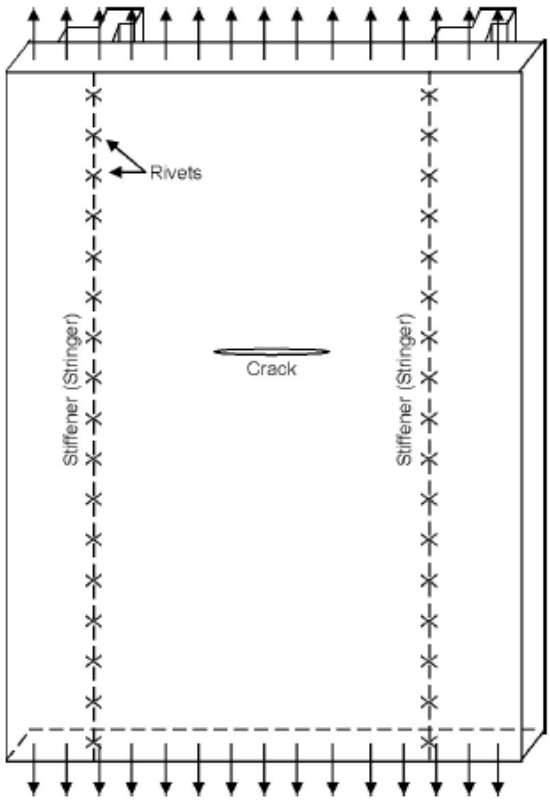

Figure 2.28: Skin-Structure Built-Up Structure

Assuming that the fasteners are rigid, the displacements of adjacent points in skin and stringers will be equal. (If skin and stringers are made from the same material, the stresses in the two will also be equal for the case of no crack.) Let a transverse crack develop in the skin. This will cause larger displacement in the skin, and the stringers must follow this larger displacement. As a result, they take load from the skin, thus decreasing the skin stress at the expense of higher stringer stress. Consequently, the displacements in the cracked skin will be smaller than in an unstiffened plate with the same size of crack. This implies that the skin stresses are lower and that the stress-intensity factor is lower. The closer the stringers are to the crack, the more effective is the load transfer. If the stress-intensity factor for a small crack in an unstiffened panel is approximated by $K = \sigma\sqrt{\pi a}$, the stress-intensity factor for the stiffened plate will be $K = \beta\sigma\sqrt{\pi a}$.The reduction factor β will decrease when the crack tip approaches a stringer. Since the stringers take load from the skin, the stringer stress will increase from σ to Lσ, where L increases as the crack tip approaches the stringer. Obviously, $0 < \beta \leq 1$, and $L \geq 1$. These values depend upon stiffening ratios, the stiffness of the attachment, and the ratio of crack size to stringer spacing.

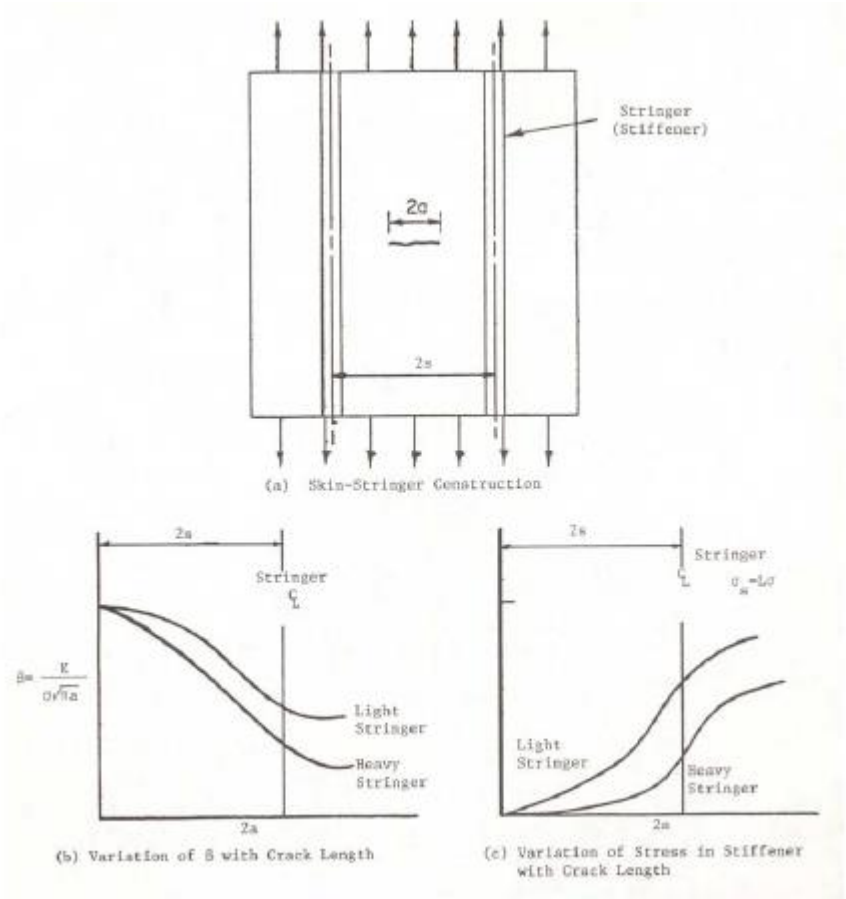

Figure 2.29: Variation of B and L with Crack Length in Stiffened Panel with a Crack Between the Stiffeners

Due to the complexity of stiffened skin structure, the construction of a residual strength diagram is considerably more difficult. Consider first the condition where an abrupt failure in the skin occurs. When the crack is small as compared to the stiffener spacing, the residual strength of the skin is not influenced by the stiffeners and the initial portion of the diagram follows the plot for an unstiffened panel. Once the crack size is long enough that the skin cannot sustain the applied load any further, the stringer will take some of the load from the skin, thus decreasing the skin stress. Consequently, the crack-tip stress-intensity factor will be lower due to the reduced stress and so the residual strength of the skin structure will increase with crack length. As the crack size increases further toward the stiffener location, the load transferred from the skin to the stiffener also increases significantly, thus reducing the stress-intensity factor. The residual strength of the stiffened panel continues to increase as shown in the figure for longer cracks. It can also be noted from the figure that the residual strength diagram for an unstiffened panel would have followed the dotted line, i.e., the continuous decay in the residual strength as the crack size increases. This is because there is no inherent feature present in the single load path structure to decrease the crack tip stress-intensity factor.

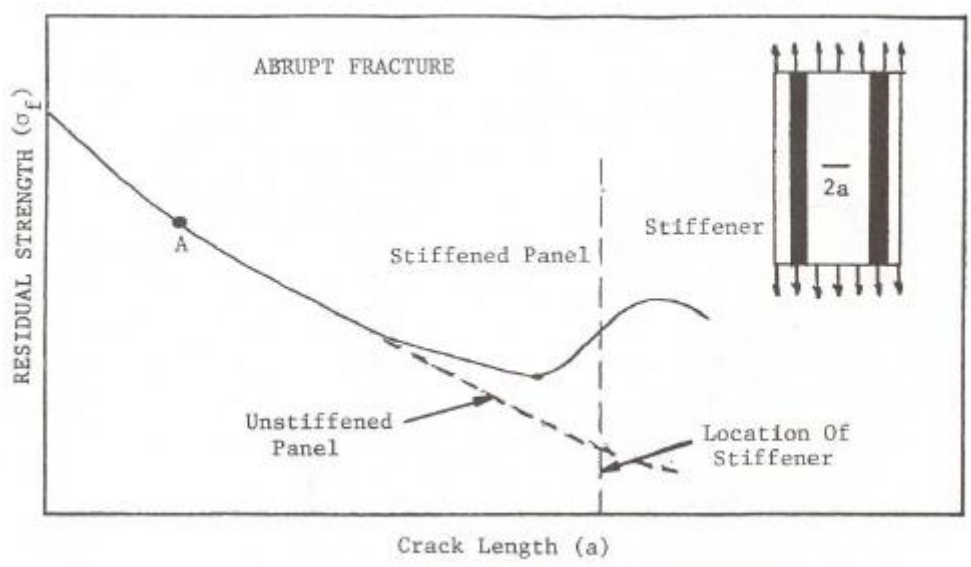

Figure 2.30: Residual Strength of the Cracked Panel as a Function of Crack Length for Built-Up Skin-Stiffened Structure Compared with Unstiffened Panel. Abrupt Failure Criterion Used to Determine Residual Strength

For a structure with a crack of length a_A, the residual strength is identified as point A. Since point A is associated with a failure stress that is above the peak stress (σ_{peak}), the crack extends abruptly and completely fails the panel. If the structure contains a crack of length a_C, in the range between a_B and a_D, the crack extends abruptly but then arrests at crack length a_E, where the residual strength available is greater than the applied (failure) stress. This crack extension and arrest feature of skin-stringer construction greatly facilitates meeting inspection requirements for fail-safe structures.

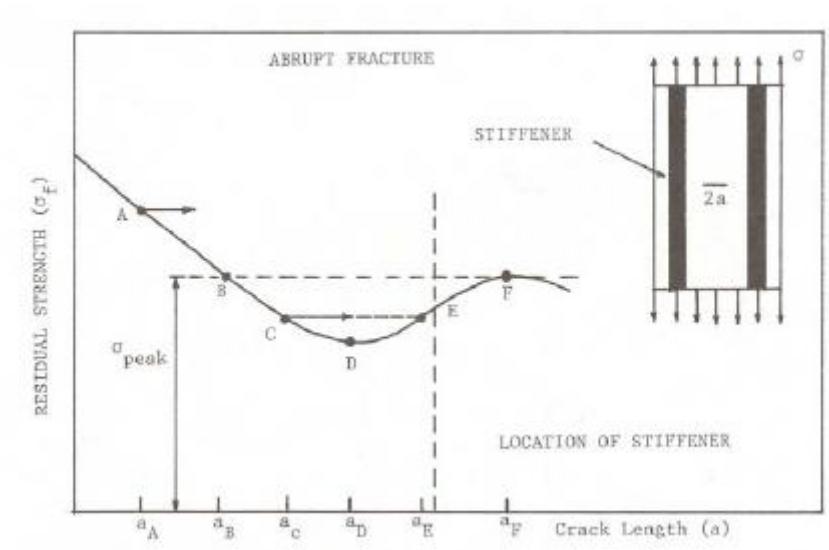

Figure 2.31: Residual Strength of the Cracked Panel as a Function of Crack Length for Built-Up Skin Stiffened Structure. Only Skin Failure Mode Considered. Abrupt Failure Criterion Used to Determine Residual Strength

Before the panel fails completely, the failure stress level at point C/E must be increased to the level associated with point F, i.e. to σ_{peak}. As the stress is increased above the level of point E, the crack extends from a_E to maintain an equilibrium between the input stress and

the residual strength. When the stress reaches σ_{peak}, the crack has extended to a_F, at which point the crack abruptly extends causing failure of the panel.

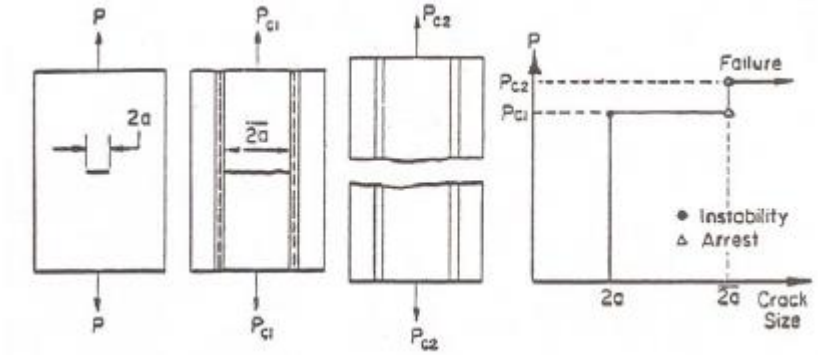

Figure 2.32: Load-Crack Length Behavior Observed in Skin-Stiffened Construction with Arrest Features

In the design of fail-safe structure, a frequent objective is to design the structure for limiting or arresting unstable crack growth so that catastrophic failure can be prevented. The fundamental concept in crack arrest design is to provide within the structure a means to reduce the crack tip stress intensity factor. This concept requires the use of additional stiffening members such as stiffeners, reinforcing rings, etc., to produce a decrease in the stress. These are inherently present in built-up structures, such as aircraft wings, fuselages, etc… In general, the residual strength analysis of a structure with crack arrest capabilities may involve more than one failure criterion. For instance, in a stiffened skin structure or an aircraft wing, the analysis should consider stringer failure, fastener failure, and skin crack failure criteria. Built-up panels loaded to fail-safe levels tend to exhibit substantial local deformations of critical elements. Failure criteria are thus dependent also on elastic-plastic deflection allowables for both fastener and skin/stringer elements. The residual strength diagram for the structure that exhibits slow crack growth behavior will contain two curves. The lower curve corresponds to the critical level of stress at which slow crack extension starts. The onset of slow tearing is then described by this lower curve. The upper curve provides the critical stress level at which the unstable rapid crack extension occurs. When the crack approaches the stiffener, as explained earlier, the residual strength levels, corresponding to the onset of slow cracking and the rapid extension, start increasing. For a crack length a_i, the slow crack extension begins at point B. This stable extension continues up to point B′ where the rapid failure is supposed to occur. However, due to the continuous rise in the residual strength of the stiffened panel, the stable crack extension continues to occur beyond point B′ and up to point C. Since the residual strength of the panel starts reducing at this point, any further increase in the applied load will lead to the rapid unstable crack extension.

The construction of the residual strength diagram has already been presented. Due to the complexity of the structural geometry, however, estimating requires the calculation of the loads that are transferred to the stiffening or secondary members from the main load carrying member of the structure. Depending upon the complexity, the K vs. a curves can be obtained either through an appropriate numerical method or through the method of superposition.

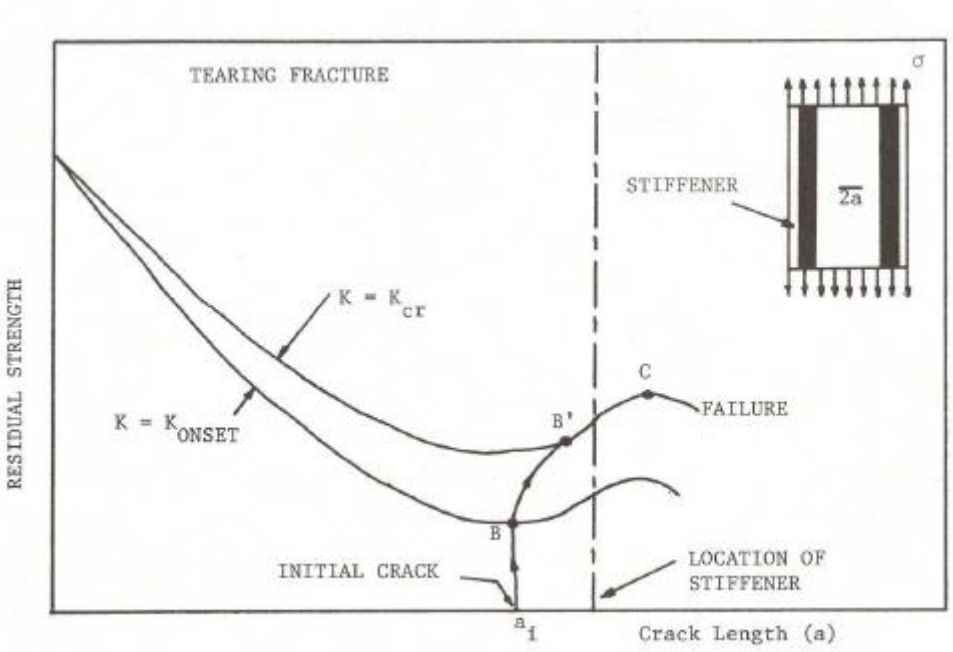

Figure 2.33: Residual Strength of Cracked Panel as a Function of Crack Length for Built-up Skin-Stringer Structure. Tearing Failure Criterion Used to Determine Residual Stress

SECTION 2.4: LIFE PREDICTION METHODOLOGY

Currently, within the Air Force, airframe life predictions are based on a crack growth damage integration package that uses a data base and analysis to interrelate the following six elements:

a) The initial flaw distribution which accounts for size variations and location of cracks in a given structure;

b) Aircraft usage describing the load spectra data base;

c) Constant amplitude crack growth rate material properties accounting for stress ratio and environmental effects;

d) Crack tip stress intensity factor analyses which account for crack size, shape, and structural interactions;

e) Damage integrator model which assigns a level of crack growth for each applied stress application and accounts for load history interactions; and

f) The fracture or life limiting criterion which establishes the end point of the life calculation.

The damage integrating equation showing how the various elements interact is:

$$a_{cr} = a_o + \sum_{j=1}^{t_f} \Delta a_j$$

where Δa_j is the growth increment associated with the j^{th} time increment. The purpose of this numerical expression is to determine the life t_f. The various elements affect the quantities in the following manner:

1. a_{cr} is determined interrelating elements b, d, and f.
2. a_o is determined using element a.
3. Δa_j is determined by interrelating elements a, b, c, d, and e.

A measure of initial quality in a component of service hardware is given by the distribution of initial crack sizes.

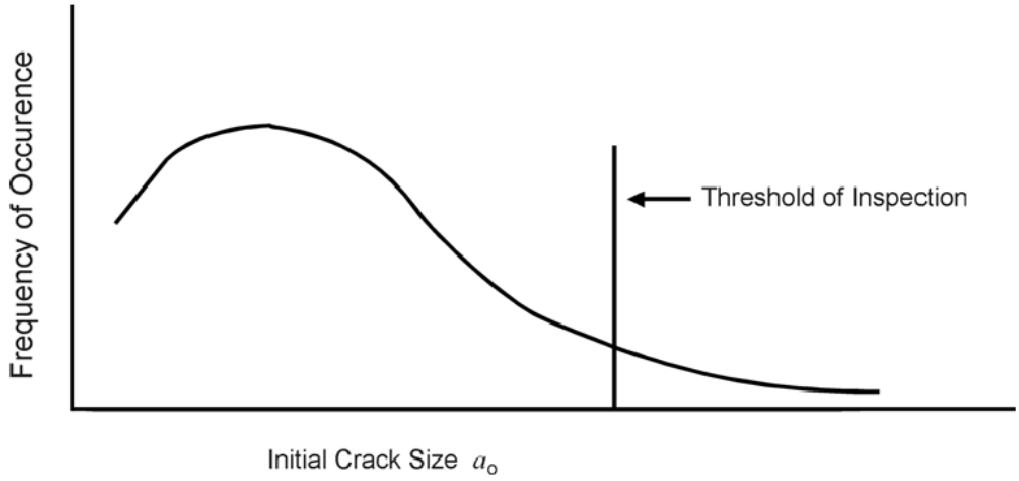

Figure 2.34: Distribution of Initial Crack Size for a Given Type of Crack

For predictions of safety limits, the initial cracks larger than the nondestructive inspection (NDI) detectability limit are of principal concern. Current specifications detail NDI limits and require verification/certification of contractor capability to detect cracks smaller than the specified NDI limits. Normally, such certification is demonstrated with curves.

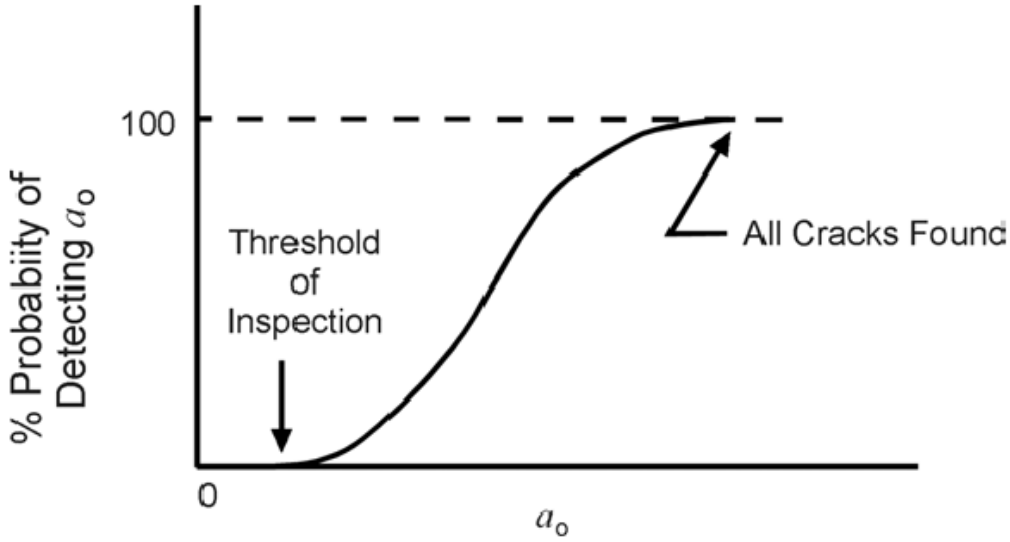

Figure 2.35: Certification of NDI Capability

The program of certification for a contractor's quality control inspector/inspection techniques allows the USAF to assess the probability and confidence limits associated with detecting a given crack.

Results generated by the F-4 Independent Review Team (IRT) provided a method of characterizing the initial flaw population (apparent initial quality) based on full-scale fatigue test-induced cracking behavior [Lozano, et al., 1974]. Given the measurable flaw distribution in a structure at some time subsequent to test startup, the initial flaw population can be backtracked by analysis. The "back" extrapolation of the flaw population is conducted using the damage integration package.

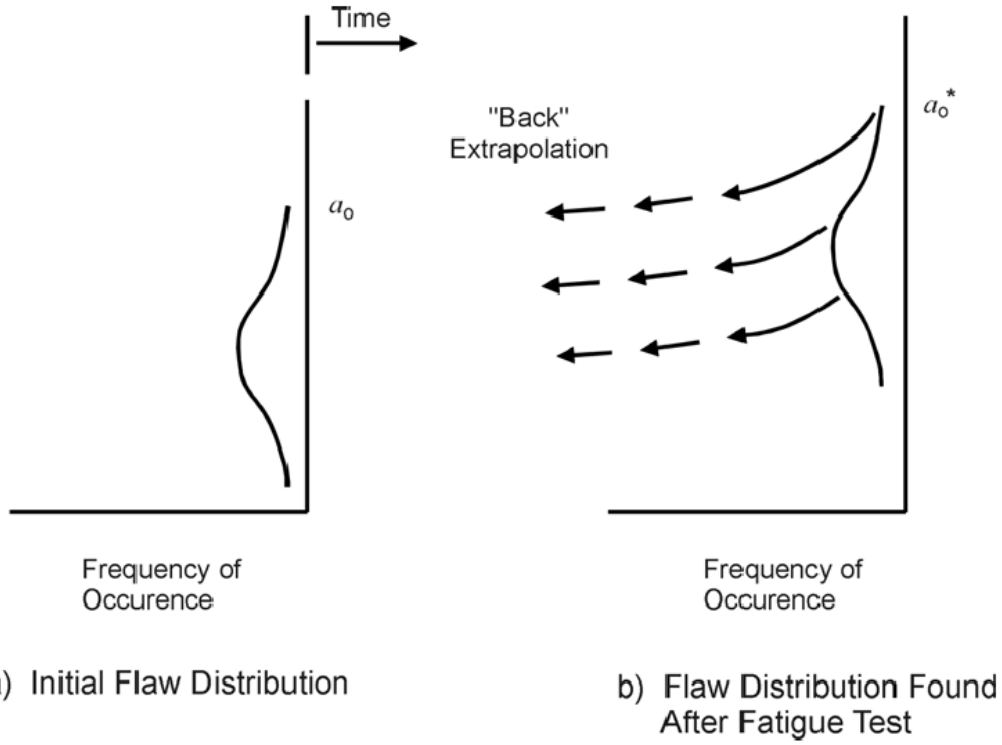

Figure 2.36: Determining Initial Quality by Back Calculation

The initial flaw distribution can be used to estimate influence of load factors, mission profiles, and usage changes on the life of service hardware. The F-4 IRT study also provided an evaluation of statistical methods for describing the large crack length extremes for initial flaw distributions established in this manner.

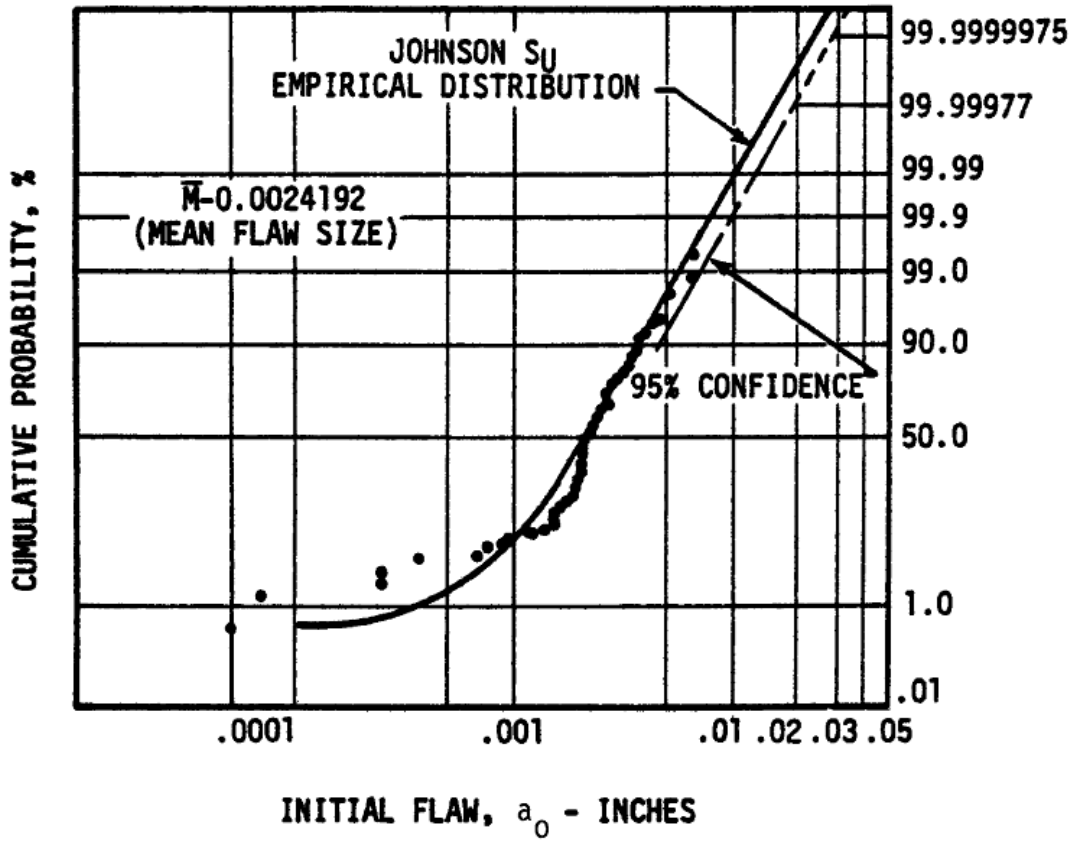

Figure 2.37: Initial Flaw Distribution for F-4 Based on Back Calculation

The sum of the load levels that a structure is expected to experience is determined by a projection of the amount of usage expected over the life in the various possible missions; e.g., hours in training, air-to-air combat, reconnaissance, weapons delivery, etc. The mission mix includes the relative amounts of time spent in each mission. The most basic information needed is the load factor exceedances at the center of gravity (CG) of the aircraft.

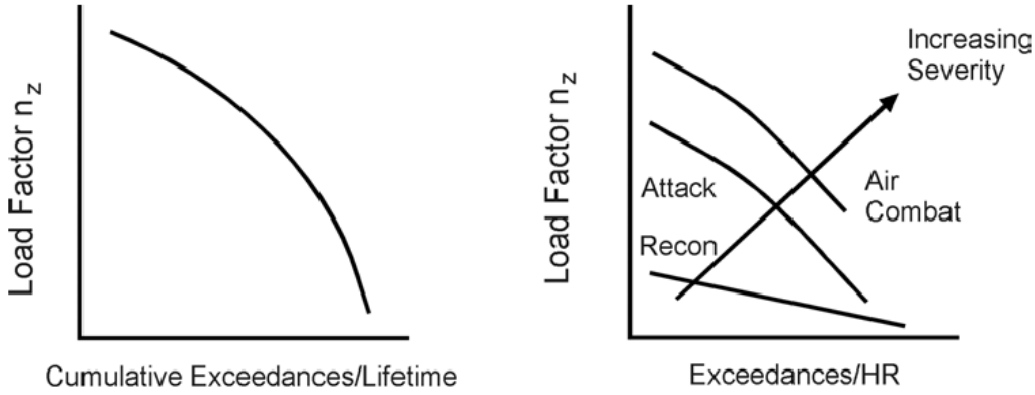

Figure 2.38: Typical Load Factor Exceedance Information Indicating Usage

For new designs, this data is derived from actual measured exceedances from operational aircraft flying similar missions. The USAF specifications contain such data. The Air Force Guidelines Handbook for developing Load/Environmental Design Spectra [Giessler, et al., 1981] summarizes the techniques that are currently being utilized to develop the loading and environmental spectra based on these data for various types of structures. The specific sequence of loads applied to the structure is necessary to the crack growth damage accumulation analysis. Current practice is to simulate the overall life on a flight-by-flight basis. Each flight in the design, analysis, or test load spectrum consists of a series of cycles that combine the deterministic and probabilistic events describing the type of mission. The deterministic events include takeoff and landing, and certain basic maneuver loads during each flight. Probabilistic events such as gusts or rough field taxiing occur periodically. Although it is possible to estimate the number of times these events occur, their position in the load sequences is determined in a probabilistic manner. In developing the load spectrum for crack growth damage analysis, it is necessary to determine the stress history for each critical area on the airframe. This is accomplished by determining the relationship between the load history derived above and the stress response.

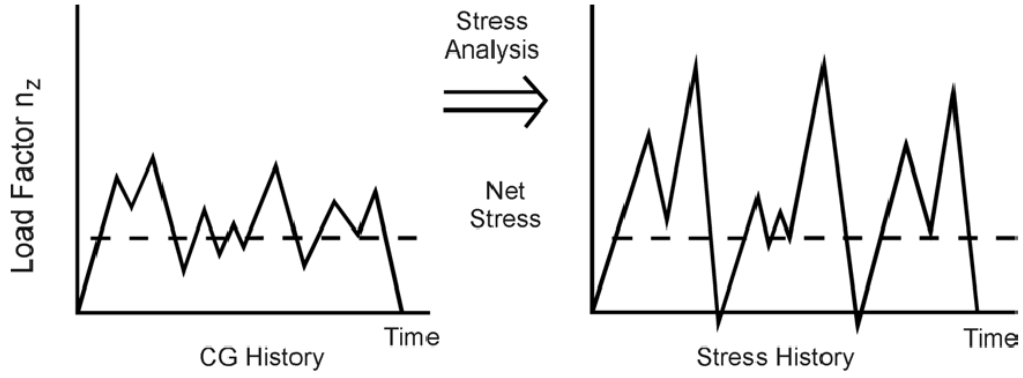

Figure 2.39: Load Factor to Stress History Transformation

Differences in crack growth resulting from mission mix can be significant. A fighter aircraft that is used primarily for air-combat or air-combat training typically accumulates more damage than one that is used for the same number of hours on a reconnaissance-type mission.

The material properties enter the damage integration package in the form of constant amplitude crack growth rate data. Crack growth data are generated in the laboratory under constant cyclic loading on simple specimens with accepted characterizing stress intensity factors. Crack growth rate data are developed and correlated on the basis of growth rate (da/dN) as a function of stress intensity factor range, ΔK. The ASTM defines $K_{min} = 0$ and thus $\Delta K = K_{max}$ whenever $R < 0$ ($R = \sigma_{min}/\sigma_{max}$).

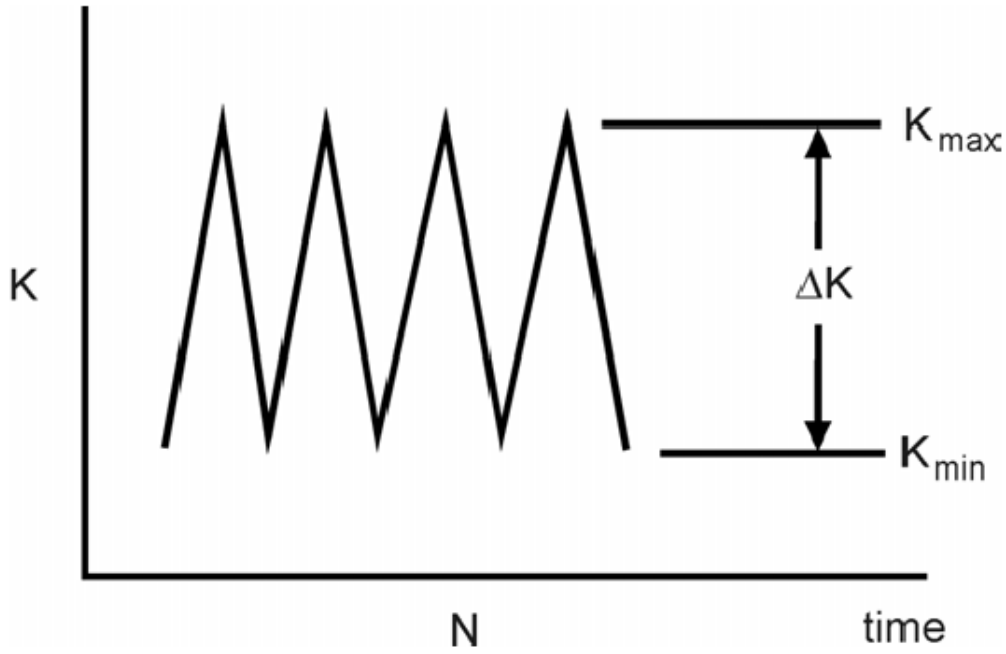

Figure 2.40: Stress-Intensity Factors – Cyclic Loading

For a given ΔK, the crack growth rate increases with increasing stress ratio, R for $R > 0$. Hence, the constant amplitude crack growth rate properties for a given material or alloy consist of a family of curves. The crack mechanics approach considers that for a given ΔK, R combination, there is a da/dN that is independent of geometry. Thus, the damage integration package has available a growth rate for each ΔK determined for the given crack configuration and loading.

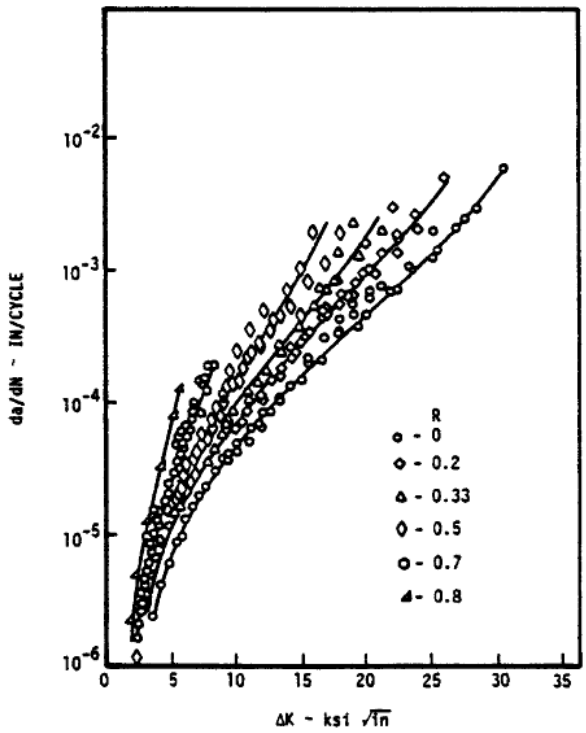

Figure 2.41: Constant Amplitude Crack Growth Rate Data for 7075-T6 Aluminum.

When necessary, thermal or chemical environment and time (frequency of loading) effects are also included in the crack growth rate data generated for use with the damage integration package.

The interrelationship between critical crack length, loading, and residual strength of a structure has been extensively presented above. The residual strength (σ_{res}), the load-carrying capacity of the cracked structure, can be shown to monotonically decrease with increasing crack length in the following manner:

$$\sigma_{res} = K_c/f(a)$$

where K_c = the material resistance to fracture, termed fracture toughness, and
f(a) the structural property, termed the stress intensity factor coefficient.

When the residual strength decays to the level of the maximum stress in the service load history, fracture of the structure occurs. The crack length associated with fracture (i.e., a_{cr}) is normally determined by solving this equation for crack length, assuming that the residual strength equals the maximum stress in the stress history. The rate of growth of a crack is directly related to the rate of loss of residual strength, thus justifying the selection of the crack to quantify structural fatigue damage.

The critical crack length (a_{cr}) is thus a function of material, structural geometry, and loading.

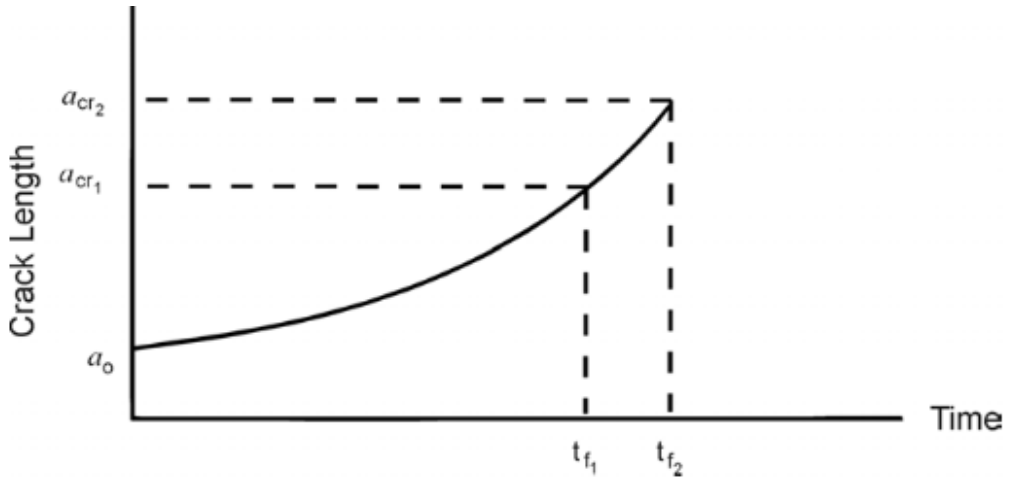

Figure 2.42: Effect of Critical Crack Size on Life

The primary advantage of designing for a large critical crack length is the increased inspectability it provides. A large critical crack length increases the probability of locating the crack before it becomes critical, thereby enhancing aircraft safety.

Determination of the critical crack size would ordinarily be sufficient for safety limits; however, durability considerations often dictate that the final crack size, a_f, be chosen smaller than a_{cr} to represent rework of repair limits.

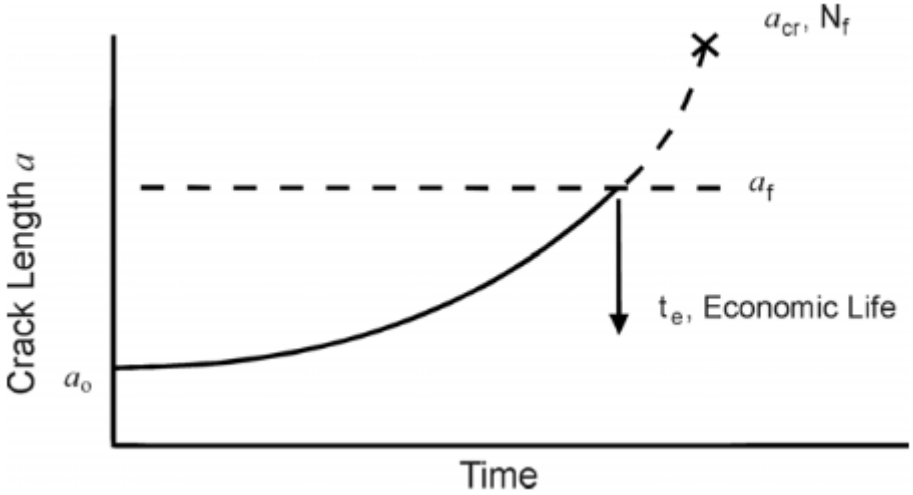

Figure 2.43: Economic Final Crack Size

SECTION 3: DAMAGE SIZE CHARACTERIZATION & ANALYSIS OF DAMAGE GROWTH

For quantifying the damage sizes that may be present in the structure at the beginning of an operational period, the following schematic is used.

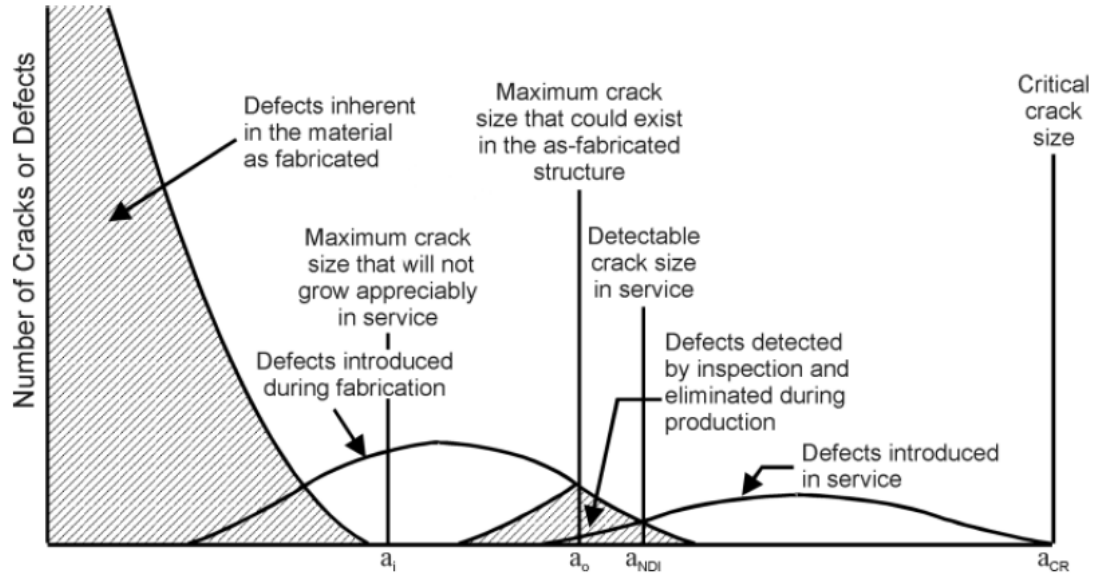

Figure 3.1: The Effect of Defects Distribution in Structural Integrity Planning

The distribution of crack lengths in any given structure can be considered to consist of the composite of several distributions. The material as received from the vendor will contain very small flaws or defects such as inclusions, cracks, porosity and surface pits, scratches, and machine marks. These inherent material flaws are considerably below the detection capability of the non-destructive inspection (NDI) and should be sufficiently small to not grow appreciably in service. These small flaws form the basis of the continuing damage crack size assumption and are characterized by a single crack length, a_i, which is assumed to be an upper bound on the distribution.

A distribution of larger defects can exist as a result of the fabrication process or as large inherent flaws. The production quality control process is designed to detect and eliminate as many of these cracks as possible but those which are not detected will propagate due to fatigue mechanisms during service. The largest crack size that could remain undetected in the newly fabricated structure after the final inspection is designated as a_o. This crack length provides the starting point for crack growth projections which demonstrate adequate service life or the necessity for an in-service inspection.

Cracks smaller than a_o will propagate in service operations and others, due to fatigue crack initiation, corrosion, and foreign object damage, will be initiated. If any of these cracks can propagate to critical size, a_{cr}, before the end of the service life, they must be detected and repaired at scheduled maintenance intervals. The largest crack size that can remain undetected after an inspection is designated as a_{NDI} and becomes the initial crack size for the next usage period.

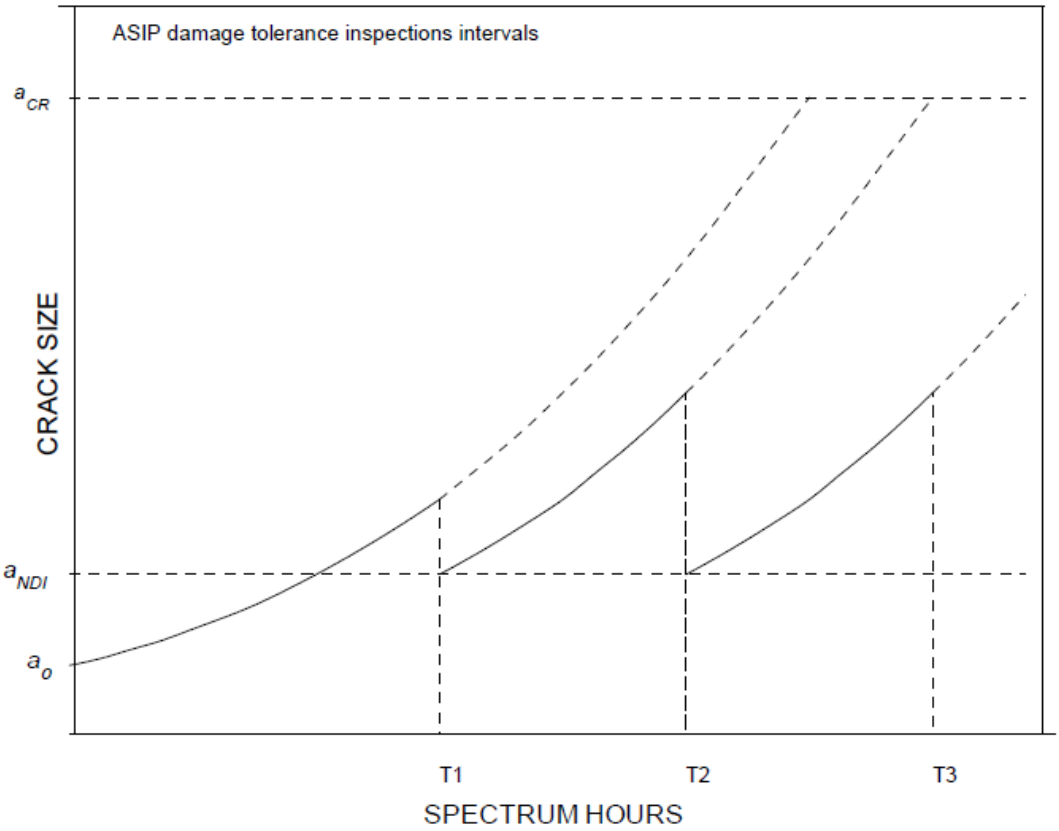

Figure 3.2: Crack Growth-Life Curve after Second Inspection

The assumed crack sizes depend on:

1) the design concept (slow crack growth or fail safe);

2) inspectability level (inspectable or non-inspectable) with and without component removal; and

3) continuing damage after initial primary damage.

Smaller initial crack sizes (a_o) may be assumed for slow crack growth structures based on the contractors demonstrated capability to eliminate all cracks greater than the smaller value. This demonstration may be based on an NDI system or on a proof test.

The continuing damage crack size assumption can also be reduced if the contractor can demonstrate an improved manufacturing quality. One method for such a demonstration is based on the determination of the distribution of equivalent initial flaws.

NDI, proof testing, and the equivalent initial quality method can be applied under the current airplane damage tolerance requirements and may receive greater emphasis in future specifications.

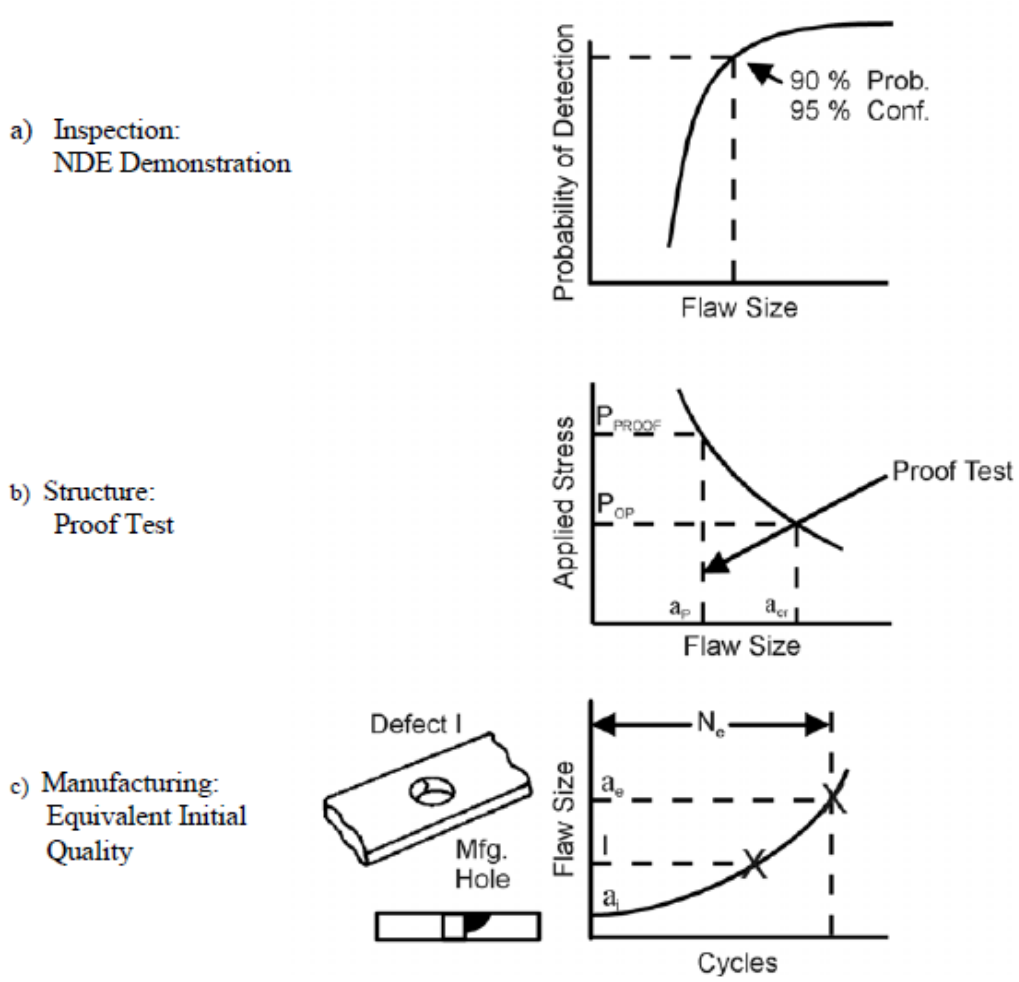

Figure 3.3: Various Qualification Processes

SECTION 3.1: NDI METHODS

Non-destructive inspection (NDI) methods are commonly used to determine the condition of a structure during production and at in-service inspections. A distinction between inspections for cracks and for corrosion is made for capability evaluations even though the physical principles of the techniques are common.

There are six commonly-used NDI techniques, and two others are expected to receive widespread acceptance and application. These eight methods are visual, liquid penetrant, eddy current, ultrasonic, magnetic particle, radiography, thermographic and acoustic emission inspections.

In a sense, all inspections in which the find/no find decision is made by a human are visual. However, in categorizing NDI methods, visual inspections are generally interpreted as inspections in which the inspector is aided, at most, by optical devices, such as magnifying glasses and mirrors. In the context of JSSG-2006, the in-flight evident, ground evident, walk-around evident, and special visual inspections are all visual inspections and play an important role in the maintenance of structural integrity through damage tolerance. Visual inspections are the most common and the most economical of the inspections to perform. However, visual inspections are also the least reliable in terms of the size of the cracks that can be detected. Since the efficacy of visual inspections is highly dependent on the alertness and acuity of the inspector, an additional level of human factors is introduced in discerning the physical attributes of a crack from its environment.

Liquid penetrant inspection is a non-destructive method for finding discontinuities that are open to the surface of parts fabricated from essentially nonporous materials. After cleaning the surface, the penetrant is applied and will seep or be drawn into various types of minute surface openings. The excess penetrant is removed and a developer is applied which highlights the cracks under ultraviolet light. The process is well-suited for the detection of all types of surface cracks, laps, porosity, shrinkage area, laminations, and similar discontinuities.

Indications of cracks can be found regardless of size, configuration, internal structure, or chemical composition of the workpiece being inspected and regardless of the orientation of the crack to the workpiece.

Liquid penetrant inspections are relatively simple and inexpensive (as compared to the other NDI methods) and can be applied to a broad range of materials. Very small cracks can be found. However, they can only detect surface cracks and their effectiveness can be adversely influenced by surface coatings, surface roughness, and porosity. Extreme care is required in pre- and post-inspection cleaning and, in some cases, etching may be required prior to inspection.

The principles of electromagnetic induction are used in eddy current inspections to detect surface and near-surface cracks in electrically-conductive metals. When an electrically-conductive material is subjected to an alternating magnetic field, small circulating electric currents are generated in the material. Since these eddy currents are affected by variations in conductivity, magnetic permeability, mass, and material homogeneity, the conditions that affect these characteristics can be sensed by measuring the eddy current response of the material. In practice, eddy currents are induced in the part to be inspected with a coil carrying an alternating current. The induced eddy currents generate their own magnetic field, which interacts with the magnetic field of the exciting coil, and changes the impedance of the exciting coil. By measuring the impedance of the exciting coil, or a separate indicating coil, the inspector can infer the presence of cracks in the material.

An important use of the eddy current NDI method has been in the detection of fatigue or stress corrosion cracks around fastener holes after the cracks have grown beyond the fastener head. Special bolt hole probes have also been devised for use after the fastener has been removed for locating cracks emanating from the wall of the fastener hole. This inspection process has been automated to remove operator influence, speed inspections, and produce a permanent inspection record.

Eddy current methods do not require contact with the specimen or clean up, and are generally faster than liquid penetrant and radiographic methods. Although eddy current methods can detect both surface and subsurface cracks, the depth of inspection below the material surface is limited (approximately 0.25 in.). Since eddy currents are influenced by many material variables, masked or false indications can easily be caused by sensitivity to part geometry, lift-off, edge effects and permeability variations. Finally, eddy current methods require well-trained operators to man the test instruments and reference standards are necessary.

Ultrasonic inspection uses high frequency sound waves as a probing medium to detect subsurface, as well as surface cracks. The sound waves travel through the part with attendant energy loss and are reflected at material-crack interfaces. Ultrasonic inspection devices detect cracks by monitoring one or more of the following: (a) reflection of energy from interfaces or discontinuities within the metal; (b) time of transit of a sound wave through the test piece; and (c) attenuation of the beams by absorption and scattering within the test piece.

Ultrasonic inspection is one of the most widely used NDI methods. Cracks, laminations, shrinkage cavities, bursts, flakes, pores, bonding faults, and other discontinuities that act as

metal-gas interfaces can be detected. Inclusions and other non-homogeneity in the metal being inspected can also be detected by causing partial reflection or scattering of the wave, even though they may not act as a metal-gas interface. Although the primary application of ultrasonic inspection in metals is the detection and characterization of internal cracks, it is also used to detect surface cracks, define bond characteristics, measure extent of corrosion and, (much less frequently) determine physical properties such as structure, grain size, and elastic constants. The penetrating power of ultrasound waves allows the detection of cracks deep within a part. Due to the sensitivity of the instruments, very small cracks can be detected but, if the gain is set too high, at the expense of many false indications. Ultrasonic methods provide greater accuracy than other NDI methods in determining the position of internal cracks, estimating their size, and characterizing their orientation, shape and nature. The limitations of ultrasonic methods are governed by the requirement for experienced technicians, the difficulty in developing inspection procedures, the need for reference standards for equipment calibration, and the physical limitations of the hardware. Since couplants (light oil or water) are needed to provide effective transfer of ultrasonic wave energy between transducers and material, parts that are rough or irregular in shape are difficult to inspect. Similarly, parts that are very small are difficult to inspect. Finally, since discontinuities in a shallow layer immediately below the surface may not be detectable, inspection results of very thin components are questionable.

Magnetic particle inspection is effective in the detection of surface and near-surface cracks in ferromagnetic parts. The inspection is accomplished by inducing a magnetic field in the part and applying either a dry magnetic powder or a liquid suspension of iron particles to the surface being inspected. Defects in the part cause local bipolar perturbations in the magnetic field which attract the magnetic particles, producing visible indications by color contrast or by fluorescence under “black light”. The magnetically-held particles form the outline of the discontinuity and generally indicate its location, size, shape, and extent to an experienced inspector.

The magnetic particle method is a relatively fast and inexpensive method for locating small and shallow surface cracks in ferromagnetic materials. Discontinuities that do not break the surface are detectable, but deeper cracks must be larger to be found. Elaborate pre-cleaning is not necessary, but thin coatings of paint or other non-magnetic coverings, such as plating, adversely affect the sensitivity of this inspection technique. Following the inspection, the material must often be de-magnetized, and post-cleaning to remove the clinging magnetic particles is usually necessary. This NDI method can be used only on ferromagnetic materials, which include most of the iron, nickel and cobalt alloys. Many of the precipitation-hardening steels, such as 17-4PH, 17-7PH, and 15-4PH stainless steels, are magnetic after aging. Non-ferromagnetic materials that cannot be inspected by this method include aluminum, magnesium, copper, and titanium alloys and austenitic stainless steels.

Radiographic NDI is based on the differential absorption of penetrating radiation by the structure being inspected. In conventional radiography, the object is bombarded by a beam of X-rays and the portion of the radiation that is not absorbed by the object impinges on a sheet of film. The unabsorbed radiation exposes the film emulsion similar to the way light exposes film in photography. Development of the film produces an image that is a two-dimensional “shadow picture” of the entire volume of the object. Variations in density, thickness, and composition of the object being inspected cause variations in the intensity of the unabsorbed radiation and appear as variations in shades of gray in the developed film. Evaluation of the radiograph is based on a comparison of the differences in photographic density with known characteristics of the object or with standards derived from radiographs of similar objects of acceptable quality.

Radiographic inspection provides the capability to probe the internal characteristics of materials and components. It can disclose structural weaknesses, assembly errors, and mechanical malfunctions, as well as revealing voids, long cracks, and other material anomalies. Radiography is, however, expensive, slow, and not sensitive to detecting certain type cracks. Cracks cannot be detected unless they are parallel to the radiation beam. Tight cracks in thick sections cannot usually be detected even when properly oriented. Laminations are almost always non-detectable. Minute discontinuities such as inclusions in wrought material, flakes, microporosity and microfissures cannot be detected unless they are sufficiently segregated to produce a detectable gross effect. Finally, due to the hazards of exposure to X-rays, strict controls are required to prevent biological damage to the inspectors.

Thermographic inspection uses relative differences in heat transmission to detect internal features and defects, such as delaminations in layered materials. In active thermography, heat is applied to the object under test and surface temperatures are monitored by an infrared camera as the heat propagates through the object. In the reflection method, heat is applied to the surface that is monitored; relatively warm areas indicate possible internal defects. In the transmission method, heat is applied to the opposite side of a panel from a detector, and relatively cooler areas will indicate areas of poor thermal transmission. Heat may be applied by a laser, warm air, heat lamps, flash lamps, or other methods. While heating is most common, cooling may also be used to create thermal transients within the material. Passive thermography, with no external heat source, may be used if thermal contrasts are produced within the object under test by other means, such as electrical heating at a poor solder joint.

Thermographic methods are most appropriate for use with materials that have low thermal conductivity, such as ceramics and polymers. Heat propagates more slowly in these materials, which decreases the image acquisition rate needed from the infrared camera. In addition, interference with the thermal excitation can obscure near-surface data, with "near-surface" measured in time of thermal transmission, so that much less data is lost when the heat is propagating slowly. High emissivity surfaces radiate heat better and, therefore, produce better sensitivity. Coatings, such as a flat black paint, may be applied to low emissivity or reflective surfaces to increase emissivity. Flaws, such as delaminations that are perpendicular to the propagation of thermal energy through the object, are the best candidates for detection by thermography. Other flaws that disrupt heat flow, such as fluids trapped in honeycomb materials, can also be detected with relative ease. The resolution of this method decreases with depth, because the thermal energy is conducted in all directions, not just directly through the material. Surface flaws, such as cracks, may be detected if heat can be forced to propagate along the surface of the material. Thickness or composition variations may be detected by transmission thermography.

Thermography has a long history, but has not achieved the widespread use of other methods, such as ultrasonic, eddy current, and radiography. Disadvantages of this method include the expense of equipment, the reliance on surface emissivity, and the generally low signal-to-noise ratio. Advantages include area inspection nature of the technology, speed, noncontact nature, and versatility. Currently, thermographic methods are used for delamination detection in layered composites, coatings evaluation, honeycomb inspection, thermal barriers, bond evaluation, and thickness evaluation. Improvement in the sensitivity of infrared detectors and better thermal sources indicate that the use of thermographic methods will increase as the supporting technologies continue to mature.

Acoustic emission (AE) is the term used for dynamic stress waves that are created within a material due to the application of a force. Some examples are the sound of fibers breaking when a piece of wood is bent, high-frequency stress waves created when a crack grows in

a metal structure undergoing mechanical fatigue, and the pulse of stress waves emanating from the impact site of a meteorite colliding with a spaceship hull. AE differs from most of the other NDI methods in that no directed energy is put into the test object. Whole-body forces create the localized stress waves that propagate through the test object to AE sensors.

AE NDI is done by placing multiple acoustic sensors on the object being inspected and then recording and correlating the signals generated when stress waves reach the sensors. The sensors typically are responsive to acoustic frequencies between 50 kHz and 1 MHz. The lower limit is important in order to limit acoustic noise, although it should be noted that common objects such as jingling car keys or grinding wheels produce acoustic energy above 100 kHz. The upper limit is strongly dependent on the bandwidth of the AE sensor. Occasionally, AE tests utilize sensors with the upper limit extending into the 2-3 MHz range. The sensors are connected to AE instruments that amplify, filter, store, and process the signals produced by the sensors. Typical results from AE tests are the number of AE "events" recorded; the energy, time, and duration of each event; and the location of the event within the test object.

Some advantages of AE NDI are: 1) the method is sensitive to stress waves emanating from anywhere within the test object; the sensors do not have to be focused or scanned across the object; 2) triangulation of the time of detection of the stress wave at different sensors allows identification of the location of the emission, and 3) sensors can be placed on objects with very limited access.

Disadvantages of AE NDI are: 1) the instrumentation is expensive, 2) appropriate signal processing to eliminate unimportant signals can be complicated, 3) large amounts of data often are generated, creating data storage problems.

The five principal non-visual NDI methods are in widespread use. For damage tolerance considerations, the key characteristic of an NDI system is the size of the flaws that can be missed when the system is applied in the field. Quantifying inspection capability in terms of flaw size is referred to as inspection or NDI reliability. Because of the many differences in material and geometry of structural details and the many approaches to the application of any of the methods, there is no single characterization of capability in terms of a reliably-detected crack size for any of the methods. Further, because of the difficulty and cost of quantifying NDI reliability, relatively few capability demonstrations have been conducted. Only very general statements can be made comparing the NDI reliability of the five methods.

Because of the random nature of inspection response to flaws of ostensibly the same size, NDI capability is characterized in probabilistic terms and estimated using statistical methods. In particular, NDI reliability is quantified in terms of the probability of detection as a function of flaw size, POD(a). There is no practical flaw size for which there is 100 percent assured detection. For damage tolerance applications in the aircraft industry, it has become customary to characterize inspection capability in terms of the crack size for which there is a 90 percent probability of detection, the a_{90} crack size. To reflect the statistical uncertainty in the estimate of a_{90}, a 95 percent confidence bound can be calculated yielding the $a_{90/95}$ crack size characterization of capability. There is 95 percent confidence that at least 90 percent of all cracks of size $a_{90/95}$ will be detected. The reliably detected crack size for a system is usually taken to be either a_{90} or $a_{90/95}$. Note that cracks smaller than $a_{90/95}$ are readily detected by the NDI systems since POD(a) functions for production inspections increase over a relatively large crack size region. Typically, the 50 percent detectable crack size is less than half the a_{90} crack size for a non-automated inspection.

The following table presents approximate lower limits of reliably-detected crack sizes for the NDI methods in common use in the aircraft industry. These limits are achievable on some structures by well-trained inspectors working in a good production environment. Because these crack sizes represent the limits of the methods, such capabilities must be demonstrated before use in a damage tolerance based inspection schedule. Note that most routine inspections are not designed for these target crack sizes.

Method		Location	Dimension	Size (in.)
Eddy Current	Manual	Near Surface	Length	0.030-0.040
	Semi-Automated	Near Surface	Length	0.020-0.030
	Automated	Near Surface	Length	0.005-0.010
Ultrasonic	Manual	Subsurface	FBH*	0.032-0.064
	Automated	Subsurface	FBH*	0.016-0.032
Fluorpenetrant	Manual	Surface	Length	0.075-0.100
	Automated	Surface	Length	0.060-0.075
Magnetic Particle	Manual	Near Surface	Length	0.010-0.020

*FBH – capability based on flat bottom holes

While all of the NDI systems are capable of finding "small" cracks, damage tolerance analyses are based on the largest crack that might be in the structure after an inspection. Thus, the focus of NDI capability evaluation for damage tolerance is the largest crack that might be missed at an inspection. NDI techniques do not always produce a correct indication when applied by inspectors to cracks of the same size. The ability and attitude of the operator, the geometry and material of the structure, the environment in which the inspection takes place, and the location, orientation, geometry and size of the crack all influence the chances of detection. When considering the efficacy of an NDI system as a function of only crack size, uncertainty is introduced as a result of ignoring the other factors. This uncertainty is quantified in terms of the probability of detection (POD) of cracks of a fixed size. POD(a) is defined as the proportion of all cracks of size a that will be detected by the NDI system when applied by representative inspectors to the population of structural elements in a defined environment. At present, demonstrating the capability of an NDI system for a specific application requires a carefully controlled experiment with a valid statistical analysis of the resulting data.

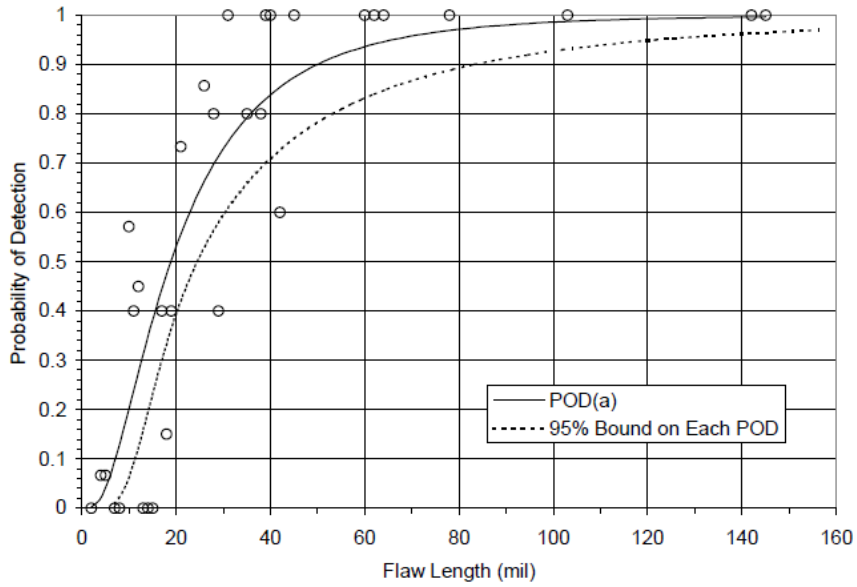

Figure 3.4: Example POD(a) Curve with Confidence Bound for Liquid Penetrant Inspections

The statistically-based characterization of NDI capability has two significant ramifications. First, for a given NDI application, the true probability of detection as a function of crack size (or for a single crack size) will never be known exactly. The capability of an NDI system can only be demonstrated by inspecting representative structures with known crack sizes. The true POD(a) function is estimated from the responses to the inspection stimuli or by the observed percentages of correct positive indications. The estimated POD(a) is subject to the statistical variation that can result from all of the uncontrolled factors that lead to variability in positive indications for all cracks of a particular size. However, statistical methods (which depend on the experimental procedure) are available which yield confidence limits on the true probability of detection. Protection against making a wrong decision on the basis of a set of non-typical results is provided by the confidence limits.

Second, in the real-world structural integrity problem, no inspection procedure will provide 100 percent assurance that all cracks greater than some useful size will be detected. Current NDI capabilities at the short crack lengths of interest in aircraft applications dictate that a reliably detectable crack size, can only be specified in terms of a size for which a high percentage of cracks will be detected. To reflect the statistical uncertainty, a confidence bound is often placed on this estimate of crack size. Such single crack size characterizations of NDI capability are expressed in terms of the crack sizes for which there is at least a given POD at a defined level of confidence (the POD/CL crack size). Such characterizations provide a stand-alone measure of the NDI system that is valid for applications represented by the demonstration test conditions.

There are three major limitations associated with the POD/CL type characterization:

1) The choice of particular POD and confidence limits has been made on a rather arbitrary basis. For example, 90/95 values were selected for JSSG-2006 recommended crack sizes even though there is no real interest in a crack length that is detected only 90 percent of the time. Rather, 90/95 limits were selected because higher POD or confidence limit values would have required much larger sample sizes in the demonstration programs for the analysis methods being used. The 95 percent confidence limit is assumed to provide the required degree of conservatism.

2) A POD/CL limit is not a single, uniquely defined number but, rather, is a statistical or random quantity. Any particular POD/CL estimate is only one realization from a

conceptually-large number of repeats of the demonstration program. Berens & Hovey [1981] showed there can be a large degree of scatter in these POD/CL estimates and the scatter depends on the POD function, analysis method, POD value, confidence level and number of cracks in the demonstration program.

3) The POD/CL characterization is not related to the size of cracks that may be present in the structure after an inspection. To calculate the probability of missing a large crack requires knowledge of both POD(a) for all cracks sizes and the distribution of the sizes of the cracks in the population of structural details being inspected.

There are two distinct strategies for quantifying NDI capability for damage tolerance analyses. These are: a) estimating POD(a) as a function of crack size and b) demonstrating capability for a fixed crack size. To estimate a POD(a) function, the structural details to be inspected would comprise a range of crack sizes in the expected domain of increasing POD. A parametric equation is assumed for the POD(a) function, the parameters of the equation are estimated from the inspection results, and the statistical properties of the estimates are used to place a confidence limit on the selected detection probability. To demonstrate capability for a fixed crack size, only cracks of the size of interest are inspected. The proportion of the cracks that are detected is the estimate of POD (for cracks of that size) and binomial theory is used to place a lower confidence bound on the detection probability. Because of the greater utility of the POD(a) function, the approach based on estimating the entire function is preferred by many, including the Air Force [MIL-HDBK-1823]. The fixed crack size approach is used by NASA for qualifying the inspection capability of vendors [Salkowski, 1993]. It might be noted that a binomial approach to estimating POD as a function of crack size was extensively considered in the 1970's, but later abandoned. Very large numbers of cracked specimens were needed to ensure an adequate sample size within reasonably small intervals of crack size.

Inspection results are recorded in two distinct formats and the format determines the analysis method to be used in modeling the POD(a) function. When the results of an inspection are expressed only in terms of whether or not a crack was detected, the data are known as find/no find, hit/miss, or pass/fail data. Such dichotomous inspection results are represented by the data pair (a_i, Z_i) where a_i is the size of the i^{th} crack and Z_i represents the outcome of the inspection of the i^{th} crack: $Z_i = 1$ for the crack being found (hit or pass) and $Z_i = 0$ for the crack not being found (miss or fail). Examples of such data would be the results of visual, magnetic particle, or fluorescent penetrant inspections or any inspection for which the magnitude of the response to the inspection stimulant was not recorded. POD(a) analysis for data of this nature is often called hit/miss or pass/fail analysis. Maximum likelihood estimates of the parameters of the POD(a) model are obtained from the (a_i, Z_i) data. Asymptotic properties of the maximum likelihood estimates are used to calculate the confidence bound on the estimate of the reliably detected crack size.

When the results of the inspection are based on the quantified magnitude of a response to the inspection stimulus and the response is recorded, the POD(a) function can be estimated from the statistical scatter in the response magnitudes as a function of crack size. The data pair comprising size and signal response are designated as $(a_i, \hat{a}_i)$ in which $\hat{a}_i$ is the response to the inspection stimulus for the i^{th} crack. If $\hat{a}_i$ is greater than a pre-set threshold, $\hat{a}_{th}$, a crack is indicated. Data of this nature are often referred to as â vs a (a-hat vs a). Data from automated eddy current systems are of this nature. Data from ultrasonic and liquid penetrant inspections have also been recorded and analyzed in the â vs a format. The parameters of the POD(a) function are estimated from the scatter in â values about the mean response to cracks of size a. Maximum likelihood is used to estimate the parameters and to place confidence bounds on the estimate of the reliably detected crack size when desired [MIL-HDBK-1823; Berens, 1988].

The demonstration of NDI capability is a consumer or quality concern. The primary objective of such demonstrations for a particular application is to estimate the POD(a) function and, consequently, the reliably detected crack size, say a_{NDI}. For damage tolerance considerations, a_{NDI} is commonly accepted to be the crack sizes designated as a_{90} or $a_{90/95}$. The a_{90} crack size is defined as the size for which POD(a_{90}) = 0.90 and $a_{90/95}$ is the upper (conservative) 95% confidence bound on the estimate of a_{90}. (The estimate of the a_{90} crack size is often referred to as the $a_{90/50}$ crack size under the wrong assumption that the estimate of a_{90} is the median of the sampling distribution of the estimates.)

NDI reliability experiments have also been conducted to optimize the inspection protocol and to ensure process control. System optimization with respect to POD(a) would have the objective of determining system configurations that produce acceptable a_{90} or $a_{90/95}$ values. The design of system optimization programs is of a different character.

Sample sizes in NDI reliability experiments are driven more by the economics of specimen fabrication and crack characterization than by the desired degree of precision in the estimate of the POD(a) function. Reasonable appearing POD(a) functions can often be obtained from applying the maximum likelihood analysis to an inspection of relatively few specimens. Totally unacceptable results can also be obtained from inspecting specimens containing too few cracks or from inspection results that are not reasonably represented by the assumptions of the models. Therefore, it must be recognized that the confidence bound calculation for a POD(a) analysis is based on asymptotic (large sample) properties of the estimates and that there are minimal sample size requirements that must be met to provide a degree of reasonable assurance in the characterization of the capability of the system.

Larger sample sizes in NDI reliability experiments will, in general, provide greater precision in the estimate of the POD(a) function. However, the sample size is determined from the number of cracks in the experiment and there is an information content coupling with the crack sizes that must also be considered. The effect of this coupling manifests itself differently for the â versus a and hit/miss analyses. Sample sizes for the binomial analysis that is used to demonstrate a capability at a single crack size are dictated strictly by the selected value of the target POD and the degree of confidence.

When the crack decision is made on the basis of a recorded response, â, to the inspection stimulus, the data are known as â versus a inspection results and a better POD(a) analysis is available. When the inspection response is greater than a pre-set detection threshold, a crack is indicated for the site. In a capability demonstration, the minimum signal threshold is set as low as possible with respect to noise. Detection thresholds are later set that will yield a desired a_{90} value with an acceptable rate of extra indications. Extra indications are crack indications at sites with no known cracks. Extra indications can be the result of noise or large responses from insignificant cracks. However, they can also result from anomalies that do not impair structural integrity.

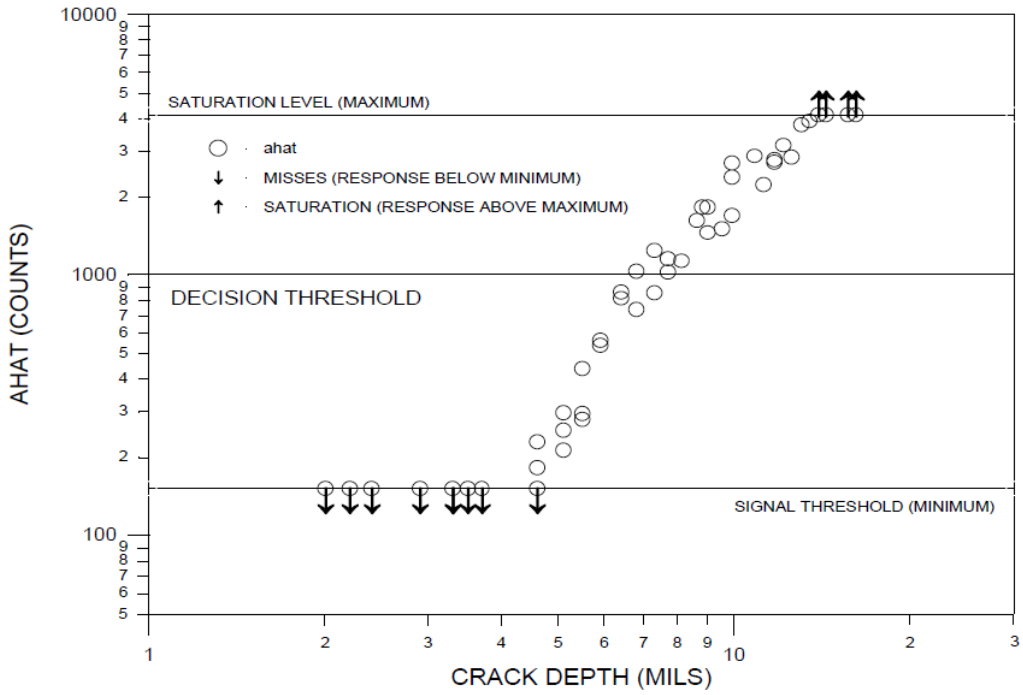

Figure 3.5: Example Plot of â versus a Data

The recorded signal response, â, provides significantly more information for analysis than a simple crack or no crack decision of a hit/miss inspection response. The POD(a) model is derived from the correlation of the â versus a data and the assumptions concerning the POD(a) model can be tested using the signal response data. Further, the pattern of â responses can indicate an acceptable range of extrapolation. Therefore, the range of crack sizes in the experiment is not as critical in an â versus a analysis as in a hit/miss analysis. For example, if the decision threshold was set at 1000 counts, only the cracks with depths between about 6 and 10 mils would provide information that contributes to the estimate of the POD(a) function. The larger and smaller cracks are always found or missed and would have provided little information about the POD(a) function in a hit/miss analysis. In the â analysis, however, all of the recorded â values provided full information concerning the relation between signal response and crack size and the censored values at the signal minimum and maximum limits provided partial information. The parameters of the POD(a) function are derived from the distribution of â values about the median response for cracks of size a. Assumptions necessary for characterizing this distribution are readily evaluated with the â versus a data.

Because of the added information in the â data, a valid characterization of the POD(a) function with confidence bounds can be obtained with fewer cracks than are required for the hit/miss analysis. It is recommended that at least 30 cracks be available for demonstrations whose results can be recorded in â versus a form. Increasing the number of cracks increases the precision of estimates. Perhaps, more importantly, increasing the number of cracks provides a broader population of the different types of cracks that the inspection will address. Therefore, the demonstration specimen test set should contain as many cracked sites as economically feasible. The analysis will provide parameter estimates for smaller sample sizes but the adequacy of the asymptotic distributions of the estimates is not known.

In a hit/miss capability demonstration, the inspection results are expressed only in terms of whether or not the crack of known size was detected. There are detection probabilities associated with each inspection outcome and the analysis assumes that the detection probability increases with crack size. Since it is assumed that the inspection process is in a

state of control, there is a range of crack sizes over which the POD(a) function is rising. In this crack size range of inspection uncertainty, the inspection system has limited discriminating power in the sense that detecting or failing to detect would not be unusual. Such a range might be defined by the interval ($a_{0.10}$, $a_{0.90}$), where a_p denotes the crack size that has probability of detection equal to p; that is, POD(a_p) = p. Cracks smaller than $a_{0.10}$ would then be expected to be missed and cracks greater than $a_{0.90}$ would be expected to be detected.

In a hit/miss capability demonstration, cracks outside the range of uncertainty do not provide as much information concerning the POD(a) function as cracks within this range. Cracks in the almost certain detection range and almost certain miss range provide very little information concerning probability of detection. In the hit/miss demonstration, not all cracks convey the same amount of information and the "effective" sample size is not necessarily the total number of cracks in the experiment. For example, adding a large number of very large cracks does not increase the precision in the estimate of the parameters of the POD(a) function.

Ideally, all of the cracks in a hit/miss demonstration would have 80 percent of their sizes in the ($a_{0.10}$, $a_{0.90}$) range of the POD(a) function. However, it is not generally possible to have a set of specimens with such optimal sizes for all demonstrations. The demonstrations are being conducted to determine this unknown range of sizes for the NDI system being evaluated. Further, because of the high cost of producing specimens, the same sets of specimens are often used in many different demonstrations. To minimize the chances of completely missing the crack size range of maximum information and to accommodate the multiple uses of specimens, the sizes of cracks in a specimen set should be uniformly distributed between the minimum and maximum of the sizes of potential interest. A minimum of 60 cracks should be distributed in this range, MIL-HDBK-1823, but as many as are affordable should be used. This minimum sample size recommendation was the result of subjective considerations as to the number needed to make the asymptotic assumptions reasonable, experience in applying the model to data, and the results of analysis from a number of simulated POD demonstrations [Berens & Hovey, 1981; Berens & Hovey, 1984; and Berens & Hovey, 1985].

When capability is to be demonstrated by using specimens with cracks of the same size and the binomial analysis, the number of cracks in the specimens can be determined exactly from the POD level and the desired degree of confidence. The best (maximum likelihood) estimate of the POD at the crack length of interest is the proportion of cracks in the specimen set that are detected. A lower bound on the estimate is then calculated for the desired confidence level using binomial distribution theory. For example, to demonstrate that there is 95 percent confidence that at least 90 percent of all cracks of the size under consideration will be detected requires at least 29 cracks of that size. If all 29 cracks are detected, the maximum likelihood estimate of POD is 1.0 and the lower 95 percent confidence bound is slightly greater than 0.9. If any crack is missed, the lower confidence bound on the estimate of POD is less than 0.9.

It must be emphasized that the sample size is determined by the number of different cracks, not the number of inspections. Different cracks can respond differently to inspection stimuli. Multiple inspections of the same crack are not independent and, therefore, cannot be treated as independent samples from the population of cracks of the given size. There is a tendency to re-inspect specimens to increase the sample size. For example, if one of 29 cracks is not detected, the inspection does not qualify for an $a_{90/95}$ capability at that size. The specimen set cannot be re-inspected with the expectation of passing the test for a sample size of 58. New specimens with different cracks must be used or the analysis is not valid.

In the context of the preceding discussion, sample size refers to the number of known cracks in the specimens to be inspected during the capability demonstration. The complete specimen set should also contain inspection sites that do not contain any known cracks. If the inspection results are of the hit/miss nature, at least twice as many uncracked sites as sites are recommended. The uncracked sites are necessary to ensure that the NDI procedure is truly discriminating between cracked and uncracked sites and to provide an estimate of the false call rate. If the NDI system is based on a totally automated â versus a decision process, many fewer uncracked sites will be required. If any â values are recorded at the uncracked sites, their magnitude would provide an indication of the minimum thresholds that might be implemented in the application.

The impact of corrosion on the sustainment costs of an aging fleet is significant, particularly for transport aircraft. The presence of corrosion indicates a failure of the corrosion protection system and necessitates some sort of action in the maintenance plan. Regardless of the corrosion control maintenance strategy, NDI plays an important role in its implementation and the need exists to quantify the corrosion detection capability of the inspection system.

Several types of corrosion are typically found in aging airframes – uniform, pitting, intergranular, exfoliation, crevice (uniform and pitting), and stress corrosion cracking. Although there is a need to quantify the corrosion detection capability of an NDI system, at present there is no commonly accepted procedure for doing so. When characterizing the NDI capability for detecting cracks, the natural metric for measuring crack damage was the linear crack dimension used in damage tolerance analyses. The selection of the appropriate metric for corrosion damage, however, is not immediately apparent. There are different types of corrosion damage and different metrics can be used to quantify the damages. For example, in hidden corrosion in lap joints and doublers on fuselage structures there are several possible metrics: thickness loss, pit depth and/or frequency, surface roughness, and joint pillowing. When inspecting for intergranular and exfoliation corrosion, around fasteners, useful metrics might be the maximum radial distance that the corrosion extends from the fastener hole or the corrosion area about each fastener. In some sense, each metric plays a role in the effect that the corrosion defect has on the structure. Consequently, it is important to consider all of the metrics for a given application. Each corrosion type must be considered separately, but the important aspect of the metric is that it measures corrosion severity. Ideally, the metric should be based on an “effect of defects” study; however, in practice the important metrics are generally known, and, in order to keep the assessment focused, it becomes necessary to select only one metric at a time for detection assessment. If it is absolutely essential to include an evaluation of more than one metric, then multiple evaluations must be performed (one evaluation per metric). There is a necessary relation between the corrosion metric and the NDI technique. Obviously, the NDI technique must be responsive to changes in the corrosion damage metric. For example, in inspecting for hidden corrosion in lap joints, eddy current is responsive to thickness loss but may not be sufficiently responsive to pit depth. If pit depth is a critical parameter, a different NDI technique would be needed. In the case of a crack detection assessment, representative cracks can be grown quite successfully in the laboratory. Since methods of corrosion growth are not well established, most notably for hidden corrosion, at present it is necessary to include real aircraft pieces with real corrosion in the specimen sets to be used in NDI capability demonstrations. Finding specimens with appropriate levels of corrosion is not a trivial problem. Potential specimens can be obtained from obsolete aircraft and from depots. While such specimens may contain real corrosion, they are not necessarily representative for a particular application. Further, a “good” NDI system for detecting hidden corrosion would be needed to select the specimens with

varying degrees of corrosion damage. On the other hand, this situation does not eliminate the need for engineered and manufactured specimens. These specimens provide a level of control not available with the aircraft specimens. The type, location, and size of the defect (as measured by the chosen metric) can be controlled. The particulars of the engineered specimens must be determined from the specific metric chosen and the application. For thickness loss between layers, engineered specimens might include machined out areas of various depths and lateral dimensions. Experiment objectives also impact specimen designs. For example, a spatial resolution test would require a specially designed and manufactured specimen.

SECTION 3.2: EQUIVALENT INITIAL QUALITY METHOD

The Equivalent Initial Quality Method is presented for fastener holes since this is the most prevalent source of cracking in aircraft structures [Rudd & Gray, 1978]. Quality may be defined as a measure of the condition of the structure relative to imperfections, flaws, defects, or discrepancies that are either inherent in the material or introduced during manufacturing of the structure. The approach is to quantify these imperfections by representing them with fatigue cracks of a particular size and shape, such as corner cracks. If an initial quality representation is performed for each of a number of fastener holes, an equivalent initial quality statistical distribution can be used to quantify the quality of the fastener holes produced by certain manufacturing and processing procedures [Potter, 1978]. The initial quality representation, defined as the equivalent initial quality, can be obtained in the following manner. Consider a piece of structure with a fastener hole containing the defect of characteristic dimension l. This defect results in fatigue crack initiation and propagation when subjected to some known load history. Upon failure of the structure, a fractographic examination of the fracture surface is performed to obtain as much of the crack growth curve as possible. Analytical crack propagation analyses are performed until there is good agreement between the analytical prediction and the fractographic test data. The initial crack length (crack length when the load history is first applied), a_i, of the analytical crack growth curve that correlates best with the fractographic test data is defined as the equivalent initial quality. Hence, a_i is said to be the analytical equivalent of the actual defect of characteristic dimension, l, if each results in a crack size a_e after N_e cycles of the same load history have been applied. Hence, fastener holes that contain actual crack lengths less than a_e after N_e cycles have been applied are of better quality than those that contain actual crack lengths equal to or greater than a_e after N_e cycles.

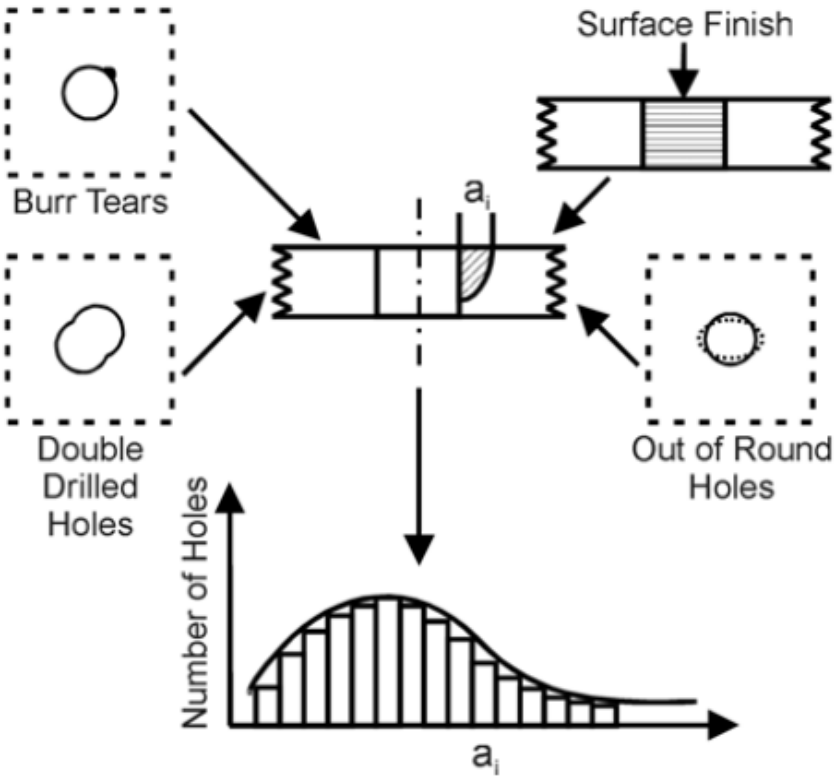

Figure 3.6: Parameters that Affect Fastener-Hole Initial Quality

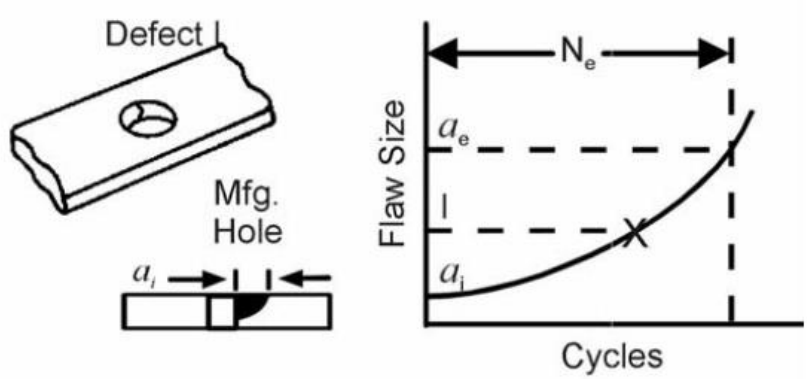

Figure 3.7: Definition of Equivalent Initial Quality

SECTION 3.3: PROOF TEST METHOD

Tiffany and Masters [1965] utilized the proof test as a means of guaranteeing that a potentially cracked structure would not fail during a defined period of operation. This guarantee results from the fact that all the cracks remaining in a proof-loaded structure must be smaller than those cracks which would have failed the structure during the proof test. Since the proof test loadings are typically larger than the maximum operating conditions, the post proof-tested structure's cracks are also expected to be substantially smaller than the cracks which would cause failure under operating loads.

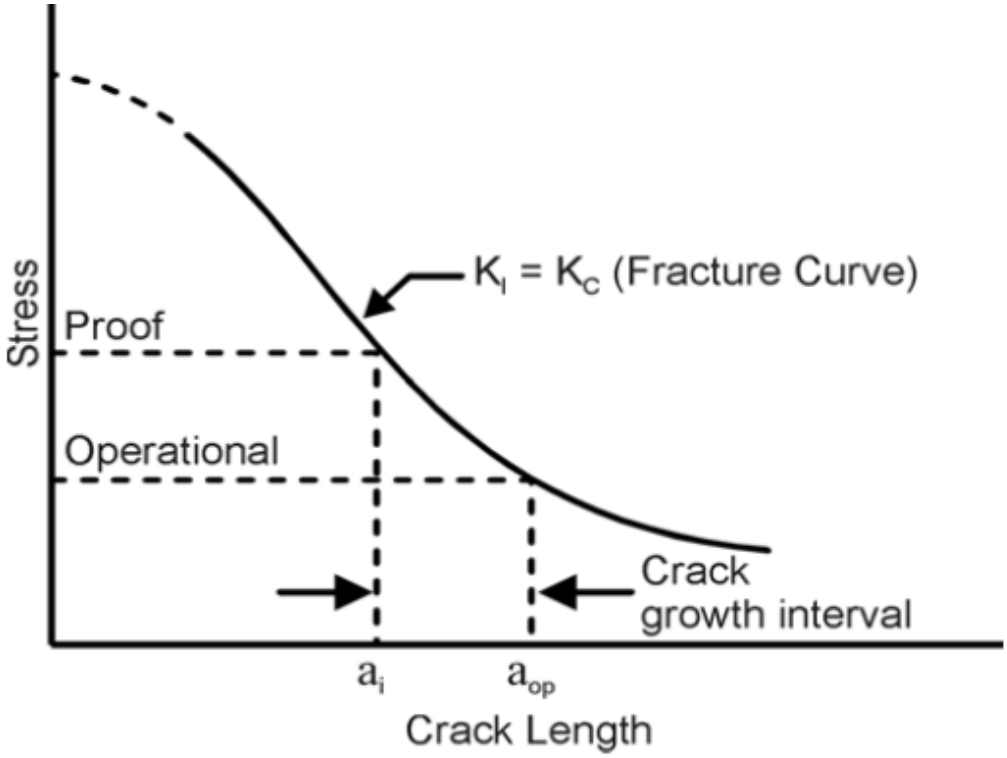

Figure 3.8: Fracture Critical Curve Defining Relationship Between Stress and Crack Length Associated with Fracture

All cracks larger than a_i will cause the structure to fail during the proof test loading, thus guaranteeing a "minimum" safe crack growth interval between a_i and the crack size (a_{op}) at which the operating conditions will cause failure. The interval established is the minimum safe interval because the structure may initially have cracks that are substantially smaller than the guaranteed initial size (a_i).

Tiffany and Masters [1965] designed the proof test conditions so that all cracks initially present in the structure and of sufficient size that they could grow to failure during the planned service operating period would fail the structure during the proof test. If the operating conditions and the crack growth mechanisms are known, then a crack growth life calculation can be performed to establish the minimum safe crack growth interval during which failure will not occur during service. The minimum safe crack growth interval extends from the largest allowable initial crack size (a^*_i) and the crack size (a_{op}).

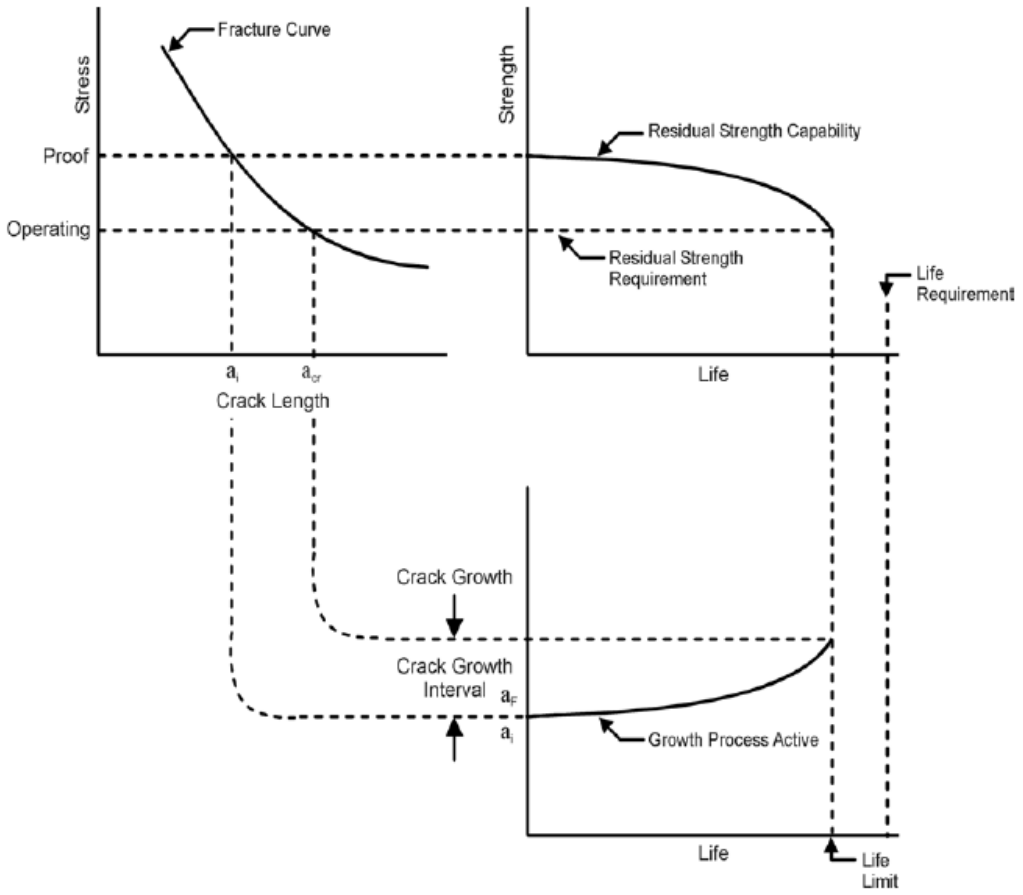

Figure 3.9: Schematic Illustrating the Relationship Between the Proof Test Diagram, the Residual Strength Capability and Crack Growth Life Interval

The life limit associated with the crack growth process and the decay of the residual strength capability is lower than the service life requirement. An increase in the proof stress if required, therefore, to decrease the corresponding crack size (a_i) to the maximum allowable crack size (a^*_i) and thus ensure a safe period of operation. Note that the stress-crack size diagram indicates that all cracks greater than a_i , present at the time of the proof test, will cause structure failure. Thus, the proof test ensures that when the structure enters service, its initial cracks will be no larger than the size associated with the proof test conditions.

The levels of proof test stress and the material's fracture toughness combine to establish the maximum initial crack size guaranteed by the proof test. Because material and stress variations will exist throughout any proof loaded structure, the designer of a proof test must be aware of several important material variations which could significantly affect the post-proof test crack size distribution. These important material variations are caused by changes in temperature, loading rate, thickness, and yield strength.

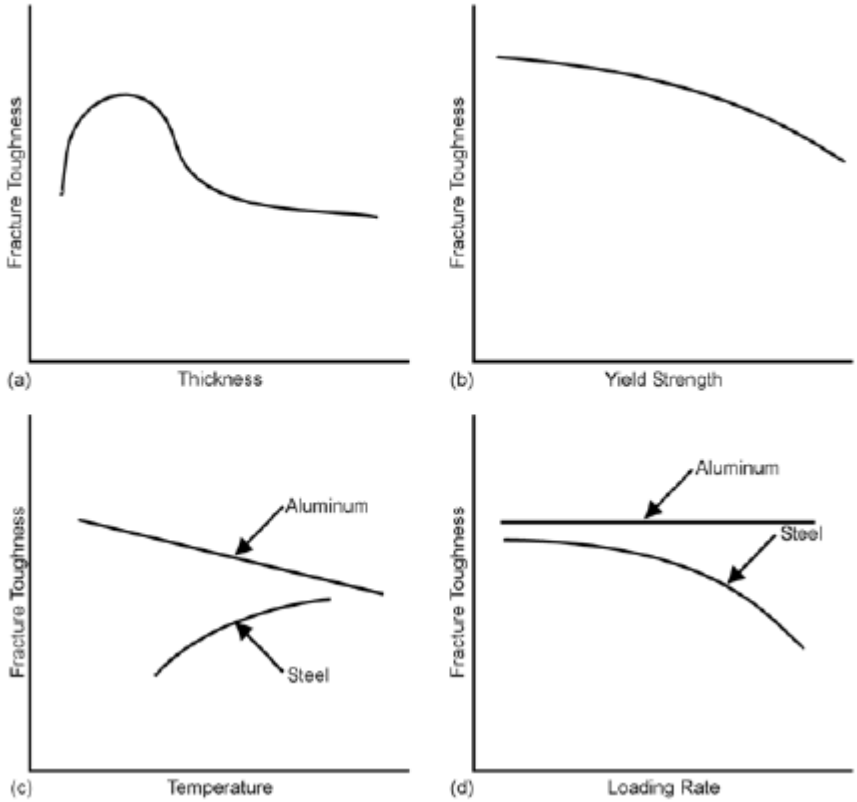

Figure 3.10: Fracture Toughness Varies as a Function of (a) Thickness, (b) Yield Strength, (c) Temperature, and (d) Loading Rate

A material's known response to temperature is utilized to select a low temperature condition for conducting the proof test. The lower fracture toughness exhibited at the low temperature is shown to extend the minimum safe crack growth interval substantially beyond what would have been expected for the same proof stress at the operating temperature conditions.

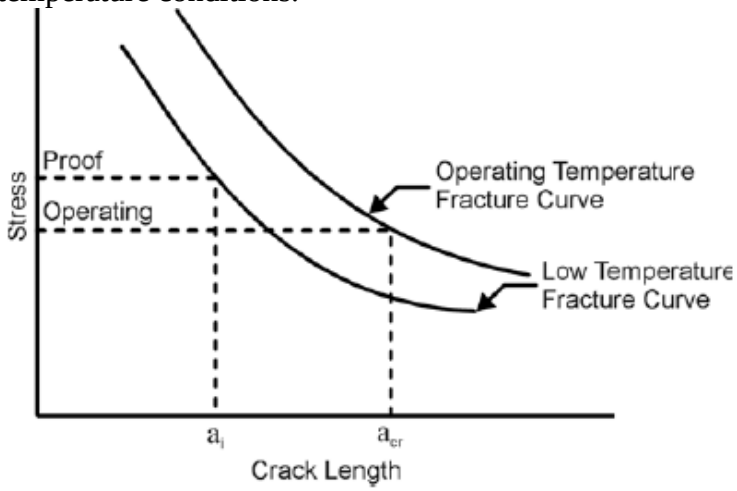

Figure 3.11: Using a Material's Low Temperature Fracture Sensitivity to Decrease Initial Crack Size and thus Increase the Minimum Safe Crack Growth Interval for a Given Proof Stressing Condition

"The minimum assumed initial flaw size shall be the calculated critical size at the proof test stress level and temperature using procuring activity approved upper-bound of the material fracture toughness data." The concept of using an approved upper-bound for the

fracture toughness ensures a worst case assumption for the maximum allowable initial crack size and the minimum safe crack growth interval.

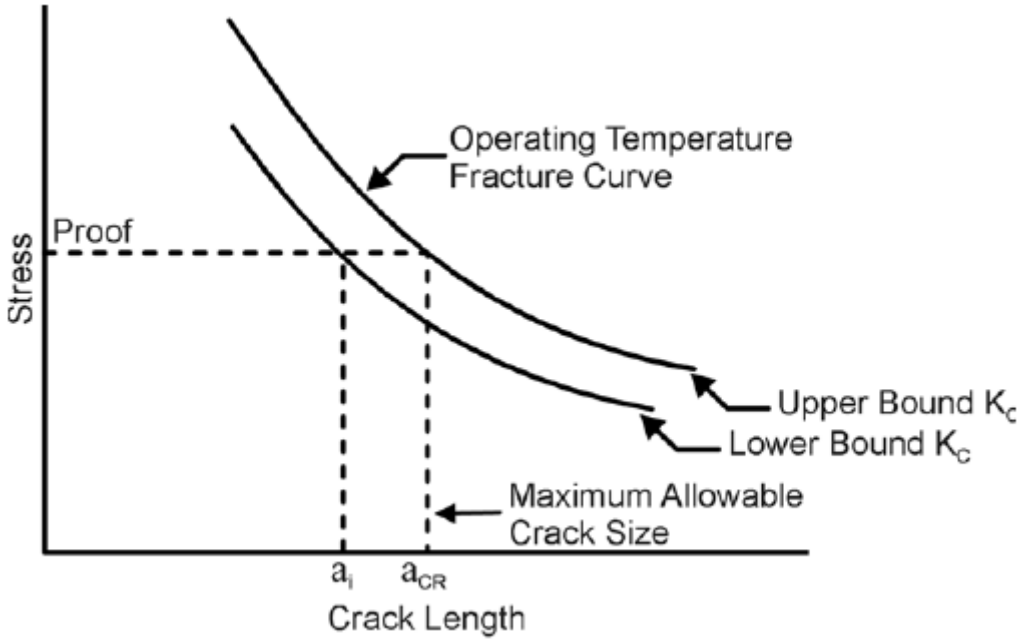

Figure 3.12: Influence of Fracture Toughness Variation on the Maximum Allowable Crack Size

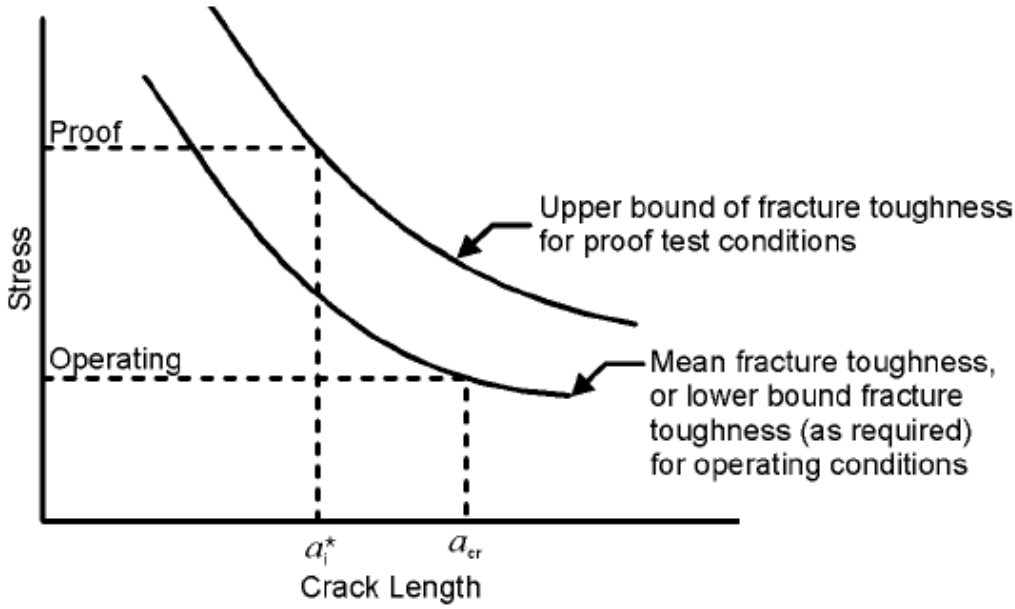

Figure 3.13: Description of Procedure Used to Establish Initial Crack Size and the Minimum Safe Crack Growth Interval According to JSSG-2006, A.3.12.1

SECTION 3.4: ANALYSIS OF DAMAGE GROWTH

The cracks existing in all primary aircraft structure shall not grow to a size to cause loss of the aircraft at a specified load within a specified period. Showing compliance with these requirements implies that the rate of growth of the assumed flaws must be predicted.

The analysis procedure for crack-growth prediction requires the following steps:

1. Find baseline crack growth data
2. Select a retardation model; select and apply an integration routine

3. Establish a stress history and mission mix
4. Determine the stress-intensity factor

Crack growth is a result of cyclic loading due to gusts and maneuvers (fatigue cracking), or of the combined action of sustained loading and environment (stress-corrosion cracking), or both. The most common crack growth mechanisms are fatigue crack growth and environment-assisted (corrosion) fatigue crack growth. Certain aircraft parts, especially high-strength forgings, may be liable to stress-corrosion cracking. Since there is a design threshold for stress corrosion, proper detail design and proper material selection can minimize or prevent stress corrosion. Fatigue cracking is difficult to prevent, but it can be controlled.

To predict crack growth behavior, the following information must be available:

• The stress-intensity factor, described as a function of crack size, for the relevant structural and crack geometry;

• The stress (load) – time history, described for the structural location component or structure under consideration;

• The baseline crack growth properties (constant amplitude crack growth rate data), described as a function of the stress intensity factor, for the material and for the relevant environment;

• A damage integration routine that integrates the crack growth rate to produce a crack growth curve, and uses the proper stress-time history, the proper stress intensity formulation, and an appropriate integration rule.

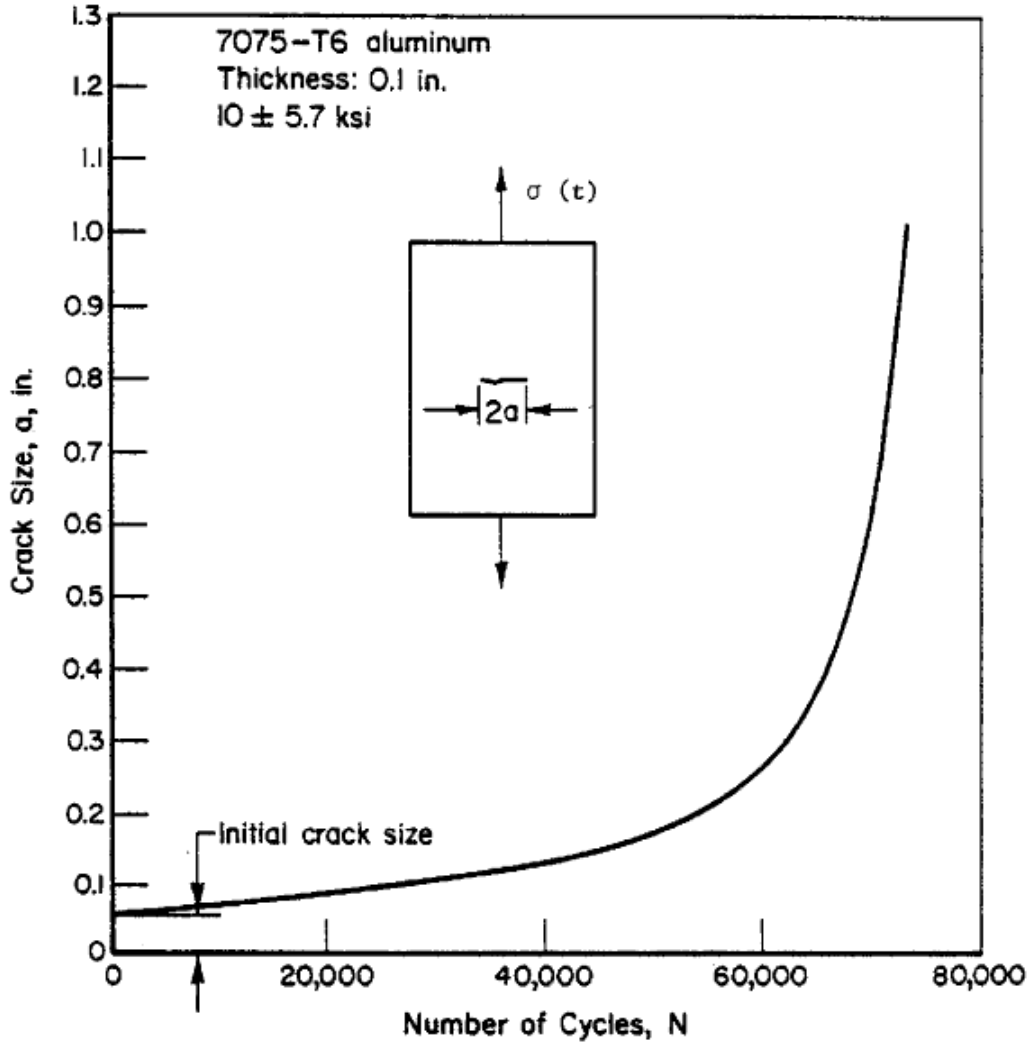

Figure 3.14: Typical Crack Growth-life Curve

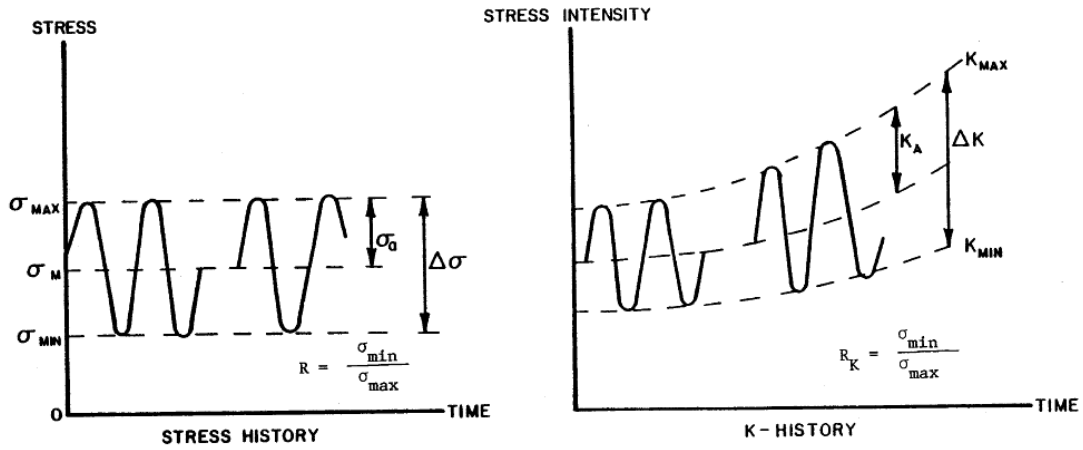

Figure 3.15: Definition of Terms for Fatigue Crack Growth and Stress Intensity

The stress history can be converted into a stress intensity factor history at a given crack length by multiplying the stress history by the stress intensity factor coefficient. It is theoretically difficult to define a negative stress intensity factor that happens if the stress becomes compressive. In this case, the crack closes and the crack tip stress field loses its singularity character; thus, the stress intensity factor ceases to have meaning. The operational quality of the negative stress intensity factors calculated for compressive stress situations has been given a lot of consideration by the aerospace industry and by ASTM, specifically its subcommittee on sub-critical crack growth (ASTM E24.04). ASTM has chosen to provide the following definitions when the minimum stress (σ_{min}) is less than zero:

$$K_{min} = 0 \text{ if } \sigma_{min} < 0 \qquad \Delta K = K_{max} \text{ if } \sigma_{min} < 0$$

In the elastic case, the stress-intensity factor alone is sufficient to describe the stress field at the tip of a crack. When the plastic zone at the crack tip is small compared with the crack size, the stress-intensity factor gives a good indication of the stress environment of the crack tip. Two different cracks that have the same stress environment (equal stress-intensity factors) will behave in the same manner and show the same rate of growth. Since two parameters are required to characterize the fatigue cycle, two parameters are required to characterize crack growth rate behavior. The crack growth rate per cycle, da/dN, can be generally described with:

$$\frac{da}{dN} = f(\Delta K, R) \quad or = g(K_{max}, R)$$

where a is the crack length, N is the number of cycles, and R is the stress ratio associated with the stress cycle.

Currently, the fatigue crack growth rate (FCGR) descriptions are carefully selected to provide accurate mean trend descriptions of the specific data collected to support a materials evaluation or structural design.

One modeling procedure that has consistently shown itself to range among the most accurate FCGR descriptions for predicting lives is the table look-up scheme . For life prediction purposes, many aircraft companies have gone to a table look-up scheme in which they describe crack growth rate as a function of ΔK for specific values of fatigue crack growth rate or vice versa, i.e., da/dN is described for specific values of ΔK.

Unlike tensile strength and yield strength, fatigue crack growth rate (FCGR) behavior is not a consistent material characteristic. The FCGR is influenced by many uncontrollable factors. As a result, a certain amount of scatter occurs. Therefore, crack growth predictions should be based on factors relevant to the conditions in service.
Among the many factors that affect crack propagation, the following should be taken into consideration for crack growth properties:

Material production:
• Type of product (plate, extrusion, forging)
• Heat treatment
• Orientation with respect to grain direction
• Manufacturer and batch
• Thickness
Environmental conditions:
• Environment
• Temperature
• Frequency
Several factors pertaining to the material production affect crack growth. The crack propagation characteristics for a particular alloy differ for plates, extrusions, and forgings. The latter may exhibit large anisotropy, which may have to be considered in the growth of surface flaws and corner cracks, which grow simultaneously in two perpendicular directions. Closely related to this are other processing variables, particularly the heat treatment.
In view of the factors that influence crack growth properties, predictions of crack growth should be based on material data that pertain to the product form. Spot checks may be necessary to account for variability in heats and/or manufacturer.
The factors pertaining to environmental conditions are associated with the environmental circumstances. A lightly corrosive environment (humid air) gives rise to higher crack growth rates than a dry environment. At low temperatures, the reaction kinetics are slower and the air contains less water vapor. This may reduce crack propagation rates in certain alloys. In view of the effect of environment on crack growth, the data used for life predictions should represent the effect of the expected environment and temperature.
Accurate mean trend FCGR descriptions result in accurate fatigue crack life descriptions. People have worried in the past about trying to account for the substantial amount of scatter that exists in the crack growth rate data. The amount of crack growth between crack measurements and the accuracy of this incremental crack growth measurement determines a large part of the scatter. Another inherent reason for data scatter is due to the differentiation techniques that one uses to reduce the data. Worrying about the random (within specimen) scatter in fatigue crack growth rates is really not that important from a life estimation standpoint. What has been found from analyses of multiple specimen data sets is that the width of the scatter-bands associated with specimen to specimen mean trend variations in FCGR is closely related to the variability in crack growth-life behavior. The coefficient in variation of crack growth lives is sometimes similar in magnitude to the root mean square (percentage) error associated with fatigue crack growth rate modeling. When conservative estimates in crack growth lives are desired, the upper bound of the real scatter-band determined on the basis of four or more specimens should be used.

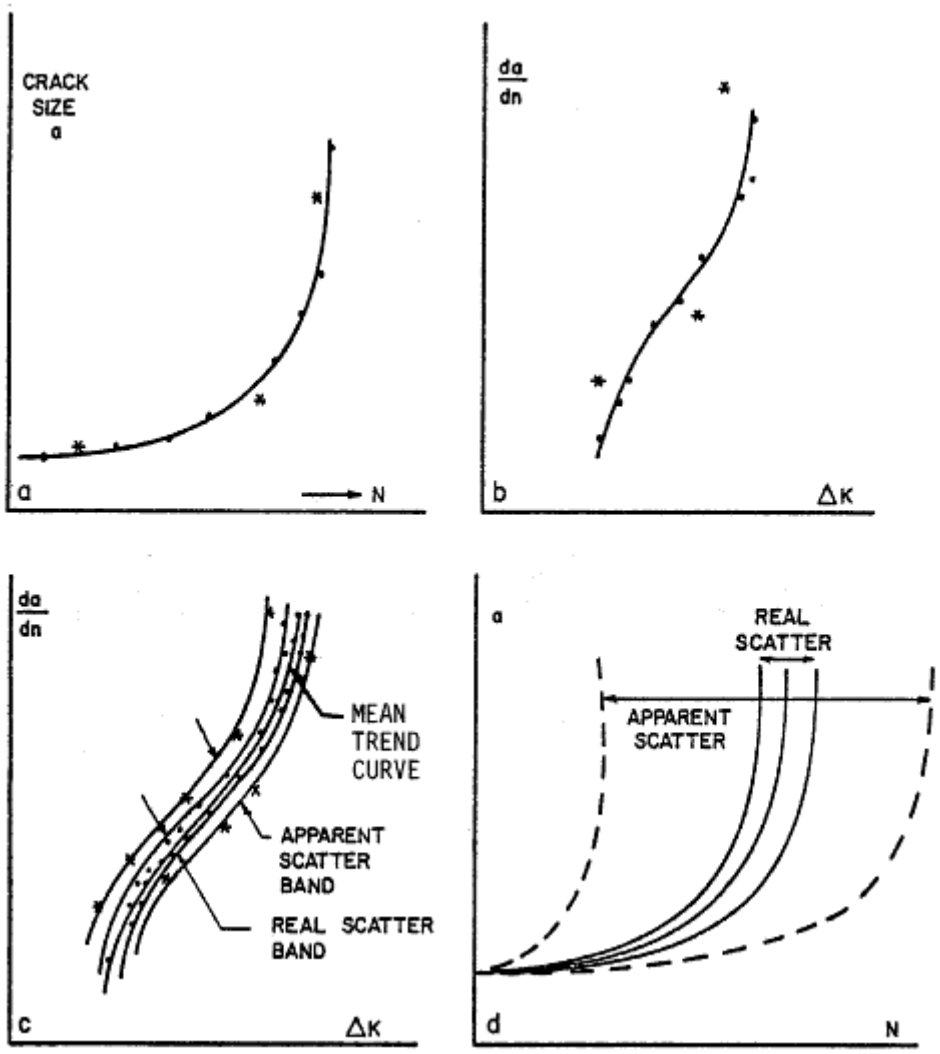

Figure 3.16: Crack Growth Data Scatter for Identical Conditions

Many engineering materials exhibit some cracking behavior under sustained loading in the presence of an environment (thermal and/or chemical). The type of cracking behavior for many chemical environments is referred to as stress-corrosion cracking behavior. The mechanism for this attack process has been attributed to the chemical reactions that take place at the crack tip and to diffusion of reactive species (particularly hydrogen) into the high stressed region ahead of the crack. The cracking process has been noted to be a function of time and it is highly dependent on the environment, the material, and the applied stress (or stress-intensity factor) level.

For a given material-environment interaction, the stress-corrosion-cracking rate has been noted to be governed by the stress-intensity factor. Similar specimens with the same size of initial crack but loaded at different levels (different initial K values) show different times to failure [Brown, 1968; Sullivan, 1972; Chu, 1972].

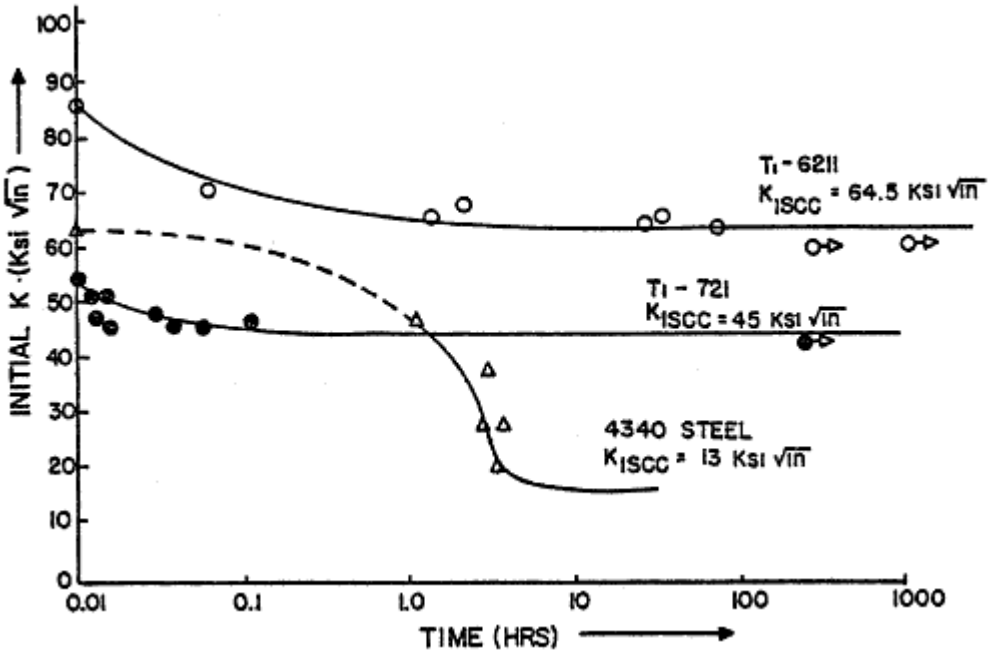

Figure 3.17: Stress Corrosion Cracking Data

If the load is kept constant during the stress-corrosion-cracking process, the stress-intensity factor will gradually increase due to the growing crack. When the crack has grown to a size so that K becomes equal to $K_{Ic,}$ the specimen fails. The stress-corrosion threshold and the rate of growth depend on the material and the environmental conditions.

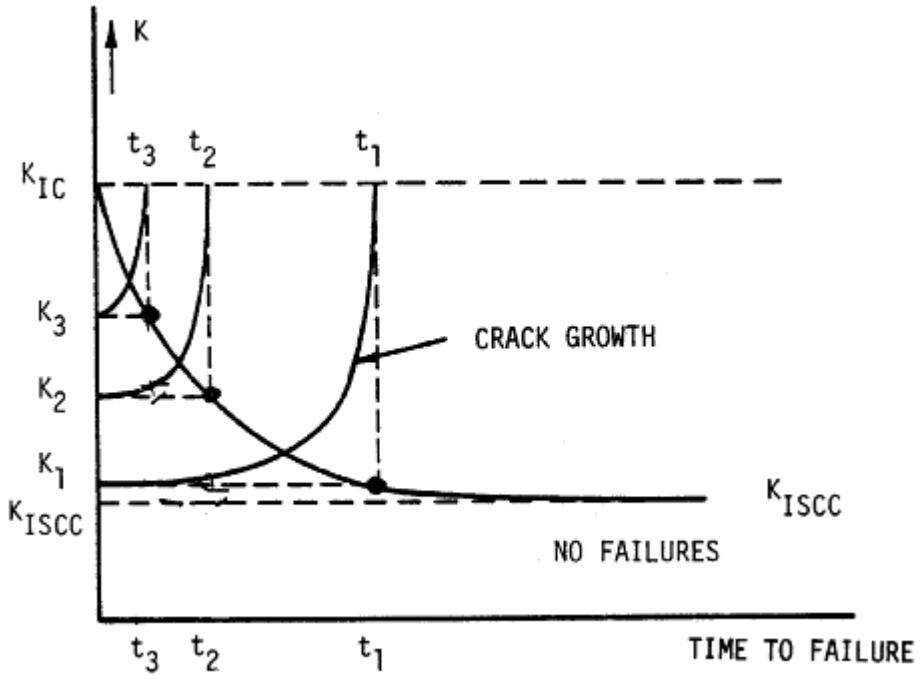

Figure 3.18: Stress Corrosion Cracking

Baseline fatigue data are derived under constant-amplitude loading conditions, but aircraft components are subjected to variable amplitude loading. If there were not interaction effects of high and low loads in the sequence, it would be relatively easy to establish a crack-growth curve by means of a cycle-by-cycle integration. However, interaction effects of high and low loads largely complicate crack-growth under variable-amplitude cycling.

A high load occurring in a sequence of low-amplitude cycles significantly reduces the rate of crack-growth during the cycles applied subsequent to the overload. This phenomenon is called retardation.

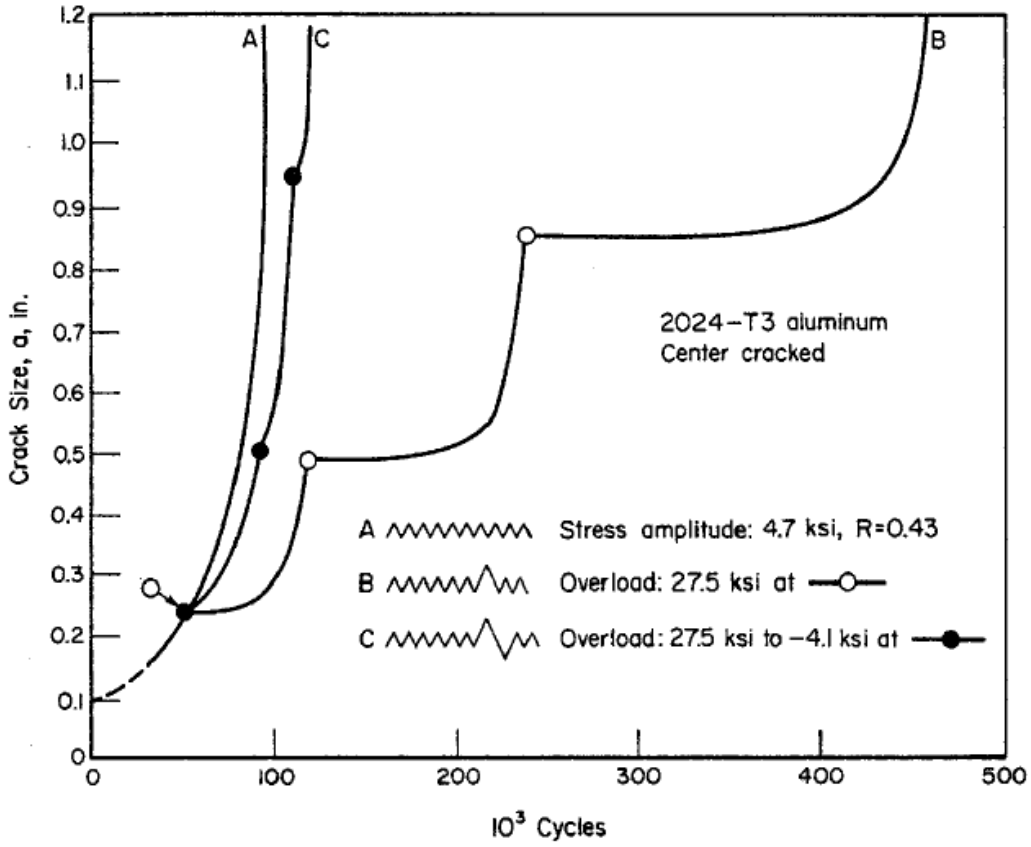

Figure 3.19: Retardation Due to Positive Overloads, and Due to Positive-Negative Overload Cycles

In other experiments, the same constant-amplitude loading was interspersed with overload cycles. After each application of the overload, the crack virtually stopped growing during many cycles, after which the original crack-growth behavior was gradually restored. Retardation results from the plastic deformations that occur as the crack propagates. During loading, the material at the crack tip is plastically deformed and a tensile plastic zone is formed. Upon load release, the surrounding material is elastically unloaded and a part of the plastic zone experiences compressive stresses. The larger the load, the larger the zone of compressive stresses. If the load is repeated in a constant amplitude sense, there is no observable direct effect of the residual stresses on the crack-growth behavior; in essence, the process of growth is steady state. Measurements have indicated, however, that the plastic deformations occurring at the crack tip remain as the crack propagates so that the crack surfaces open and close at non zero (positive) load levels. These observations have given rise to constant amplitude crack-growth models referred to as closure models [Elber, 1971] after the concept that the crack may be closed during part of the load cycle.

When the load history contains a mix of constant amplitude loads and discretely applied higher level loads, the patterns of residual stress and plastic deformation are perturbed. As the crack propagates through this perturbed zone under the constant amplitude loading cycles, it grows slower (the crack is retarded) than it would have if the perturbation had not occurred. After the crack has propagated through the perturbed zone, the crack growth rate returns to its typical steady state level.

Two basic models have been proposed to describe the phenomenon of crack retardation. The first model is based on the concept of the compressive residual stress perturbation and the second on the concept of plastic deformation with enhanced crack wedging and more closure.
If the tensile overload is followed by a compressive overload, the material at the crack tip may undergo reverse plastic deformation and this reduces the residual stresses. Thus, a negative overload in whole or in part annihilates the beneficial effect of tensile overloads. Retardation depends upon the ratio between the magnitude of the overload and subsequent cycles. Sufficiently large overloads may cause total crack arrest. Hold periods at zero stress can partly alleviate residual stresses and thus reduce the retardation effect [Shih & Wei, 1974; Wei & Shih, 1974], while hold periods at load increase retardation. Multiple overloads significantly enhance the retardation.

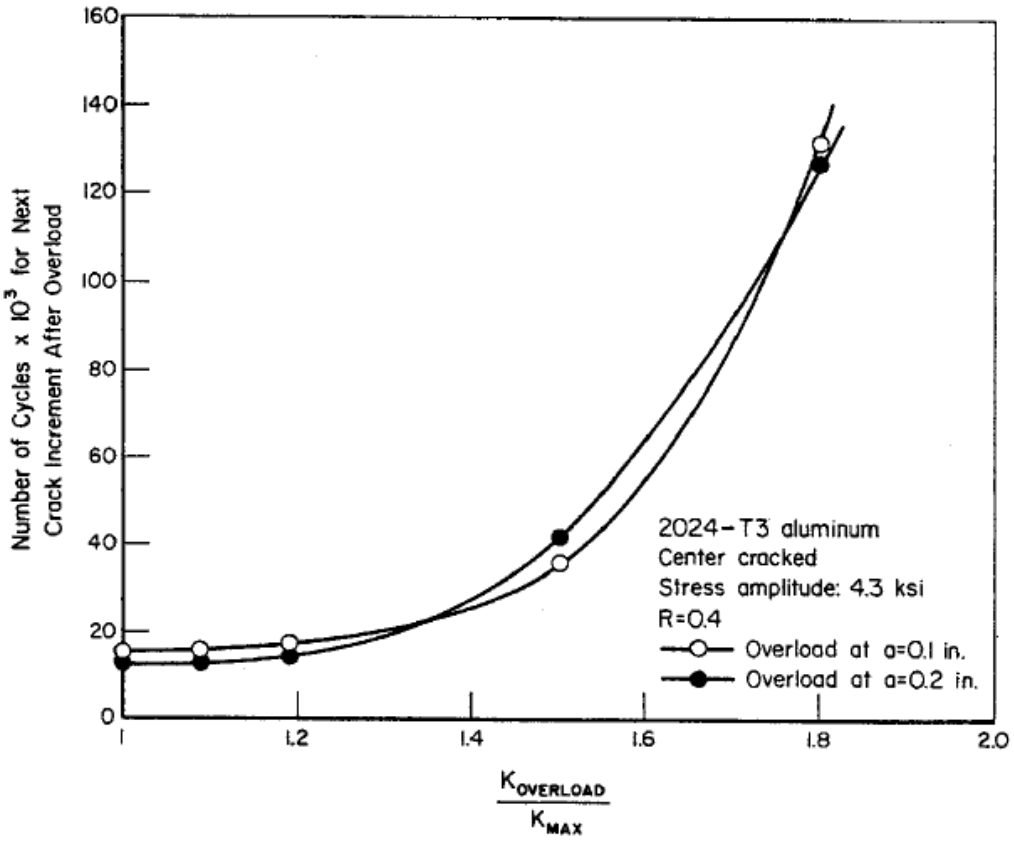

Figure 3.20: Effect of Magnitude of Overload on Retardation

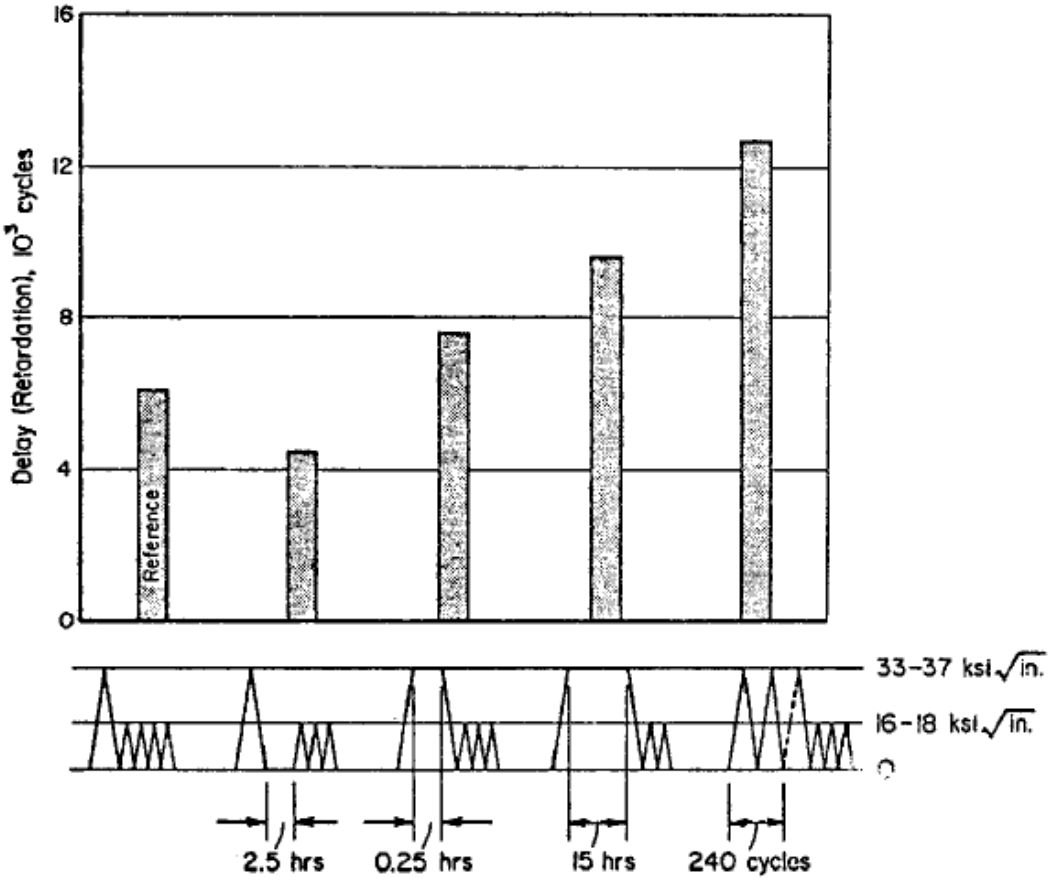

Figure 3.21: Retardation in Ti-6V-4Al; Effect of Hold Periods and Multiple Overloads

An actual service load history contains high- and low- stress amplitudes and positive and negative "overloads" in random order. Retardation and annihilation of retardation becomes complex, but qualitatively the loading produces behavior that is similar to a constant-amplitude history with incidental overloads. The higher the maximum stresses in the service load history, the larger the retardation effect during the low-amplitude cycles. Negative stress excursions reduce the retardation effect and tend to enhance crack-growth. When the magnitude of the higher loads are reduced (or clipped) without eliminating the cycle, i.e., higher loads are reset to a defined lower level, the cracking rates are observed to speed up.

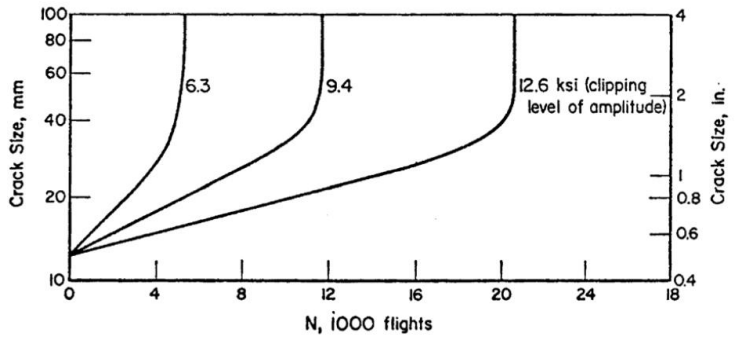

Figure 3.22: Effect of Clipping of Higher Loads in Random Flight-by-Flight Loading on Crack Propagation In 2024-T3 Al Alloy

It was also observed that negative stress excursions reduce the retardation effect and omission of the ground-air-ground (G-A-G) cycles (negative loads) in the tests with the highest clipping level resulted in a longer crack growth life for the same amount of crack

growth. Ordering the sequences of the loads, low-high, low-high-low, or high-low increases the crack-growth life, the more so for larger block sizes. Hence, ordering should only be permitted if the block size is small.

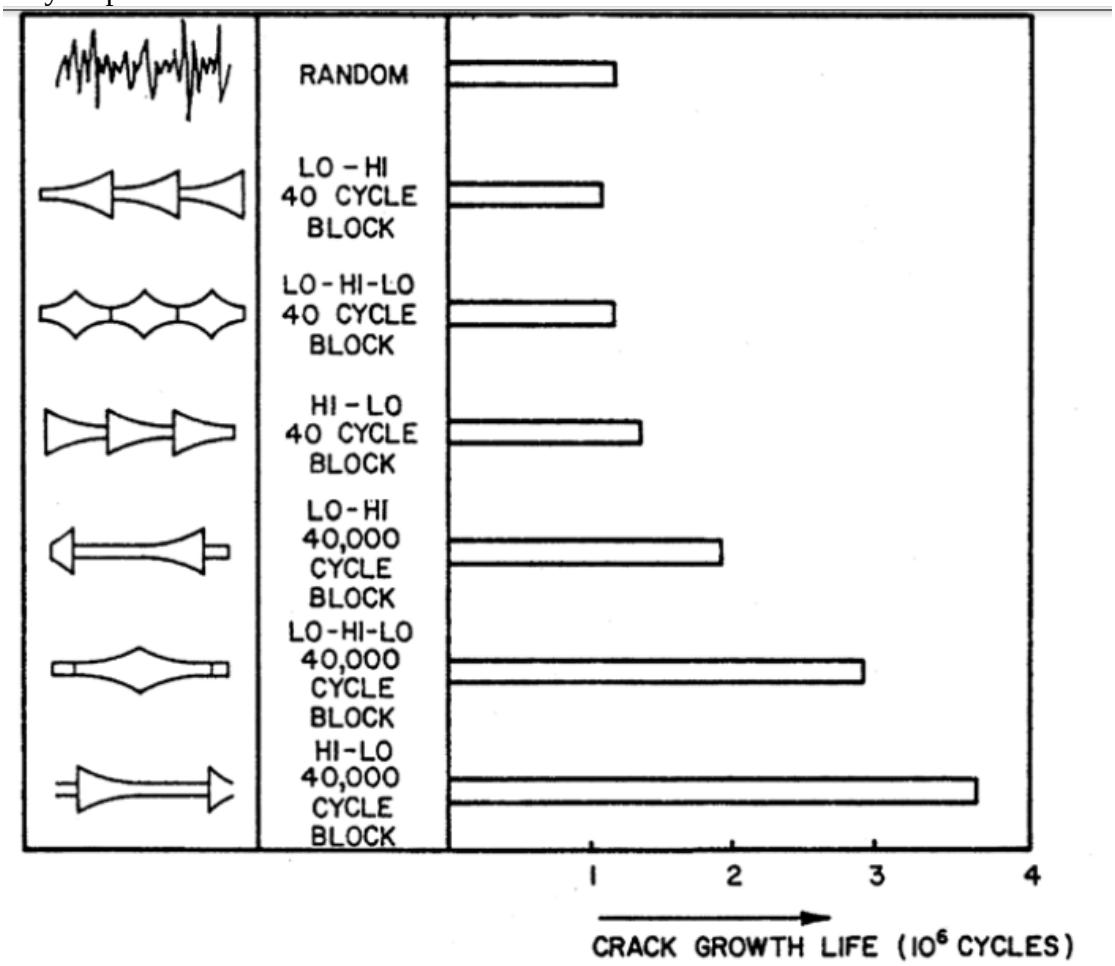

Figure 3.23: Effect of Block Programming and Block Size On Crack Growth Life All Histories Have Same Cycle Content; Alloy: 2024-T3 Aluminum

Several computer programs are available for general uses that include one or more of the retardation models in a crack-growth-integration scheme. Most airframe companies, have their own in-house computer program for performing variable-amplitude fatigue life calculations.

In order to predict the crack-growth behavior of an aircraft structure, the designer needs to know the sequence of stress cycles applied during the life of the structure. This stress history for a new design is developed from the service life requirements and the mission profile information specified by the procurement activity. Based on this information a repeated load history due to ground handling, flight maneuvers, gusts, pressurization, landing, store ejection, and any other load source is developed. The stress history at any given point is then determined from the applicable load/stress relations.

The load sequence developer works from the service life requirement summary and the mission profiles as given by the aircraft procurement documents. The service life data contains the total flight hours, expected calendar year life, number of missions to be flown, identification of mission types, and number of touch and go and full stop landings. The mission profile description provides the time variation of the airspeed, altitude, and gross

weight. Each mission is divided into segments, as shown, which can be easily characterized by the type and frequency of the various load sources.

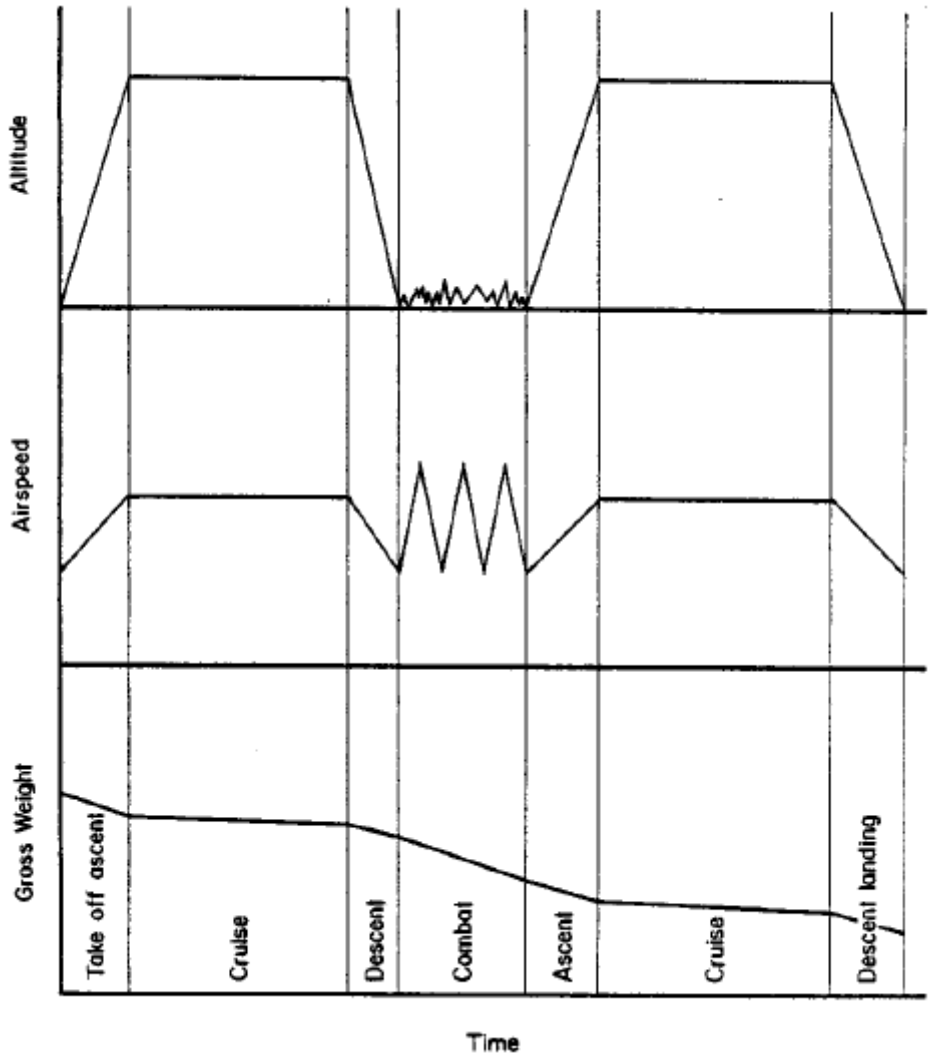

Figure 3.24: Mission Profile and Mission Segments

The load spectrum for each mission segment is characterized by a table of occurrences of a load parameter. The commonly used parameter is the normal load factor at the aircraft center-of-gravity, n_z. Such a table can be presented as an exceedance plot, which shows the number of occurrences that exceed specified values during a specified time period. MIL-A-8866 presents tabular exceedance data for six classes of aircraft, broken out by mission segment. The number of identified segments varies from three to seven. These tables give the number of exceedances per 1,000 mission hours. The total number of exceedances is on the order of 10^5 - 5 x 10^5.

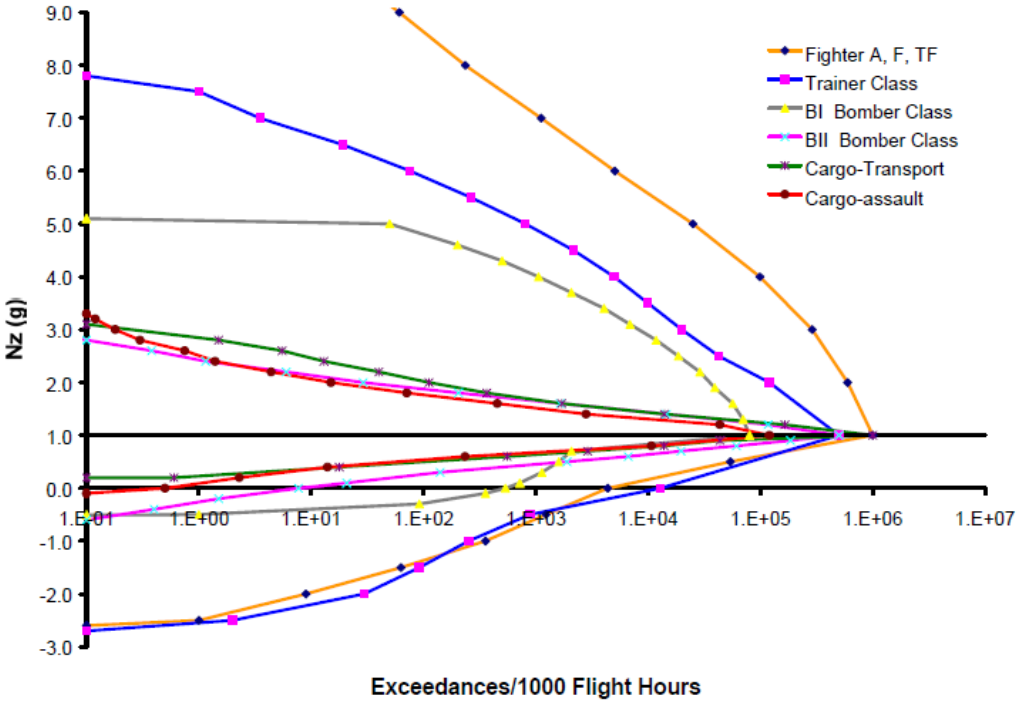

Figure 3.25: Maneuver Spectra According to MIL-A-8866

These three basic pieces of information, the service life summary, the mission profiles, and the load factor spectra are converted into the loads history and the stress history at critical locations on the aircraft.

The preparation of a flight-by-flight load sequence is done in five essential steps:

1. Prepare the representative life history mission ordering.
2. Define mission segment flight conditions.
3. Determine the number of maneuver and gust load cycles at each load level in each mission segment.
4. Order the maneuver and gust load cycles within each mission segment.
5. Place load cycles from other sources within each mission segment.

The establishment of the mission sequence for the life history of the aircraft is usually done in a deterministic manner and is based on past observations of similar type aircraft. It is reasonable to assign missions in blocks as flying assignments usually follow specific groupings of missions as various flying skills are being stressed. Missions occurring relatively few times are usually interspersed throughout the sequence either singly or in small numbers. It is recommended that the severest missions be somewhat evenly spaced throughout the sequence. It is common to treat the sequence as a repeating block. Each block would contain all mission types and represent some proportion of the total flight history. Blocks of five hundred or one thousand flight hours have been found to be convenient. For example: for a 6,000 hour aircraft life, a 500 hour block would be repeated twelve times to obtain the total sequence.

Each mission is divided into segments for ease in defining the loading cycles. This division is specified in the mission profile. The same ordering of mission segments is used each time a mission occurs. This division is useful in two ways: it facilitates the identification of load spectra and it provides for the definition of the flight condition parameters. The flight condition parameters are the values of airspeed, altitude, gross weight, configuration, and time used for each mission segment. These conditions are selected from the mission profile to give a set of representative loading conditions for each segment. These are combined with the load level indicator to compute the loads.

The determination of the number and severity of loads assigned to each mission segment is based on a spectrum of a load level indicator. For most applications this is the normal load factor, n_z. This spectrum is obtained from analysis of previous usage of similar aircraft in the case of a design specification, or from current usage of the aircraft being analyzed in the case of an update to the design analysis.
The load information for an aircraft structure is usually in the form of an exceedance spectrum. The spectrum is an interpretation of in-flight measurements of center-of-gravity accelerations or stresses at a particular location. The interpretation consists of a counting procedure, which counts accelerations (or stresses) of a certain magnitude, or their variation (range).

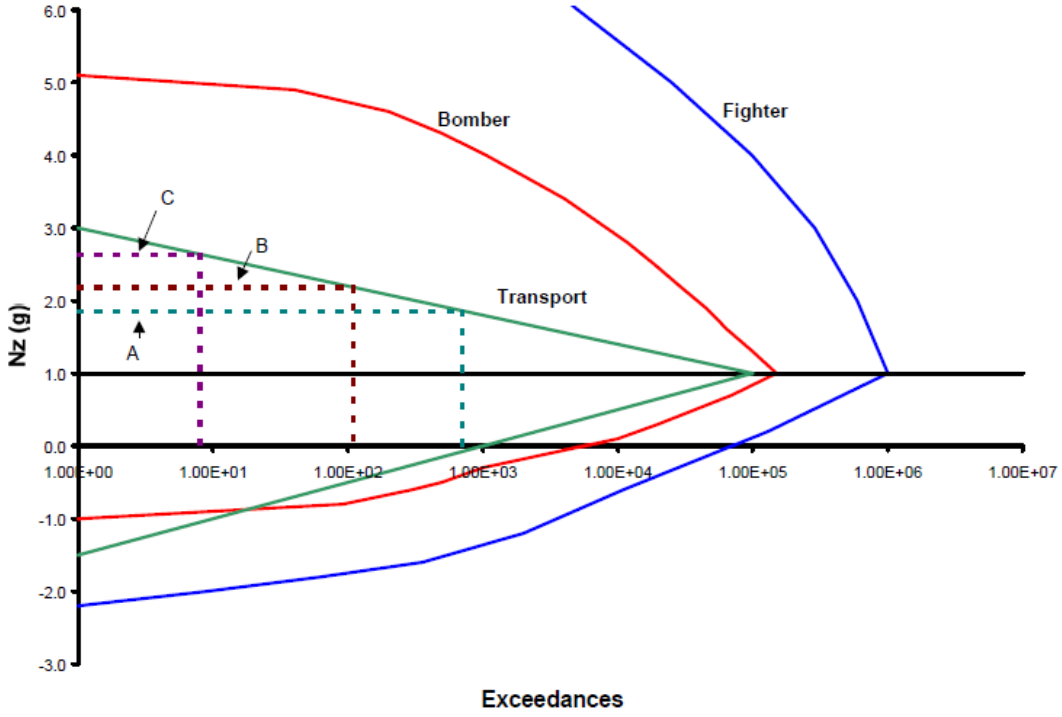

Figure 3.26: Exceedance Spectra for 1000 Hours

Level A is exceeded n_1 times and level B is exceeded n_2 times. This means that there will be n_1-n_2 events of a load between levels A and B. These loads will be lower than B, but higher than A. The exact magnitude of any one of the n_1-n_2 loads remains undetermined.
One can define an infinite number of load levels between A and B. However, there are only n_1-n_2 occurrences, which means that while the number of load levels to be encountered is infinite; not every arbitrary load level will be experienced. Strictly speaking each of the n_1-n_2 occurrences between A and B could be a different load level. If one chose to divide the distance between A and B into n_1-n_2 equal parts, ΔA, each of these could occur once. Mathematically, a level $A+\Delta A$ will be exceeded n_1-1 times. Hence, there must be one occurrence between A and $A+\Delta A$. In practice, such small steps cannot be defined, nor is there a necessity for their definition.
If measurements were made again during an equal number of flight hours, the exceedance spectrum would be the same, but the actual load containment would be different. This means that the conversion of a spectrum into a stress history for crack-growth analysis will have to be arbitrary because one can only select one case out of unlimited possibilities.
Going to the top of the spectrum, level C will be exceeded 10 times. There must be a level above C that is exceeded 9 times, one that is exceeded 8 times, etc. One could identify these levels, each of which would occur once. In view of the foregoing discussion this

becomes extremely unrealistic. Imagine 10 levels above C at an equal spacing of ΔC, giving levels C, C+ΔC, C+2ΔC, etc. If level C is exceeded 10 times, all of these exceedances may be of the level C+3ΔC for another aircraft.
As a consequence, it is unrealistic to apply only one load of a certain level, which would imply that all loads in the history would have a different magnitude. Moreover, if high loads are beneficial for crack growth (retardation), it would be unconservative to apply once the level C+ΔC, once C+2ΔC, etc., if some aircraft would only see 10 times C.
Hence, the maximum load level for a fatigue analysis should be selected at a reasonable number of exceedances. (This load level is called the clipping level). From crack-growth experiments regarding the spectrum clipping level, it appears reasonable to select the highest level at 10 exceedances per 1,000 flights. The same dilemma exists when lower load levels have to be selected. Obviously, the n loads in 1,000 hours will not be at n different levels. A number of discrete levels has to be selected. This requires a stepwise approximation of the spectrum. The more discrete load levels there are, the closer the stepwise approximation will approach the spectrum shape. On the other hand, the foregoing discussion shows that too many levels are unrealistic. The number of levels has to be chosen to give reliable crack-growth predictions.
If the stepped approximation is made too coarse (small number of levels) the resulting crack-growth curve differs largely from those obtained with finer approximations. However, if the number of levels is 8 or more, the crack-growth curves are identical for all practical purposes. A further refinement of the stepped approximation only increases the complexity of the calculation; it does not lead to a different (or better) crack-growth prediction. Crack-growth predictions contain many uncertainties anyway, which means that one would sacrifice efficiency to apparent sophistication by taking too many levels. It turns out that 8 to 10 positive levels (above the in-flight stationary load) are sufficient. The number of negative levels (below the in-flight stationary load) may be between 4 and 10.

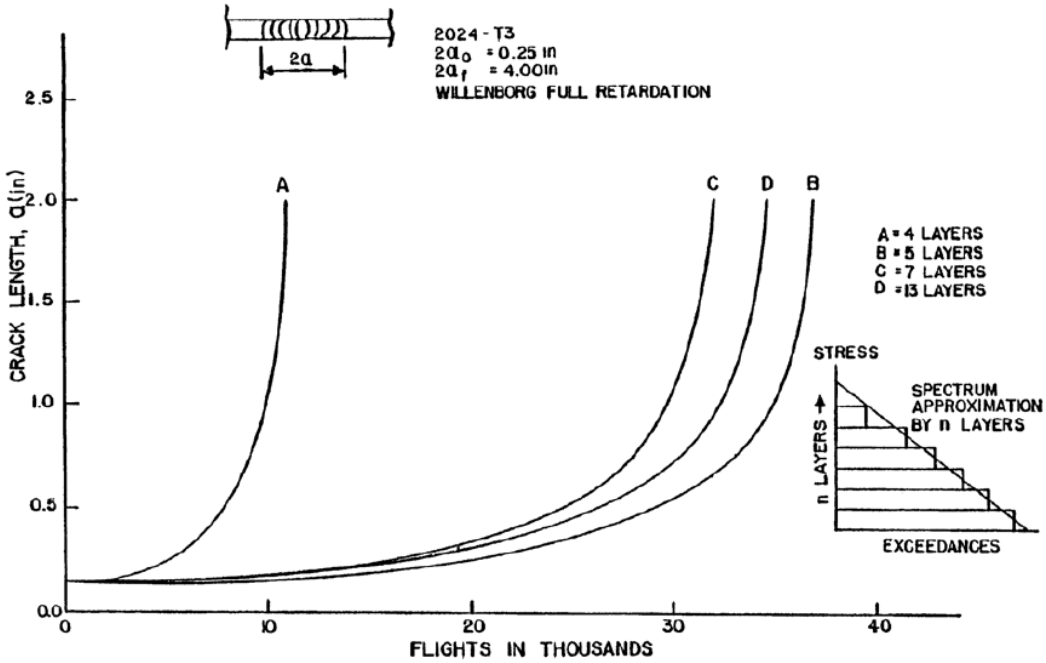

Figure 3.27: Fatigue-Crack Growth Behavior Under Various Spectra Approximations

Selection of the lowest positive level is also of importance, because it determines the total number of cycles in the crack-growth analysis. This level is called the truncation level. Within reasonable limits the lower truncation level has only a minor effect on the outcome of the crack-growth life. Therefore, it is recommended that this lower truncation level be

selected on the basis of exceedances rather than on stresses. A number in the range of 10^5 - 5 x 10^5 exceedances per 1,000 flights seems reasonable.

SECTION 4: DAMAGE TOLERANCE TESTING AND EVALUATION

Tests that support the development of damage tolerant aircraft structures range from simple element tests used to collect basic material properties to the full-scale article tests used to verify the damage tolerant characteristics of the complete structure. The damage tolerant tests have been subdivided into four categories: materials tests, quality control tests, analysis verification tests, and structural hardware tests.

The materials tests provide the basic materials data for structural life analyses and for residual strength calculations. For the most part, these tests are conducted as early in the design phase as practical, in order to aid in the selection of materials and in the sizing of the structure. Materials data covered by this category of tests include fracture toughness and crack growth resistance properties, as well as basic tensile, compression, bearing and shear data.

The quality control tests provide data that support the initial quality design assessments or ensure the uniformity of the production product. Requirements for these tests are defined after the preliminary sizing and the identification of fracture critical parts have been accomplished. Quality control data covered by this category of tests include equivalent initial quality (EIQ), fracture toughness, tensile strength and notch tensile strength data.

The analysis verification tests provide data that define the accuracy of the damage tolerance analysis tools relative to their ability for predicting the crack growth behavior of the structure under operational conditions. These tests are typically conducted during the design analysis and development testing phase of the contract prior to testing the full-scale structure. Additional testing may also be required subsequent to the full-scale flight and ground tests to support interpretation and evaluation of cracking problems. Analysis verification tests include those tests that are used to verify stress-intensity factor calculations, residual strength methods, crack growth calculations and test spectrum truncation procedures.

The structural hardware tests have two functions: (a) to support the verification of the complete structural design, and (b) to define those areas of the structure that need additional attention. These tests are scheduled so that there is sufficient time to incorporate structural changes into production aircraft. In fact, production go-ahead is predicated on achieving one design lifetime of flight-by-flight loading in the full-scale durability test per JSSG-2006 paragraph 3.11.1. Structural hardware tests include joint tests, component tests, assembly tests, as well as full-scale structural tests.

SECTION 4.1: MATERIALS TESTS

The material tests provide the basic materials data for conducting structural crack growth life and residual strength analyses. The tests are relatively simple to conduct compared to many of the tests in the other categories. Typically, a large number of material tests are conducted in the early part of the design phase so that the appropriate materials can be selected to meet design objectives. The materials selection process may concentrate on specific design criteria relative to requirements of cost, weight, strength, stiffness, fracture toughness, corrosion resistance, and crack growth resistance to fatigue loading. The damage tolerance materials tests must, of course, be supplemented by other tests, e.g. tensile tests, exfoliation tests, etc., in order to ensure that preliminary material trade studies result in the appropriate choices for the given application. Typically, before the final bill of materials for the structure is signed off, additional in-depth structural tests must be accomplished to verify initial material choices and to identify additional criteria not initially considered.

Residual strength and crack growth life analyses are supported by a damage integration package that requires the definition of fracture toughness and crack growth rate properties for the materials being considered. A material's crack growth behavior is a function of a wide number of different factors such as anisotropy, environment, loading rate, processing variables, product form, thickness, etc. The damage integration package accounts for these effects by utilizing data collected from specimens (a) that are representative of the material variables of interest, (b) that contain cracks which grow in the appropriate direction, and (c) that are loaded in the manner representative of operational conditions. Standardization of test methodologies, data reduction and reporting procedures are to a large part responsible for the success of the current life prediction models.

The predictive accuracy of any lifing model is only as good as the quality of the baseline crack growth and fracture data inputs. The American Society for Testing and Materials (ASTM) is the world leader in producing consensus testing standards to accurately identify materials behavior in general – and most important to the DTDH – have been the leader in developing procedures usable for damage tolerance applications. The ASTM Book of Standards is published yearly to give all users of the test methods and analytical procedures the latest versions available.

Standard	Title	Specimens	Results
E399	Standard Test Method for Plane-Strain Fracture Toughness of Metallic Materials	C(T), SE(B), A(T), DC(T), A(B)	K_{Ic}
E561	Standard Practice for R-Curve Determination	M(T), C(T), C(W)	K_R
E647	Standard Test Method for Measurement of Fatigue Crack Growth Rates	M(T), C(T), ESE(T)	da/dN vs ΔK
E740	Standard Practice for Fracture Testing with Surface-Crack Tension Specimens	SC(T)	K_{Ie}
E812	Standard Test Method for Crack Strength of Slow-Bend Precracked Charpy Specimens of High Strength Metallic Materials	Charpy	σ_c
E1304	Standard Test Method for Plane-Strain (Chevron-Notch) Fracture Toughness of Metallic Materials	Chevron-notch	K_{IvJ}, K_{IvM}
E1457	Standard Test Method for Measurement of Creep Crack Growth Rates in Metals	C(T),	da/dt
E1681	Standard Test Method for Determining a Threshold Stress Intensity Factor for Environment-Assisted Cracking of Metallic Materials	MC(W), SE(B), C(T)	K_{IEAC}, K_{EAC}
E1820	Standard Test Method for Measurement of Fracture Toughness	SE(B), C(T), DC(T)	K_{Ic} , J_{Ic}, CTOD
E1823	Standard Terminology Relating to Fatigue and Fracture Toughness	All	NA
E1942	Standard Guide for Evaluating Data Acquisition Systems Used in Cyclic Fatigue and Fracture Mechanics Testing	All	NA

Figure 4.1: ASTM Standards for Damage Tolerant Testing

Each of the Standard Test Methods used for damage tolerance testing have a selection of test specimens that are preferred for each test.

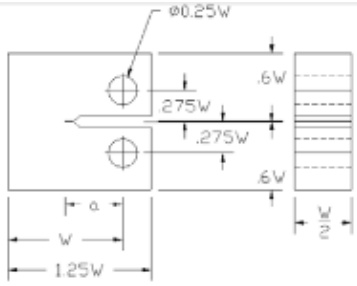

	K_{IC}	R	EAC	J_{IC}
W/B	2-4	Plane Stress	1-2	2-4

(a) Compact Tension Specimen

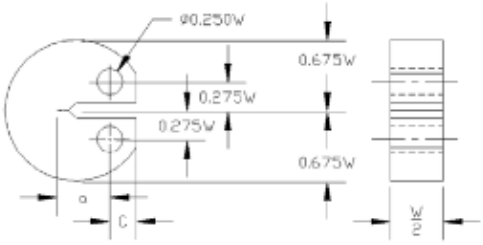

	K_{IC}	J_{IC}
W/B	2-4	2-4

(c) Disk-Shaped Compact Specimen DC(T)
Standard Proportions

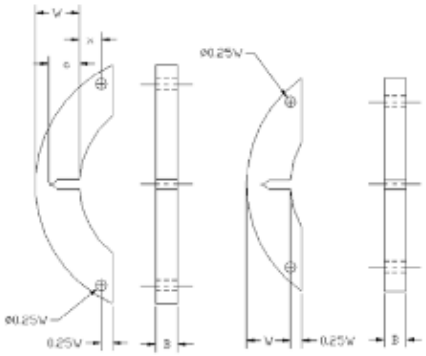

	K_{IC}
W/B	2-4

(b) Arc-Shaped Specimen Designs A(T)
Standard Proportions

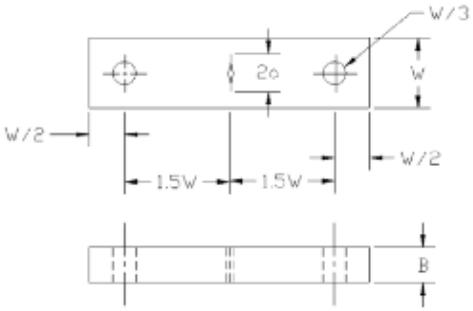

	B	ECG
W/B	Plane Stress	Var

(d) Standard Middle Tension Specimen
when W≤75 mm

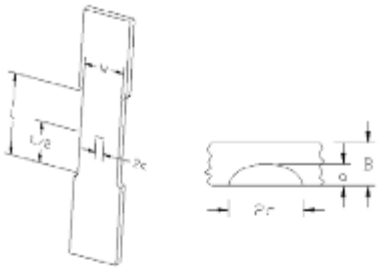

(e) Part-Through Crack

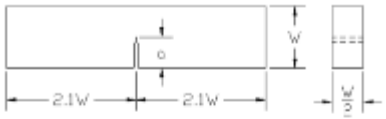

	K_{IC}	EAC	J_{IC}
W/B	1-4	1-2	1-4

(g) Bend Specimen SE(B) – Standard Proportions

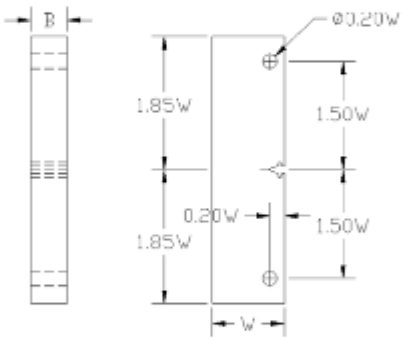

	FCG
W/B	4-20

(f) Standard Eccentricaly-Loaded Single Edge Crack Tension Specimen

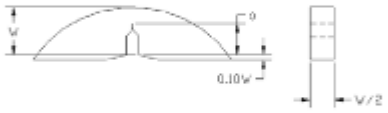

(h) Arc-Shaped Bend

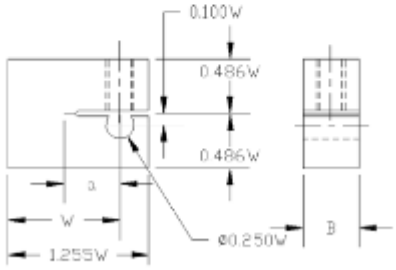

	EAC
W/B	1-2

(i) Bolt-Loaded Wedge-Opening-Loading MC(W) Specimen

Figure 4.2: Specimens for Damage Tolerance Testing

As a result of the concerns about the effects of anistropy on material fracture toughness and crack growth resistance properties, standard nomenclature relative to directions of mechanical working (grain flow) has evolved.

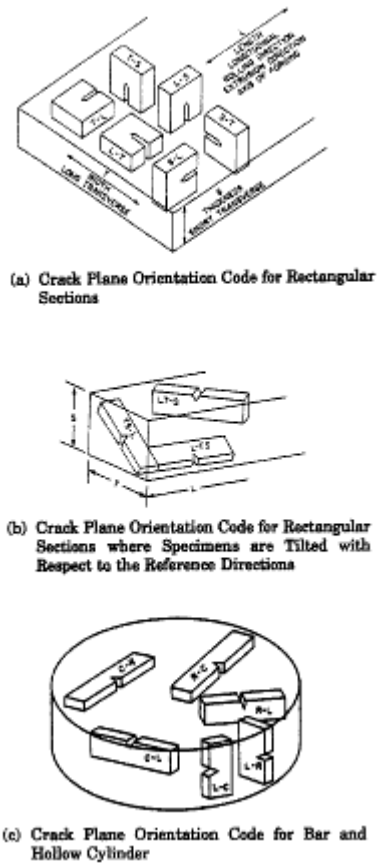

(a) Crack Plane Orientation Code for Rectangular Sections

(b) Crack Plane Orientation Code for Rectangular Sections where Specimens are Tilted with Respect to the Reference Directions

(c) Crack Plane Orientation Code for Bar and Hollow Cylinder

Figure 4.3: Crack Plane Orientation Code for Rectangular Sections and for Bar and Hollow Cylinders [ASTM 2001]

The same system would be useful for sheet, extrusions, and forgings with non-symmetrical grain flow:

L – direction of principal deformation (maximum grain flow)

T – direction of least deformation

S – third orthogonal direction.

When reporting crack orientation in rectangular sections, the two letter code, such as T-L is used when both the loading direction and direction of crack propagation are aligned with the axes of deformation.

For specimens tilted with respect to two of the reference axes, a three-letter code, e.g. L-TS, is used. The designation used can be interpreted by considering the codes as a composite pair in which the first element in the pair designates the direction normal to the crack plane and the second element designates the expected direction of crack propagation. The code T-L for a cracked specimen indicates that the fracture plane has a stress application normal in the T direction (width direction of the plate) and the expected direction of propagation in the L direction (in the longitudinal direction of the plate). The code L-TS means that the crack plane is perpendicular to the L direction (principal deformation) and the expected crack direction is intermediate between T and S.

For cylindrical sections where the direction of principal deformation is parallel with the longitudinal axis of the cylinder, such as for drawn bar stock and for extrusions or forged parts having a circular cross section, the specimen reference directions are described. The three directions used here are:

L – directional of maximum grain flow (axial) R – radial direction, and C – circumferential or tangential direction

Interpretation of the specimen designations relative to the location of the crack plane and crack path is similar to that employed for the rectangular sections.

Fracture toughness data have provided the basis for estimating the crack length-residual strength behavior of aerospace structures since the late fifties. Initial correlation tests for airplane skin-stringer type structures were typically conducted using wide, center crack panel tests of the skin material. It was soon realized that such tests were inappropriate for estimating the fracture behavior of thicker material/structure for a number of reasons. By the late sixties, ASTM had evolved a fracture toughness test for materials that fail by abrupt fracture. This test method eventually became the plane-strain fracture toughness (K_{Ic}) test standard, ASTM E399, in 1972.

Additional work by ASTM throughout the seventies resulted in several additional fracture toughness methods. One such method appropriate for tougher (or thinner) materials which fail by tearing fracture is ASTM Standard E561, which covers the development of the K_R resistance curve. The K_R resistance curve test has found wide acceptance in the aircraft industry since calculation procedures were already in place to utilize the data for residual strength estimates. Another recently-approved standard, ASTM E1820, covers the determination of fracture toughness using several methods. One such method applicable to materials which lack sufficient thickness for plane-strain fracture toughness (K_{Ic}) per ASTM E399 is the J-integral approach to determine the plane-strain toughness J_{Ic}.

The plane-strain fracture toughness (K_{Ic}) measures crack resistance to abrupt fracture under tri-tensile crack tip stress conditions where the constraint against crack tip deformation is maximized. As such, K_{Ic} data represent a lower bound on the fracture toughness that a material might experience under a wide range of cracking and geometric configurations. The ASTM E399 standard that covers plane-strain fracture toughness of metallic materials was developed to obtain values of fracture toughness using relatively thick specimens (thus maximizing the crack tip constraint) subjected to quasi-static loading conditions. The determination of K_{Ic} is also covered in the common fracture toughness method ASTM E1820.

A variety of specimen configurations are currently recommended for collecting K_{Ic} data. The compact tension [C(T)] and the single edge notched bend specimen [SE(B)] were initially the only specimens recommended for the measurements and most laboratories are well equipped to support these tests. The arc-shaped tension [A(T)], disk-shaped compact tension [DC(T)], and arc-shaped bend [A(B)] specimens have since been added as these configurations evolved to characterize the resistance of specific structural product forms, i.e. tube/pipe type structures and cylindrically shaped bar stock.

It should be noted that ASTM E399 uses linear elastic fracture mechanics as its basis for calculating fracture toughness. For this reason, specimen sizing requirements are predicated on maintaining a crack tip plastic zone size that is a small fraction of the planar dimensions of the specimen. The test method is also specific about ensuring that the thickness of a K_{Ic} specimen is substantially larger than the crack tip plastic zone size so that a crack tip tri-tensile stress state is established which maximizes the constraint on plastic deformation. Basically, the specimens are sized so that the dimensions of crack size (a), thickness (B), and remaining ligament size (W-a) are greater than the ratio of 2.5 $(K_{Ic}/\sigma_{ys})^2$, i.e., so that

$$a, B, (W - a) > 2.5\left(\frac{K_{Ic}}{\sigma_{ys}}\right)^2$$

where σ_{ys} is the 0.2 percent offset yield strength and the K_{Ic} value meets all the test criteria.

The procedures for determining fracture toughness outlined in ASTM E1820 are essentially identical to E399 for samples sufficiently thick to provide valid K_{Ic} measurements. The plane-strain crack toughness test is unusual in that there can be no advanced assurance that the fracture toughness established by a given test will be a valid K_{Ic} value. The fracture toughness calculated after a given test must be validated through a series of criteria checks that are thoroughly described in E399 and E1820. The principle advantage of E1820 is that one can analyze the test information using different criteria to come up with valid toughness measurements if the thickness is too thin for valid K_{Ic} values.

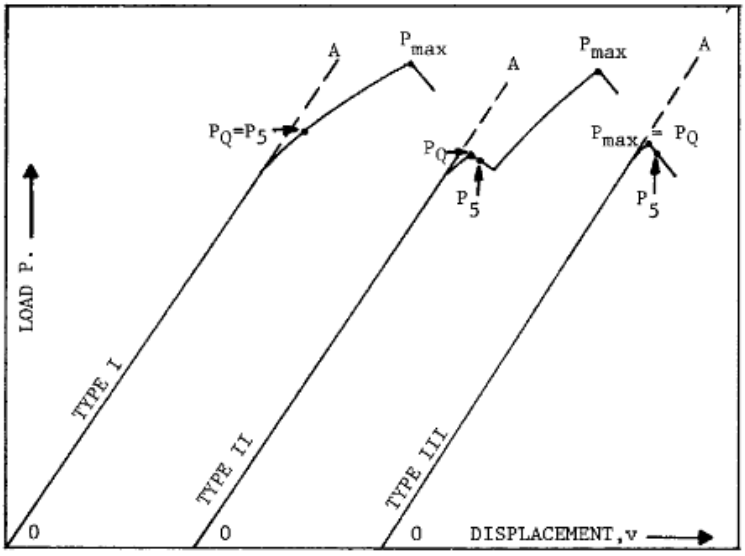

Figure 4.4: Principal Types of Load-Displacement Records [ASTM 2001]

The collection of such load-displacement data is a requirement of most ASTM fracture related standards. The objective of this test record is to establish the load, P_Q, which will be used in the calculations of the test fracture toughness value (K_Q), and the level of maximum test load (P_{max}). The test fracture toughness (K_Q) is a conditional result that must be validated through checking the size requirements before accepting K_Q as a valid plane-strain fracture toughness (K_{Ic}) value. If K_Q is a non-valid test result according to ASTM E399, K_Q should not be utilized as an estimate for K_{Ic} for design purposes since the value may be very non-conservative.

The R-Curve measures crack resistance to tearing fracture for situations where the material thickness employed within a structure is below the requirement for plane-strain fracture toughness conditions. The R-curve describes the extent of crack movement from an initial starting condition as a function of the level of applied stress-intensity factor (K) and as such represents a complete history of quasi-static crack growth up until fracture occurs. It has been shown for several materials that the R-curve for a given thickness is independent of crack size and structural geometry [McCabe, 1973].

For the detailed reasons stated already, the R-curve is not as easily employed in design as abrupt fracture criteria. Early work on aerospace materials with thicknesses below that required for K_{Ic} was directed at obtaining the limits on the R-curve, i.e. on obtaining K_{ONSET}, associated with the K conditions at the start of crack movement, and K_c, associated with the K conditions at the moment of instability. After it was realized that the plane-stress fracture toughness (K_c) was a function of crack size and structural geometry as well as thickness, attention was focused on obtaining the complete history of the tearing fracture.

ASTM evolved a standard practice for determining the R-curve to accommodate the widespread need for this type of data. While the materials to which this standard practice

can be applied are not restricted by strength, thickness or toughness, the test specimens utilized in tests must be of sufficient size to remain predominantly elastic throughout the duration of the test. The reason for the size requirement is to ensure the validity of the linear elastic fracture mechanics calculations. Specimens of standard proportions are required, but size is variable, to be adjusted for yield strength and toughness of the material considered.
The ASTM Standard E561 covers the determination of R-curves using middle cracked tension panel [M(T)], compact tension [C(T)], and crack-line-wedge-loaded [C(W)] specimens.

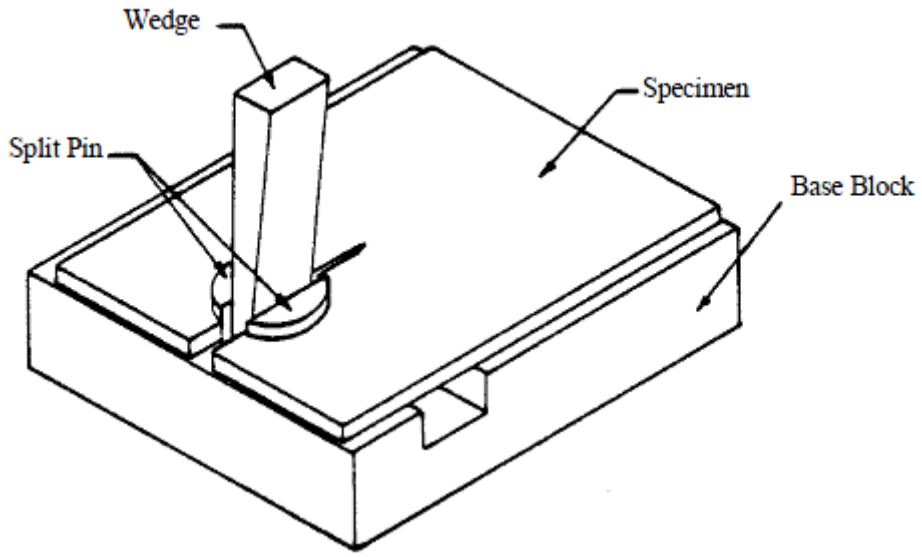

Figure 4.5: Crack-Line-Loaded Specimen with Displacement-Controlled Wedge Loading [ASTM 2001]

The crack-line-wedge-loaded configuration and loading conditions are such that, as the crack grows, the stress-intensity decreases under fixed-displacement conditions. Such an arrangement facilitates collecting the complete R-curve using one specimen since the crack growth remains stable under decreasing K conditions. Load control conditions ensure that the stress-intensity factor will increase as the crack grows. This arrangement results in limiting the K_R versus crack extension (Δa) data to a level associated with the fracture of the test specimen.
While the C(W) specimen had gained substantial popularity for collecting K_R curve data, many organizations still conduct wide panel, center cracked tension tests to obtain fracture toughness data. As with the plane-strain fracture toughness standard, ASTM E399, the planar dimensions of the specimens are sized to ensure that nominal elastic conditions are met. For the M(T) specimen, the width (W) and half crack size (a) must be chosen so that the remaining ligament is below net section yielding at failure. It is recommended in ASTM E561 that the M(T) specimen be sized so that the dimensions can be referenced to the plane stress plastic zone size (r_y).

$$r_y = \frac{1}{2\pi}\left(\frac{K}{\sigma_{ys}}\right)^2$$

where the specimen sizes are chosen on the basis of the maximum stress-intensity factor expected in the test.

K_{max}/σ_{ys} ($in^{1/2}$)	Width (in.)	Crack Size (in.)	Specimen Length (in.)
0.5	3.0	1.0	9
1.0	6.0	2.0	18
1.5	12.0	4.0	36
2.0	20.0	6.7	30*
3.0	48.0	16.0	72*

* Panels wider than 12 in. will require multiple pin grips and the length requirement is relaxed to $1.5W$

Figure 4.6: ASTM E561-98 Recommended M(T) Dimensions

It should be noted that the initial crack length is sized to be W/3 to minimize the potential for net section yielding prior to a stress-intensity factor controlled fracture. Based on data collected from a number of aluminum panels with different widths, it appears that there is a tendency for the calculated fracture toughness K_c to increase with increasing panel width. While it is difficult to generalize the observation based on these results to all materials, such data indicates that it is possible to develop conservative predictions of the plane-stress fracture toughness by using sub-size specimens.

Material	Crack Orientation	Buckling Restraint	Specimen Thickness (in.)	Specimen Width (in.)	Kapp (ksi $in^{1/2}$)	Kc (ksi $in^{1/2}$	No. of Measure.
2020-T6	L-T	No	0.063	2.0	29.6	34.6	5
				3.0	29.1	30.1	2
				15.8*	36.1	36.9	4
2020-T6	T-L	No	0.063	2.0	25.9	30.5	5
				3.0	26.9	27.8	2
				15.8*	34.5	34.5	5
2024-T81	T-L	No	0.063	2.0	35.6	--	9
				6.0	51.2	57.9	3
				9.0*	55.2	61.2	2
2024-T851	T-L	No	0.250	3.0	26.7	31.3	6
				4.0	38.0	47.1	7
				20.0*	38.6	48.4	12
7075-T6 clad	L-T	No	0.040	7.5	47.3	--	3
				9.0	51.4	55.0	12
				30.0*	64.9	85.6	6/2+
7075-T6 clad	L-T	Yes	0.080	5.9	53.5	60.1	9/6+
				11.8*	61.5	70.1	17
				23.6*	62.4	69.3	20
7075-T6 clad	L-T	No	0.090	3.0	49.4	--	11
				9.0*	64.5	70.0	16/12+
				20.0*	56.4	61.8	10
7075-T7351	L-T	Yes	0.250	8.0	59.7	--	13
				15.9	77.2	--	8
				36.1*	93.0	119.9	3/2+
7075-T7351	L-T	No	1.00	8.0	43.1	45.9	3
				16.0*	47.3	52.7	9
				20.0*	77.9	96.7	16/12+

*Width requirements meet ASTM E 561 requirements.
+First number represents number of Kapp calculations, the second represents Kc [ASTM 2001]

Figure 4.7: Room Temperature Plane-Stress Fracture Toughness Values for Several Aluminum Alloys Presented as a Function of Thickness and Width

Another test condition important to consider during R-curve (or plane-stress fracture toughness) testing is the amount of buckling restraint that should be built into the test fixtures. Most tests are conducted either with no buckling restraint or with extensive fixturing that tends to maintain inplane loading by preventing buckling. With tests conducted with limited buckling restraint, the spurious stress distributions created when buckling occurs (at the specimen edges or in the crack tip region) can lead to mechanical driving factors that either enhance or degrade the calculated levels of applied stress-intensity factor. The ASTM E561 method places restrictions on the amount of buckling exhibited during the R-curve test. The data collected during an R-curve test includes load and crack size readings. The stress-intensity factor associated with a given increment of crack size, i.e. K_R, is calculated using the stress-intensity factor formula for the specimen, the applied force (P), and a plasticity enhanced crack size. The plasticity enhanced crack length is referred to as the effective crack (a_{eff}) and is calculated by adding the plane stress plastic zone radius (r_y), to the current physical crack, i.e.

$$a_{eff} = a_0 + \Delta a + r_y$$

where a_o is the initial crack length and Δa is the increment of crack movement.

Visual and non-visual methods of measuring crack size are available for collecting the data. Within ASTM E561, the details associated with making crack length measurements based on compliance (force-displacement) methods are fully described. In fact, for those situations where extensive crack tip plasticity can occur, the compliance methods are recommended since these methods yield an estimate of crack length that already accounts for a plasticity correction.

ASTM E561 recommends that the R-curve be presented using an effective crack increment ($\Delta a_{eff} = \Delta a + r_y$) so that the instability predictions can be directly made from the plots. Thus, the R-curve is a plot of $K_R = K(a_{eff}, P)$ versus Δa_{eff}. The test engineer must describe how Δa_{eff} and a_{eff} were calculated so that structural engineers using the data have a full report of the behavior.

The J_{Ic} can be used as a toughness value at the initiation of crack tearing from a sharp fatigue crack in metallic materials. This toughness value can serve as a basis for screening tough materials or for evaluating materials utilized in sub-K_{Ic} thicknesses. Requirements for a valid J_{Ic} value according to ASTM E1820 are based on the ratio of the J_{Ic} to yield strength, i.e.,

$$B, b_0 > 25\left(\frac{J_Q}{\sigma_{ys}}\right)$$

where B is thickness and b_0 is the initial ligament.

The relationship between the J-integral and the stress-intensity factor is

$$J = \frac{K^2}{E'}$$

where $E' = E$, the elastic modulus, for plane stress, and $E' = E/(1-\nu 2)$ for plane strain, and ν = Poisson's ratio.

Thus, at the critical condition ($J = J_{Ic}$, $K = K_{JIc}$), the thickness requirement becomes

$$B > 25\left(\frac{\sigma_{ys}}{E'}\right)\left(\frac{K_{JIc}}{\sigma_{ys}}\right)^2$$

For the typical condition where the ratio of yield strength to elastic modulus (σ_{ys}/E) is below 0.1, J_{Ic} values can be obtained using specimens thinner than that required by the K_{Ic} standard (ASTM E399).

The K_{JIc} value, however, does not normally correspond to the K_{Ic} value that would be obtained using the plane-strain fracture toughness standard. The K_{Jic} value based on J_{Ic} measurements is typically lower and thus leads to conservative estimates of the ASTM E399 K_{Ic} value. The differences in K_{JIc} and K_{Ic} arise as a result of differences in the amount of allowable physical crack growth associated with the two standards; there is less growth allowed for the J_{Ic} value than for the K_{Ic} value.

While the use of a toughness standard for sub-K_{Ic} thickness specimens provides additional opportunities for characterizing material resistance to fracture, the J_{Ic} concept appears somewhat limited relative to the design of aerospace structures. A single test of a J_{Ic} type specimen might be similar in cost to a K_{Ic} type test; but a number of J_{Ic} type specimens must be tested to develop the required crack resistance data prior to estimating the J_{Ic} value. Through unloading compliance testing, it is possible to reduce the number of tests.

Since the early sixties, sub-critical crack growth data have provided the basis for estimating the crack growth behavior of structural components under service conditions. In the initial stages of damage tolerant design methodology and test development, the effects of stress ratio, environment and load sequencing were poorly understood. Thus, the initial damage integration packages did not account for these effects; furthermore, testing capability was for the most part limited to constant amplitude or to block loading. By the early seventies, understanding and capability had progressed to the point where evaluation of each major damage producing element in the service history could then be modeled by damage integration packages.

The ASTM Committee E08 on Fatigue and Fracture Testing also played an important part in developing standards for collecting data which could be used to support damage integration packages. Throughout the seventies, inter-laboratory testing programs were conducted which further refined the testing conditions that could be standardized by consensus. The AF Materials Laboratory funded development of a standard test method to ensure a stable methodology for information used in aircraft damage tolerance assessments [Hudak, et al., 1978]. In 1978, ASTM issued the first standard based on these developments, ASTM E647, on fatigue crack growth rate (da/dN) testing. Additional standards or additions to existing standards such as ASTM E1681 on environmentally assisted cracking testing (K_{IEAC}), on corrosion fatigue, on automated methods and on threshold testing have and continue to evolve. Methods for non-visual crack size monitoring such as compliance and electric-potential have been developed over the last 15 years and incorporated into nearly all of the fracture related standards.

Fatigue crack growth rate data that support standard damage integration packages of the type described already are based on constant amplitude testing of cracked specimens. Typically, multiple specimen tests are conducted at a number of fixed stress ratio (R) conditions so that the complete range of crack growth rate is covered for the mechanical and environmental variations of interest. For the most part, all tests of this type are covered by ASTM E647 on fatigue crack growth rate testing.

Test conditions that deal with the conditions essential for obtaining near threshold growth rates are further described by ASTM E647. Substantial care is necessary for correctly

controlling the precracking operation and the stress-intensity-factor control conditions in the near threshold region of the fatigue crack growth rate curve (da/dN vs ΔK) [Yoder, et al., 1981; Wei & Novak, 1982]. Also, ASTM E647 must be supplemented with information relative to control of environmental conditions when these conditions affect behavior.

The ASTM E647 describes the test, as well as the data collection, reduction and reporting requirements. The test itself requires standard fatigue test capability and utilizes precracked specimens which have widely accepted stress-intensity factor solutions. The standard currently recommends three specimen configurations, the middle-cracked tension [M(T)], the compact tension [C(T)], and the eccentrically-loaded single edge tension [ESE(T)] specimen geometries.

While the M(T) specimen is generally recommended for all stress ratio conditions, it should be noted that the C(T) and the ESE(T) specimens can only be used for positive stress ratio conditions.

The primary control exercised during a test is the control of the fatigue forces that are being applied to the test sample. Most modern servocontrolled, electrohydraulic test machines that are periodically recalibrated using force cells traceable to the National Institute of Standards and Technology (NIST) will result in force control well within the ASTM E647 requirements. Force cells, of course, should be selected such that fatigue crack growth rate tests are being conducted using forces that are at the higher end of the load cell range to maximize force accuracy.

Specific care should be taken to minimize force errors. Such errors can cause major errors in reported crack growth rate data since stress-intensity factor (K) is a linear function of force.

Fatigue crack growth rate data are derived from the crack length data (discrete pairs of crack length and cycle count data) and test load data. Significant errors in crack growth rate behavior can also result if systematic errors in crack length measurement occur since such errors directly affect the calculated stress-intensity factor parameters. ASTM E647 places strict requirements on the measurement of crack size and recommends a frequency of crack length measurement based on the gradient (rate of change) of the stress-intensity factor through the crack length interval in the given test specimen.

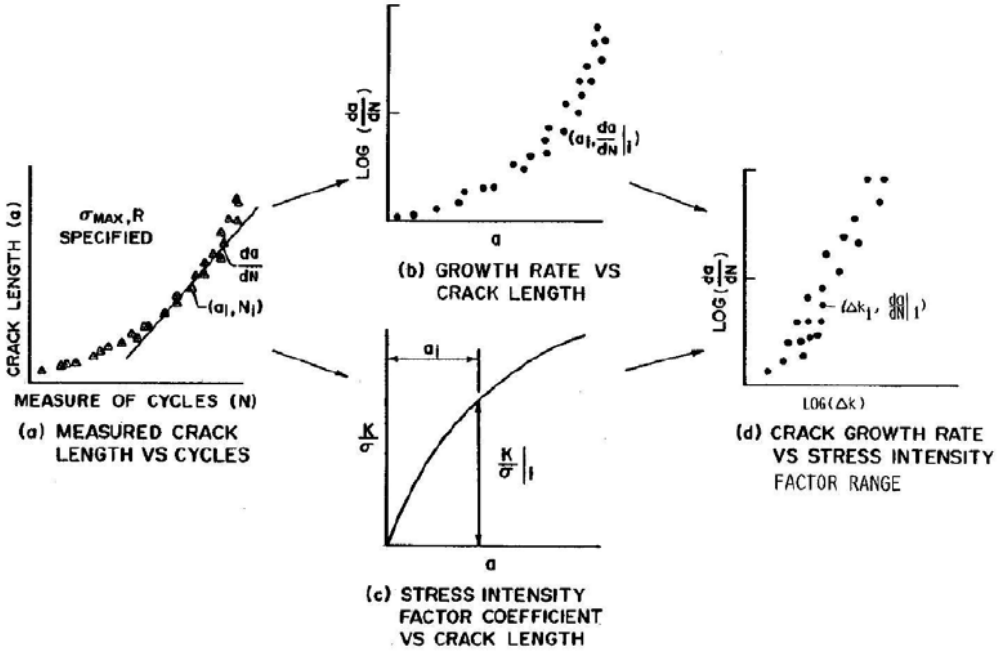

Figure 4.8: Fatigue Crack Growth Rate Data Reduction Procedure

The procedures that one uses to differentiate the crack length data have some effect on the individual da/dN vs ΔK discrete data points. To ensure some uniformity in this part of the data reduction process, ASTM E647 recommends that either the secant or the 7-point incremental polynomial methods be utilized. In fact, the standard includes a listing of a FORTRAN computer program that can be utilized to reduce the crack length data according to the 7-point incremental polynomial method. Other differentiation methods leading to the same data trends for a given test include 5, 7, 9 point incremental, linear, quadratic, and power law least squares fitting schemes and the three-point average incremental slope method utilized by MIL-HDBK-5. The specific differences that result from differentiating a set of crack length data using different methods are primarily associated with point-to-point data scatter in the a vs N data.
ASTM E647 recommends that duplicate tests be conducted to establish the crack growth rate behavior for a given set of test conditions (constant and environment). However, if a complete definition of the growth rate behavior between threshold and fracture is required for a given set of test conditions, six constant load type tests with three different load levels might be required to cover the range. For determining general trends under a given set of test conditions, shortcut methods are available. These methods include:
• methods of periodically increasing the constant amplitude load (by less than 10 percent) as the crack grows, and
• methods of periodically modifying either the stress ratio or cyclic load frequency during a test.

These shortcut methods are designed so that only selected intervals of the fatigue crack growth rate data are generated, although a description of the complete da/dN vs ΔK curve is possible since the entire range of behavior is covered.
When shortcut methods are utilized to obtain a design database, it is recommended that a preliminary test program be conducted to verify the accuracy of these shortcut methods. The preliminary test program would be based on a sufficient number of both constant load amplitude and shortcut tests to justify the shortcut test methods, since changing test loads, stress ratio levels, cyclic load frequencies and environmental conditions can introduce crack growth transients. The crack growth transients of most concern are those that modify the interpretation of the mean trend behavior exhibited by the material under the test variations considered. The preliminary test program should determine the magnitude of the transient and the crack growth increment required to establish steady-state behavior after a new condition is introduced. The approving agency should review the results of the preliminary test program relative to the impact of transient behavior and to the development of data reduction methods that exclude those intervals of crack length where transient behavior might be exhibited.
Stress corrosion or environmentally-assisted cracking data which support standard damage integration schemes, as well as materials evaluation and selection studies, are based on either constant load or constant displacement type tests of fatigue cracked specimens placed in simulated service environments. There are two types of stress corrosion cracking data properties measured by such tests:
1) the threshold property (K_{IEAC}), which is the level of the stress-intensity factor associated with no cracking in the given environment, and
2) the crack growth rate resistance property (da/dt as a function of the static stress-intensity factor K).

ASTM E1681 covers determination of stress corrosion threshold. Three types of test specimen configurations utilized in the ASTM standard are:

• a bolt-loaded, compact [MC(W)] specimen,
• a constant load single-edge specimen [SE(B)], and
• a compact tension specimen [C(T)].

As can be noted from the figure, the bolt-loaded MC(W) specimen is a self-loading specimen. The force loaded SE(B) and C(T) specimens must be placed in a test figure that supports the specimen while under load, which is typically applied using weights attached to one end of the specimen.

As with other sub-critical crack growth resistance tests, the materials test engineer must pay particular attention to the pre-cracking, loading, and crack size measurement details. In addition, because the environment has a more important influence on the crack growth resistance of many materials, specific controls must be instituted here also.

Crack growth tests conducted in aqueous or similar deleterious environments lead to difficult crack length measurement problems since typically the direct use of visual techniques is restricted to conditions whereby the specimen is removed from the environment. Use of visual techniques under these conditions is acceptable if it can be shown that removing the specimen from the environment introduces no major crack growth transient effects. Collecting crack length data using electric potential difference (EPD) methodology and the relationships between crack size and potential voltage difference has gained credibility in recent years as a means of automating the measurement of crack size in both SE(B) and C(T) specimens. Since stress-corrosion cracking tests are conducted over longer periods of time (~ 10,000 hours) than other mechanical tests, stability of the crack size measurement system must be given a great deal of attention.

Differences of opinion exist between the experts relative to the use of either the increasing (constant load) or decreasing (constant displacement) stress-intensity factor (K) type specimens for collecting threshold stress corrosion cracking data. These differences result from the influences of test conditions and of crack growth transients. Since the objective of the K_{IEAC} test is to obtain a threshold level of K associated with a preset growth rate limit, a series of tests should be conducted which would minimize these effects.

The K_{IEAC} results obtained using constant load specimens are influenced somewhat by the fact that the test time includes both the time associated with initiating the crack movement from the sharp precrack and that associated with subsequent propagation. For K_{IEAC} data collection programs using increasing K specimens, a number of tests should be conducted such that the precracked specimens are loaded above and below the level of the expected stress-intensity factor condition associated with zero crack movement. Subsequently, each unbroken specimen should be broken open and examined for evidence of crack movement during the test period. In all cases, the K_{IEAC} value is lower than the lowest value of the stress-intensity factor associated with the broken specimens. If no stress-corrosion cracking movement is observed when the unbroken specimens are examined, the K_{IEAC} is taken as the highest stress-intensity factor level associated with the unbroken specimen group. When stress-corrosion cracking movement is observed in the unbroken specimen group, the amount of crack movement should be divided by the test time in order to ascertain if the average growth rate associated with any test is below that required to obtain the K_{IEAC} value. The highest level of stress-intensity factor that yields an average growth rate below that required is taken as the K_{IEAC} value.

The K_{IEAC} results obtained using the bolt-loaded (K-decreasing type) specimen can be influenced by crack growth transients that occur after loading. For K_{IEAC} data collection programs using decreasing K specimens, a number of tests should be conducted such that the precracked specimens are loaded to levels that are slightly above (10 to 25 percent) the level of expected K_{IEAC}. High initial stress-intensity factor levels (relative to K_{IEAC}) result

in a number of problems in determining K_{IEAC} accurately. These problems sometimes result from the fact that once the precrack starts to move it has a longer distance to travel before arresting as a result of the high initial K condition and the slowly decaying K gradient associated with the bolt-loaded conditions. Another problem associated with high initial K conditions is that cracks will sometimes initiate and arrest prematurely due to crack blunting (under first loading) and crack front tunneling. In the decreasing K specimen, as soon as crack movement occurs from the precrack, the crack front loses the sharpness of a fatigue crack; this sometimes results in a value of K_{IEAC} that is somewhat above that measured in the increasing K specimen.

Some of the problems in estimating K_{IEAC} using either constant-load (increasing K) and bolt-loaded (decreasing K) specimens are alleviated when crack growth measurements are continuously made throughout the test. Specifically, measurement of the first crack movement that occurs in constant-load specimens provide a better time basis for estimating the crack growth rate from unbroken specimens. Even periodic measurement of the crack length in the bolt-loaded C(T) specimens will increase the test engineer's confidence that transient or abnormal crack growth behavior has not occurred during the test. Crack growth rate data used for sensing a material's resistance to environmental attack is collected and reduced in a manner similar to fatigue crack growth rate data. The principal difference in an environmental attack testing program is that the loads or displacements are held constant during the test. K_{IEAC} is used primarily for ranking materials for sub-critical crack growth resistance in environments. Because fatigue testing is conducted extensively in similar environments during the design of airframe structures, a high level of interest continues in combining the time dependent rate information with the cyclic dependent data into a common predictive model. It is therefore suggested that when such tests are necessary to support damage integration packages, that stress-corrosion cracking rate tests follow the basic guidelines of the fatigue crack growth rate tests in ASTM E647.

SECTION 4.2: QUALITY CONTROL TESTS

The quality control tests provide data that (a) support the initial quality design assessments and non-destructive inspection (NDI) requirements, or (b) ensure the uniformity of the production product. Because many of these tests will be conducted during the production run they are fairly simple tests. Requirements for these tests are defined after the preliminary sizing and the identification of fracture critical parts. Quality control data covered by this category of tests include equivalent initial quality (EIQ) data, continuing assessment of the non-destructive evaluation (NDE) capability, and component prolongation tests for fracture toughness and crack growth resistance.

One sure method for minimizing damage tolerant problems due to the presence of the manufacturing induced rogue flaw is to take ample precautions on the production line to minimize the probability that such defects could be present in safety-of-flight structures. The manufacturer, during design, will typically suggest methods for ensuring strict production line control of material preparation, fabrication and joining techniques. The manufacturer's control can be periodically checked using the same type of testing and analysis approaches that were utilized in design to justify the choices of materials and defect sizes for the airframe's damage tolerant analysis.

Throughout the procurement cycle of several recent weapon systems, fracture toughness was controlled to specified design minimum levels for airframe safety-of-flight type structure. The particular fracture toughness property used for quality control was the plane-strain fracture toughness – K_{Ic}. Since some manufacturing processes are such that they alter the microstructure of some materials (and thus the fracture resistance), it was

believed necessary to monitor the behavior of material subjected to the gamut of processes that precede final assembly. In fact, the B-1A material quality control program was designed so that the fracture toughness was sampled for each fracture critical part after each major manufacturing process; such a sampling program provided an immediate indication if any process was detrimental to the fracture toughness.

In almost all the past cases where fracture toughness was controlled, ASTM E399 was employed to obtain a valid plane-strain fracture toughness (K_{Ic}) value. As a result of the difference in cost between a K_{Ic} test and other much simpler mechanical tests such as the tensile test, engineers have been giving attention to the development of tests that are both simple and representative of the fracture toughness property of interest. The double-edge notched specimen and the round edge-notched specimen are two notched geometries that have been examined. Both notched geometries are prepared with sharp root radii, i.e. radius < 0.002 inch, but do not contain fatigue precracks. A Chevron Notch Test for K_{IV} (ASTM E1304) can also be used as a K_{Ic} indicator.

For quality control purposes, the manufacturer might prepare a series of round-edge notched specimens and K_{Ic} specimens with the same microstructure (from the same lot of material) and determine the relationship between, for example, notched tensile strength and fracture toughness. The series of tests would be repeated for different microstructure (different lots of material) until every possible combination of microstructure was covered. The manufacturer would then formulate a global relationship between notched tensile strength and fracture toughness of this material. Using standard statistical techniques, the manufacturer could then establish the required level of notch tensile strength that should be measured during production in order to achieve the minimum allowable level of fracture toughness.

While the crack growth property is actually of greater concern than the fracture toughness property, controlling the level of subcritical crack growth resistance via a quality control test has not been attempted for any large weapon system due to the expense and complexity of the crack growth rate test. The Air Force funded one study to explore the possible development of an inexpensive crack growth test but the results of this program were mixed [Creager & Sommers, 1977]. With the advent of automated fatigue crack growth rate test methods, future quality control programs could incorporate a test for controlling the subcritical crack growth resistance of fracture critical parts.

SECTION 4.3: ANALYSIS VERIFICATION TESTS

The analysis verification tests provide data that define the accuracy of the damage tolerance analysis tools relative to their ability to predict the crack growth behavior of the structure under operational conditions. In essence, these tests are conducted to verify individual or collective elements of the damage integration package that will be used to conduct damage tolerant life analysis studies. Analysis verification tests include those tests that are used to verify stress-intensity factor calculations, residual strength methods, crack growth calculations, and test spectrum truncation procedures. The tests range in difficulty from constant amplitude tests on fairly simple structural geometries to flight-by-flight load type tests conducted on structures that simulate isolated design features contained in full-scale structural components. These tests are typically conducted during the design analysis and development testing phase of the contract prior to testing the full-scale structure and major components. Additional testing may also be necessary subsequent to the results of

the full-scale flight and ground tests to support interpretation and evaluation of cracking problems.

The current analytical procedures for developing the stress-intensity factor (K) associated with two-dimensional structural geometries have been extensively verified. The verification of the tools required to solve three-dimensional structural geometry problems, however, is still receiving major attention.

For the two-dimensional crack geometries, the engineer has the opportunity to employ four different types of experimental tests to verify the stress-intensity factor solution for the given problem: compliance (displacement/load) measurements [Bubsey, et al., 1973], moiré fringe techniques [Kiu & Ke, 1975], photoelastic procedures [Kobayashi, 1973], and crack growth rate testing [James & Anderson, 1969]. In the realm of the three-dimensional problem, only two of the above tests can be relied upon: photoelastic procedures [Smith, 1975], and crack growth rate testing [Grandt & Sinclair, 1972; Grandt & Hinnerichs, 1974].

The residual strength analysis was discussed which requires a material model describing the fracture process, the specific materials data that support the model for the structural thickness and loading conditions, and the ability to derive the value of the controlling structural parameter (such as the stress-intensity factor) for the cracked structure. There are a series of residual strength tests that can be conducted during the course of the design analysis and development test activity (JSSG-2006 paragraph 4.12.2) that will support the verification of residual strength analysis capability in aircraft safety-of-flight critical structure. For example, a manufacturer could choose to conduct some constant amplitude fatigue crack growth rate tests using radial-corner-cracked-hole type specimens or part-through thickness cracked type specimens in order to verify the stress-intensity factor analysis part of the damage integration package. Instead of cycling such constant amplitude tests to failure, the tests could be stopped prematurely and the specimens pulled to fracture. By monitoring these fracture tests and recording critical events as a function of load, the manufacturer can build a database that can be utilized to verify the applicability of various material (fracture) models proposed for the residual strength analysis.

An example illustrating some of the initial steps in verifying the applicability of a new type of fracture model can be obtained from a review of the work of Wang and McCabe [1976]. One of the first steps in verifying any residual strength analysis is to demonstrate the transferability of the data between simple cracked geometries.

Wang and McCabe considered the applicability of the R-curve (K_R) analysis to the prediction of residual strength of aircraft structures. At the time of their study, there was almost no documentation that supported the transferability of R-curve data. Wang and McCabe employed two types of crack-line-wedge-loaded compact [C(W)] specimens to provide the basic materials data and then performed a residual strength analysis on middle-crack tension [M(T)] panels. They also directly compared the R-curves from the two cracked geometries.

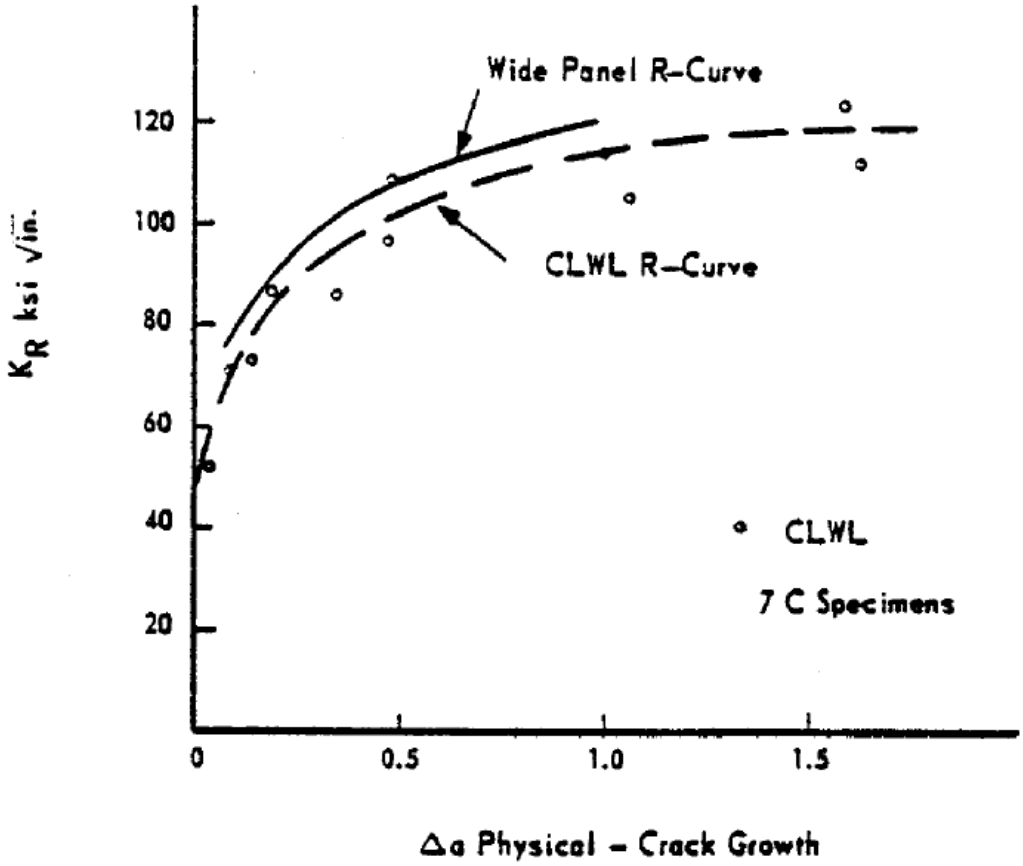

Figure 4.9: R-Curve Comparison for 7475-T61 Aluminum [Wang & McCabe 1976]

They were able to predict the gross stress at fracture, i.e. the residual strength, on the average to within 5 percent (on the conservative side) of the experimental results. Their most non-conservative prediction was only about 8 percent higher than the experimental value.

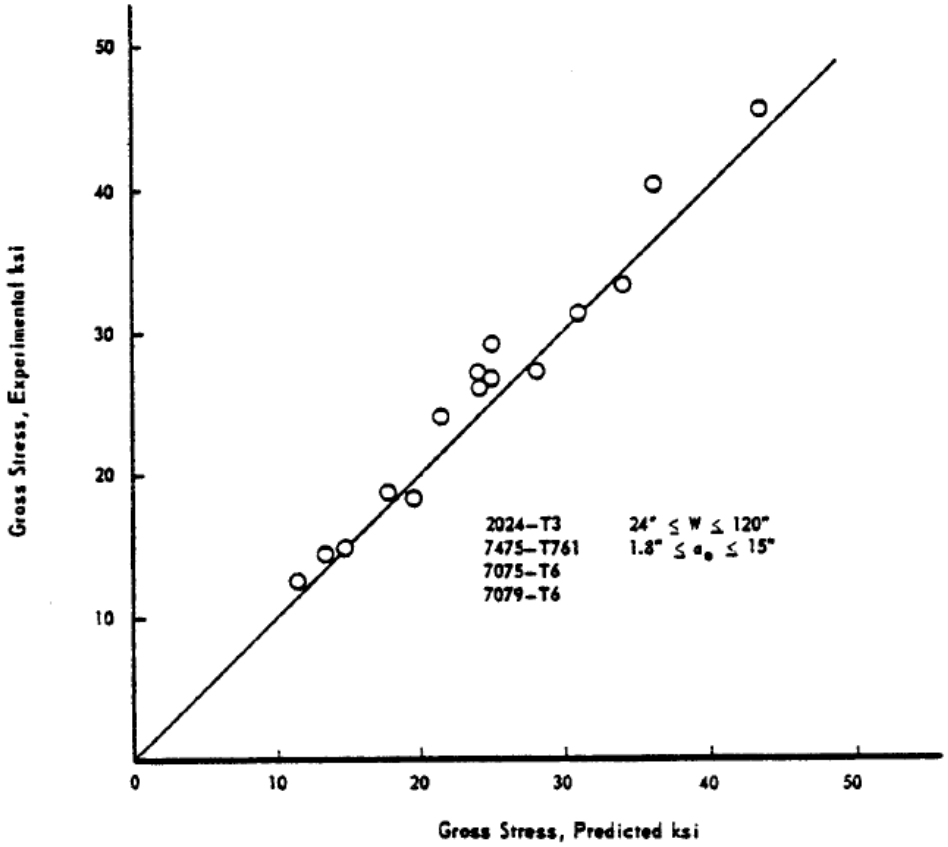

Figure 4.10: Summary of the Capability of the R-Curve Method for Predicting the Residual Strength of Center-Cracked Panels Using CLWL Specimen Data [Wang & McCabe 1976]

			Half Crack Length (in)		Gross Stress, Fracture (ksi)		K_c ksi √in.		Net Section Stress, predicted ksi
Material	Width (in.)	a_o (in.)	Predict	Exper.	Predict	Exper.	Predict	Exper.	
2024-T3	24	4.0	5.64	4.79	24.9	26.7	121.9	116	46.6
	36	5.4	7.43	7.03	24.1	26.1	130.5	134	40.8
	120	10.0	12.57	13.46	21.6	24.22	139.5	162	27.3
	120	15.0	17.66	19.05	17.8	18.7	140.1	156	25.2
7475-T761	36	1.8	2.91	2.65	43.5	45.2	133.8	133	51.8
	36	3.6	4.85	4.75	34.1	33.1	139.4	135	46.6
	36	5.4	6.70	6.50	28.1	27.2	141.1	134	44.8
	48	4.8	6.12	5.90	31.1	31.2	142.2	139	41.7
	120	10.0	11.46	11.05	23.8	27.2	146.1	164	29.3
	120	15.0	16.50	16.05	19.5	18.1	147.3	133	26.9
7075-T6	30	4.87	5.28	5.23	13.4	14.35	59.2	63	20.7
	48	7.0	7.42	7.3	11.5	12.5	59.0	63	16.6
7079-T6	48	7.0	7.49	8.05	14.9	14.95	77.0	78	21.6
7475-T61	36	1.8	2.54	2.65	35.9	39.8	102.6	118	41.8
	48	4.8	6.13	5.7	25.1	29.25	114.8	129	33.7
	120	10.0	11.67	-	19.3	-	119.7	-	24.0

Figure 4.11: Comparison Of CLWL Predicted Instability Conditions To Experimentally Determined Values In Middle-Cracked Panels.

The next step in verifying the residual strength prediction model is through the testing of built-up (multiple-load-path) type structure. Such structures have the attributes of transferring load during crack propagation as well as of possibly arresting the running crack before a catastrophic failure of the complete structure occurs. The development of an accurate value of the structural parameter K, the stress-intensity factor, requires that the structural analyst properly account for load transfer, joint deformations, fastener effects, etc. As such, the testing of built-up structures can result in the verification of the stress-intensity factor (or other appropriate parameter) estimates as well as the material failure model and its supporting data.

As an example of results obtained to validate the use of a residual strength model for built-up structure with fracture arrest features, consider the work of Swift and Wang [Swift, 1971; Swift & Wang, 1970]. They tested extremely large flat panels with longerons and frames. The longerons were either T or hat sections. The frames were attached to the skin with shear clips; in some cases, extra tear straps were used as crack stoppers.

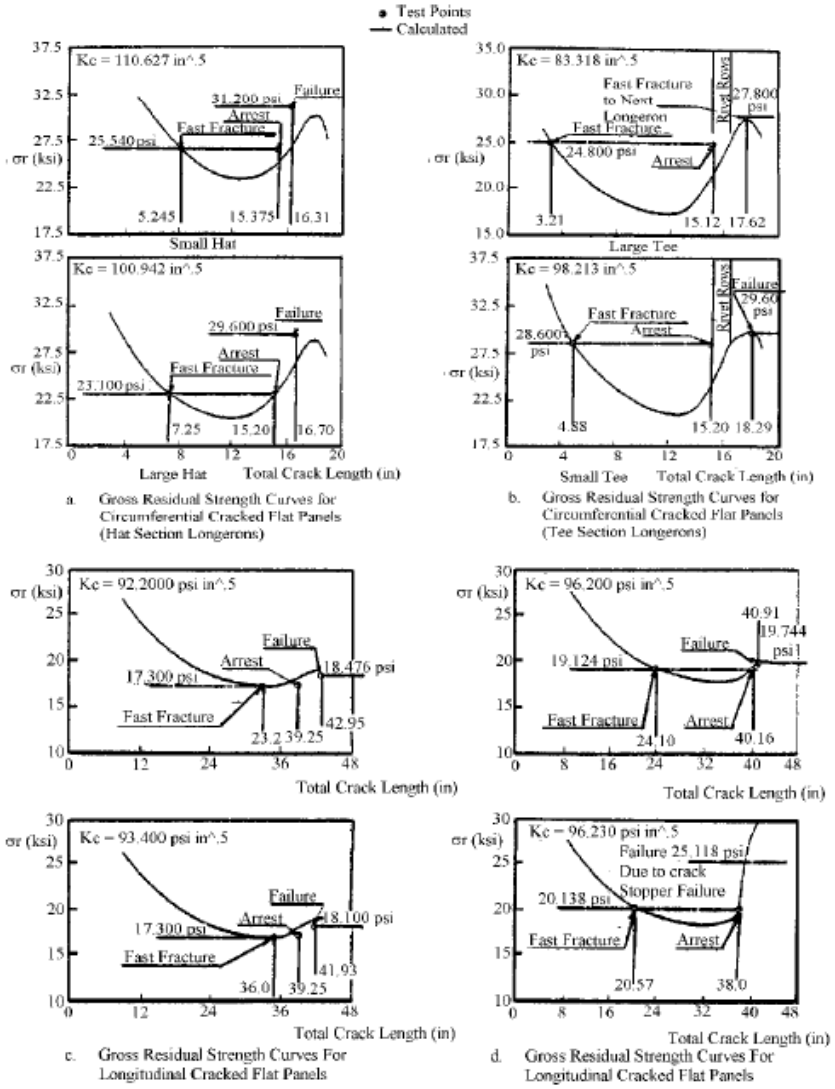

Figure 4.12: Test Results of Swift and Wang on 120 Inch Wide Panels with 7075-T73 Skin

In most cases, the analysis was shown to be within 5 percent of predicting the experimental observation. Additional examples of residual strength verification tests for model transferability using single-load-path and built-up structures can be found in Liu & Eckvall [1976], Verette, et al. [1973, 1977], Liebowitz [1974], and Potter [1982].

A similar program was conducted by Dawicke, et al. [1999]. Under the auspices of the NASA Aircraft Structural Integrity (NASIP) and Airframe Airworthiness Assurance/Aging Aircraft (AAA/AA) programs, a residual strength prediction methodology has been experimentally verified for aircraft fuselage structures.
The fracture criteria selected for use on the (mostly) thin gage aluminum fuselage structure was the crack tip opening angle (COTA). A detailed description of the testing methodology used for determining the COTA is given in Dawicke [1997] and Dawicke & Sutton [1993]. The COTA was selected to handle the diverse loading problems of large scale yielding, and significant stable crack growth which limited the applicability of more normal linear elastic fracture mechanics. Two finite element codes were used in the program: a) ZIP3D was used for the simple laboratory specimens which did not exhibit large out of plane displacements, b) STAGS, which is a nonlinear shell analysis code, was used for the residual strength analysis for larger specimens with large out of plane displacements.
A typical fuselage skin material, 2024-T3, was used throughout the program. Specimen thicknesses were 0.040, 0.063, and 0.090 inches. The laboratory test results of the CTOA were used to predict the results from larger structural element and full scale structure validation tests. The final test in the series was a full size fuselage segment with combined internal pressure loading and axial tension loads to simulate fuselage body bending.
The CTOA fracture criteria projects that crack growth will occur when the included angle of the two crack surfaces with respect to the crack tip reaches a critical value. The critical angle for a given material is nearly constant after growth exceeds the half thickness point. An increase in the thickness of the specimen causes a decrease in the CTOA.

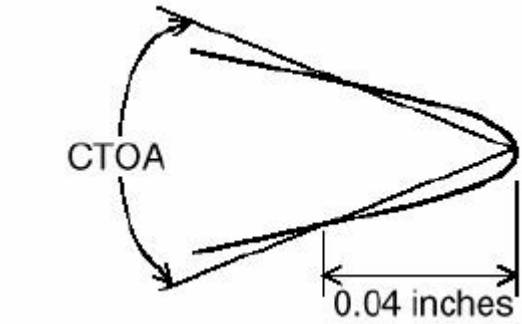

Figure 4.13: Schematic of the Definition of Critical Crack-Tip Opening Angle (CTOA) [Dawicke, et al., 1999]

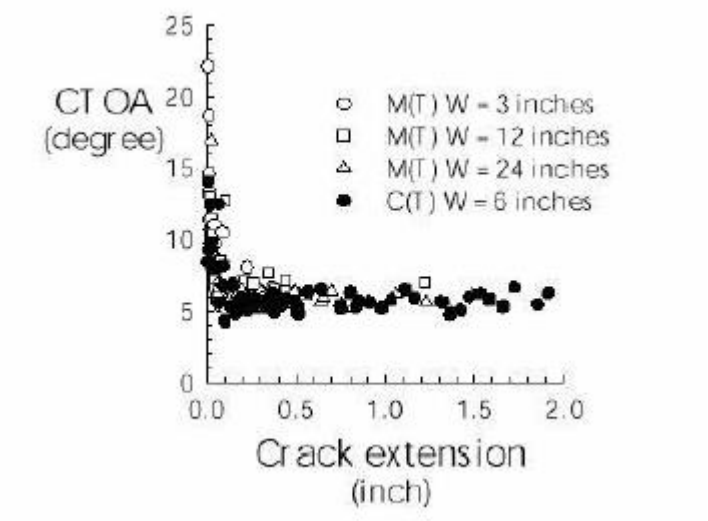

Figure 4.14: CTOA Measurements For 0.063-Inch-Thick, 2024-T3 Aluminum Alloy [Dawicke, et al., 1999]

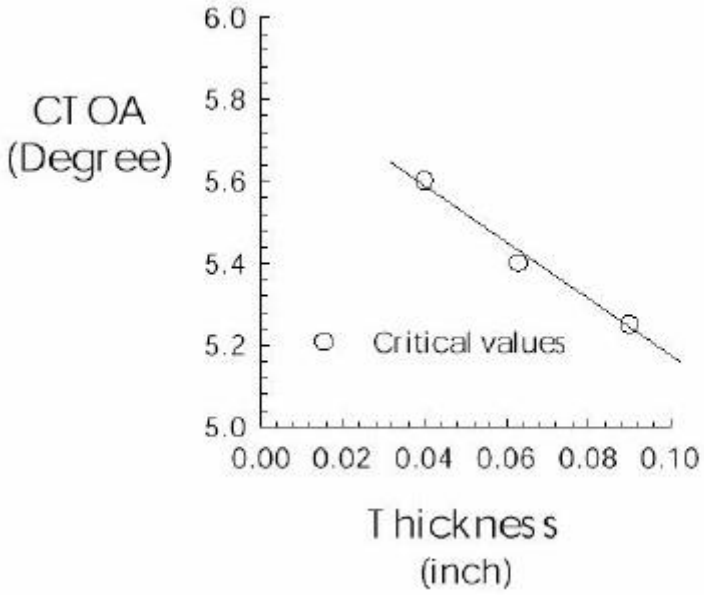

Figure 4.15: Influence Of Specimen Thickness On The Critical CTOA For 2024-T3 Aluminum Alloy [Dawicke, et al., 1999]

Another complexity that was introduced by using the STAGS 2D FEM was the necessity to account for the through-thickness constraint effects by using an approximation for the plane strain core (PSC). This approximation of the PSC height is nominally equal to or less than the specimen thickness.

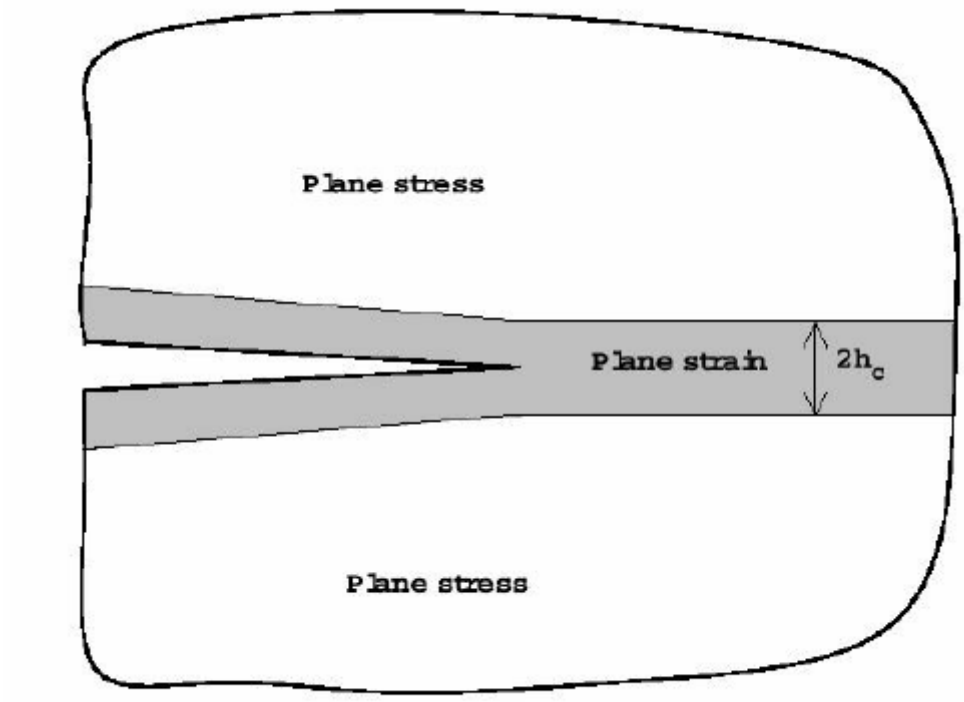

Figure 4.16: Illustration of the Plane Strain Core Around a Crack [Dawicke, et al., 1999]

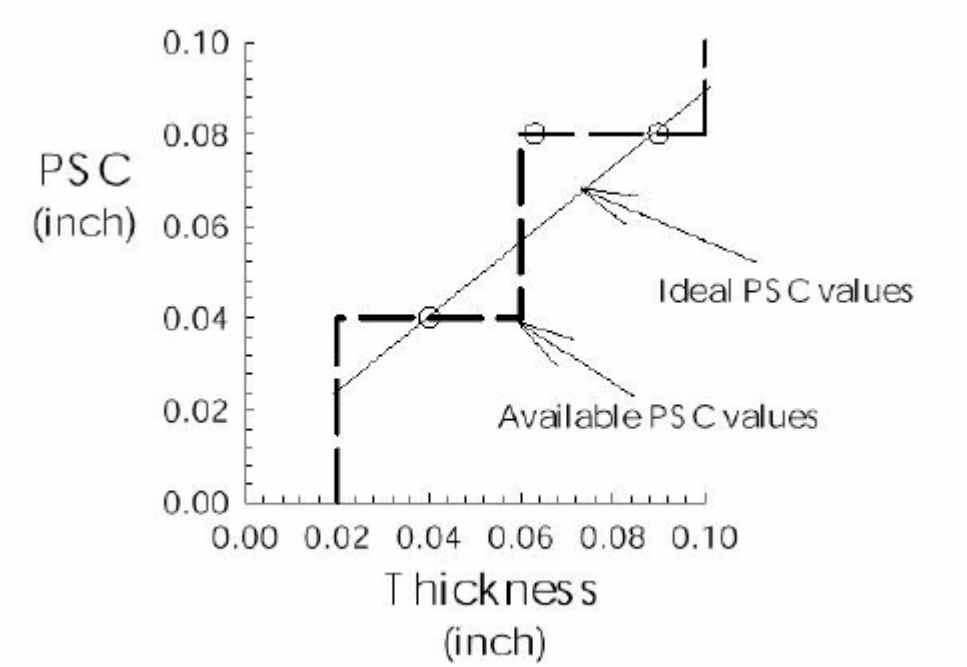

Figure 4.17: Plane Strain Core Heights (PSC) for the 0.04, 0.063, and 0.09-inch-thick 2024-T3 Aluminum Alloy Specimens [Dawicke, et al., 1999]

The report summarizes a successful application of the CTOA fracture criteria in conjunction with a 2D non-linear FEM model. The critical CTOA and the plane strain core (PSC) were acquired from small laboratory size specimens and the results were projected for wide panel (40 inches) and full scale fuselage structural components. For a specified thickness, the predicted value to the experimental test value was within 10% for all the program specimens.

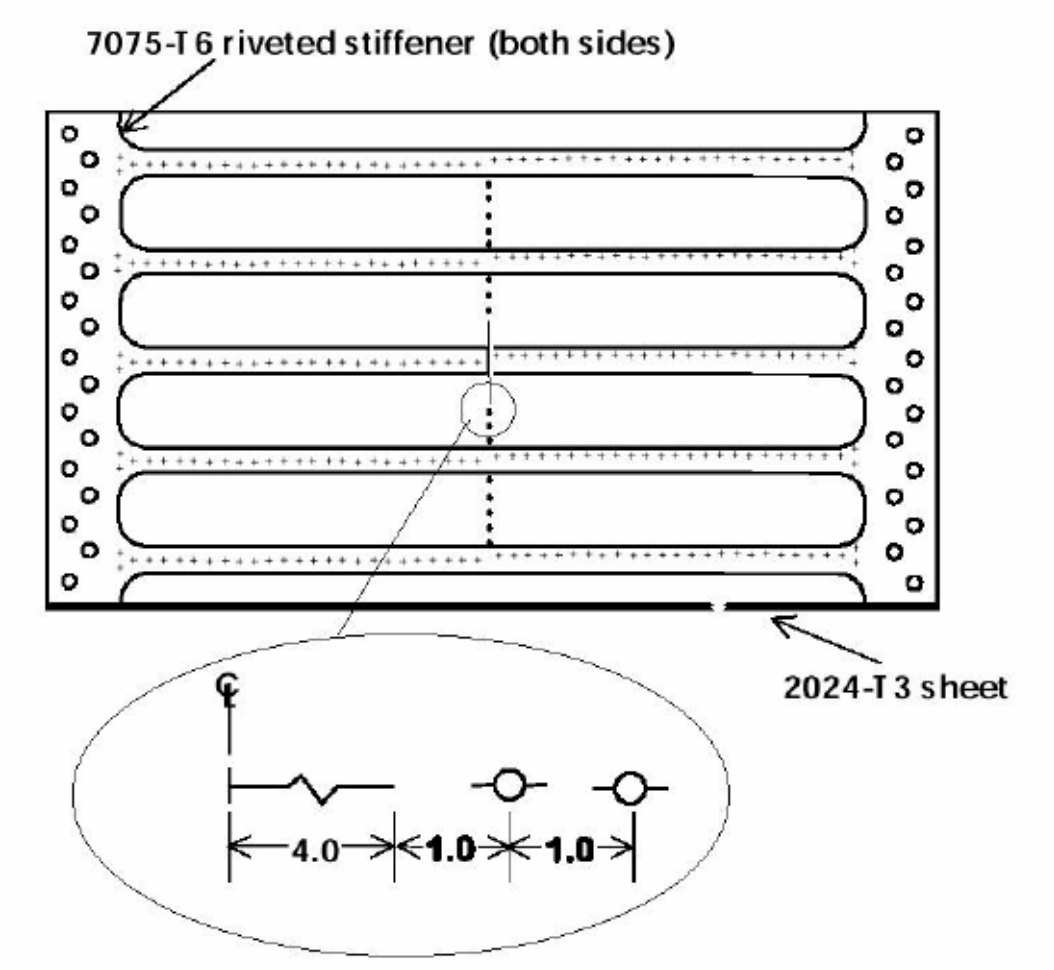

Figure 4.18: Stiffened Panel and MSD Crack Configuration [Dawicke, et al., 1999]

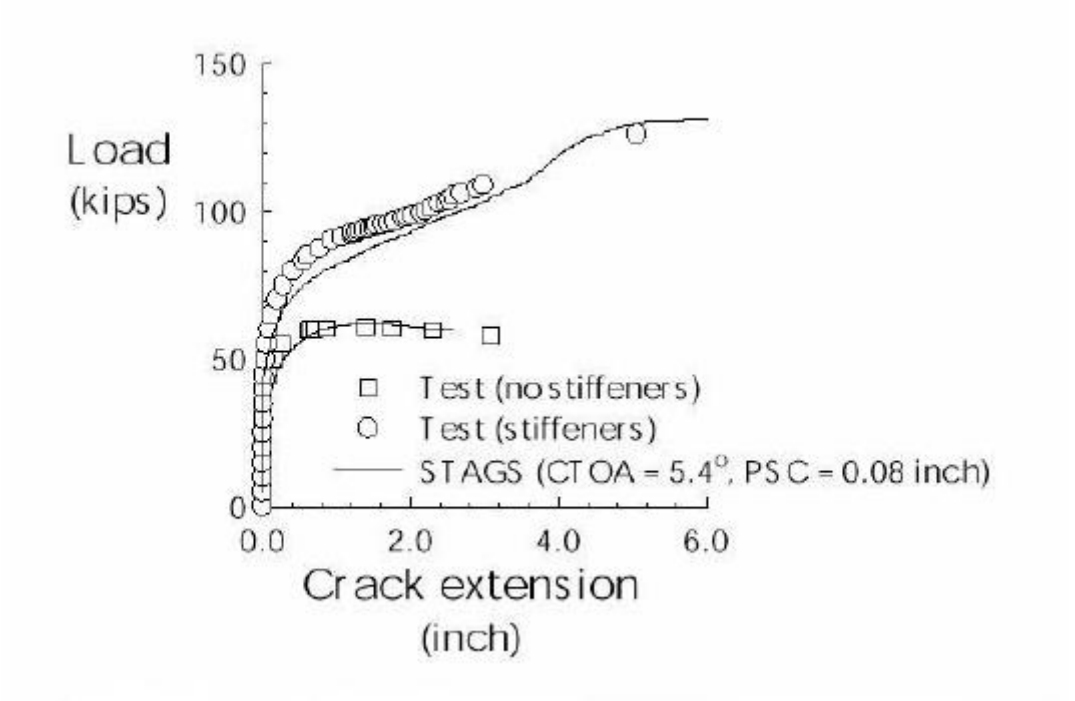

Figure 4.19: Fracture Test Results For 2024-T3, B=0.063-Inch-Thick, 40-Inch-Wide M(T) Specimens With and Without Stiffeners and STAGS Predictions Using CTOA=5.4° and PSC=0.08 Inch [Dawicke, et al., 1999]

The residual strength verification testing continues through both the design analysis and test development phase and the full-scale flight and ground test phase of an aircraft development contract (JSSG-2006 paragraph 4.12.2 and A4.12.2). For cost-effectiveness, it is useful to terminate a number of fatigue tests (used to verify the crack growth analysis or test spectrum design) with a controlled fracture test. Continuing a fatigue test until failure occurs may give incomplete or false information about the residual strength characteristics of the structure. Hence, it would not be appropriate to use fatigue failures to verify residual strength. The problems associated with attempting to verify residual strength analysis or characteristics using the information from fatigue test failures are summarized below:

1) The damage tolerance requirements specify residual strength loads, P_{xx}, which are all on the order of limit load. Stresses on the order of the limit load stress may occur seldom in the test stress history; they may not occur at all during the last part of crack growth. As a result, the cracks may grow much longer than the critical size associated with the stress level at the Pxx load. Then final failure will occur at a much lower stress.

2 Letting failure occur in the course of a crack growth test introduces a difficulty in determining the stress at fracture. If the loading is constant amplitude, it is reasonable to assume that fracture occurs at the peak stress. In variable-amplitude loading a series of low stress cycles may be followed by one high stress cycle during which fracture occurs. It is not certain now whether fracture took place at the peak or at a somewhat lower stress.

3) The critical crack size may be difficult to determine. Usually some crack growth has occurred since the last measurement. During the last cycles, crack growth may accelerate fast. This usually means that the fracture surface is very similar to that of a static fracture. As a result, the size of the fatigue crack at which fracture occurred is not well delineated on the fracture surface.

4) The crack growth at low stresses may continue so long that fracture occurs at a crack size that is too long with respect to specimen dimensions. A rational comparison with other test data is complicated due to the remaining ligament requirements and could be misleading.

Therefore, it is useful to perform a controlled residual strength test near the end of the crack growth test. For this purpose, the critical crack size is estimated on the basis of the stress at the required P_{xx}. The test is discontinued when this crack size is reached. Then an appropriately instrumented fracture test is performed. In this respect, it is important that the specimen is of sufficient size. There can be no question about this when a complete component is tested. In that case, any size requirement is overruled.

The basis of all crack growth calculations is the damage integration package discussed already, which includes the models and procedures used in estimating the effects of the load and environmental events in the operational history that must be verified. To model the impact that a variable amplitude load history has on the crack propagation characteristics of a structure, the damage integration package must be able to predict the effects of load amplitude, stress ratio (R), load sequences, and hold time events, as well as load frequency and waveshape in the case of a material sensitive to environmental effects.

Testing for verification of the crack growth models in the damage integration package should be conducted using middle-cracked panels. The middle-cracked panel geometry is characterized by widely accepted stress-intensity factor calibration and the results of spectrum tests with this geometry are easiest to correlate. It is recommended that the procedures outlined already and in ASTM E647 relative to geometry, crack measurement,

and pre-cracking be employed when using the middle-cracked panel specimen for non-constant amplitude loading.

Additional tests should be performed on specimens with radial corner cracked hole geometries and on specimens containing surface flaws in order to verify methods that describe the change in crack shape as the crack grows. It is important that corner-crack and surface-crack geometries be included in any crack growth verification test program in view of their relevance to the damage tolerance criteria. Radial corner-cracked-hole specimens and other part-through thickness specimens require special preparation techniques. Typically, the radial corner-cracked hole specimens are prepared in two steps. The first step is to introduce damage (EDM notch, saw cut, etc.) into a hole that is undersized and pre-crack the specimen until a crack of sufficient size appears. The second step is to enlarge the hole, remove the initial damage, and leave a crack with the required size in the specimen. It is necessary in the first step during pre-cracking to limit the stress-intensity factor levels so that the crack tip is not exposed to levels higher than what will be experienced during the test start up. Sometimes to preclude overload effects, the radial-cracked specimen is pre-cracked subsequent to the second step.

The surface flaw (part-through-crack) specimens are normally prepared along the lines suggested by ASTM E740. While the objective of this standard is to describe a fracture test of a part-through-crack type structural geometry, the standard details damage preparation techniques as well as pre-cracking procedures.

Because each material responds differently to the same spectrum, and because each load history will cause different amounts of damage in different materials, a crack growth damage integration package will be based on a combination of models and experimentally established constants. Typically, the effects of load amplitude, stress ratio and load sequence are addressed through the use of a model that effectively combines a crack-growth-rate-based stress-ratio model with a crack-growth-retardation model which in turn accounts for the effect of tensile and compressive overloads, as well as multiple overload occurrences. The stress-ratio models as well as the retardation models are empirically based as was discussed previously. The tailoring of the retardation model so that it adequately represents effects of a given spectrum and material is one of the more difficult tasks of the damage tolerant design analysis and test development activities.

The tailoring of the retardation model is based on crack growth life predictions of test results using reliable baseline (constant amplitude) crack growth rate data. In terms of developing a good correlation between prediction and test results, the following guidelines apply for each test. First and foremost, there should be a good estimate of the crack growth life based on the growth from crack initiation to test termination. Second, and normally just as important, the shapes of the predicted and test crack growth curves should match as closely as possible.

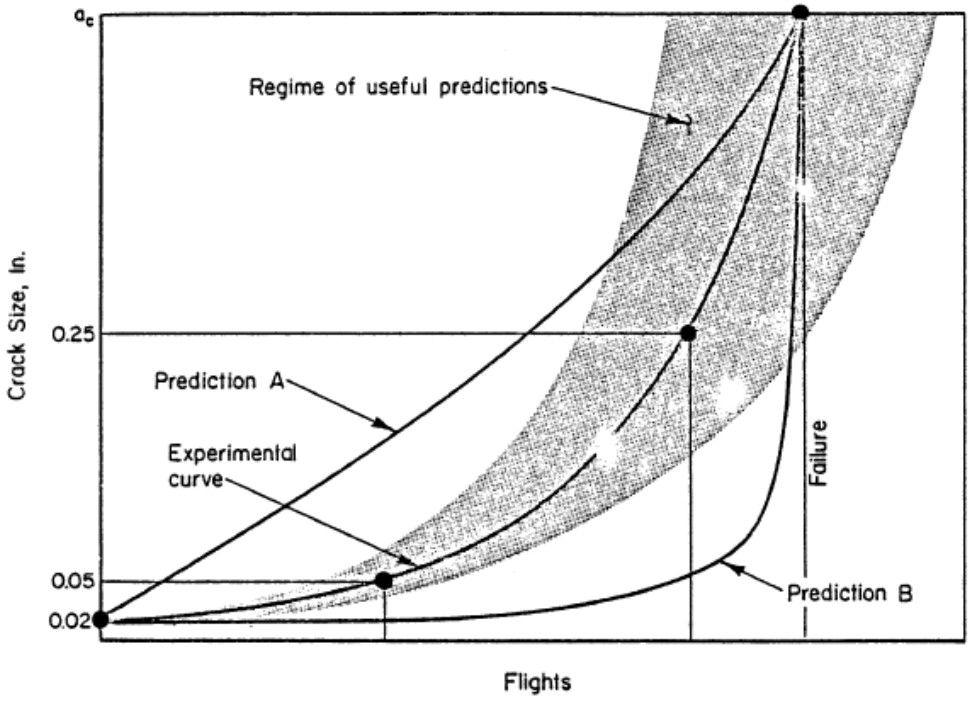

Figure 4.20: Comparison of Analytical and Experimental Crack Growth Curves

Predictions A and B would be considered bad, even though the life to failure was predicted correctly. Correlations are considered good if the prediction of all relevant points are within about 20 percent of the test data, as indicated by the shaded region of the figure. Typically, a number of tests with different conditions must be conducted before the damage integration package can be accepted with confidence. It is recommended that each crack growth test be summarized with crack growth life curves (predicted and test). The next several paragraphs describe a verification test program for an improved damage integration package.

In a study for the (then) Flight Dynamics Laboratory, Chang [Chang, et al., 1978; Chang, et al., 1981; Chang, 1981] conducted a series of crack growth tests on 2219-T851 aluminum alloy that were used to verify the accuracy of an improved damage integration package imbedded within the computer code EFFGRO. In Chang, et al., [1981], Chang summarizes the results of ten constant amplitude tests (different stress ratios), 20 tests where single and periodic overloads were applied, and 30 tests where multiple overloads and block loading conditions were studied. In Chang [1981], Chang summarized thirteen tests where different flight-by-flight loading conditions were applied; eleven tests involved fighter histories, two tests involved transport type histories.

Chang's Table No.	Number of Tests	Type of Load History	Life Prediction Ratios (N_{pred}/N_{test})		
			Mean ± Standard Deviation	Lowest Value	Highest Value
2*	10	Constant amplitude	1.340 ± 0.500	0.81	2.48
3*	19+	Single and periodic overload	0.783 ± 0.240	0.37	1.18
4*	30	Multiple overload and block	0.938 ± 0.30	0.15	1.60
2* and 3*	29	See above	0.974 ± 0.44	0.37	2.48
2*, 3* and 4*	59	All simple	0.956 ± 0.37	0.15	2.48
2++	13	Flight-by-flight	1.131 ± 0.22	0.80	1.46
2*,3*,4* and 2++	72	All	0.987 ± 0.35	0.15	2.48

+ one additional test reported but life estimate vague
* from Chang, et al. [1981]
++ from Chang [1981]

Figure 4.21: Summary of Chang's Improved Spectrum Prediction Results Based on Tables in Chang, et al.[1981] and Chang [1981]

Probability of Maximum Error Occurring (%)	Formula For Estimating Errors	Life Prediction Data For Estimating Errors (See Table 7.4.2)	Lowest Error Expected (N_{pred}/N_{test})	Highest Error Expected (N_{pred}/N_{test})
±1	Mean ± 2.58 Std. Dev.	0.987 ± 2.58×0.35	0.084	1.89
±5	Mean ± 1.96 Std. Dev.	0.987 ± 1.96×0.35	0.301	1.67
±10	Mean ± 1.645 Std. Dev.	0.987 ± 1.645×0.35	0.411	1.56

Figure 4.22: Error Estimate in Life Prediction Ratio Based on Assumed Normal Distribution of All Chang's Results (72 Tests)

By collectively evaluating the life prediction ratios for the individual tests, for selective test groupings, and for the total number of tests conducted, the engineer can evaluate both the effectiveness of the modeling approach as well as the accuracy of individual tests. Improvements in the more fundamental segments of the model might yield substantial improvements in all the life prediction ratios, whereas isolated modification of some empirical constants might only improve the predictability of a limited number of tests. It is recommended that life prediction ratio data provide the basis for justifying selection of damage integration packages. In fact, by using such schemes for different crack geometries or load transfer situations, the engineer will have the necessary confidence that crack growth life predictions for more complicated cases can be made with the best possible reliability. See Saff & Rosenfeld [1982], Wozumi, et al. [1980], Rudd, et al. [1982], Dill, et al. [1980], Abelkis [1980] and Lambert & Bryan [1978] for other examples of test programs designed to verify the capability of a damage integration package.

In the design of a given airplane component, generality is not required if the damage integration package applies well to the spectrum and history of that component. The most applicable prediction method has to be found. The only basis for judgment of the applicability is a series of tests with the relevant spectrum and stress history. Therefore, it is recommended that some substantiation testing be performed as soon as there is

reasonable certainty with respect to the spectrum shape. The experiments should be performed on a flight-by-flight basis, with landing loads included. A reasonable number of stress levels should be used. The stress sequence within a flight should be representative for service usage or arranged in a lo-hi-lo sequence. Block loading should not generally be applied. Experiments should be run for a few different design stress levels and one or two clipping and truncation levels in order to evaluate the effect of these changes on crack growth behavior, and to justify proposed changes to the design spectrum for component and full-scale fatigue testing.

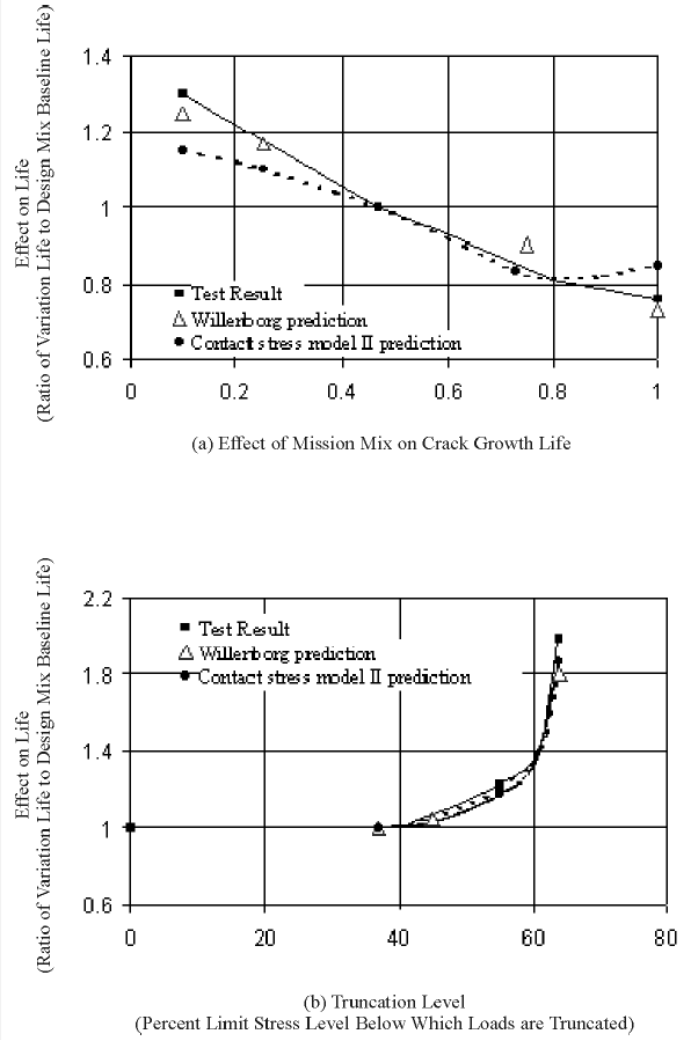

Figure 4.23: Effect of Spectrum Variations on Crack Growth Life Compared to Baseline (Design Mix) and to Two Damage Integration Packages [Dill, et al., 1980]

SECTION 4.4: STRUCTURAL HARDWARE TESTS

The structural hardware tests have two functions: to support the verification of the complete structural design, and to define those areas of the structure that need additional attention. These tests are scheduled so that there is sufficient time to incorporate structural changes into production aircraft. In fact, production go-ahead is predicated on completing at least one design lifetime of flight-by-flight loading in the full-scale durability test (see JSSG-2006 paragraph A.4.11.1.2.2.b). Structural hardware tests include joint tests, component tests, assembly tests, as well as full-scale structural tests.

Examples of variables that may be considered for the study of different design concepts, design details and structural materials are:

- fastener systems
- type of joints and joint detail
- forged versus machined or built-up structure
- production method
- reinforcement or tear strap shape, size, and spacing
- multiple or single load path
- materials or combination of materials
- effect of design stress level

Structural hardware testing can be a form of comparative testing during the development phase. That means that the test conditions do not always have to be an exact simulation of service conditions as long as the variables considered are tested the same way. However, it is strongly recommended that service conditions be approximated as closely as possible. How closely the test conditions have to resemble service conditions depends upon the predictability of the effect of a change in conditions.

The following guidelines are applicable to structural hardware testing for damage tolerance. First, the specimen should contain the design and manufacturing details that are the subject of the investigation. The load should be properly distributed at the point of interest. Second, if the purpose is to validate a piece of structure for damage tolerance, then load sharing, load interaction, and load transfer among different members should be simulated or otherwise accounted for. Type of loading (bending, tension) should be as in service, or be such that the stress distribution at the critical location is as in the actual structure. Special care should be taken that no undesired bending is introduced due to load eccentricities. This requires intelligent grip design. It may also require some special structure to distribute the loads properly from these areas into the specimen. Third, the nominal stress at the critical location should be as in service. Experiments should be performed on a flight-by-flight basis with landing loads included. A reasonable number of stress levels should be used. The stress sequence within a flight should be representative of service usage or arranged in lo-hi-lo sequence. Block loading should not generally be applied.

In JSSG-2006 Tables XXX and XXXI, certain initial damage assumptions and continuing damage assumptions are prescribed. These assumptions form a basis for analysis but they cannot always be rigidly adhered to in damage-tolerance testing.

A 0.05 inch initial crack is assumed in slow-crack growth structure and in fail safe structures. If the specimens for design development testing are not provided with artificial defects, the cracks, once initiated, will grow through the sizes mentioned above. Crack-growth records would automatically cover the span of the requirements, provided the cracks can be detected. Otherwise the recorded crack-growth curve would have to be extrapolated backwards. If initial flaws are provided, it is recommended to make them the size assumed in the requirements or close to the size for analysis substantiation.

Continuing damage, from a testing standpoint, is more difficult to make as a result of the small initial sizes and the different growth requirements for different cases.

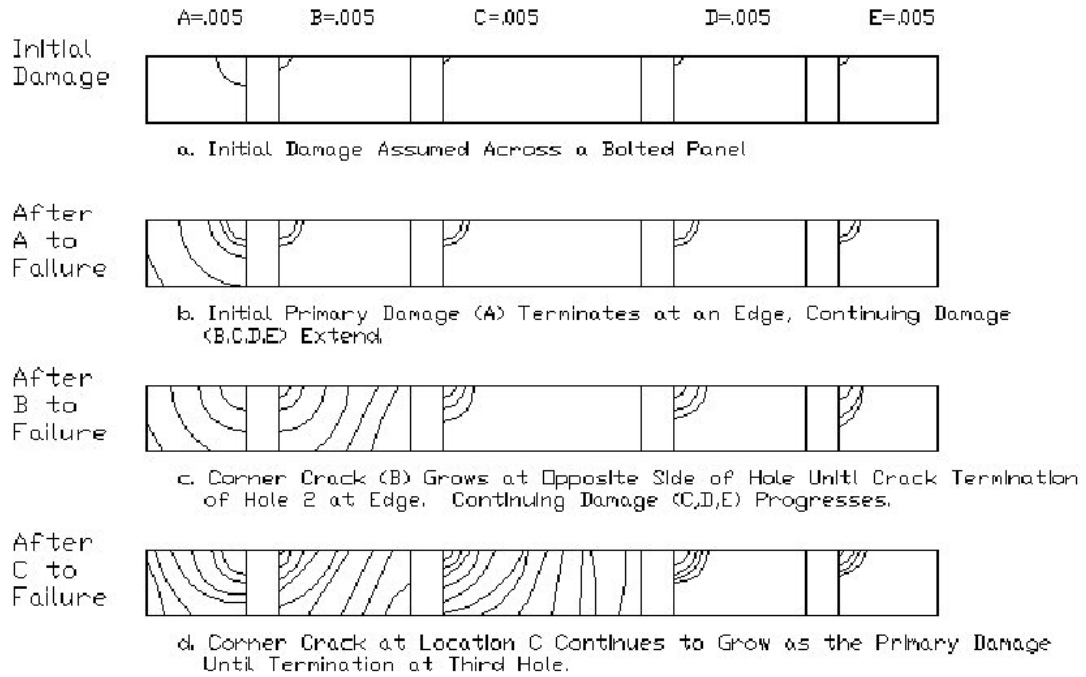

Figure 4.24: Primary and Secondary Damage Sites and Continuing Damage

Consider the example configuration where A is the primary damage site, and B, C, D, & E are continuing damage sites. The four parts of the figure show (a) the initial damage assumed in the panel per JSSG-2006 paragraph 3.12.1 and Tables XXX and XXXI, (b) the initial damage and growth until the primary damage terminates at the edge, (c) the continuing damage that starts at B, the opposite side of the primary damage site which terminates in hole 2, and (d) the growth of continuing damage at C until termination at hole three. While the analysis can follow the assumptions required by JSSG-2006, it would be difficult (if not impossible) to manufacture the necessary continuing sizes either prior to test or after the primary damage (segment A) terminated at the edge. Therefore common practice is to put in the primary damage and continuing damage starter flaws and let the specimen crack growth proceed without additional perturbations. Post test analysis of the crack growth data and fracture surface striation morphology will document this logic.

In a AFRL/VA contracted study, Brussat et al. [1977] were able to show that the experimental fatigue lives of built-up structure with and without continuing damage flaws were about the same and that the primary crack damage chose the most effective path through the structure. Secondary cracks developed in a natural way during the test. Dormant periods when a crack ran into a hole could be estimated and subtracted if the results were used for a check of the analysis.

Residual strength tests of fail safe structure are of special importance. Interruption of a fatigue test at the critical crack size for intact structure is crucial. If the crack grows longer, the stress for rapid propagation is too low to give proper information on crack arrest capabilities and on the strength of the remaining structure at that stress (times the dynamic factor). Since these properties are essential for the qualification as fail safe structure, a proper evaluation is justified, even during design development tests.

After instability and arrest (or load path failure), if successful, fatigue testing should be continued. At that point the JSSG-2006 Damage Tolerance Requirements assume remaining structure damage. In testing, this poses the same problems as the continuing

damage. Therefore, it is recommended that the remaining structure damage be developed in a natural way during damage tolerance testing; artificially induced damage may also be incorporated where necessary consistent with the initial flaw assumptions of the component. Again, fatigue cycling is discontinued when the (calculated) critical size for the remaining structure damage is reached. Then a final residual strength test is performed.
During the development cycle, the manufacturer will subject major assemblies and structural components to flight-by-flight fatigue loadings that approximate the operational environment. Some tests are specifically identified as damage tolerant tests or as durability tests, but other tests serve a dual function - first as a durability test (two lifetimes) and then as a damage tolerant test. Component durability tests or component dual function tests are normally scheduled to precede the full-scale durability test by a sufficient amount of time that would allow incorporating suggested structural modifications into the full-scale durability test article. The scheduling of the full scale damage tolerant test follows (and uses) the full scale durability test article.
The major assemblies and components selected for damage tolerant testing are chosen to provide further assurance that major elements will not fail during service and thus impact the operational readiness of the force due to safety-of-flight failures. Several examples of major assemblies and components selected during recent weapon system acquisition programs are listed below.
The damage tolerant articles will include artificially induced damage such as scratches, elox notches, sawcuts, and other types of non-crack damage, and are then subjected to an interval (about one-quarter lifetime) of flight-by-flight loading that is designed to initiate the desired starter cracks. The test interval subsequent to the precracking is up to one design lifetime with a P_{xx} loading applied at the end of the lifetime to verify residual strength capability. Crack growth should be monitored throughout the test. In-service inspection procedures should be employed whenever possible to evaluate the ability of these procedures to locate and measure the cracks.

F–16	A–10	B–1A	KC–10
Wing/Fuselage Box Beam Components	Wing Lower Center Panel	Wing Carry Through Article*	Fuel Tank Panel and Fuselage Floor Beam Structure
Horizontal Tail Component	Engine/Nacelle Forward Support Frame Fuselage Support Lug	Aft Fuselage Article*	Aerial Refueling Boom
	Horizontal Tail Support Aft Frame Fitting and Attachment Lug		
	Nacelle Thrust Fitting Assembly		

* Damaged subsequent to durability test (2 lifetimes).

Figure 4.25: Major Assemblies and Components Tested to Support Damage Tolerant Design Verification

Throughout the structural hardware test program, there is substantial attention given to cracking problems. Such problems, when they surface, identify areas where the design should be modified to ensure the soundness of the final product. Each structural problem is

analyzed to determine the specific cause of the problem so that appropriate candidate solutions can be incorporated into production aircraft.

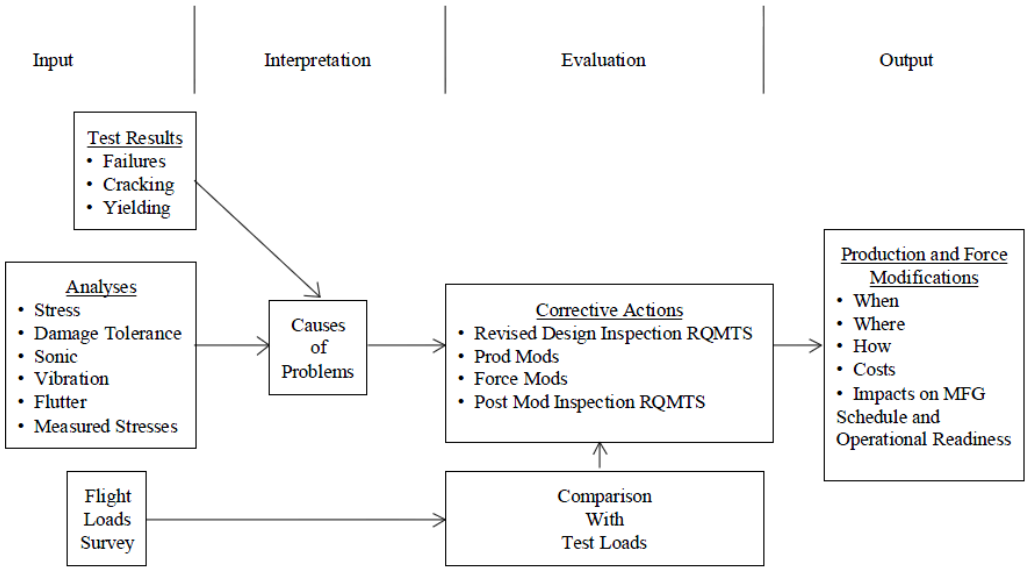

Figure 4.26: Summary of Interactions Resulting from Structural Failure Per JSSG-2006 Requirements

One final check on the adequacy of the structural design is the teardown inspection that follows the full-scale durability test (two lifetimes or economic life) and the damage tolerance test (one lifetime). The teardown inspection is required by JSSG-2006 paragraph 4.11.1.2.2.e to provide assurance that no critical area has been overlooked in the course of normal inspections, and to characterize the state of crack development in selected structural areas. In relation to the characterization of the state of crack development, the teardown inspection will typically include the sectioning of the structure for additional fatigue testing, residual strength testing, and/or microscopically tracking cracks back to the start of the durability test. The crack population at the end of the durability test and damage tolerance test becomes the basis for assessing the quality of the production structure through the use of the equivalent initial quality concept.

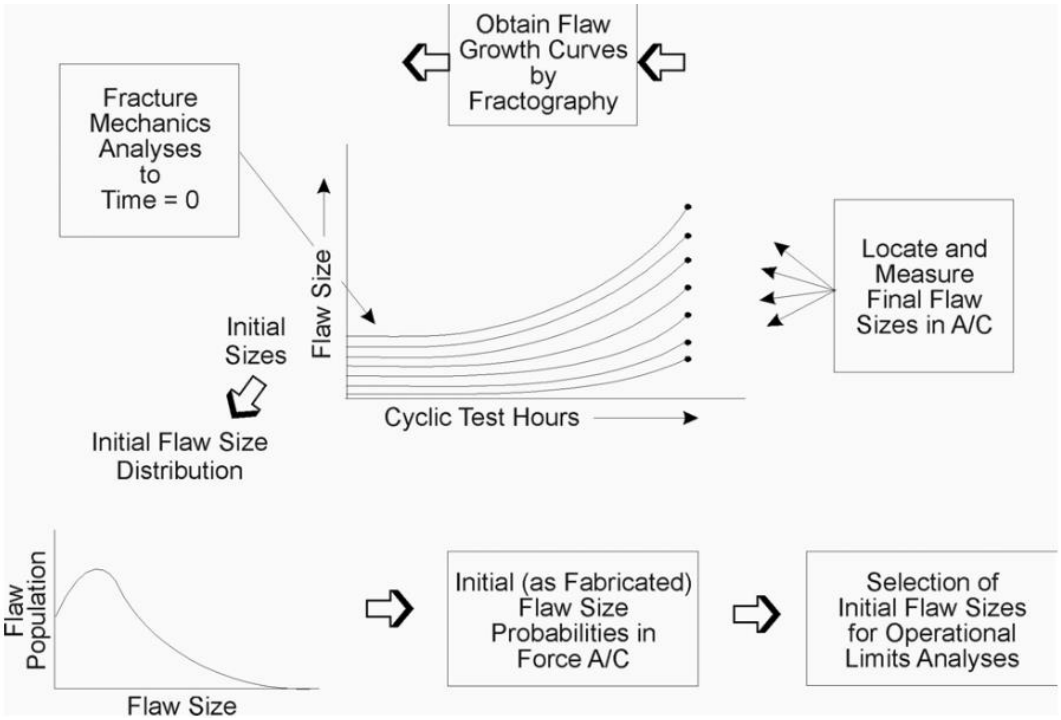

Figure 4.27: Equivalent Initial Quality Distribution Obtained by Backtracking Cracks Found in Durability Test Articles. Backtracking Procedures Involve Fractography and Fracture Mechanics Crack Growth Analyses

SECTION 5: STRUCTURAL ELEMENTS AND LOAD ARRANGEMENT

The identification of structural elements should begin with a review of the following four basic definitions.

SECTION 5.1: STRUCTURAL ELEMENTS DEFINITIONS

Principal structural elements (PSEs) are those which contribute significantly to carrying flight, ground, and pressurization loads, and whose failure, if it remained undetected could result in catastrophic failure of the airplane.

Critical structural elements (CSEs) are those elements whose failure would result in catastrophic failure of the airplane.

Primary structure is that structure which carries flight, ground, or pressure loads.

Secondary structure is that structure which carries only air or inertial loads generated on or within the secondary structure.

These definitions provide some useful guidelines, but they give no easy clues about how to accomplish the identification. Evidently, primary structure ought to consist of PSEs and CSEs, but what should the breakdown be, and what about secondary structure? The answers to these questions depend upon analysis of function and judgement of failure consequences. The approach to getting the answers should begin with a checklist that covers the entire airframe.

WING AND EMPENNAGE:

- ✓ Control surfaces, slats, flaps, spoilers, and their mechanical systems and attachments (hinges, tracks, and fittings);
- ✓ Integrally stiffened plates;
- ✓ Primary fittings;
- ✓ Principal splices;
- ✓ Skin or reinforcement around cutouts or discontinuities;
- ✓ Skin-stringer combinations,
- ✓ Spar caps;
- ✓ Spar webs;
- ✓ Spar "kick" details in swept wings.

FUSELAGE:

- ✓ Circumferential frames and adjacent skin;
- ✓ Door frames;
- ✓ Pilot wine 3w posts;
- ✓ Pressure bulkheads;
- ✓ Skin and any single frame or stiffener around a cutout;
- ✓ Skin and/or skin splices under circumferential loads;
- ✓ Skin and/or skin splices under fore-and-aft loads;
- ✓ Skin around a cutout;
- ✓ Skin and stiffener combinations under fore-and-aft loads;
- ✓ Door skins, frames, and latches;
- ✓ Floor skins and beams;
- ✓ Window frames.

LANDING GEAR AND THEIR ATTACHMENTS:

- ✓ Trunnions;
- ✓ Main struts (inner and outer parts).

ENGINE MOUNTS:

- ✓ Struts;
- ✓ Thrust links;
- ✓ Pitch and yaw reaction force fittings;

ENGINE CONTAINMENTS AND CASINGS

An average structure area is considered critical stress areas and needs to be evaluated for crack propagation. The number is often reduced to about 90 PSEs by area similarity. The following selection criteria for PSEs are proposed:

- Elements in tension or shear
- Low static margin
- High stress concentration
- High load transfer
- High spectrum density
- High stresses in secondary members after primary member failure
- Materials with high crack growth rates
- Areas prone to accidental damage
- Component test results
- Results of full-scale fatigue test

SECTION 5.2: STRUCTURAL LOAD ARRANGEMENTS

The main structural boxes in the wings, horizontal stabilizers, and vertical stabilizer are primary structures which possess generally similar configuration and function, The pressure loads on each corresponding pair of aerodynamic surfaces (upper and lower) are gathered chordwise to the box and then carried spanwise to the fuselage. The net upward load is the difference between the aerodynamic lift and the downward acting wing weight (structure, fuel and wing-mounted engines). The box bends and shears upward due to the spanwise loads and also twists nose-up because the center of pressure is offset forward of the elastic axis. The aerodynamic drag loading also bends and shears the box aft, but the effect on stresses is small when compared with the effects of upward deflection and twisting.

The resulting stresses are compression in the upper components, tension in the lower components, and shear in the skins and webs. A transport wing box is generally designed to make the most efficient possible use of stressed-skin construction because transport aircraft are designed for high wing loadings to cruise at high speeds. An exploded view of one comer of the box shows how the stresses act on the lower panel (skin, spar caps, and webs). The schematic also shows how the shear associated with twist is carried from the skin through the front spar cap to the front web. (The webs also carry the shear associated with upward bending.) Each fastener participates by exerting equal and opposite bearing loads on the components which it joins. Similar systems of forces act at splices and repair patches. Spanwise skin splices transfer shear from one skin panel to the next via equal and opposite fastener bearing loads. Chordwise splices transfer both tension (in the lower skin) and shear in a similar manner. Fastener bearing is also the mechanism for diverting some of the skin stress through the doubler in a repair patch. The wing box lower panel acts as a unit carrying the tension due to bending. A failure of the panel would immediately separate the wing from the aircraft, which would then enter an uncontrollable roll. Thus, the lower panel is an obvious CSE.

What about the empennage? The spars in a stabilizer structural box are often designed to carry a greater proportion of the bending load, in relation to the skins, because the stabilizer dimensions are much smaller and stabilizer loadings are generally much lower than wing loadings.

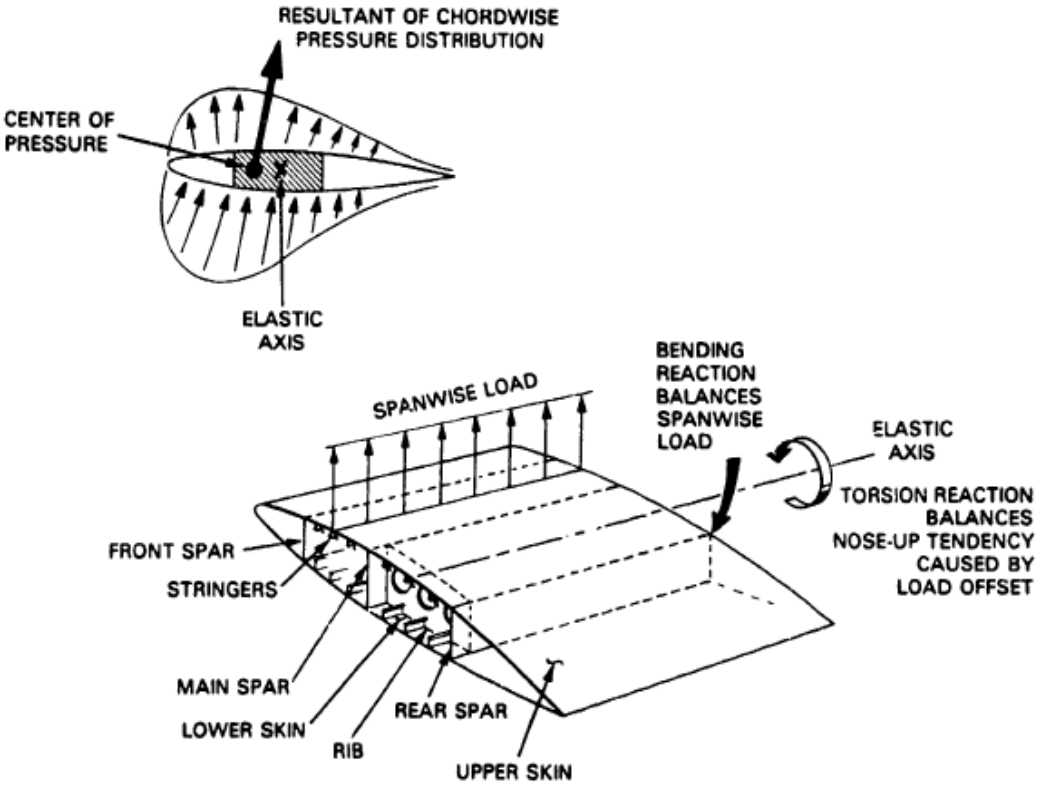

Figure 5.1: Wing box configuration and function

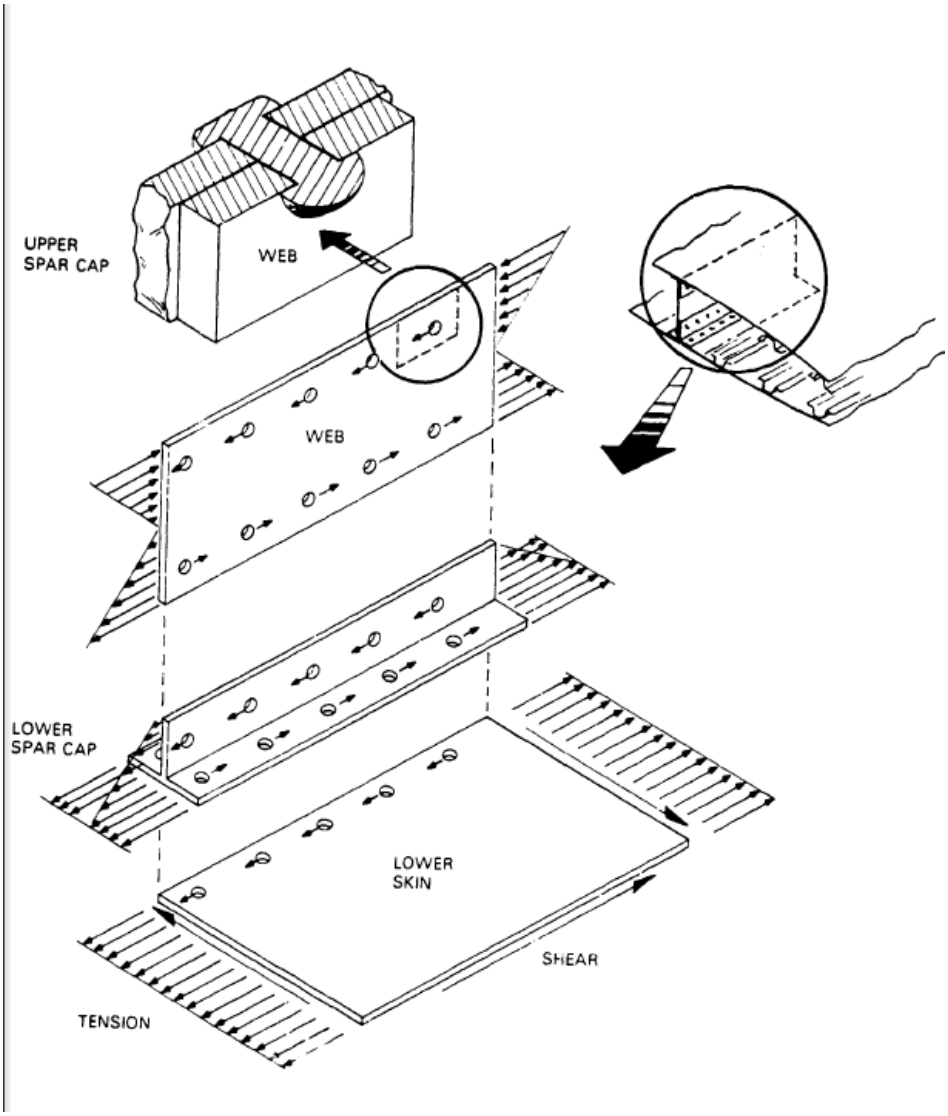

Figure 5.2: Stress in a wingbox

The horizontal stabilizers are normally under down load to maintain pitch trim', so attention must be paid to the upper panel (or simply the spar caps in a small stabilizer). Loss of one side would cause an immediate nose-down pitch; it is also likely that the damage would prevent control of the elevator on the other side, leaving the aircraft in an unrecoverable dive. It is not so easy to predict what will happen if the vertical stabilizer fails, since it does not normally bear any significant trim load. The consequent immediate loss of the rudder is serious but not necessarily fatal. Case studies suggest that judgements based on specific aircraft configurations and characteristics (under-wing versus fuselage-mounted engines, coupling between yaw and roll modes, spiral divergence rate, etc.) should determine whether the vertical stabilizer is a PSE or CSE. The fittings which attach wings and stabilizers to the fuselage continue the carriage of major flight loads. Therefore, these attachments are also primary structure and, for the most part, critical elements.

Conversely, the control surfaces are secondary structure because they carry only their own self-generated air loads. Elevators are obvious CSEs, and rudders can be argued either way, for the same reasons just given in the discussion of primary structure panels. Flaps, slats, ailerons, and spoilers are probably in the PSE category; in any case, the decision should depend on the specific control system design. Do normally operating spoilers provide adequate roll control if one aileron is lost? Can the spoiler control be disabled (spoilers stowed) and the airplane flown with ailerons alone if spoilers are lost on one

side? If flaps and/or slats are lost on one side, can the airplane be landed flaps-up, or does the spoiler/aileron system have enough roll control authority to keep the wings level in a partially deployed split-flap situation? Positive answers to questions like these would suggest PSE or lower classification.

The stressed-skin stiffened shells that form transport aircraft fuselages are primary structures in which panel assemblies again play a major role as structural elements. Most fuselage panels would probably be classified as PSEs, based on the history of aircraft accidents caused by fuselage panel failures. In some cases, the remaining structure prevented in-flight breakup and gave the flight crew enough margin to land at the nearest airport.

How did these fuselages manage to hold together under circumstances that would have led to immediate in-flight breakup, had the failure occurred in a wing box panel? One reason is that a fuselage panel failure quickly relieves the pressurization. A second reason is that the pressure design limit load requirements may lead to structure that is overdesigned for the bending that a damaged fuselage must still continue to carry due to the weight of its own structure plus equipment and payload. On the fuselage crown at a station over the wing attachments, the axial stress due to bending can approach the magnitude of the pressurization stress. A simplified model, which overestimates the bending stress, is summarized below to illustrate this point. This part of the crown area is usually designed with some local reinforcement, in any case, to accommodate the transfer of major loads between the wing and fuselage.

The ratio of maximum bending stress to pressure hoop stress can be quickly estimated by treating the fuselage as a circular cylinder of radius R, thickness t, and length *L* loaded by a total weight W distributed uniformly along its length and supported at mid-length, where the wing-fuselage attachments are assumed to be concentrated. The effect of stiffeners is neglected. Based on simple beam theory, the maximum bending stress is then given by:

$$\sigma_B = \frac{WL}{8\pi R^2 t}$$

The pressure hoop stress is:

$$\sigma_P = \frac{PR}{t}$$

where P is the internal pressure. Combining these two formulas leads to the ratio:

$$\frac{\sigma_B}{\sigma_P} = \frac{WL}{8\pi PR^3}$$

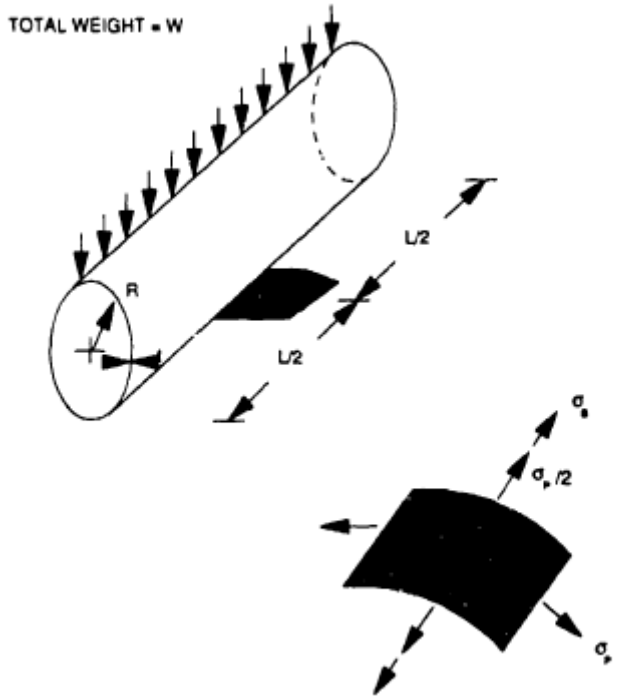

Figure 5.3: Simplified fuselage model

The following results are based on published nominal dimensions and weights of several typical transport airplanes. A pressure P = 9 psi was assumed, and the model weight was estimated as:

$$W \cong W_{ZF} - 0.2W_G$$

where W_{ZF} and W_G are the maximum zero fuel weight and the maximum gross weight respectively.

The bending stress is much lower at other locations. At any fuselage station, it decreases in linear proportion to vertical distance below the crown, passing through zero at about the fuselage mid-height and changing to compression in the lower half of the fuselage. It also decreases fore and aft of the wing attachments, in approximate proportion to the square of distance from the station considered to the nose or tail cone. Conversely, the pressurization stresses are approximately constant over the mid-body section, where the fuselage shape is close to a circular cylinder.

The pressure stresses are thus the dominant components over most of the fuselage. The design limit and ultimate load factors for pressurization can thus provide a margin of safety in bending, even after the fuselage has been severely damaged, as long as the aircrew can keep the aircraft close to unaccelerated flight until landing. It is logical to rely on the accident history and to classify most of the pressurized fuselage structure as PSEs. However, the CSE classification should be considered for panels near the wing-fuselage attachments.

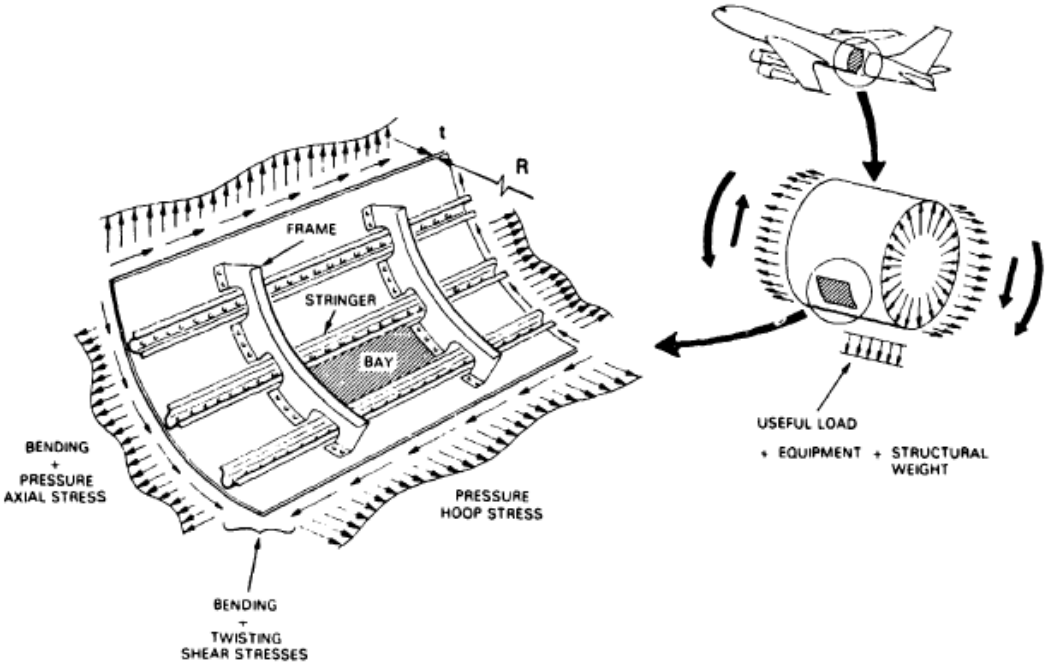

Figure 5.4: Stress in a fuselage shell

The skin stresses, shown along the panel edges, vary from maximum values at mid-bay to minimum values over the frames and stringers. The variation is a consequence of the effect of' pressure loading on a stiffened cylinder. If the fuselage were simply a skin, its radius would expand uniformly under pressure, The frames and stringers restrain the expansion to a great extent near their own centerlines and to a decreasing extent toward mid-bay. The maximum pressure stresses at mid-bay are less than the simplified model stresses. The skin also carries shear stresses, which are generally low compared to the other stresses. Shear associated with fuselage bending is greatest at stations near the wing attachments and at approximately fuselage mid-height, decreasing to zero at the crown and keel. Shear due to twist is approximately independent of location (within the cylindrical portion of the fuselage). The shear due to twist is caused by transient forces, such as vertical stabilizer yaw loads, and is generally much less than the magnitude of shear due to bending. Only minor fastener bearing loads are encountered over large areas of continuous skin. The minor loads occur mainly near frame-stringer crossovers, where most of the local load transfer between skin and stiffeners takes place as the stiffeners act to restrain the skin expansion. These bearing loads are related to the skin stress variation, which is typically about 30 percent of the nominal skin stress. If the skin in a bay is cracked, of course, the nearby fastener bearing loads must increase in order to redistribute load away from !he cracked area to the surrounding stiffeners. A longitudinal crack sheds pressure hoop stress to the adjacent frames; a circumferential crack sheds axial stress to the adjacent stiffeners.

Another important local effect of the restrained expansion phenomenon is secondary bending in the stiffeners. Since the pressure hoop stress generally exceeds the pressure axial stress, longitudinal cracks are of the most concern in a damage tolerance assessment, and frame bending is thus the most important secondary bending effect.

The floor structure create, a similar bending effect on a larger scale. The cabin floor is supported in part by cross-beams, which carry the floor loads into the fuselage structure via ties to the frames. The floor loads include pressure in those areas of the cabin located above unpressurized cargo bays or wheel wells.

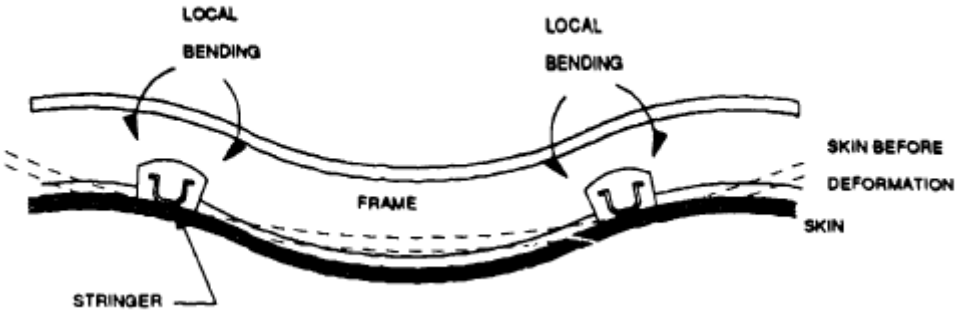

Figure 5.5: Frame bending

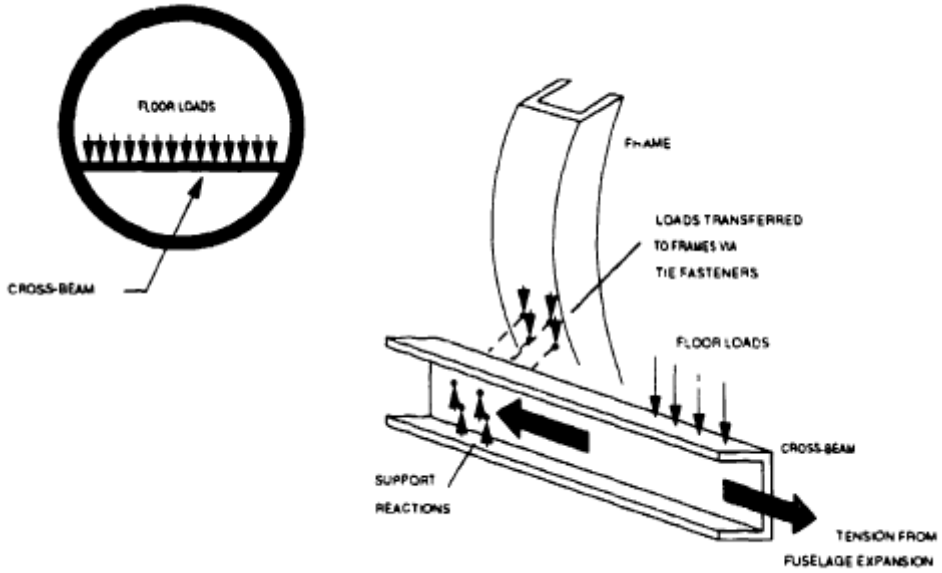

Figure 5.6: Floor cross-beam function

When the fuselage expands under pressure, it must impose tension on the cross-beams. However, cross-beams are extremely stiff in tension and are able to locally restrain the expansion much more effectively than other parts of the structure. As a result, the skin and frames are bent inward near the floor when the fuselage is pressurized, as depicted in the exaggerated deflection schematic below. This local bending effect also appears as additional fastener bearing loads at the frame tie details.

How should the floor structure be classified? The floor consists of flat panel assemblies (skin, stringers, and cross-beams) that carry mainly passenger and cabin furnishing loads into the fuselage shell. These loads do not appear in the definition of primary structure, so most floor panels would be classified as secondary. Conversely, panels located above unpressurized bays must carry the pressure load and, therefore, should be classified as primary.

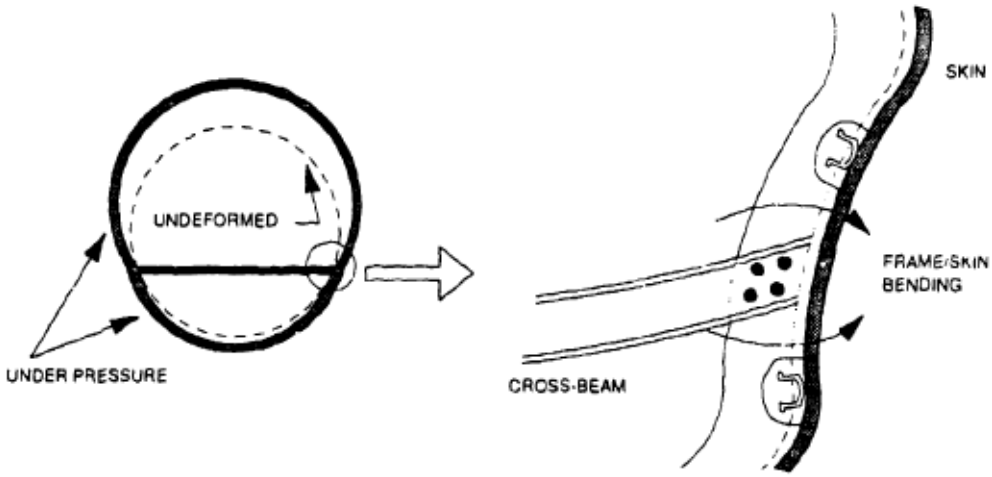

Figure 5.7: Local bending of fuselage at floor.

Further classification of primary panels as PSEs or CSEs is unlikely without exceptional circumstances peculiar to a specific design. A primary panel fracture is not likely to cause further structural damage to the panel itself before the pressure is relieved. However, the classification should take into account the possible effects of collateral damage. The meaning of the term "collateral damage" is illustrated by the sequence of events in an accident where a corrosion-cracked nose wheel failed in flight, breaking into a few large fragments. One of the fragments became a discrete damage source when forces from the tire pressure propelled it upward through the cabin floor, causing the cabin pressure to be vented into the wheel well. The wheel well doors, which were not designed for pressurization, were blown open. Two children who had been playing in the aisle when the accident occurred were immediately sucked out of the aircraft. The aircraft was able to return to and land safely at the airport from which it had departed.

The door failure was the collateral damage in this case. As serious as it was, this accident itself would not suggest that the floor panel be classified as a PSE because the door failure did not compromise flight safety. On the other hand, suppose that a similar floor panel failure could damage flight-critical systems, such as hydraulic lines routed through an unpressurized bay. Are the lines adequately protected? Are backup lines routed through a different area? Could the aircraft be flown in a normal manner if these lines were lost? Negative answers to all of these questions would suggest a PSE classification. Like wings, fuselages must be designed with skin splices to facilitate manufacture from sheet stock of standard width and to allow for practical handling of subassemblies. Circumferential joints are generally designed as butt splices over heavier-than-normal frames; the design may also include internal or external doublers, or provisions for staggering skin and stringer splices. Longitudinal joints are generally located over stringers and may be designed as either reinforced butt splices or lap splices, depending on model and manufacturer. Also, depending on the manufacturer, splices may be either mechanically fastened and sealed with a nonstructural sealant, or they may be fastened and bonded with a structural adhesive. The pressure bulkheads are skin-stringer panels that provide end closures for the pressurized volume in the fuselage. The forward and intermediate bulkheads are generally flat, and the pressure load creates panel bending stresses. The larger aft bulkhead may be curved, but in that case it is usually a shallow spherical cap which, for practical purposes, can be treated as a flat panel.

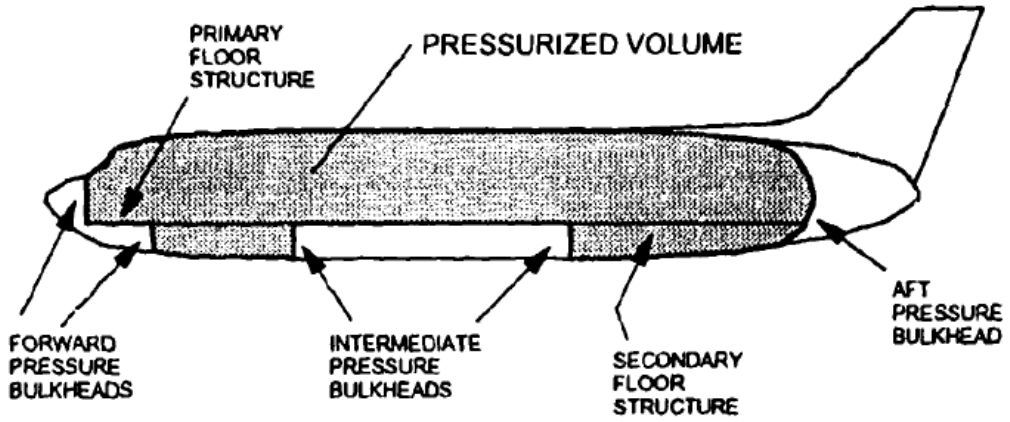

Figure 5.8: Typical bulkhead arrangement

It is useful to represent a full bulkhead by a simplified model, in the present case, an unstiffened circular panel of thickness t supported on its periphery of radius R. Both the location and magnitudes of the maximum bending stresses depend on the support stiffness. The radial σ_r and circumferential σ_θ stresses at the panel outer surface can be expressed in the form:

$$\sigma_r = P\left(\frac{R}{t}\right)^2 f_r(r)$$

$$\sigma_\theta = P\left(\frac{R}{t}\right)^2 f_\theta(r)$$

where f_r and f_θ are scaling functions.

The maximum stresses in an unstiffened panel would be quite high because they are proportional to the square of R11, which may exceed 200 for typical bulkhead radii and skin thicknesses. Therefore, actual bulkheads are stiffened with stringers to share the bending and reduce the skin stresses to tolerable levels. These structures can have quite complicated geometry; moreover, the structure which supports a bulkhead cannot be realistically approximated by either the knife-edge or built-in idealization. Thus, the reverse bending area is likely to be smaller than would be estimated assuming built-in support, but the actual area can be determined only from a detailed structural stress model.

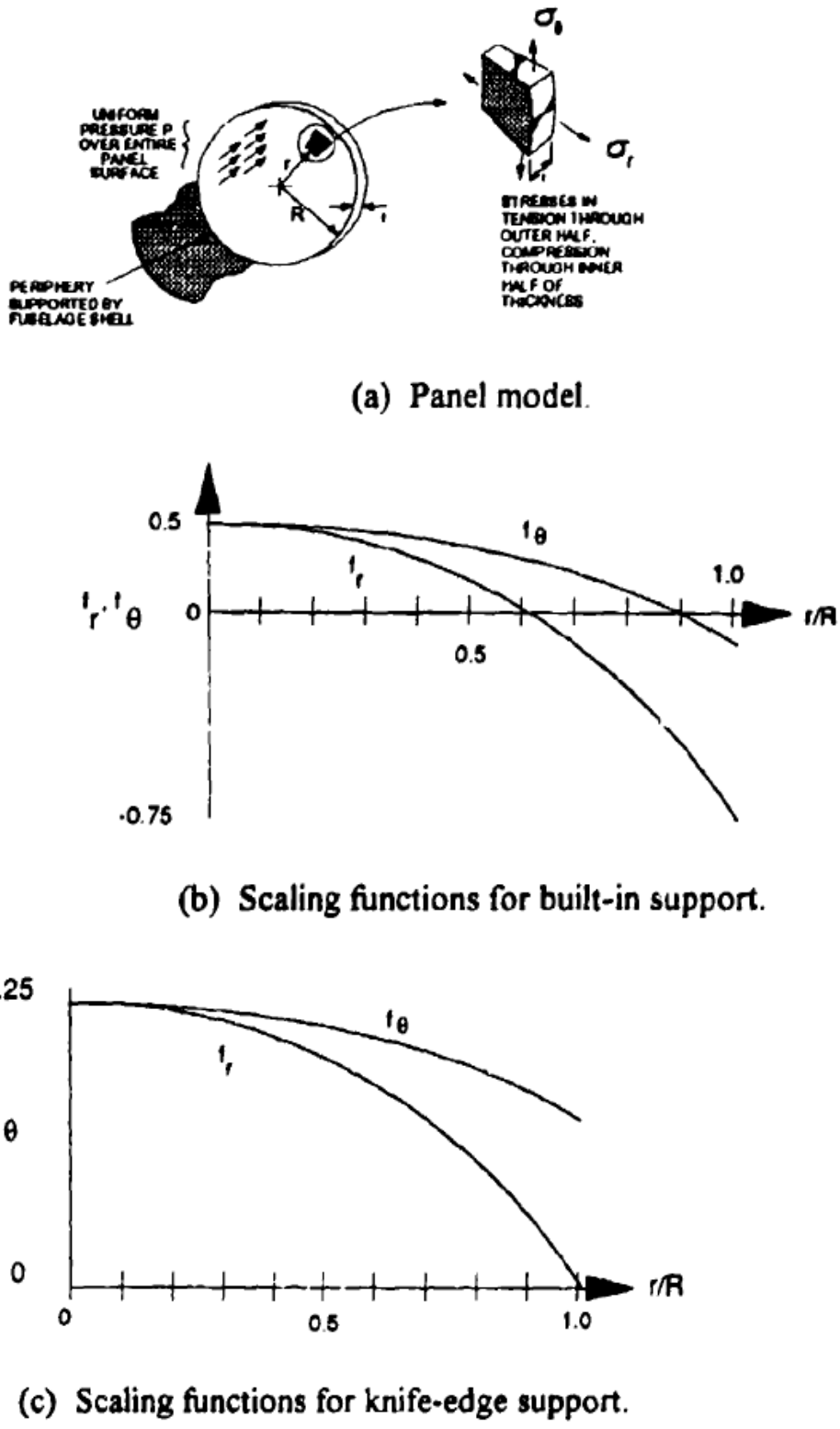

(a) Panel model.

(b) Scaling functions for built-in support.

(c) Scaling functions for knife-edge support.

*Figure 5.9: Bending stress distributions in a flat circular panel loaded **by** pressure.*

Floor panels over unpressurized bays are subjected to the same kind of load as pressure bulkheads, but the floor panel stringers are usually on the nonpressure side, whereas bulkhead stringers are often located on the pressure side.

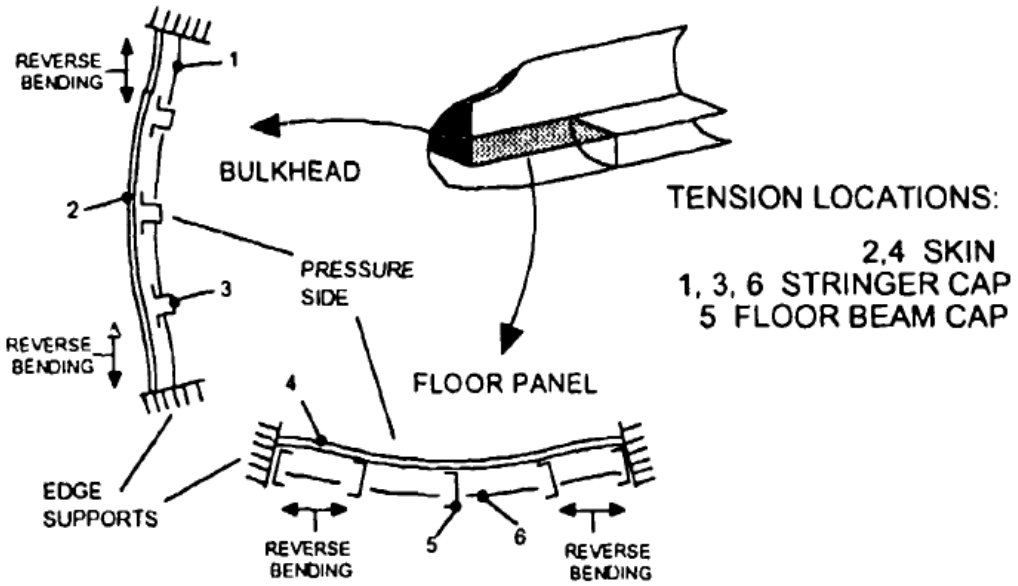

Figure 5.10: Floor panel and bulkhead evaluation sites.

No summary of fuselage structure would be complete without a discussion of doors and windows. All windows and some of the doors are subjected to fuselage pressurization loads. They carry only the pressure on their own surfaces, and this load is passed directly to the fuselage shell. Therefore, doors and windows are secondary structure. If a door or window should fail in flight, the consequences could be serious or even fatal for nearby occupants, but no blowout has ever caused the loss of an aircraft Therefore, neither doors nor windows need be classified as PSEs. However, it is important to consider the supporting structure, especially with regard to its effect on the surrounding fuselage panel, which is a PSE or CSE. A simplified window construction as ellipses with the ratio of minor to major axis selected to equalize the local axial and hoop stresses. The designers took advantage of the fact that the nominal axial stress is only half the nominal hoop stress. They accepted a larger stress concentration factor on axial stress in order to reduce the factor on hoop stress.

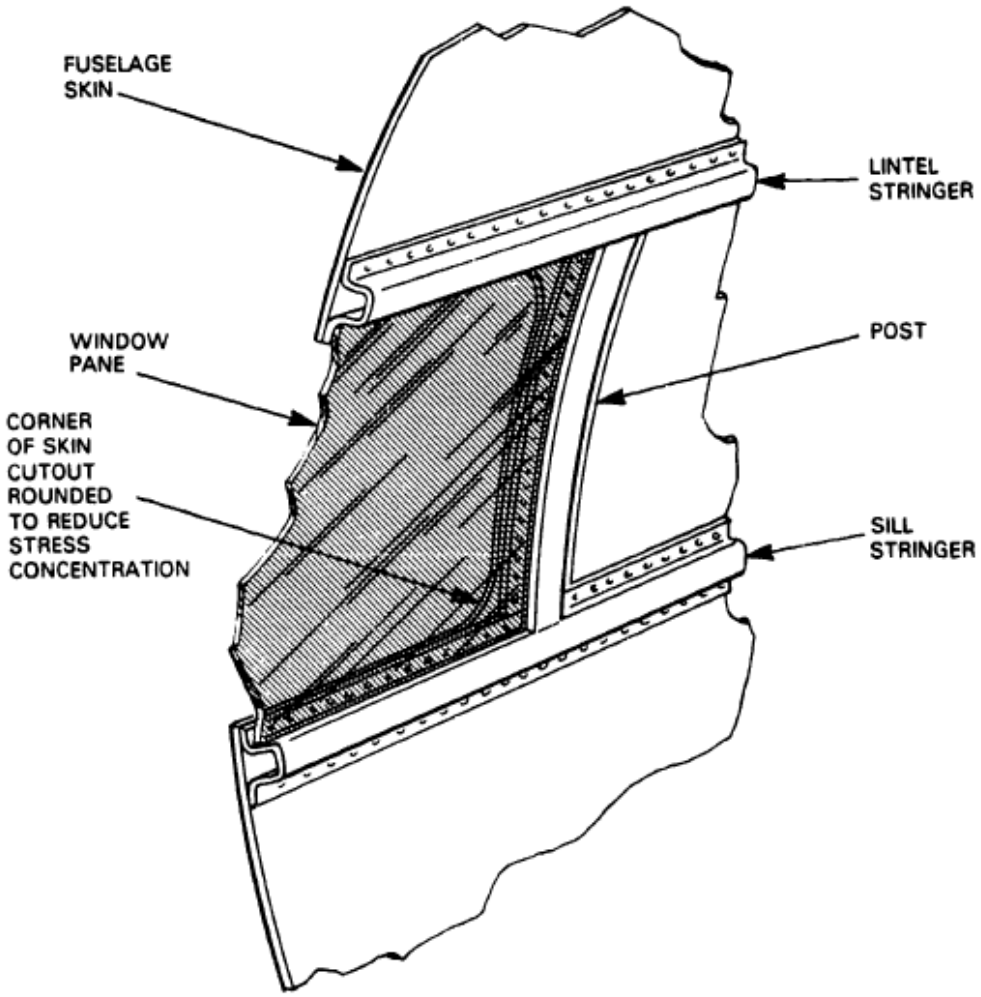

Figure 5.11: Cutaway view of window detail.

Splices parallel to the major stress axis are effective crack stoppers as long as the structure has not entered the widespread cracking condition. A stiffener attached to a continuous skin can also arrest a running skin fracture under the right conditions. The following simple experiment will demonstrate the crack-arrest capabilities of stiffeners. Inflate two balloons to the same size, using balloons that assume a sausage shape when pressurized. Apply ordinary cellophane tape to one balloon, making two hoops spaced 2 to 3 inches apart. Any tape from 1/4 to 1/2 inch wide will do, as long as it adheres well to the balloon's skin. Quickly cut each balloon with a sharp knife or razor blade, making the cut parallel to the balloon's axis. (The cut in the taped balloon should be made between the "stiffeners.") The balloon with no tape will burst catastrophically, but the tape on the other balloon will arrest the crack and control the deflation.

The crack-stopping experiment works because the much stiffer and stronger tape adheres well to the skin of the balloon. Getting stringers to stop a crack in an aircraft skin depends on analogous characteristics. In a good design, enough of the strain energy released from the skin by the running crack will be diverted into the stringers to reduce the energy available for further extension below the amount needed to create new crack surface.

In the structure, "adherence" means how close to the line of the advancing crack can load be transferred from skin to stringers. In mechanically joined structure, this depends on the fastener pitch and stiffness. Stiffer, more closely spaced fasteners produce better load

transfer but other design constraints limit what can be achieved in practice. Bonded construction is an alternative approach which generally produces better load transfer than can be obtained from fasteners, provided that the integrity of the bond is maintained. In this case load transfer improves as the bond layer's thickness decreases and its shear modulus increases. The stringers provide a route to bypass panel load around the cracked skin. How much load can actually be transferred depends on how stiff the stringers are, relative to the skin. Since both components are normally made of material with the same Young's modulus, the ratio of stringer to skin area in a typical section determines the stiffness ratio. The stiffness ratio can be increased by using heavier stringers and/or by decreasing the bay width between stringers.

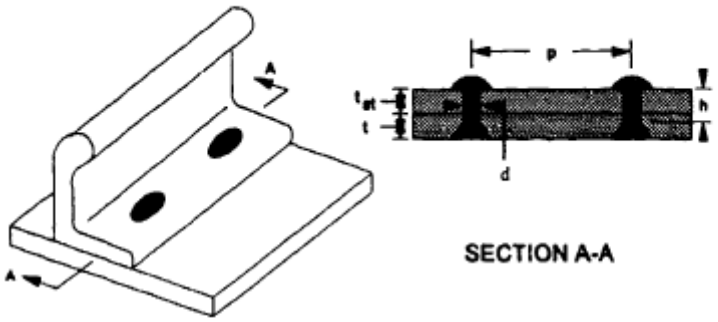

$t + t_a$	-	thick enough to take major tension load
h	-	determined by $(t + t_a)$ and fastener type
d	-	limited by stringer leg width
p	-	enough to prevent interactions of stress concentrations ($p/d \geq 4$)

Figure 5.12: Fastener design constraints.

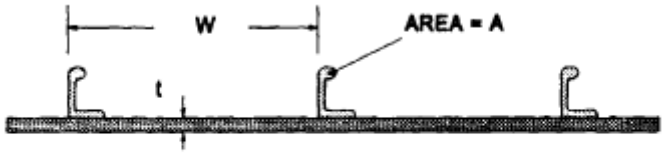

STIFFNESS RATIO ≈ A/Wt

Figure 5.13: Stringer/skin ratio

The strength available in the bypass route restricts the amount of load that can be transferred. Limits imposed by both the stringers themselves and the attachment design must be considered. If the local stress in a stringer reaches its ultimate strength before the skin crack is arrested, the stringer fails and cannot divert any more of the strain energy being released by the running crack. A common design practice to guard against stringer failure is to use a material of higher strength. For example, tension panels are often made with 2024-T3 skins and 7075-T6 stringers (ultimate strengths of 50 and 77 ksi, respectively). Since the panel is uniformly stressed when intact, the allowable stress is controlled by the strength of the 2024-T3 alloy, and the extra strength of the 7075-T6 alloy

provides a reserve for the stringer. A basic characteristic of the attachment system is that it is most heavily loaded close to the line of advance of the skin crack. If the concentrated load is high enough to cause local attachment failure, the concentration shifts away from the crack line and decreases as the efficiency of load transfer is reduced. The attachment failure thus progresses away from the crack line to a distance at which the concentrated load is no longer enough to cause further failure. This distance depends on the shear strength of the fasteners or bond. If the attachment failure distance is long enough, stringer "adherence" is reduced to the point where too little energy is diverted to prevent the crack from running past the intact stringer. Like the multiplank panels, the continuous-skin panel is a multiple path structure. As the preceding discussion has shown; however, the multiple path character of the continuous-skin panel is quite different because the independent paths all go through stringers. Continuous skins are found in wing and empennage boxes as well as in fuselages, but fuselage panels require additional consideration because of certain historical factors and the effects of pressurization.

High-altitude piston-engine transports began to come into widespread service in the late 1940s and by the early 1950s there had been a number of incidents and accidents precipitated by propeller blade failures in flight. In a few cases, a blade may have been thrown through the fuselage skin, causing extensive structural damage that brought the airplane close to catastrophic failure.

Concern for prevention of such failures led to the FAA's first damage tolerance regulation, later embodied in FAR 25.571(b)(3)(ii), requiring manufacturers to demonstrate that a pressurized fuselage could arrest a long crack suddenly introduced by a discrete source, under 1g flight loads and 110 percent of normal cabin pressure. The worst case is assumed for test and evaluation purposes, namely: an axial crack (Mode I loading by the pressure hoop stress) located midway between longerons. Different designers have made different assumptions about the initial damage.

Today, a crack extending into two frame bays with the central frame also cut is generally assumed. The structure is considered to comply with FAR 25.571(b)(3)(ii) if, under the specified conditions, it arrests the skin crack within two frame bays.

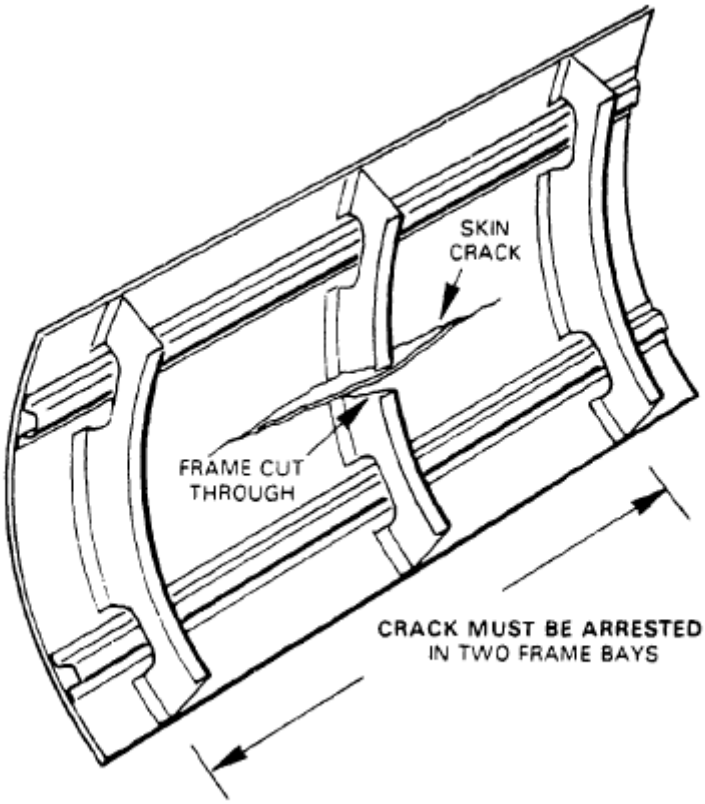

Figure 5.14: Definition of fuselage tolerance to discrete source damage.

Once a fracture has been initiated, the crack runs quite rapidly. In a typical skin fracture, the advance speed builds up to about 1,000 ft/sec in less than 100 microseconds. Thus, the crack reaches the frame at the end of the bay while the fuselage is still almost fully pressurized. Simultaneously, unable to carry the pressure as hoop tension, the cracked skin bulges outward and sheds its load into stringer bending which exacerbates the local frame bending already present at the stringer crossing. The added stress on the reduced frame section at the mousehole may be enough to cause a local frame failure. Even if the frame does not break, it is unable to support further bending in the yielded condition. If the frame section on the crack advance line also yields under local overload, the frame acts as if it is hinged at the three points A,B,C shown in the figure below. The effects of the skin bulging are then transmitted back to the crack, driving it past the frame.

As more was learned from service experience with pressurized fuselages, designers came to recognize that the practice of attaching frames directly to the skin did not produce the best possible damage tolerance for the least structural weight. In aging airframes, fatigue cracks were frequently found originating at the mousehole corners in the frames. If numbers of such cracks could accumulate in an airframe, then the further reduction of frame bending strength might rob the fuselage of its fail-safe character.

Since there is no convenient way to attach a frame directly to the skin without cutting in mouseholes to let the stringers through, designers began to experiment with offset frames. Besides getting rid of the mousehole, offset frame design improved tolerance of single fastener hole fatigue damage. In the older design, a crack at a skin-to-frame fastener could lead to the two-frame-bay crack with a broken central frame; an undesirable effect of aging, even though the airframe should be able to contain the damage. Conversely, a similar crack at the skin-to-frame attachment in the new design would leave the frame

intact. Despite its obvious benefits, the offset frame design also has one disadvantage: the shear clip attachments are more flexible and spaced further apart than the older direct fastener system. Thus, while the offset design guards against frame bending failure, it also reduces the diversion of released energy from the skin to the frame. This problem was solved by adding a tear strap to the design. The tear strap is usually about the same thickness as the skin and is attached directly to it. In some designs, additional effectiveness may be gained by using a stiffer material for the tear strap (e.g., titanium). In other designs, extra tear straps may be placed in the middle of each frame bay in a trade-off for a lighter frame section.

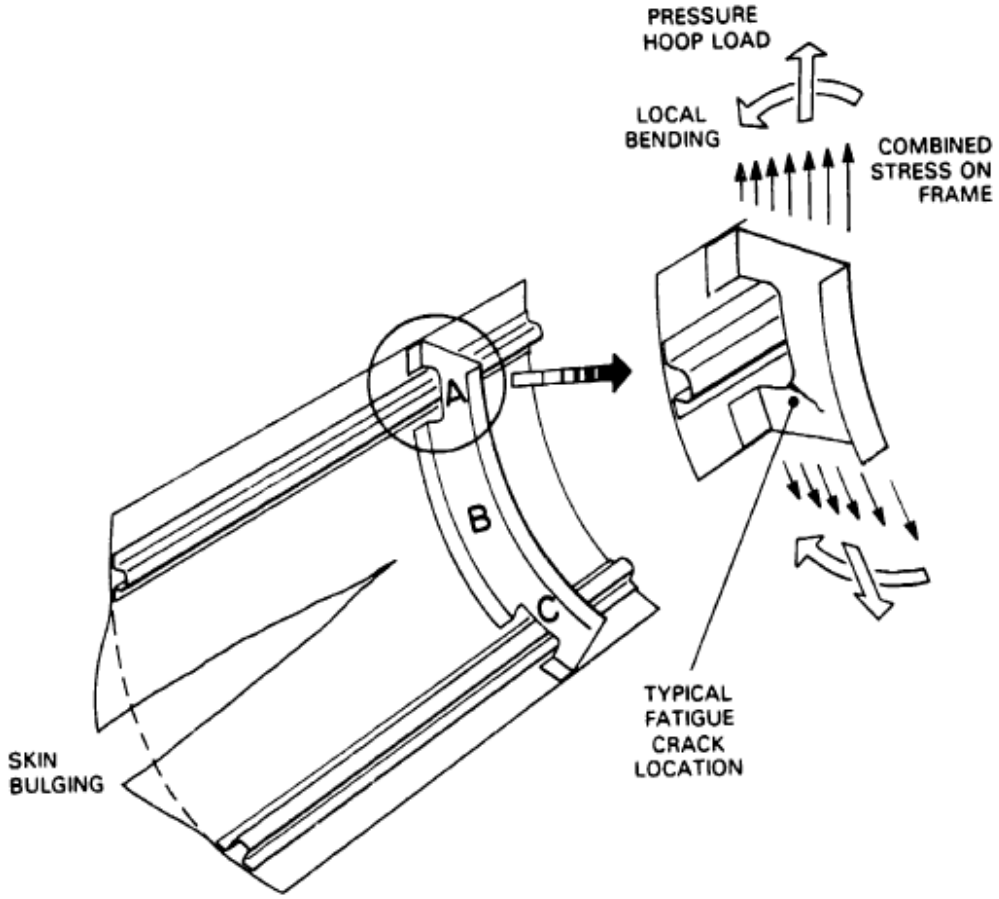

Figure 5.15: Frame collapse mechanism.

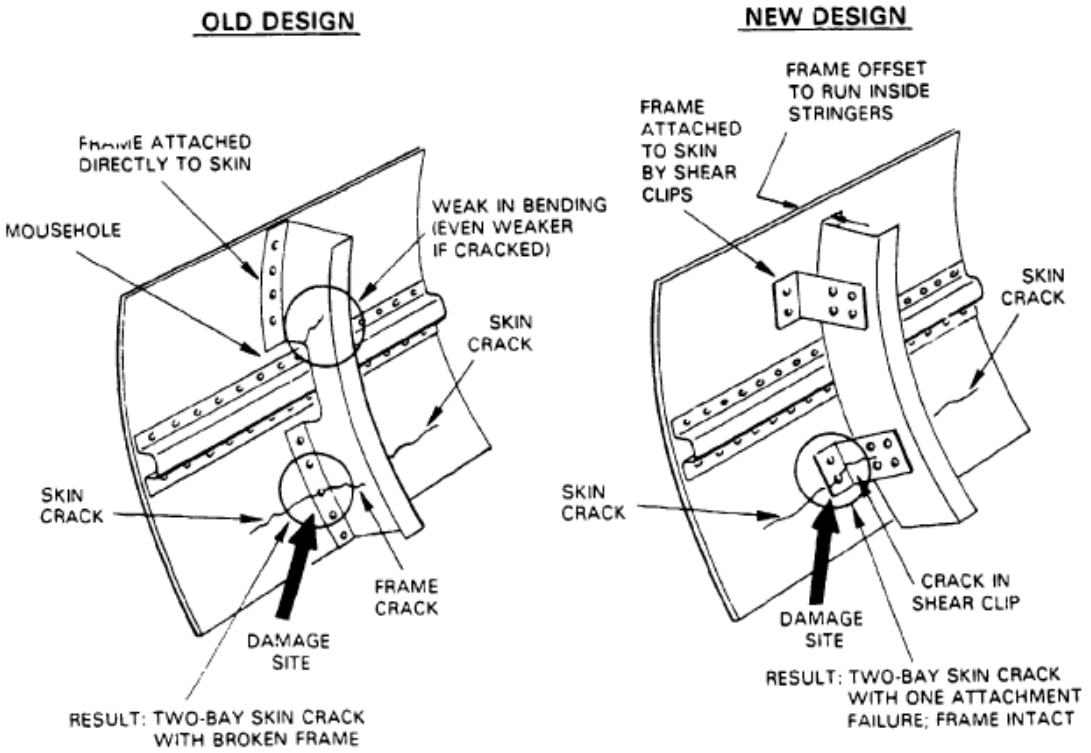

Figure 5.16: Comparison of old and new design details.

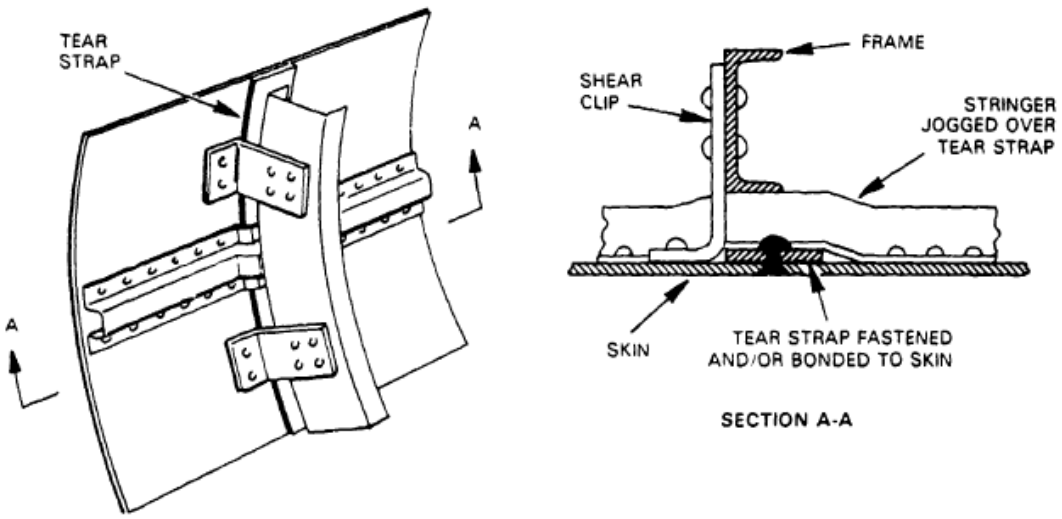

Figure 5.17: Offset frame with tear strap.

When a major load crosses a mechanically joined skin splice, the entire load must be transferred by means of fastener bearing. Crosswise splices are thus more sensitive to

fastener detail fatigue than parallel splices, in which fastener bearing transfers only secondary load. Good fatigue design requires extra material and multiple fastener rows in crosswise splices. Extra material reduces the local skin stress, and multiple fastener rows reduce the bearing stresses. Both factors affect fastener detail fatigue life. Extra material means abrupt change of thickness, a feature which tends to overload the outer fastener rows. The best splice designs employ some combination of the following measures to produce an equitable distribution of fastener bearing loads: (1) multiple fastener rows on each side of the splice; (2) greater fastener pitch in the outer rows, (3) smaller fastener pitch between rows; (4) stepped doublers; (5) doubler taper in the plan view; and (6) fastener flexibility.

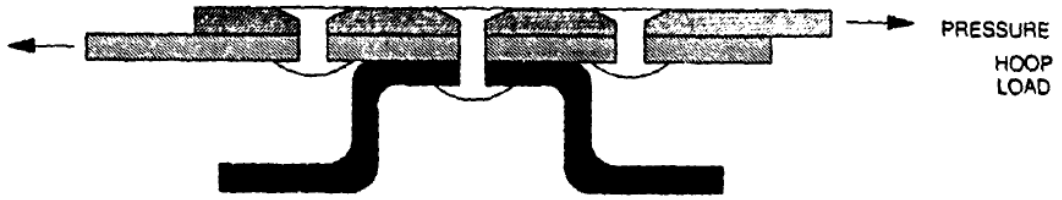

(a) Lap splice over fuselage stringer.

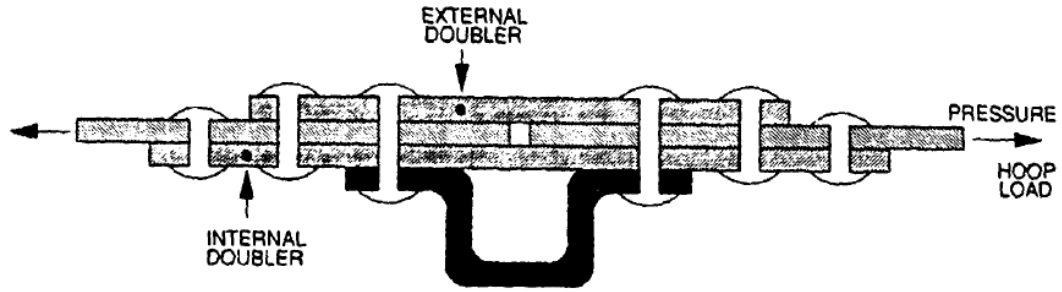

(b) Butt splice over fuselage stringer.

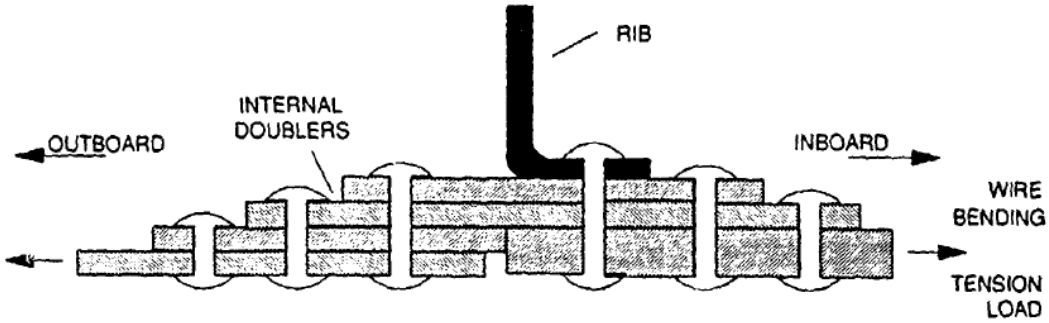

(c) Chordwise butt splice at skin thickness drop in a wing box.

Figure 5.18: Example of splice details

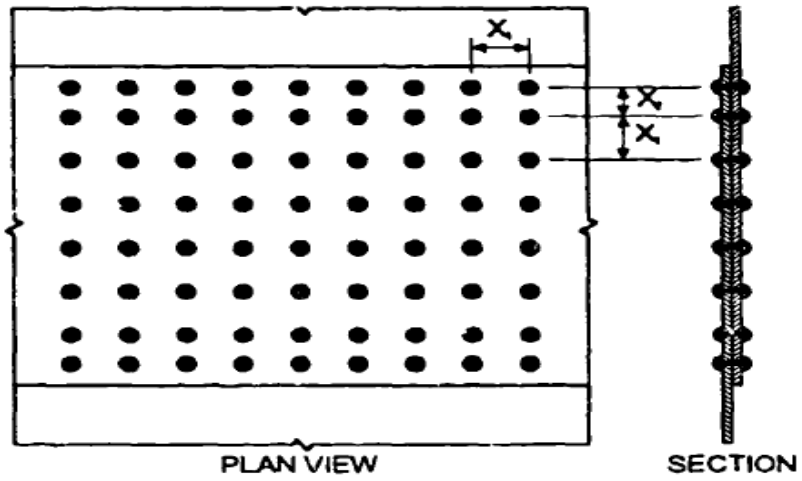

(a) Lap joint with pitch change between rows.

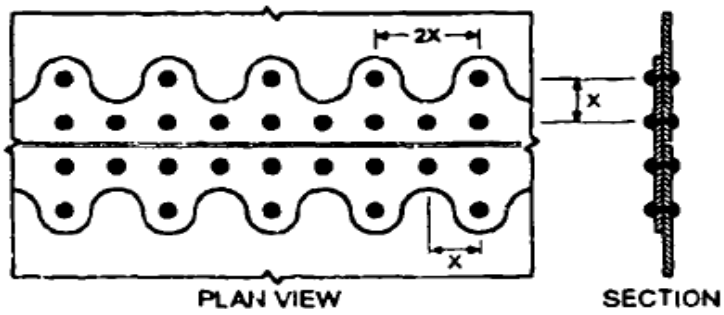

(b) Tapered "finger" doubler with outer row pitch doubled.

Figure 5.19: Examples of pitch change and taper.

Airframe repairs are often designed as riveted doubler patches on skin areas which have either been damaged or are being reinforced to avoid or delay cracking. Repair doublers transfer load in the same way as doublers at splices, i.e., the bearing loads are concentrated toward the outer fastener rows. However, the bearing loads in a repair patch are less than those in a crosswise splice because the skin underneath the repair is still stressed. Another difference between patches and splices is that most patches are subject to Poisson effects because they do not span the full width of the skin. As a result, the fastener bearing loads also tend to concentrate toward the corners of a patch.

Older repair doubler designs were generally based on static strength considerations. The doubler skin thickness, number and size of fasteners, number of rows, and fastener pitch were selected to provide sufficient strength for the doubler to carry the entire load in its

area. However, fatigue and damage tolerance considerations suggest that some doubler designs are better than others, even though they may have identical static margins.

Two alternative but statically comparable repair designs for a 0.04-inch thick damaged skin with a nominal stress of 15 ksi are presented. Design (a) is a 0.05-inch thick conventional single doubler patch with four rows of rivets on each side of the damage. The 8x25-inch doubler covers a skin area where damage has been cut out. The effect of the cutout on the ability of the underlying skin is represented by a crack (length = 2a) in the numerical analysis model. Design (b) is a patch consisting of two doublers: a 0.025-inch thick internal doubler which extends to a fifth fastener row on each side, and a 0.032-inch thick external doubler.

A finite element stress analysis was performed for each of the designs, in order to determine the fastener bearing loads. The underlying skin damage was represented by a 2-inch crack.

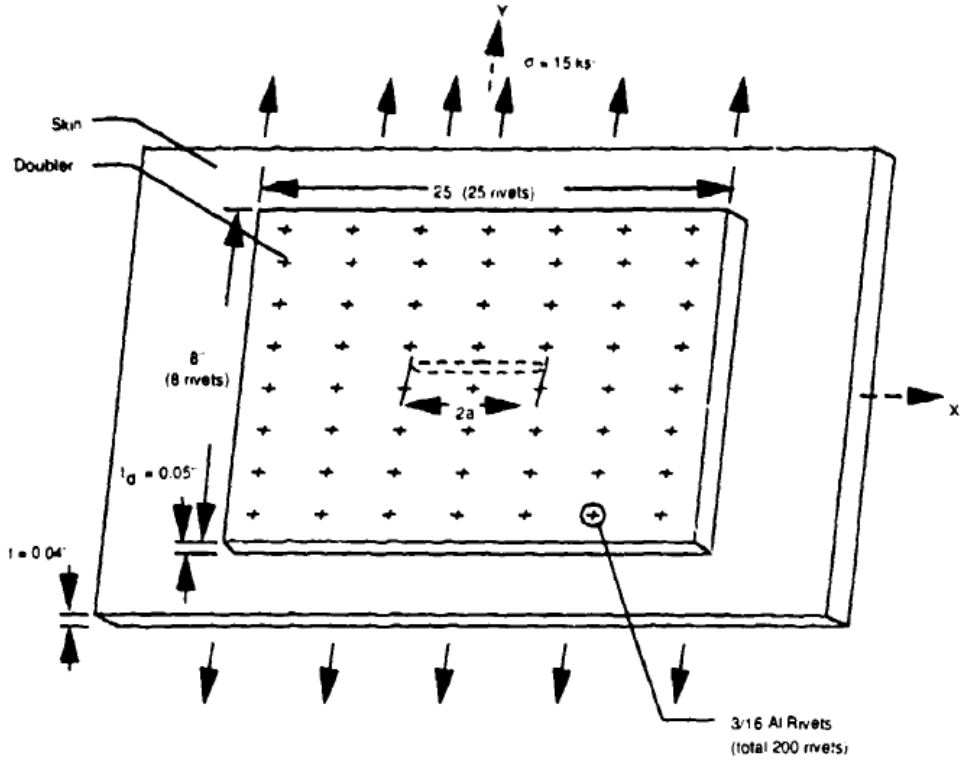

(a) Conventional single doubler.

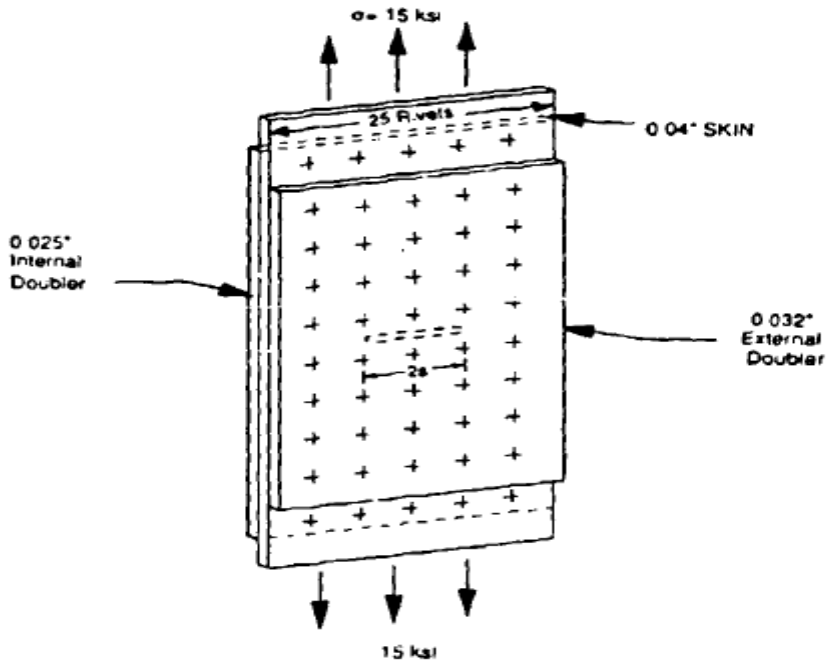

(b) Stepped inside/outside doubler.

Figure 5.20: Damaged skin with repair patch.

The plot at the right compares the bearing load component parallel to the applied stress with results obtained from a compatibility model solution by Swift. Swift's model considered only one-dimensional behavior (no Poisson effect). The concentration of bearing load toward the outer rows is evident and, near the center of the patch, the results agree with Swift's results. The finite element results, which do include the Poisson effect, show an additional concentration of load toward the lateral edges of the patch. The component parallel to the applied stress is 227 lb. (18 percent higher than the 187 lb. load on the interior upper and lower fasteners). There is also a 76-lb. lateral force component acting on the corner fasteners, i.e., their total bearing load is 239 lb.

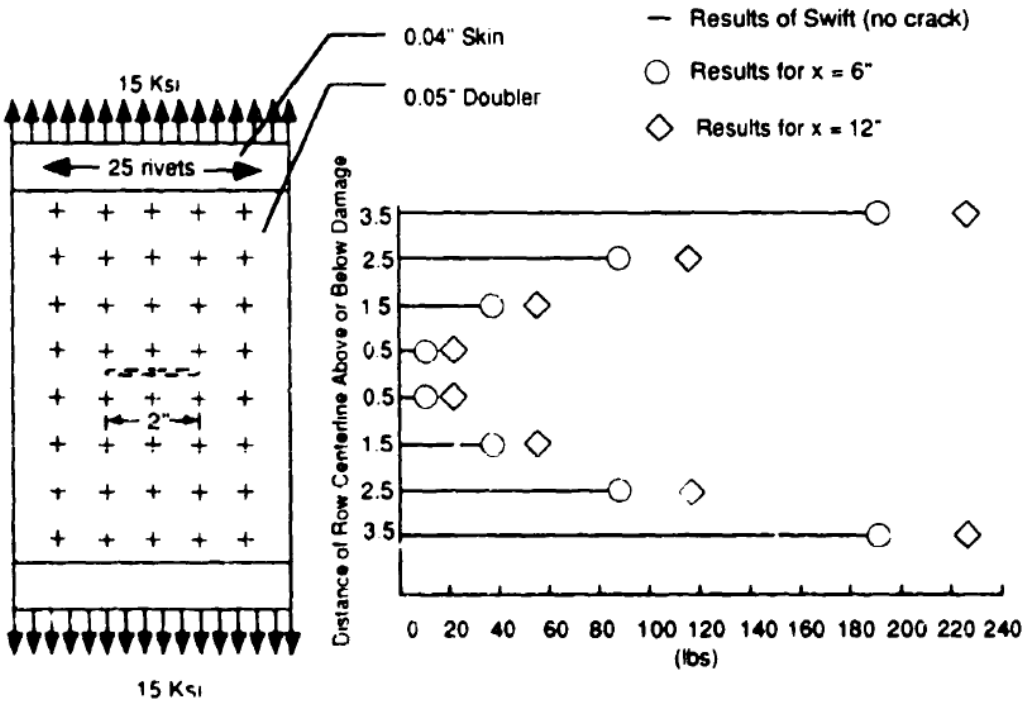

*Figure 5.21: Rivet load distribution in **a** single doubler.*

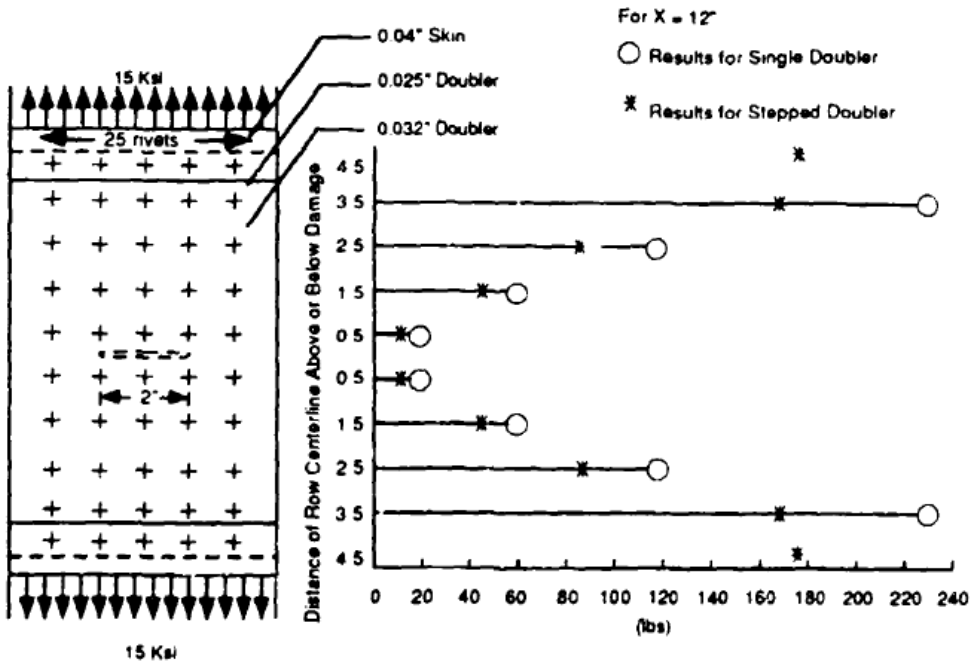

Figure 5.22: Comparison of rivet load distributions in stepped and single doublers.

A conventional fatigue analysis using open hole data (stress concentration factor of 3) for 2024-T3 aluminum skins and assuming R=0 gives a safe-life of 160,000 cycles for the basic structure. Similar analyses for the doublers give much shorter safe lives because of the fastener bearing load concentrations. The life was estimated to be 39,000 cycles for the single doubler, but improved to 55,000 cycles for the stepped doubler. Another lesson to be learned from the foregoing example is that one should expect recurring damage at repair patch sites. If the example is considered as an approximate model for a fuselage repair, the estimated safe lives represent numbers of flight cycles that could easily be

accumulated on the patch. Thus, it would be a good idea to evaluate the damage tolerance of such repairs as multiple path structure (keeping in mind the possibility of widespread cracking).

SECTION 5.3: STRUCTURAL FAILURES & REPAIRS

The structural integrity of a force of operational aircraft is primarily ensured by implementing the periodic inspection and maintenance program defined in the Force Structural Maintenance (FSM) plan in the associated technical order (T.O.)-3 repair and -36 inspection manuals. In addition to this formal method of addressing known or potential cracking problems, the structural integrity of individual aircraft is also ensured through the timely identification of new cracking problems and by implementing repairs that will return cracked structure to a safe operational condition. This section is presented as a supplement to the other sections and only specifically addresses those guidelines applicable to ensuring that adequate damage tolerance exists in structural repairs. Adequate damage tolerance implies that cracks do not reduce the structure's load carrying capability below a predefined level throughout a required period of in-service usage.

All repairs made to cracked structure, and all structure and structural changes made to in-service aircraft require some form of damage tolerance analysis. The degree of intensity of each analysis, however, depends on the consequences of failure in the repaired or modified structure if cracks are present. For example, the extent of the analysis of a repair to replace a compressively loaded fuselage member that is removed for corrosion damage would be minimal, while a force wide modification to the tension-loaded, primary-load-path, lower wing skin structure of a fighter aircraft would require an in-depth evaluation of expected fatigue crack growth behavior.

Examples of aircrafts structural failures are following below with photos/details detected during planned maintenance inspections, as provided by maintenance repair organizations for specific aircraft types:

AIRCRAFT TYPE: BOEING 737-400:

1) Upper hinge Forward Service Door hole

TYPE OF DAMAGE: Dent 140mm X 110mm. Depth 7mm.
CAUSE OF DAMAGE: Unknown
REPAIR: As per Boeing SRM dent in limits, for more details KLM Engineering Report (Appendix Repair01)

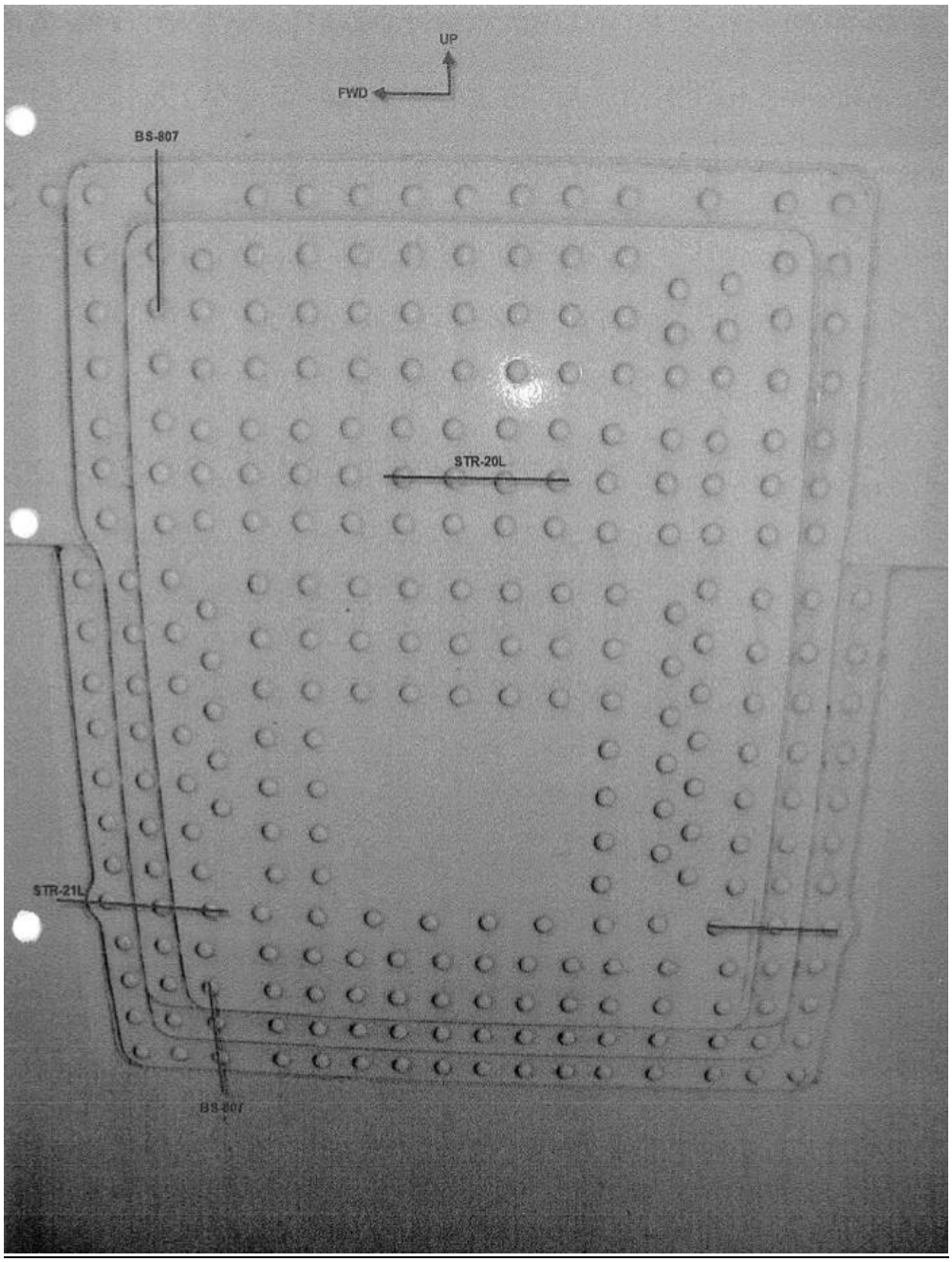

Photo 5.2a: Upper hinge Forward Service Door hole

2) Several dents in External Skin

TYPE OF DAMAGE: Structural
CAUSE OF DAMAGE: Failure
REPAIR: As per Boeing SRM was out of limits , for more details KLM Engineering Report (Appendix Repair11)

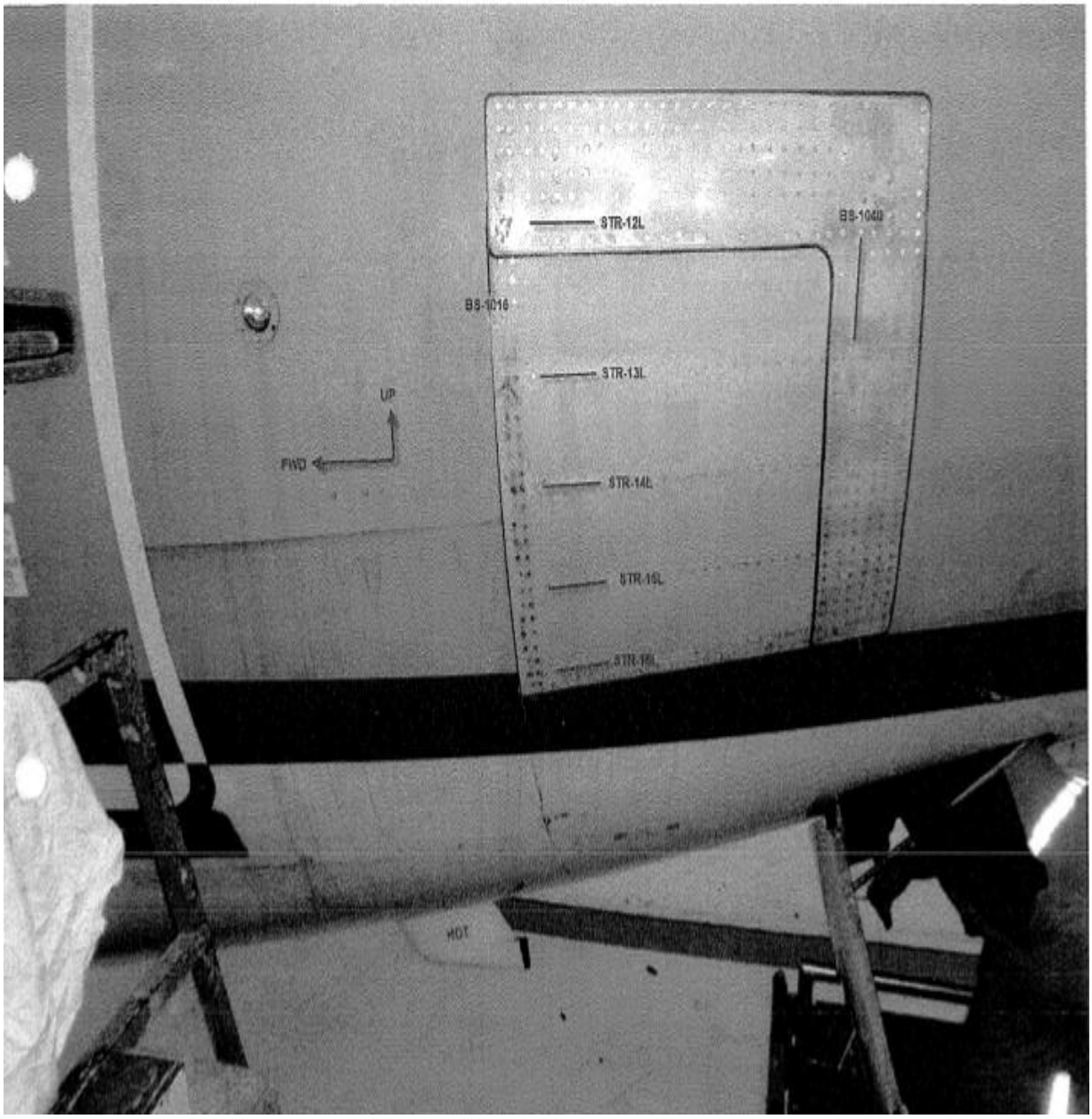

Photo 5.2b: Dents in external skin

3) Crack aft side of fuselage

TYPE OF DAMAGE: Crack
CAUSE OF DAMAGE: Failure
REPAIR: Fuselage Skin Repair as per Boeing SRM. Installed Lap Slice Repair.
For more details KLM Engineering Report (Appendix Repair17)

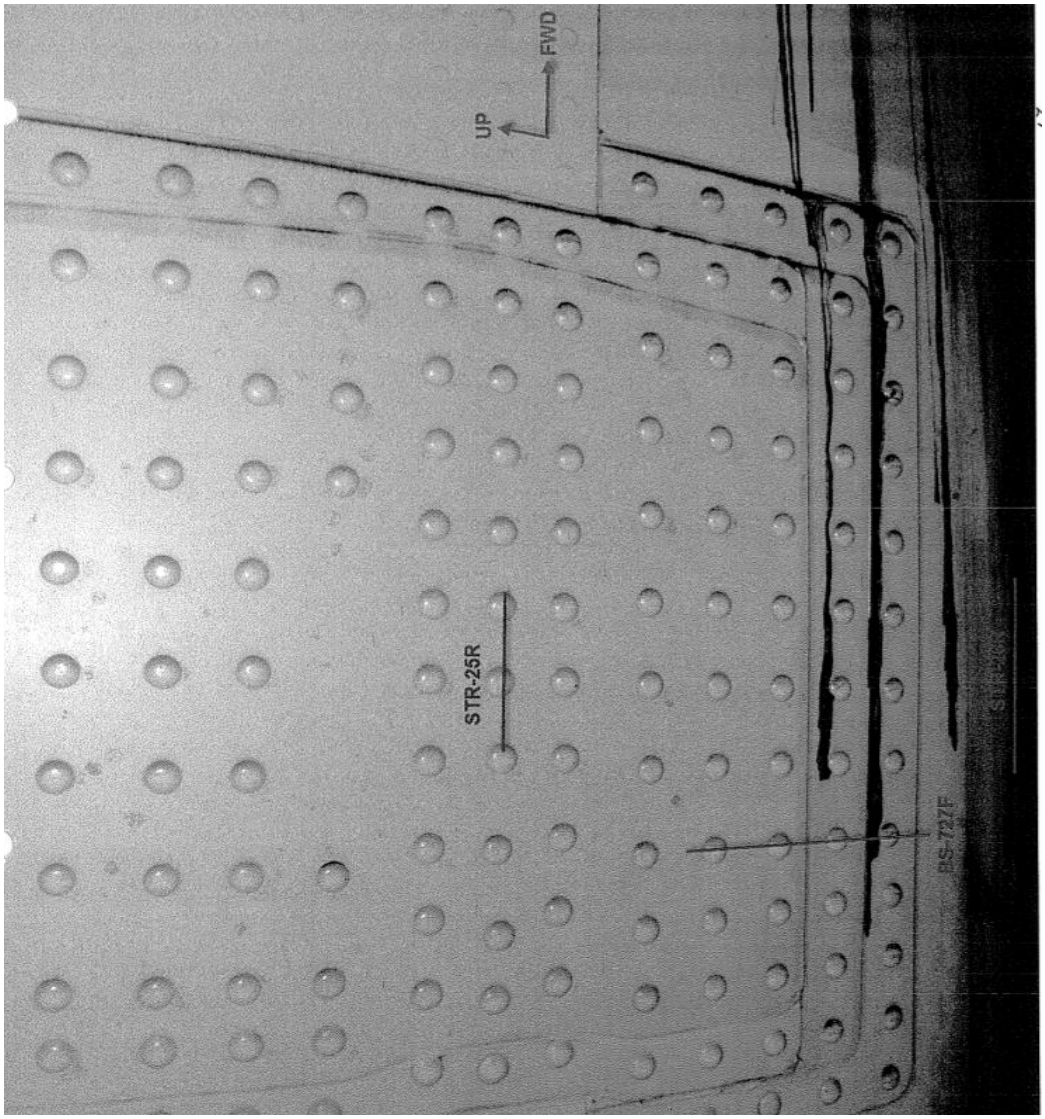

Photo 5.2c: Crack aft side of fuselage

4) Skin crack at fuselage station 727E right side

TYPE OF DAMAGE: Crack
CAUSE OF DAMAGE: Fatigue
REPAIR: First step of Repair, by making a hole 1 inch width and removed crack.
All actions as per Boeing SRM. For more details KLM Engineering Report (Appendix Repair18)

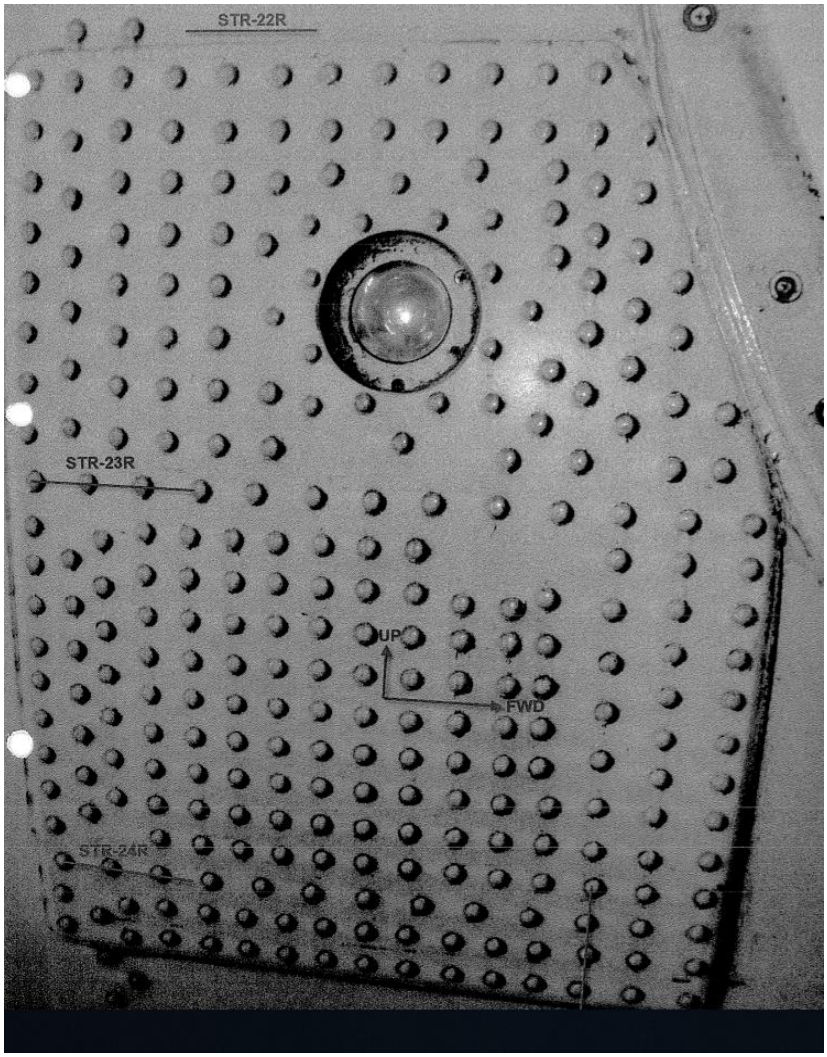

Photo 5.2d: Skin crack at fuselage

AIRCRAFT TYPE: GULFSTREAM G450

5) Corrosion wing to body contact fairing areas

TYPE OF DAMAGE: Material Corrosion
CAUSE OF DAMAGE: Operational & Environmental Conditions
REPAIR: Repair and review maintenance thickness per Gulfstream GSL40539001.
For JET AVIATION work order details (Appendix WO: CS543512)

Photo 5.2e: Corrosion in fairing areas

6) Corrosion Horizontal Stabilizer

TYPE OF DAMAGE: Material Corrosion
CAUSE OF DAMAGE: Operational & Environmental Conditions
REPAIR: Repair and review maintenance thickness. JET AVIATION work order details (GSGAB035)

Photo 5.2f: Corrosion horizontal stabilizer

If the manufacturer can conceive of potential problems associated with the repair or modification of special designed (or manufactured) safety-of-flight critical structure, then the manufacturer should identify such problems with reference to additional details in repair manual. The intensity of the analysis also varies as a function of the extensiveness of the change of the force. If the repair or modification can be incorporated into any given aircraft or will be applied to all aircraft in the force, than a more careful analysis of the impact of a crack potentially existing in the structure should be conducted. For one-of-a-kind repairs applied to an airframe in order to return the aircraft to a depot for more extensive repair, the type of damage tolerance analysis would be primarily of a residual strength type, without much consideration being given to variable amplitude fatigue loading.

This section has been prepared to present some real facts with (a) (b) dents results of a fuselage skin repairs (c) cracks growths fail-safe of aircrafts components (d) fatigue life sensitivity and a hole repair, (e)(f) decrease of the skin residual strength with corrosion effects (cracks / holes deterioration).

Not only the repairs as corrective actions, after the detection of structural findings, but also some experimental suggestions for the increase of residual strength of skin can be presented for future application and this approach is described at next section.

SECTION 6: CONCLUSION & FUTURE PROJECT

SECTION 6.1: CONCLUSION

This thesis contained a standardized procedure to make estimations on damage tolerance of a structure, and thus promoted more accurate inspection timing, which will ultimately lead to smaller costs for the company industry.

As a quick review the damage tolerance is estimated over following steps:

1.Through the determination of the most critical point in terms of stress concentration (crack initiation and propagation is easier at these locations); 2. Definition of the initial damage (length, direction, shape and quantity); 3. Definition of the spectrum to use, whether from a real aircraft or algorithm based, usually selected concerning the type of aircraft that is being analysed; 4. Residual strength limits, calculated from the airworthiness requirements, defining the maximum allowed crack length on the structure; 5. Crack growth determination will enable to compute the number of cycles for the structure to have grown a crack with a prescribed dimension; 6. Inspection procedure definition, emphasizing the definition of the inspection threshold and inspection interval. The construction of the inspection charts is made through these parameters.

When all steps are completed, and a Damage Tolerance Analysis has been conducted, the following must be provided:

- The residual strength as a function of the crack size;
- The crack growth, emphasizing the number of cycles till failure and critical crack length;
- The initial damage assumed;
- The inspection interval.

At detection of cracks/defects in aircraft structures, which needed permanent repair and modification as per manufacturers mandatory recommendations, the review of failures is taken into consideration and different suggestions for materials/time inspections or operation environment are strongly followed by air operators. For damage tolerance designing improvements, a scenario of future development of reinforced panels in fuselage is suggested below.

SECTION 6.2: DAMAGE TOLERANCE ANALYSIS OF AIRCRAFT REINFORCED PANELS

Experimental tests performed for the development of reinforced panels, typically found in aircraft fuselage are presented. The bonded reinforcements can significantly reduce the rate of fatigue crack growth and increase the residual strength of the skin. The reinforcements are of two types: stringers and doublers. The former provides stiffening to the panel while the latter controls the crack growth between the stringers. For validating a numerical method of analysis that can predict the damage tolerance of these reinforced panels, a fracture mechanics approach is used and several models (different by the geometry and the types of reinforcement constraints) are simulated with the finite element solver ABAQUS. The bonding between skin and stiffener was taken either rigid or flexible due to the presence of adhesive. The possible rupture of the reinforcements was also considered. The stress intensity factor trend obtained numerically as a function of crack growth was used to determine the fatigue crack growth rate, obtaining a good approximation of the experimental crack propagation rate in the skin. Therefore, different solutions for improving the damage tolerance of aircraft reinforced panels can be virtually tested in this way before performing experiments.

In aircraft fuselage, aluminum stiffeners are connected to panel in longitudinal and circumferential directions. A particularly significant application is the direct bonding between stringers and the surface of the fuselage skin. The main features of the reinforced bonded panels concern better damage tolerance and higher stability at different types of loads. The experiments on aluminum panels with bonded stiffeners show that a limit of the aluminum reinforcement is the premature rupture of the reinforcement caused by the load transfer from the skin to the stiffeners when the crack runs underneath it. To improve the tolerance to the fracture, the doublers or reinforcement cords should preferably be made of material resistant to fatigue, with high stiffness and static strength. Panels made of a thin metal skins stiffened with bonded reinforcements insensitive to fatigue, can ensure slow crack propagation if not its arrest, and the capability to withstand a large damage, combined with a low structural weight. The effects of this bonded reinforcements or doublers are very difficult to predict numerically or analytically, because of the complex mechanisms of failure:

- separation at the interface between skin and reinforcement around the area of nucleation and propagation of the crack;
- load redistribution between the damaged and undamaged reinforcement;
- fatigue damage of the reinforcement which may cause his premature rupture;
- crack bridging by the doublers thanks if they have a sufficiently high fatigue strength.

In addition, secondary effects, such as residual stresses generated by the bonding process and bending caused by the eccentricity of the load with respect to the neutral axis of the reinforced panel cross-section, increase the complexity of the phenomenon. Reliable predictions of crack growth and residual strength in bonded structures can be based mainly on empirical considerations. The experimental results which support the numerical analysis reported in this work refer to an experimental investigation carried out by Airbus in a period from 2002 to 2007. Through an extensive campaign of tests, several methods of reinforcement were analyzed, using bonded reinforcements in the fuselage panels. To achieve a quantitative study, in the analysis different types of connection between the

reinforcements and the skin were considered. In the literature, numerical studies on FCP (Fatigue Crack Propagation) in reinforced structures are available. However, if the damage tolerance assessments appear to be practicable in integral reinforced structures, the same assessment is not straightforward in differential structures with bonded joints between skin and chords due to the complex mechanisms mentioned previously.
The stiffened differential structures can actually be reproduced with proper models that allow replicating the stiffener effect using the "crack arrest" philosophy design. In this approach after an initial propagation, the crack arrests due to a stiffener when a given length is reached.

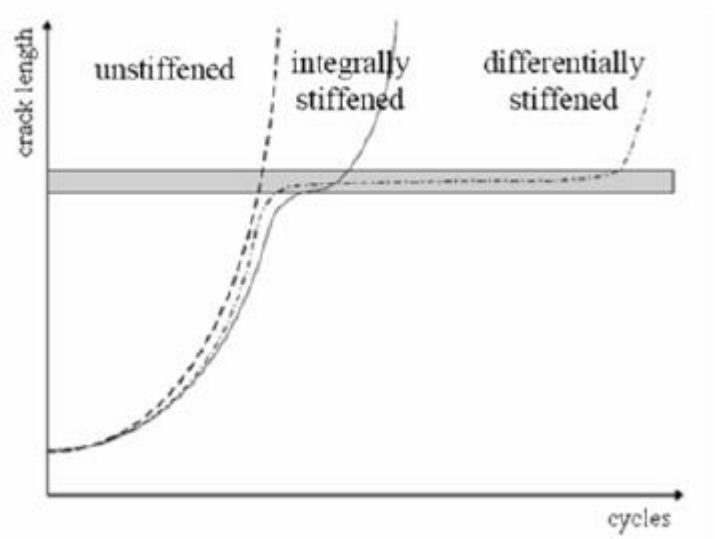

Figure 5.23: Comparison between the several design solutions according the "crack arrest" method.

In the differential structures the crack propagates typically only in the skin, then the completely intact stiffeners can control the defect evolution during the propagation, due to the load transfer from the skin to the stiffeners which, in turn, means that the stress intensity factor decreases. This fact underlines the effectiveness design of *crack arrest*. Several experiments have shown a significant beneficial effect due to the presence of reinforcements in differential structures. In many engineering fields such as aeronautics, automotive, marine or civil engineering, plates and shell made with laminate composite structures are largely used in load-bearing structural members. Important examples of these applications can be observed in aerospace engineering, where thin laminates are reinforced by a certain number of profiles (the so called stringers).

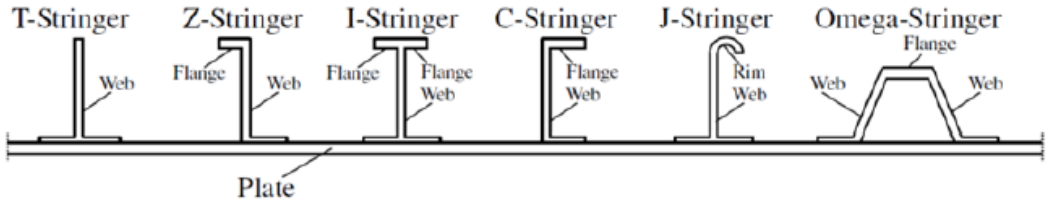

Figure 5.24: Cross sections of several kinds of stringers

Such structural parts can readily be found in fuselages, tail planes, or wind covers of aircrafts and typically consist of a thin plate or moderately curved thin shell that is stiffened by a certain number of shaped stringers. Especially stringers which have a closed-profile cross-section may provide a high torsional stiffness to the plate such that the composite plate itself can be assumed to be elastically restrained to some degrees.
Another kind of reinforcement, called *doubler*, is usually positioned in the separation zone between stringers, oriented parallel to them.

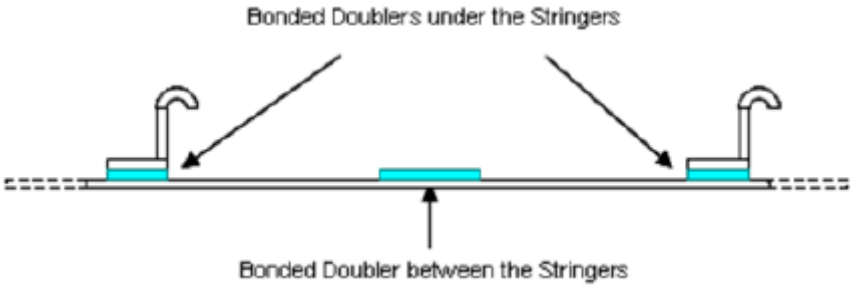

Figure 5.25: Representations of the possible placements of the doublers: in the middle of the bay (between the stringers) or under the stringers.

Because of their shape, the doublers have not a stiffening function, but they slow down the crack grow rate in the zone between the stringers (the so-called bays). The doublers are typically bonded to the skin and experimental studies are showed they are more efficient with a thick section rather than a thin section.

A total of 35 stiffened panels, representative of a typical fuselage skin of a long-range family aircraft, were manufactured and tested in the laboratories of EADS-IW Ottobrunn. The fatigue crack propagation (FCP) rate was investigated for twenty-four of them. The remaining eleven panels were tested for the residual strength. The panel shown below has been tested and it is characterized by a skin (1224 mm wide and 1455 mm long) with seven equally spaced bonded stringers. In addition to the stringers, bonded doublers are positioned below and between the stringers in order to provide additional reinforcement. All the doublers are placed orthogonal to the direction of crack propagation alike the stringers.

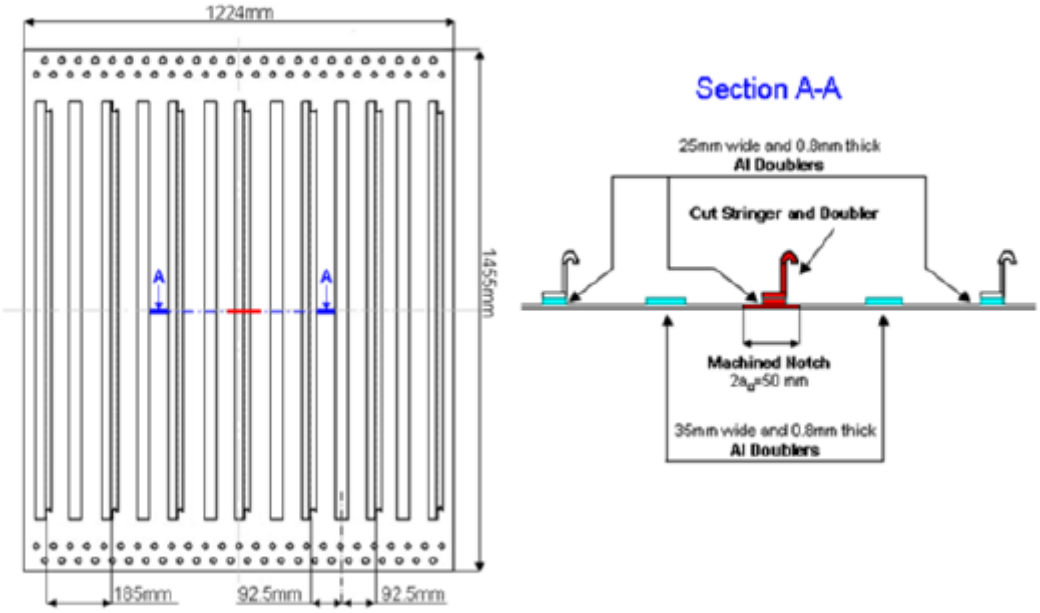

Figure 5.26: Representation of a "seven stringers" panel with doublers bonded between and under the stringers (a) and with an additional glass fiber reinforcement (b).

The tests were performed by means of a servo-hydraulic INSTRON 8805 machine with a 1MN load cell. The clamping was specifically designed for the 7-stringers panels. An anti-bending device was installed to prevent the out of plane deflection of the panel during the test. The skin, like the doublers, were made of 2024-T3 aluminum alloys with 1,4 mm thickness the former and 0,8 mm the latter. The stringers were "J"-shape extruded profiles made of high strength 7349-T76511 aluminum alloy. An antibending
device was installed to prevent the out-of-plane deflection of the panel during the test.

In the experiments, the fatigue crack propagation was investigated starting from a through-the-thickness, 50 mm-long, machined notch. The crack was placed across the middle stringer; this stringer and the underlying doubler (when present) were also cut. The loading parameters were the same for all the tested configurations (constant amplitude loading, *280 kN* maximum force and *0.1* load ratio). The tests ended when the crack was "four bays" long or in case of panel failure.

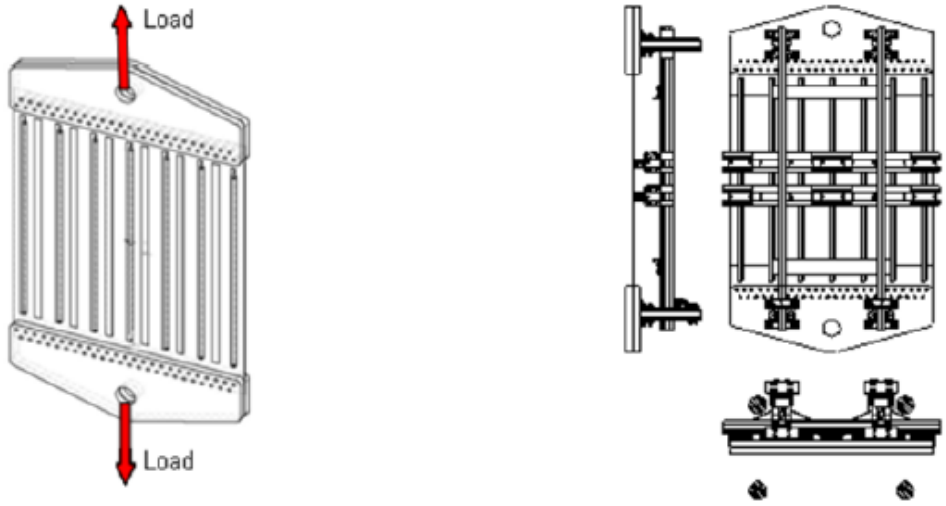

Figure 5.27: Representation of the clamping system (on the left) and of the anti-bending device (on the right).

The observed crack lengths within the two bays were practically symmetrical: this has permitted to draw the crack propagation curves [$a = f(N)$] considering the average crack length between the left and right crack tip displacement.

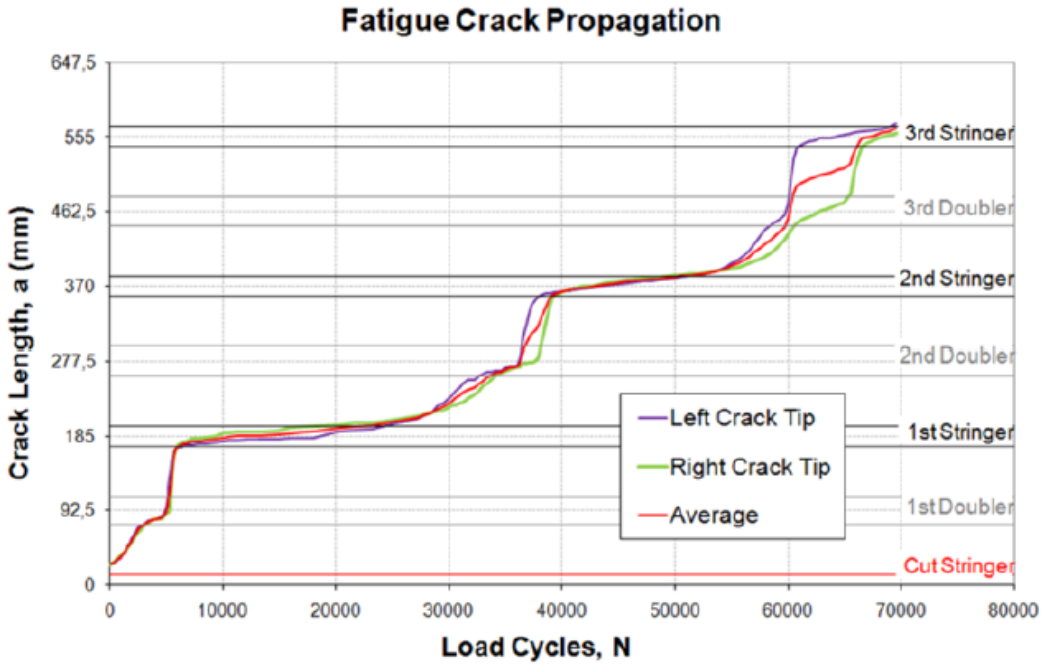

Figure 5.28: Experimental FCP curve illustration of left and right crack length and their average values (two bays-cracked panel).

The panels tested at EADS-IW are simulated using finite element analysis with the commercial software ABAQUS. A quarter of the panel was modeled so as to limit the computational complexity. Two important approximations in the FE analysis are:

- the propagation occurs in the perpendicular direction to that of load application (Mode I);
- the front of the crack is assumed to be straight and modeled with two elements in the thickness

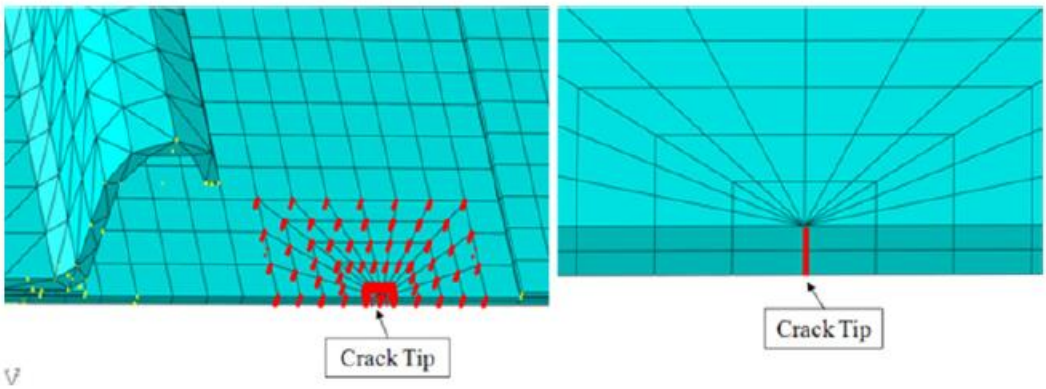

Figure 5.29: Straight crack front in the thickness direction.

In the following figures, the analysis results are shown for each of the different models. With two elements in the skin thickness, the stress contour map at the crack tip is represented.

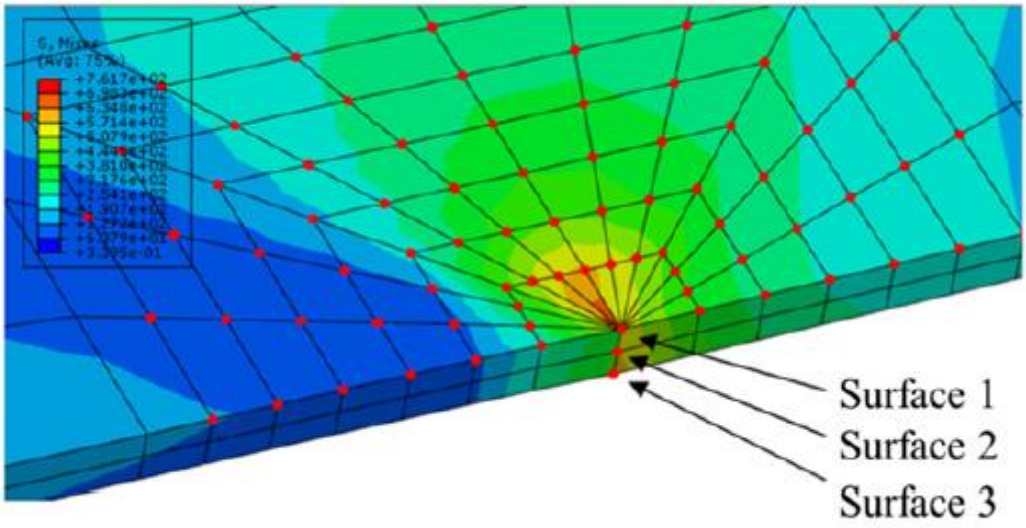

Figure 5.30: Node positions in seven contours chosen for the crack modeling. The number 1 is the surface where the stiffeners are bonded.

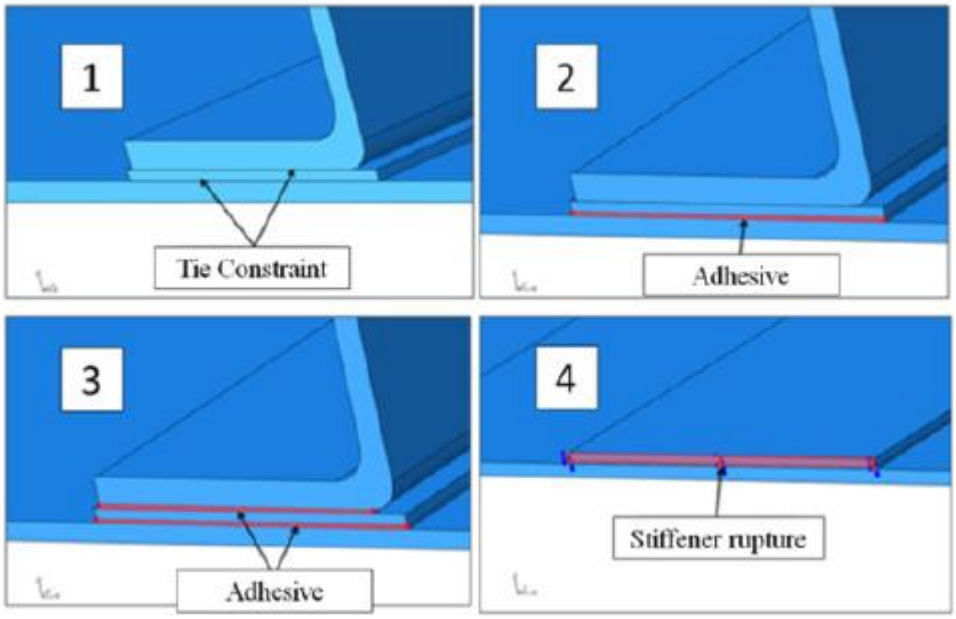

Figure 5.31: Representation of the different skin-stiffener couplings simulated.

At first, the influence of the presence of the adhesive between skin and stiffeners was assessed (Model 02 vs. Model 01). Where adhesive was introduced, the final crack length is reached in a lower number of cycles (see Fig. 15). In Model 03, the separation of the adhesive under the first doubler was modeled and an increase of crack growth rate in the first bay is observed. In the panels 4 and 4-NB, the increase of K factors after the crack runs beyond the first stiffener is caused by the (simulated) rupture of the first doubler.

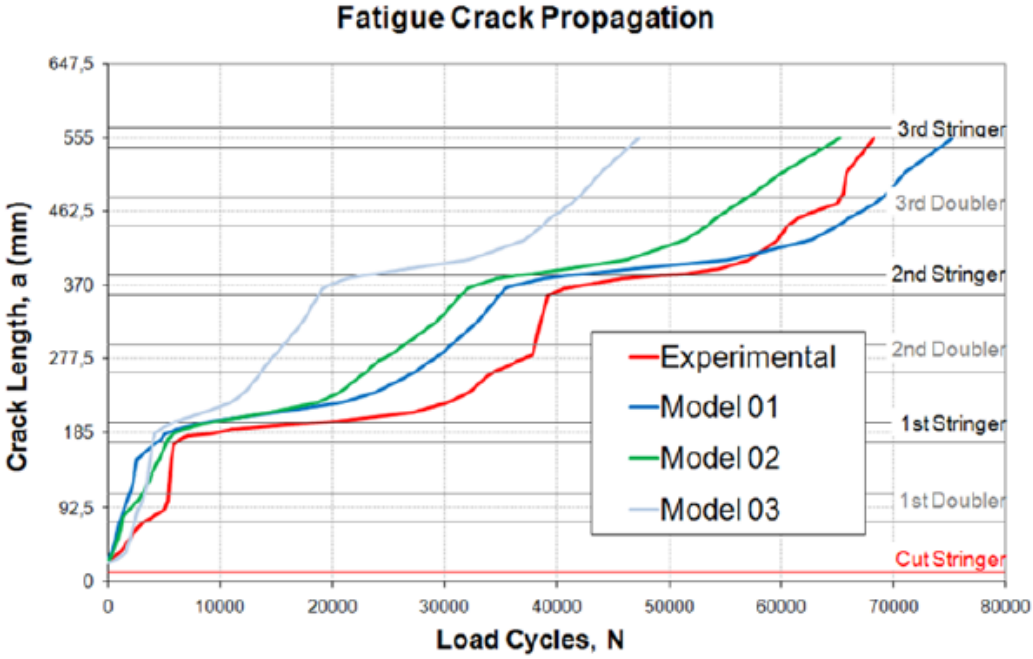

Figure 5.32: Comparison between experimental and numerical FCP curves (Models 01, 02 and 03).

The Model 01 showed the most faithful reproduction of the crack propagation. The absence of the adhesive in the simulation brings in a higher rigidity near the

reinforcements that apparently reproduces the stresses in the skin better than the other models. The inclusion of the anti-bending device in the model 04-NB until the second reinforcement leads at a more faithful reproduction of the initial stage of crack propagation.

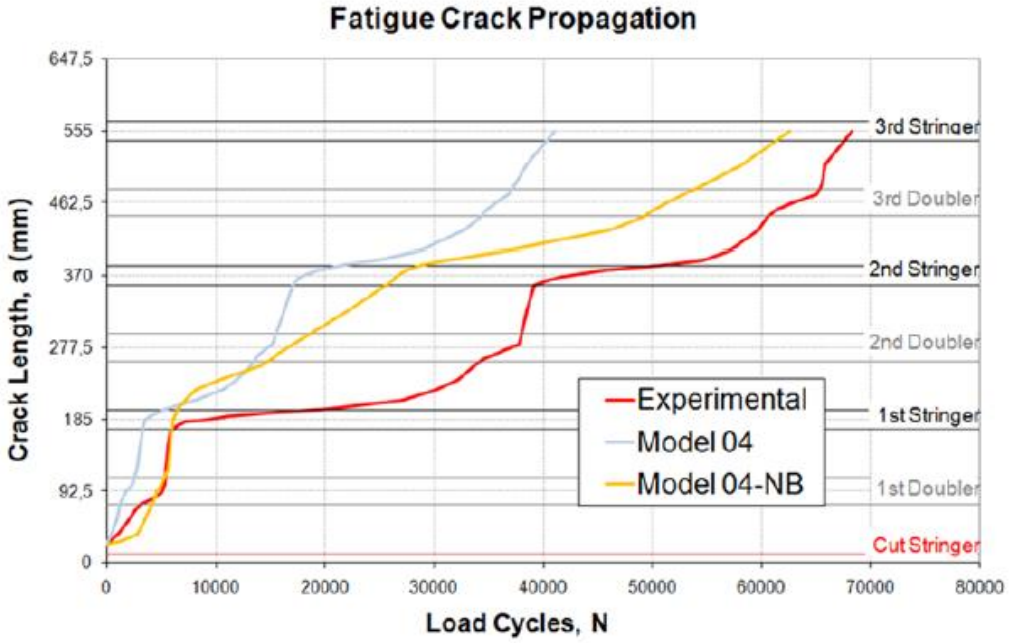

Figure 5.33: Comparison between experimental and numerical FCP curves (models 4 and 4-NB).

References

[1] Fatigue and damage tolerance assessment of aircraft structure under uncertainty. GOKSEL-THESIS, 2013
[2] Fatigue and Damage Tolerance Evaluation of Structures: The Composite Materials Response, 2009
[3] C. Mittelstedt, Composite Structures, 2008.
[4] R. S. X.B. Lin, "Stress intensity factors for corner cracks emanating from fastener holes under tension," Engineering Fracture Mechanics, vol. 62, no. 6, pp. 535-553, 1999.
[5] J. Schijve, "MULTIPLE-SITE DAMAGE IN AIRCRAFT FUSELAGE STRUCTURES," Fatigue and Fracture of Engineering Materials and Structures, pp. 329-344, 1995.
[6] S. Suresh, Fatigue of Materials, Cambridge University Press, 1998.
[7] R. M. David, "F-15B/Flight Test Fixture II: A Test Bed for Flight Research," NASA.
[8] Damage Tolerance Design Handbook, http://www.afgrow.net/applications/DTDHandbook/default.aspx
[9] AFGROW website: http://www.afgrow.net/.
[10] R. Wanhill, "Milestone Case Histories in Aircraft Structural Integrity," National Aerospace Laboratory (NLR), Amsterdam, 2002.
[11] F. Carta et alii, Frattura ed Integrità Strutturale, Damage tolerance analysis of aircraft reinforced panels, 2011.
[12] SWIFT, S. A Collective Approach to Aircraft Structural Maintenance Programs. Civil Aviation Safety Authority (CASA). [S.l.]. 2008.
[13] SCHIJVE, J. Fatigue of Structures and Materials. [S.l.]: Kluwer Academic Publishers, 2004.
[14] Damage Tolerance Design for Wing Components – Procedure Standardization. Paper: Bernardo Vilhena Gavinho Lourenço, 2010